


2021

MODELING OF RARE EARTH SOLVENT EXTRACTION PROCESS FOR FLOWSHEET DESIGN AND OPTIMIZATION

Vaibhav Kumar Srivastava

University of Kentucky, vaibhav.ism131@gmail.com

Author ORCID Identifier:

 <https://orcid.org/0000-0002-1264-5987>

Digital Object Identifier: <https://doi.org/10.13023/etd.2021.220>

[Right click to open a feedback form in a new tab to let us know how this document benefits you.](#)

Recommended Citation

Srivastava, Vaibhav Kumar, "MODELING OF RARE EARTH SOLVENT EXTRACTION PROCESS FOR FLOWSHEET DESIGN AND OPTIMIZATION" (2021). *Theses and Dissertations--Mining Engineering*. 62. https://uknowledge.uky.edu/mng_etds/62

This Doctoral Dissertation is brought to you for free and open access by the Mining Engineering at UKnowledge. It has been accepted for inclusion in Theses and Dissertations--Mining Engineering by an authorized administrator of UKnowledge. For more information, please contact UKnowledge@lsv.uky.edu.

STUDENT AGREEMENT:

I represent that my thesis or dissertation and abstract are my original work. Proper attribution has been given to all outside sources. I understand that I am solely responsible for obtaining any needed copyright permissions. I have obtained needed written permission statement(s) from the owner(s) of each third-party copyrighted matter to be included in my work, allowing electronic distribution (if such use is not permitted by the fair use doctrine) which will be submitted to UKnowledge as Additional File.

I hereby grant to The University of Kentucky and its agents the irrevocable, non-exclusive, and royalty-free license to archive and make accessible my work in whole or in part in all forms of media, now or hereafter known. I agree that the document mentioned above may be made available immediately for worldwide access unless an embargo applies.

I retain all other ownership rights to the copyright of my work. I also retain the right to use in future works (such as articles or books) all or part of my work. I understand that I am free to register the copyright to my work.

REVIEW, APPROVAL AND ACCEPTANCE

The document mentioned above has been reviewed and accepted by the student's advisor, on behalf of the advisory committee, and by the Director of Graduate Studies (DGS), on behalf of the program; we verify that this is the final, approved version of the student's thesis including all changes required by the advisory committee. The undersigned agree to abide by the statements above.

Vaibhav Kumar Srivastava, Student

Dr. Joshua M. Werner, Major Professor

Dr. Jhon Silva Castro, Director of Graduate Studies

MODELING OF RARE EARTH SOLVENT EXTRACTION PROCESS FOR
FLOWSHEET DESIGN AND OPTIMIZATION

DISSERTATION

A dissertation submitted in partial fulfillment of the
requirements for the degree of Doctor of Philosophy in the
College of Engineering
at the University of Kentucky

By

Vaibhav Kumar Srivastava

Lexington, Kentucky

Advisor: Dr. Joshua M. Werner, Assistant Professor of Mining Engineering

Co-Advisor: Dr. Rick Q. Honaker, Professor of Mining Engineering

Lexington, Kentucky

2021

Copyright © Vaibhav Kumar Srivastava 2021

<https://orcid.org/0000-0002-1264-5987>

ABSTRACT OF DISSERTATION

MODELING OF RARE EARTH SOLVENT EXTRACTION PROCESS FOR FLOWSHEET DESIGN AND OPTIMIZATION

The separation and purification of rare earth elements (REEs) into individual products has been a topic of significant interest for researchers and engineers for many decades. The prime reason for such sustained interest is due to REEs' demand and application in modern technology, as well as the challenges associated with their separation and purification. The chemical similarity of rare earth group elements is responsible for difficult separability which makes purification of individual elements challenging. Despite associated complications, processes such as solvent extraction (SX) and ion-exchange have been successfully utilized in the separation and production of REEs on pilot and commercial scales. Of the two-processes, SX is popular because of its capacity, continuous nature, fast reaction kinetics, and ease of operability. However, the literature and work on SX process design and flowsheet development for the separation of REEs is scarce.

Previous studies on the separation of REEs using SX has been focused on the experimental aspect of improving separation factors by the use of new extractants or combination of extractants. However, in a continuous SX process, the separation effects are transformed because of the multi-stage nature of operation and intricate interaction between variables, making the process more complicated and difficult to design. To have both a qualitative and quantitative assessment of such a complex process is challenging. For a rare earth system, complication compounds because of the diverse feed nature depending upon the source, multiple elements and the proportion of the individual elements present in the feed. Separations for such systems using SX require numerous stages, the determination of which is not well established and traditional methods such as McCabe Thiele becomes impractical to use because of the multiplicity of similar extracting elements. Designing and testing such processes on a pilot or industrial scale is not only time consuming but also cost and labor intensive.

This work provides a novel design framework utilizing equilibrium analysis of the rare earth SX process combined with a process modeling methodology in a modular framework to design a flowsheet for REE separation. The use of process modeling as an alternate to conventional McCabe Thiele allows analysis of a complex multi-component integrated SX system holistically. The approach is applicable to any feed composition and metal separation using SX. The equilibrium analysis for this study involved experimentally determining the separation of elements at different equilibrium pH and phase ratios. The experimental work was performed on a mixed rare earth salt solution containing yttrium,

gadolinium, samarium, praseodymium, neodymium, cerium, and lanthanum. The distribution of elements was derived from a rare earth oxide product obtained from a coal-based source, part of ongoing research at the University of Kentucky. A DEHPA and TBP mixture was used as an extractant. Similarly, stripping experiments were carried out on loaded organic at different equilibrium acid molarities and phase ratios. The results obtained from the experiments were utilized in developing non-linear separation models. The models were integrated in a process- modeling framework and programmed in Matlab/Simulink as modular function blocks to describe loading, scrubbing and stripping processes involved in a SX operation. The blocks were then arranged and interconnected to design and simulate a multi-train SX flowsheet for individual or group separation of elements. A particle swarm optimization algorithm was applied to determine stage combination, resulting in the best separation of elements based on a defined objective function using recovery and purity of elements. Simulation and optimization showed good separation for yttrium and lanthanum from the feed mixture to a purity of 99.52 and 85.41, requiring 8-12-3 and 10-3-5 loading-scrubbing-stripping stages, respectively. Simulation results also indicated moderately difficult separability between gadolinium and samarium, and difficult separability for praseodymium, neodymium, and cerium groups.

KEYWORDS: Solvent Extraction, Rare Earth Separation, Modeling and Simulation, Flowsheet Design and Optimization

Vaibhav Kumar Srivastava

4/30/2021

Date

MODELING OF RARE EARTH SOLVENT EXTRACTION PROCESS FOR
FLOWSHEET DESIGN AND OPTIMIZATION

By
Vaibhav Kumar Srivastava

Dr. Joshua Werner

Co-Director of Dissertation

Dr. Rick Honaker

Co-Director of Dissertation

Dr. Jhon Silva Castro

Director of Graduate Studies

4/30/2021

Date

DEDICATION

To my parents, teachers and friends

ACKNOWLEDGMENTS

First, I would like to express deepest gratitude to my advisors Dr. Joshua Werner and Dr. Rick Honaker for their valuable guidance and unparalleled support over the course of my studies. They provided me an opportunity to work on prestigious projects, gain operational exposure and supported my education during my program. They have been constant sources of motivation and inspiration that helped me excel. I am grateful to Dr. Werner for enriching my knowledge in the field of micro-controllers and numerical modeling, and to Dr. Honaker for educating me on the hydrometallurgy fundamentals and operational aspects of the pilot plant.

I am extremely grateful to Dr. John Groppo and Dr. Thomas Dziubla, who served as committee members on this dissertation. I very much appreciate Dr. Thomas Dziubla's course and his efforts in providing me the knowledge of equilibrium thermodynamics essential to building the foundation of the equilibrium process. Special thanks to the faculty members of the courses I took during my program. It helped me to develop knowledge and skills from mining and other disciplines, making me a knowledgeable, well-rounded engineer.

I gratefully acknowledge the help of the staff and co-workers of the Department of Mining Engineering and the pilot plant. It will be hard to list the name of all, but thanks to Megan Doyle, Douglas Addo, Glenn Brock, Xinbo Yang, Alind Chandra, Vincent Mounce, Daniel Dailey and Heather. I am grateful to Dr. Wencai Zhang for teaching me the fundamentals of ICP, which helped me analyze samples at early stages of study, and to Daniel Dailey for analyzing them at the later stages of my study. I also had the great pleasure of working with David Threlkeld of Alliance Coal in improving and applying automation techniques at the pilot plant.

The completion of this dissertation would not have been possible without the love, support and belief of my parents, Ranjana and Devendra, and brother, Anubhav Srivastava. Special thanks to my friends Ankur Sachan, Ravi Chandan Ray and Rajdeep Nath, who made my stay in Lexington memorable.

TABLE OF CONTENTS

ACKNOWLEDGMENTS	iii
LIST OF TABLES	vii
LIST OF FIGURES	ix
CHAPTER 1. INTRODUCTION	1
1.1 OVERVIEW	1
1.2 OBJECTIVE	5
1.3 OUTLINE	6
CHAPTER 2. LITERATURE REVIEW	8
2.1 RARE EARTH ELEMENTS.....	8
2.1.1 Properties of REE	9
2.1.2 Application and Market	11
2.2 SEPARATION METHODS FOR REEs	14
2.3 SOLVENT EXTRACTION (SX).....	18
2.3.1 Fundamentals	18
2.3.2 Important Variables	23
2.3.2.1 Distribution Ratio and Percent Extraction	23
2.3.2.2 Separation Factor (SF)	24
2.3.3 Continuous Processes.....	25
2.4 EXISTING SX FLOWSHEETS FOR REE SEPARATION.....	27
2.5 MODELING OF SOLVENT EXTRACTION	44
2.5.1 Thermodynamic Modeling.....	46
2.5.1.1 Concentration Method	46
2.5.1.2 Activity-Coefficient Method.....	49
2.5.2 Empirical Modeling of the Equilibrium Process	54
2.6 PROCESS MODELING.....	58
2.6.1 Steady-state modeling.....	59
2.6.2 Dynamic process modeling.....	68
2.7 SUMMARY AND GAP ANALYSIS	71
CHAPTER 3. RESEARCH APPROACH	73
3.1 FUNDAMENTAL BASIS.....	74

3.2 MODELING APPROACH USING DISTRIBUTION RATIOS	76
CHAPTER 4. MATERIALS AND METHOD.....	85
4.1 FEED.....	85
4.2 CHEMICALS	87
4.3 EXPERIMENTAL PROCEDURE	88
4.3.1 Extraction.....	89
4.3.2 Stripping.....	92
4.3.3 Phase 2 experiment	93
4.4 REE ANALYSIS	93
CHAPTER 5. EQUILIBRIUM ISOTHERM	97
5.1 EXPERIMENTAL RESULTS.....	97
5.2 MULTI-STAGE PROCESS MODELING	105
5.3 SIMULATION.....	111
CHAPTER 6. DISTRIBUTION ISOTHERM.....	117
6.1 EXPERIMENTAL RESULTS.....	117
6.1.1 Observance of Saturation Effect	122
6.2 MULTI-TRAIN MODEL DEVELOPMENT.....	124
6.2.1 Extraction and Stripping Phase Ratio Model.....	125
6.2.2 Simulink Model Library	131
6.2.2.1 Loading and Stripping Blocks:	133
6.2.2.2 Mixer, Splitter, and pH Adjustment:.....	134
6.2.2.3 Recovery and Purity.....	136
6.3 CONCLUSION.....	139
CHAPTER 7. FLOWSHEET DESIGN AND TRAIN OPTIMIZATION	142
7.1 FLOWSHEET DESIGN	142
7.2 PARTICLE SWARM OPTIMIZATION (PSO).....	147
7.3 YTTRIUM SEPARATION	152
7.4 GADOLINIUM AND SAMARIUM SEPARATION	157
7.5 LANTHANUM SEPARATION.....	161
7.6 CONCLUSION.....	167
CHAPTER 8. CONCLUSION AND FUTURE WORK	169

8.1 CONCLUSION.....	169
8.2 FUTURE WORK.....	172
APPENDICES	174
APPENDIX 1. SYMBOLS USED	175
APPENDIX 2. ADDITIONAL PLOTS.....	177
APPENDIX 3. APPLICATION CODES	180
REFERENCES	189
VITA	196

LIST OF TABLES

Table 2.1: Percentage by weight of REEs in common industrial product (Dev et al., 2020; Goonan, 2011).....	12
Table 2.2 SX separation studies performed on REEs using various extractants in different media.....	17
Table 2.3 Extractant based on their classification (ion-exchange and solvating) used in REEs extraction and separation (Jha et al., 2016; Xie et al., 2014).....	21
Table 2.4: Feed distribution of bastnaesite mineral tested via force feeding mechanism Brown et al., 1979.....	38
Table 2.5 Activity coefficient model based on electrostatic interaction (Newman et al., 1980).....	51
Table 2.6: Equilibrium and hydrolysis reactions for Co, Ni and Li separation (Vasilyev et al., 2019).....	53
Table 2.7: Models developed using power law for La, Ce, Pr, Nd and Sm (Thakur, 2000b).....	55
Table 2.8: Programs developed for process modeling of SX.....	67
Table 4.1: Specification of organic compound used.....	87
Table 4.2: Distribution of rare earth oxides and chlorides in the mixture.....	90
Table 4.3 Mean, standard deviation of measured feed samples.....	96
Table 5.1: Separation factor between element pair at different solution pH values used for extraction.....	99
Table 5.2: Separation factor between element pair at different pH values used for stripping.....	99
Table 5.3: Model parameters for distribution ratio and pH - loading.....	103
Table 5.4: Model parameters for distribution ratio and pH - stripping.....	104
Table 5.5: Parameters used for simulation.....	112
Table 6.1: pH for distribution isotherm.....	117
Table 6.2: Separation factor for element pairs at pH 1.52.....	120
Table 6.3: Separation factor for element pairs at pH 2.23.....	121
Table 6.4: Functional form explored for curve fitting.....	125
Table 6.5: Model parameters for extraction.....	127
Table 7.1: Separation condition for yttrium.....	153

Table 7.2: Optimization Parameters	153
Table 7.3: Summary of train optimazation objective function and results	165

LIST OF FIGURES

Figure 2.1 Electronic configuration of REEs showing light, middle and heavy REEs	10
Figure 2.2 Ionic radii of rare earths (Eyring et al., 2002)	11
Figure 2.3 Yearly production data of rare earth oxide (Wu et al., 2018).....	14
Figure 2.4 Mechanism involved in solvent extraction (adapted from Miller, 1978).....	19
Figure 2.5 Extractant classification on mechanism adapted from Jha et al. (2016) and Xie et al. (2014).	20
Figure 2.6: Different flow types in solvent extraction (Zhang et al., 2016b)	25
Figure 2.7: Typical solvent extraction train.....	26
Figure 2.8: Schematic of a single mixer-settler	27
Figure 2.9: Rare earth feed distributions processed using PC-88A (Zhang et al., 2016b) 29	
Figure 2.10: Flowsheet configuration for REE separation (Zhang et al., 2016b).....	30
Figure 2.11: Process A and B showing separation route developed without and using optimization respectively (Zhang et al., 2016b)	31
Figure 2.12: Plotted feed composition of HREE source (Zhang et al., 2016b)	32
Figure 2.13: Flowsheet used for separation of Europium from bastnaesite (Xie et al., 2014; originally published in Gupta et al., 1992).....	34
Figure 2.14: Flowsheet for mini plant (Preston et al., 1996)	35
Figure 2.15: Aqueous phase concentration profile for rare earth circuit of mini-plant for loading (top) and stripping (bottom) shown in Figure 2.14 (reconstructed from Preston et al., 1996)	36
Figure 2.16: Different variants of the force-feeding mechanism (Brown et al., 1979)	37
Figure 2.17: Force feeding process for separation of europium (Brown et al., 1979).....	39
Figure 2.18: Flowsheet used for separation of LREE using partial and total reflux (Brown et al., 1979)	40
Figure 2.19: Stagewise concentration profile after first treatment (top) and second treatment (bottom) (Brown et al., 1979)	41
Figure 2.20: Conceptual flowsheet for La-Nd-Y separation using TOPO and TRPO (El-Nadi, 2012)	42
Figure 2.21: Flowsheet post improvement using ANN for separation of Nd from Pr (Anitha et al., 2008)	43
Figure 2.22: Flowchart showing different methods adopted in equilibrium and process modeling and their co-dependence on each other.....	45

Figure 2.23: Distribution isotherm (Zhang et al., 2016b)	48
Figure 2.24: Reconstructed distribution isotherm surface developed for copper extraction using LXI64N (Hughes et al., 1975 data originally published in Robinson et al., 1971). 48	
Figure 2.25 Structure of neural network for predicting percent extraction from experimental data (Acharya et al., 2017)	54
Figure 2.26: Example of working of a single neuron	56
Figure 2.27: Structure of neural network model for distribution ratio of Nd and Pr (Anitha et al., 2008)	57
Figure 2.28: Multistage SX process (top, adapted from Xie et al., 2014); mass balance across a single stage showing flow and concentration variables associated with a single stage (bottom)	60
Figure 2.29: Mass balance applied successively to multistage counter-current solvent extraction adapted from Henley et al. (1981)	62
Figure 2.30: McCabe Thiele curve represented as equilibrium line and stagewise mass transfer represented by operating line	64
Figure 2.31: Equilibrium curve and operating line pair for two components.....	66
Figure 2.32: Dynamic modeling across a single stage for organic phase.....	69
Figure 3.1: Schematic showing step-by-step flow sheet development approach used in this study to model the SX system and use of optimization for flowsheet design	73
Figure 3.2: Speciation states for an individual rare earth in aqueous phase	77
Figure 3.3: Speciation states in organic and aqueous phases.....	77
Figure 3.4: Feed distribution of REO obtained from hydrometallurgical treatment of PLS obtained from Western Kentucky No.13 coarse refuse	80
Figure 3.5: Plot showing extraction results of elements present in high concentration from investigative study performed on REO mixture using DEHPA and TBP (2% v/v)	81
Figure 3.6: Plot showing extraction results of elements present in high concentration from investigative study performed on REO mixture using Cyanex 572 (2% v/v)	81
Figure 3.7: Experimental design matrix.....	83
Figure 3.8: Experimental approach and decision making involved in modeling SX process.....	84
Figure 4.1: REE distribution of the mixed oxide product recovered from West Kentucky No. 13 (Baker) seam coarse refuse	86
Figure 4.2: Reconstituted REE distribution of the mixed oxide product recovered from West Kentucky No. 13 (Baker) seam coarse refuse after ignoring REEs with less than 1% content	86

Figure 4.3: Chemical structure of DEHPA and TBP (Zhang et al., 2016b)	88
Figure 4.4: Aqueous stock (left) and organic stock (right) prepared for testing.....	91
Figure 4.5: Prior mixing (left) and phase separation (right)	92
Figure 4.6: ICP-OES Equipment (adapted form Spectro-Arcos Specofication Sheet)	94
Figure 4.7: Element chemical standard.....	95
Figure 4.8 Whisker plot of multiple feed stock concentration data used for SX tests.....	96
Figure 5.1: Equilibrium isotherm for loading showing perceent extraction of REEs at different pH's and phase ratio 1	97
Figure 5.2: Equilibrium isotherm for scrubbing & stripping at a phase ratio of 1	98
Figure 5.3 Separation route based on separation factor between the elements	101
Figure 5.4: Plot of log tranformed distribution ratio with pH for loading of REEs	103
Figure 5.5: Distribution ratio as a function of pH – stripping	104
Figure 5.6: Multi-Stage SX-Train.....	105
Figure 5.7: Mass balance of a species i for stage j.....	106
Figure 5.8: System equation matrix for a REE	108
Figure 5.9: Matlab application interface for SX train.....	110
Figure 5.10: Purity in strip bleed stream at different equilibrium pH	113
Figure 5.11: : Purity in strip bleed stream at different equilibrium pH for 3-0-1 and 6-0-1 stage combination	114
Figure 5.12: Purity in strip bleed stream at different equilibrium pH for 3-0-1 and 3-0-2 stage combination	114
Figure 5.13: Conceptual separation hirearchy	115
Figure 6.1: Percent Extraction vs O/A Ratio at pH 0.65	118
Figure 6.2: Percent Extraction vs O/A Ratio at pH 1.52	119
Figure 6.3: Percent Extraction vs O/A Ratio at pH 2.2	120
Figure 6.4: Percent Stripping vs O/A Ratio using 1M HCl (0.15 equilibrium pH).....	122
Figure 6.5: Saturation effect at pH 2.2 for Y, Gd, Sm, and Pr.....	123
Figure 6.6: Saturation effect at pH 2.2 for Nd, Ce, and La.....	124
Figure 6.7: Loading and Stripping from a single stage.....	129
Figure 6.8: Extraction and Stripping from multi-stage loading and stripping process...	130
Figure 6.9: Working of a Simulink system block	132

Figure 6.10: Solvent Extraction Model Library in Simulink.....	133
Figure 6.11: Loading and Stripping block in Simulink	134
Figure 6.12: Masked loading subsystem.....	134
Figure 6.13: Other function blocks	136
Figure 6.14: Interconnected subsystem of loading, scrubbing, and stripping process to develop SX train block.....	138
Figure 6.15: Conceptual flowsheet with updated phase ratio conditions	141
Figure 7.1 Cause and effect diagram showing factor influencing SX performance.....	144
Figure 7.2: Example of a typical system with objective function.....	145
Figure 7.3: Typical recovery-purity curve	147
Figure 7.4: Model flow diagram	151
Figure 7.5: Convergence plot for Train 1, Train 2, and Train 3 (optimized independently and plotted together) showing the minimization of objective function with iteration....	156
Figure 7.6: Yttrium separation (SX train 1).....	157
Figure 7.7: Gd-Sm combined extraction train using transformed objective function.....	159
Figure 7.8: Gadolinium and samarium separation (SX Train 2 and Train 3) using purity of gadolinium as objective function	160
Figure 7.9: Convergence plot for Train 4 and Train 5	162
Figure 7.10: Nd-Ce-Pr and La Train 4 and Train 5	163
Figure 7.11: Complete flowsheet.....	164
Figure 7.12: Sensitivity to reflux ratio	167
Figure 8.1 Stripping using acid molarity greater than 1 M.....	177
Figure 8.2: Percent Extraction vs O/A Ratio at pH 2.75	178
Figure 8.3: Saturation effect at pH 2.75 for Y, Gd, Sm, and Pr.....	178
Figure 8.4: Saturation effect at pH 2.75 for La, Ce, and Nd.....	179

CHAPTER 1. INTRODUCTION

1.1 OVERVIEW

Separation and purification of metal from contaminants is an essential and crucial step in production of any metal in usable form. Various physical and chemical methods are applied to achieve separation, exploiting differences in the metal and contaminants' characteristics. The metal of interest and contaminant may show distinct difference in characteristics which allows easier separation thus making industrial process simpler or may show poor separation characteristics resulting in complex processes. Generally, a process is feasible when metal and associated contaminants show significant differences, and therefore separation can be achieved easily and economically. However, in some instances, metal and contaminants may have similar characteristics, complex chemistry and product requirements, forcing complicated and less effective process designs. Such processes remain as preferred practice due to lack of suitable alternatives.

The separation and purification methods for traditional base metals and precious group metal is well-established. The principal reason for that is traditional metals have been utilized historically, which has promoted the continued development of the processes for their purification. However, with continued technological development, there has been an uptake in the use of more diverse kinds of metals. One such group of metals are the rare earth group of elements (REEs). This group of elements have found widespread application in modern technology, such as permanent magnets, alloys, batteries, etc. (Du et al., 2011). The products derived from these metals are used in everyday technologies, such as electric vehicles and green energy batteries, and they are also essential in defense technologies. Continuing the current trend and increasing demand of modern technology, future demand will require increasing quantities of highly purified REEs (Ganguli et al., 2018). However, scarcity of supply, difficult separation characteristics, and associated economics have created challenges in meeting the growing demand for these elements.

Currently, there are very few entities producing or attempting to produce highly purified individual REEs on a commercial scale in the United States. Mountain Pass Materials is the primary large-scale producer with an active mine in California. Rare Earth Salts is also a

known independent supplier; however, it focuses only on the separation and refining of REEs (Schmid, 2019). Other commercial companies with research in the development phase are Ucore Rare Metals, Texas Mineral Resources, and Blue Line Corporation. The reason for such low levels of commercial involvement is economic and technical difficulties in recovering and separating REEs. Factors such as trade-disputes, unregulated market supply, and geo-politics have caused significant variability in the market price of REEs, thereby negatively impacting the economics of production (Schmid, 2019). Additionally, availability of the mineable resources and difficult separability requiring large downstream processes has been a major concern on technical fronts.

To mitigate such challenges, significant research is being done to develop economically viable processes to produce REEs. Alternate sources of REEs, such as coal and fly ash, have shown potential for REE extraction (Honaker et al., 2018a). However, a major focus of ongoing research is on the extraction of REEs as a group and less about the individual separation of REEs themselves. The similar chemical behavior between individual REEs makes it difficult to exploit any property for their separation. Commercial processes that have utilized the technique of solvent extraction (SX) to individually separate rare earths for production have kept their process details largely confidential (Singh, Kotekar, & Singh, 2008). Thus, it becomes very difficult to make use of the existing knowledge of separation and purification in designing a flowsheet or developing a process for economic and effective separation.

Nevertheless, with SX being a popular and viable option for the separation of REEs, a systematic and effective procedure to develop rare earth separation processes is needed. The majority of available research on the separation of REEs using SX have been centered on improving the separability of elements. The focus has been to improve the relative separation between elements using a combination of extractants. Other aspects discussed in literature were the extraction behavior as a function of aqueous phase acidity and initial organic and metal concentration in order to identify the mechanism of extraction or study extractant behavior such as the monomeric-dimeric state. Although the studies are useful in gaining the fundamental understanding and equilibrium chemistry of the separation process, there is a need for their application in process development.

Few studies have extended the results discussed in literature in estimating the number of stages required using the McCabe Thiele method. However, most of the McCabe Thiele design methodologies are based on individual rare earth salts/elements, which fail to capture competing ion effects and organic saturation effects due to a multi-element system. In addition, McCabe Thiele plots developed on a single salt does not quantify the recovery and purity of the product from a multicomponent and multistage solvent extraction process. Thus, it is essential to have separation methods, along with a quantitative and qualitative assessment of the separation and their applicability, to develop multistage processes.

The design procedure for separation and purification of base metals such as copper, nickel, cobalt, and zinc, etc., using SX has been well-developed by researchers (Anderson et al., 2009; Rydberg, 2004; Sole et al., 2005). However, the same approach is not easily applied to the rare earth system. The process chemistry for REEs is more complicated because of the multiplicity of elements. A typical base metal separation will have 2-3 components as impurities, which will have different properties from the metal of interest. Whereas, for a rare earth system, the feed mixture usually has 5-17 different components in varying proportions with like properties. In addition, for a base metal separation using SX, the desired metal and impurities have significant differences in extraction characteristics, leading to large separation factors (ratio of distribution between elements) at various conditions. This allows engineers to effectively choose operating conditions and design a SX process to minimize the number of stages to achieve the target recovery and purity. However, the extraction characteristics of the REEs show poor chemical differentiation, resulting in low separation factors and requiring a large number of stages to achieve the desired degree of separation.

Testing such large processes on industrial or pilot projects is difficult and costly. For example, pilot-plant trials performed by researchers like Preston, et al., (1996) and Lyon et al., (2016) in the separation of REEs in group (middle and heavy) indicated the requirement of 20 or 30 stages of mixer-settlers. The process becomes tedious and unrealistic to test on a pilot scale when high purity of multiple individual REE is sought from different feed sources (Wenli et al., 2000). A more pragmatic way to achieve the design process is via modeling and simulation of the equilibrium separation process. This

assists the designer in the preliminary work of process design, while relegating physical testing to validation.

Process modeling is an effective technique used in chemical, mineral, and metallurgical industries for the design and control of industrial processes. Simulation packages like Aspen and SysCAD, commonly used by chemical engineers, are useful in analyzing the response of process due to changes in any variable, which help identify related interdependencies within a process. Simulating a process prior to physical testing not only increases the number of design iterations, but it can also decrease uncertainties in the process. However, process modeling is a challenging task as it requires successful integration of reliable experimental data and model development applied to process design. For a rare earth system, the process becomes even more complex because of the dynamic equilibrium between a large number of ionic species and the presence of large number of variables that can affect separation.

Additional complexity arises in that a single REE exists in multiple ionic states, depending upon a dissociation constant, the Eh-pH of the system. The ion then undergoes a chemical reaction with extractant of each species having a different reaction equilibrium constant. Further complicating the process is the monomeric and dimeric states of the extractant affecting the equilibria. Studying and modeling such processes from a fundamental standpoint is challenging. The mining and mineral industry is familiar with modeling complex chemical systems where fundamental solutions or approaches are not possible or cost prohibitive. Hence, a hybrid approach, combining both fundamental and empirical methods, has been used in the mining and mineral industry to adequately model non-ideal systems. Successful application of this hybrid approach, also called a phenomenological model, can be seen in areas such as grinding and flotation, where it has been successfully utilized for process design and improvement.

Therefore, the intent of this study is to understand and model the equilibrium SX process and utilize it for developing process models to provide a methodology of flowsheet development for the separation of the REEs. Doing this will require exploration and development in four different areas listed below:

- Study of solvent extraction equilibrium of REEs using experiments;

- Extraction model development using data collected from experiment;
- Application of extraction model in process design;
- Identifying and simulating the design process for different operational conditions and finding the optimum conditions for achieving optimum recovery and purity.

1.2 OBJECTIVE

It is hoped that this work will serve as a useful guide for rare earth metal separation, process modeling, simulation and optimization of complex SX circuits. The method and approach adopted will be applicable to many metal separation processes using solvent extraction or adjacencies such as ion and resin exchange. The other key objectives of the research are:

1. Reviewing prior art of solvent extraction reagents, practices, modeling techniques, and flowsheets utilized for the separation of rare earths;
2. Identify reacting species, i.e., feed composition and extractants for separation of REEs. Study the effects of these important variables on extraction such as equilibrium aqueous phase acidity (pH) and organic-aqueous volumetric ratio on separation;
3. Design and perform experiments to study the effect of the identified variables on the extraction of elements;
4. From experimental results, evaluate variables such as the concentration of metals in organic and aqueous phases, percent extraction, distribution ratios, and separation factors. Develop mathematical models for distribution and percent extraction, describing the relationship with separation variables using linear and non- linear techniques;
5. Implement distribution ratio models using a first-principal approach of mass balance to a multi-stage solvent extraction process to form a system of equations. Develop a Matlab application to solve the system of equations and predict the optimum separation pH for a given feed composition;
6. Extend the model application in the design of multi-train solvent extraction process and incorporating the organic saturation effect using distribution isotherm;

7. Develop a library of solvent extraction unit operations using distribution isotherm models in Matlab/Simulink, which can be utilized for multi-train solvent extraction flowsheet development to capture intricate interaction of the process;
8. Design a flowsheet using the modular library for separation of individual REEs;
9. Simulate the developed continuous flowsheet to study the effect of important operational variables such as organic-aqueous flow rates, reflux on recovery, and purity of elements;
10. Develop an optimization method and determine the stage configuration and resulting stage number resulting in increased recovery and purity of elements.

1.3 OUTLINE

This dissertation is a mixture of experimentation, modeling techniques, and process design for the development of an REE SX purification circuit. The material herein is progressive research and can be used for both academic and industrial applications. In addition, the experimental and chemical modeling approach is applicable to any multi-component solvent extraction system. The process modeling can be utilized in comparing alternatives for industrial process design and can be extended to process control.

The material in this dissertation was subdivided into eight chapters. The first chapter introduces the concept of separation and purification of rare earth using solvent extraction, existing practices, limitations, and challenges. It then discusses the objectives the study is aimed to fulfil. The second chapter provides a detailed literature review on rare earth separation using solvent extraction, chemistry, and reagents. This chapter further reviews existing flowsheets and processes used in industry for rare earth separation. Finally, it covers various aspects of modeling of rare earth solvent extraction and its application in design and control. The third chapter covers the fundamentals of rare earth equilibrium chemistry, lists factors affecting equilibrium processes and challenges associated with a multi-element system. It then describes the research approach to study the factors using experimentation, model extraction with respect to factors and implement developed models for SX process design. The fourth chapter introduces materials and tools required for conducting experiments. The analytical procedure adopted for performing the experiments

is discussed in detail. Experiments are performed in two phases as phase 1 and phase 2. Phase 1 experiments focused on studying REE separation with respect to pH, whereas phase 2 experiments considered the effect of phase ratios. The results obtained from the experiments are distributed into two parts, presented in Chapters 5 and 6, combined with model development. Chapter five contains the results from the developed extraction isotherms and discusses the extraction as a function of pH. Logarithmic transformation is applied to the data based on the understanding of equilibrium chemistry for model development. The models are implemented in a developed Matlab application to determine pH for the separation of individual or a combination of REEs. Chapter six utilizes results from phase ratio experiments (phase 2) to develop extraction models as a function of an organic-aqueous phase ratio, accounting for saturation effects. A library of solvent extraction unit operations containing the phase ratio model is developed in Simulink for multi-train flowsheet simulation. Chapter seven details the implementation of the model library in flowsheet development and simulation and utilizes an optimization method on developed flowsheets to determine stage requirements to achieve the desired optimum separation performance. Finally, the results from the entire process are summarized in Chapter 8, and the dissertation concludes with recommendations, suggestions, and recommendations for future research.

CHAPTER 2. LITERATURE REVIEW

Industrial processes developed for the separation of metals are usually based on the understanding of physical and chemical properties of the metal of interest and the associated impurities. Economic factors, such as market supply and demand, capital, and operating costs, are considered in determining the applicability and implementation of any process on a large scale. In the case of REEs, the property widely utilized in separation are the differences in complex forming ability of REEs at different pH values. This property is referred as basicity. Solvent extraction (SX) is one such process which utilizes this property and has been extensively implemented in preferential extraction of REEs. Another reason for wide applicability of SX process is the economic and operational advantage it offers compared to methods such as ion-exchange. Significant developments have been made by physical and organic chemists in identifying organic extractants and detailing mechanisms of extraction of REEs using SX (Thakur, 2000b). However, the methods related to the design of the SX process for REEs is limited and not well established due to multiple components. This chapter reviews and provides a background on distinct properties of REEs, their application, market supply, separation processes utilized, and progress made in SX process design for rare earth separation.

2.1 RARE EARTH ELEMENTS

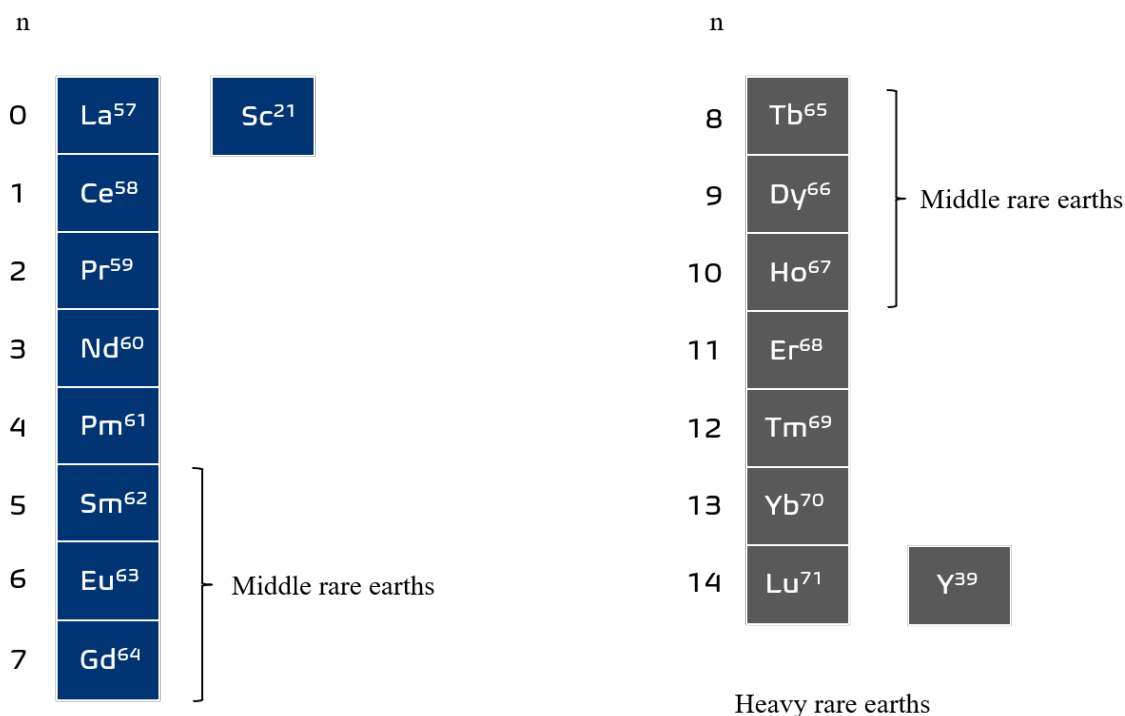
The nomenclature issued by International Union of Pure and Applied Chemistry (IUPAC) defines the rare earth elements as a group of 15 lanthanide elements from atomic number 57 to 71, along with scandium and yttrium. These elements are further classified into two groups as light rare earth elements (LREEs) and heavy rare earth elements (HREEs), based on atomic weights and slight similar properties such as double salt solubility and reactivity, etc. The LREE group consists of elements from lanthanum to gadolinium, whereas the HREE group consists of the remaining lanthanides from terbium to lutetium (Figure 2.1). Yttrium is grouped with HREEs because of additional resemblance to HREEs, whereas scandium is grouped with LREEs. This classification is generic and routinely used. In research and industry, researchers and engineers sometimes add a third category, middle rare earth elements (MREEs), based on the order of reactivity and selectivity shown by

elements to an applied chemical process (Zhang et al., 2016b). The MREE classification is utilized in group separation of REEs and contains elements from samarium to holmium.

During an applied chemical process, all REEs tend to follow an order based on a combination of chemical properties ionic radii and basicity, etc., which is responsible for their reactivity. HREEs are first to react for given chemical conditions, hence they are separated first as a group, followed by MREEs and LREEs. LREEs are last to react and often require different conditions compared to HREE and MREE. Most of the designed process, as we shall see later in the discussion, utilize this group separation as a precursor to the individual separation of REEs. Group separation allows simpler process design and the effective utilization of chemicals for separation. Nevertheless, irrespective of classification, the properties of REEs has been a topic of interest and is commonly linked to answering questions concerning their mode of occurrence and separation characteristics, etc. Subsequent sections discuss some of the important properties of REEs.

2.1.1 Properties of REE

Unlike any other metal, rare earths show a variety of physical and chemical properties. The two important properties associated to the chemical behavior is the tri-valent nature of the REEs and the lanthanide contraction. All REEs, except cerium (Ce) and europium (Eu), exist in +3 oxidation states. Ce (IV) and Eu (II) are commonly found in tetravalent and divalent states, respectively (Eyring et al., 2002). The oxidation state is responsible for compounds and complexes formed by REEs. However, it is quite unusual that, despite increasing atomic number (Z), most of them to exist in the same oxidation state. This abnormality is elucidated by reviewing the electronic configuration of REEs. A typical electronic configuration of lanthanides is given by $4f^n(5d6s)^3$ (where $n = 1$ to 14 from Lanthanum to Lutetium). In lanthanides, the electron in the outermost shell is filled prior to the inner 4f orbital. The 4f orbitals are systematically filled with an increasing atomic number (Figure 2.1). As a result, the electronic configuration and valance of the outer most shell are unchanged, leading to a +3 oxidation state, except for Ce and Eu (Brown et al., 1979). Since, oxidation states are responsible for chemical interactions, similar oxidation states are the primary reasons for difficult separability of REEs using chemical methods.



Light rare earths

$4f^n(5d6s)^3$ Electronic Configuration

Figure 2.1 Electronic configuration of REEs showing light, middle and heavy REEs

The other distinctive property of lanthanides is the lanthanide contraction. This is the decrease in the atomic and ionic radii of the lanthanides with the increase in atomic number (Figure 2.2). This phenomenon occurs because of the weak shielding effect of the 4f electron by the nucleus. With the increase in atomic number, the charge on the nucleus increases, which results in greater pull on the electrons in the outer shell, decreasing the radius. The lanthanide contraction is responsible for the difference in other property changes such as basicity and increasing coordination ability (Krishnamurthy et al., 2005; Moeller et al., 1945). The difference is normally exploited in separation of individual REEs. It is also a contributing factor in the classification criterion for REEs into light and heavy. The knowledge of similar and dissimilar properties is essential from a

hydrometallurgical standpoint because developed processes for extraction or separation utilize these properties.

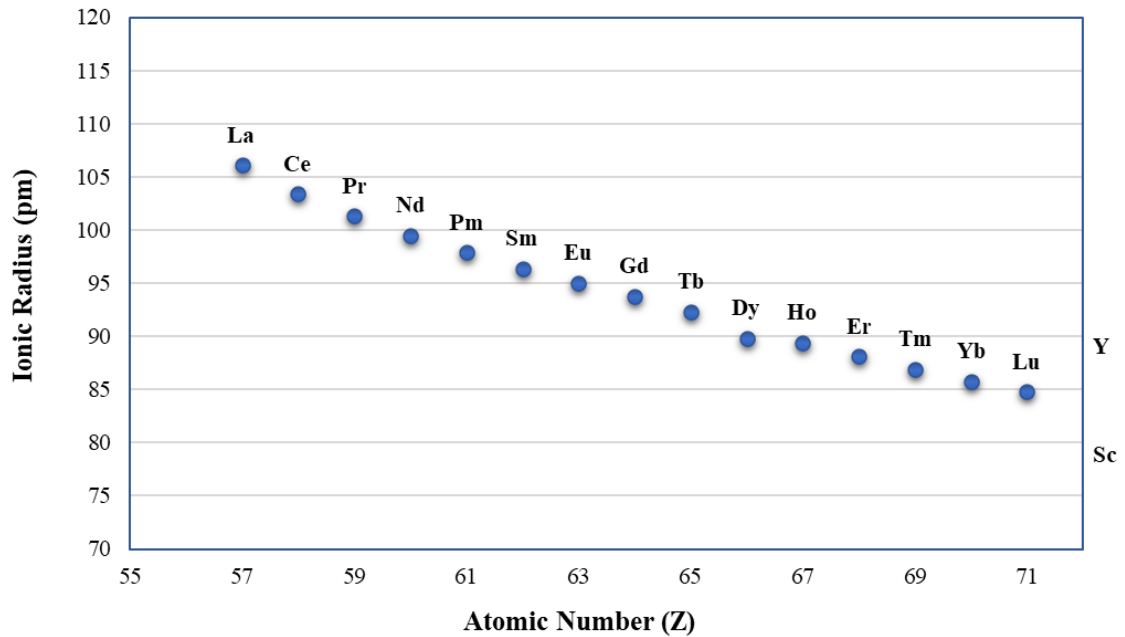


Figure 2.2 Ionic radii of rare earths (Eyring et al., 2002)

2.1.2 Application and Market

While most of the REEs have found application in technology such as batteries, magnets, electronics, etc., for their use in renewable energy production and electric vehicles REEs have been in use since the 1900s. During the 1900s, the REEs were primarily used as a mixed rare earth metal called misch metal, an alloy of cerium, lanthanum, and neodymium by the metallurgists, which improved the properties of steel (Eyring et al., 2002). A mixture of rare earth oxides was used as a catalyst in the petroleum and organic industries for hydrogenation and cracking. Other applications of individual high purity REEs, such as europium and yttrium, were in monitors and television, providing color as a synthetic fluorescent. Cerium and lanthanum oxide found usage in glass polishing and as a doping agent in glass and lenses, providing absorption characteristics. Yttrium was used in

luminesce, astronavigation, and nuclear energy. With advancement in technology and emphasis on green energy equipment, the application of individual REEs and their oxides have expanded. Neodymium, praseodymium, and dysprosium are now more popular, primarily used in making strong NdFeB permanent magnets utilized in wind turbines and electric cars. Thus, the rare earths in all the forms have diverse application. Table 2.1 summarizes percentage of REEs in common industrial products.

Table 2.1: Percentage by weight of REEs in common industrial product (Dev et al., 2020; Goonan, 2011)

Products	REE %										
	La	Ce	Pr	Nd	Sm	Eu	Gd	Tb	Dy	Y	Others
Magnets			23	69			2		5		
Battery alloys	50	33	3	10	3						
Metallurgy	26	52	5	16							
Auto catalyst	5	90	2	3							
FCC	90	10									
Polishing powders	31	65	3								
Glass additives	24	66	1	3						2	4
Phosphors	8	11				5	2	5		69	
Ceramic	17	12	6	12						53	
Others	19	39	4	15	2		1			19	

The table reveals that not all the REEs are of equal importance because demand of a rare earth is dictated by its application and availability. Thus, based on market demand and availability, they are categorized as critical and non-critical REEs (Gambogi et al., 2016). Critical REEs are the rare earths with high demand, limited supply, and essential application, which indicates that it cannot be substituted with other elements. While most of the rare earth deposits are aimed to extract critical and high priced REEs, the distribution of critical REEs may vary in terms of the feed source. Feed sources having a low proportion

of critical REEs may require a large volume of ore to produce them in needed quantities. As a result, non-critical REEs present in the feed source are also extracted (Binnemans et al., 2015). Therefore, non-critical REEs produced in the process are often stockpiled, which creates an imbalance in the market, resulting in increased supply and low prices. It is worth pointing out that the changes in the existing technology also influence the criticality of REEs. For example, samarium was initially used in manufacturing of samarium-cobalt permanent magnets which was later replaced by neodymium magnets (Zepf, 2016). Such shifts have also occurred in the mining of REEs from one ore to another, resulting some mines to run at a loss.

The world's market demand of REEs is mostly met by production from China, which contributes up to 80 percent of the world's production (Figure 2.3). As the major producer of REEs, China regulates the market price of REEs and has often surprised the market by lowering the price. This has led to the closure of some mines for intermediate periods, such as Mountain Pass in California and Mount Weld in Australia. For example, Mountain Pass was closed in 2015 as it was unable to compete with low market priced REEs. However, it was later opened in 2018 to meet the domestic requirements, whereas Mount Weld continued to operate. Thus, because of the skewed supply market, there exists a demand-supply risk of rare earths around the world. It is for the same reason which has led researchers to seek for an alternate source of REEs such as coal and coal-based source (Honaker et al., 2018). In addition, global trade and geo-political changes have also been a contributor for increased focus on the production of REEs.

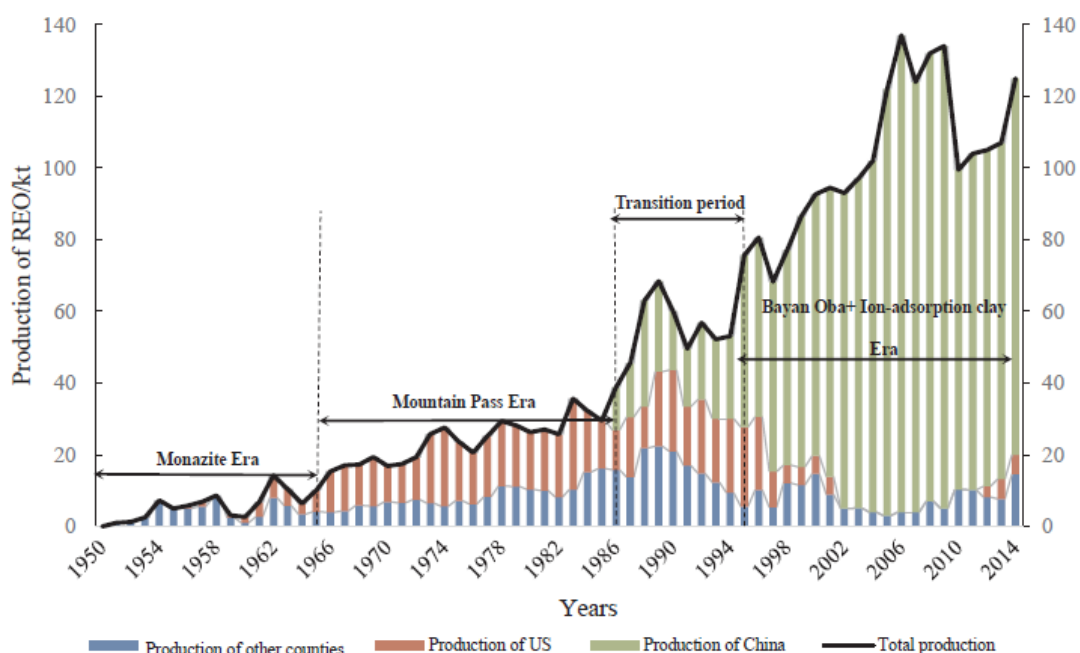


Figure 2.3 Yearly production data of rare earth oxide (Wu et al., 2018)

2.2 SEPARATION METHODS FOR REEs

The methods developed for the separation of REEs can be traced back to the early 1940s, when studies investigating the properties of the REEs, such as basicity, oxidation states, and solubilities, were initiated (Moeller et al., 1945). The knowledge gained from these pioneering studies were employed in developing potential separation techniques for REEs. Such methods include ion exchange resins, pressurized ion exchange to increase mass transfer rate, fractional precipitation, fractional crystallization, and solvent extraction. These methods involved complexation of REEs under different chemical conditions, specifically utilizing pH effects. A brief description of each method is discussed in the subsequent paragraphs.

Ion exchange is performed with a solution containing dissolved REEs, passing over a column/bed made up of ion-exchange resin or beads. The beads act as an adsorbing agent, allowing the loading of metal species onto them. The extractant in the beads acts as chelating agents to allow for the preferential exchange of cation from the aqueous solution.

Once the bead surface is loaded with ions, an eluant containing a suitable complexation agent is used to strip the loaded surface, in order to recover the element as eluate. Separation is achieved by choosing the resin-extractant and eluant, which are selective to elements. Many factors, such as complex formation, stability of complex, temperature, resin size, and pH, etc., are critical to process performance and are adjusted to achieve required separation (Nervik, 1955). Ion exchange has been very effective in producing highly purified REEs at purities greater than 99.9 percent (Royen et al., 2016). However, the limitation of the ion exchange process is that it is generally time consuming (Lusty et al., 2010). Campbell, discussed the limitation of ion-exchange resin in rare earth separation as being too slow requiring large operating times (Campbell, 1973; Uda et al., 2000). To tackle the problem, Campbell (1973) developed pressurized ion exchange for improved mass transfer rates and flowrates. However, the separation time was still 60 to 120 minutes, which is significantly higher compared to the SX process, which takes 10-20 minutes. Nevertheless, the method is still used on a small scale when very high purity analytical grade REEs are required (Xie et al., 2014).

The fractional precipitation method utilizes the difference in the solubility of the REEs by forming insoluble rare earth compounds. The precipitation is achieved by either an oxidation-reduction reaction or complex formation reactions. Precipitation using the oxidation-reduction method is achieved by changing the oxidation state of the element, resulting in the insoluble form in aqueous phase. Therefore, the oxidation-reduction method is only applicable to REEs exhibiting different oxidation states, thereby limiting it to only cerium and europium. Oxidizing agents like permanganate, chlorate, and hypochlorite have been used for converting cerium (III) to cerium (IV), making it insoluble, resulting in its separation from dissolved metal ions. Similarly, reducing agents such as zinc amalgam have been used to reduce and precipitate europium (Kronholm et al., 2013). Alternately, the complex formation method uses chelating agents like oxalic acid to form complexes, which are insoluble in aqueous phase, without altering the oxidation state (Weaver, 1954). The rate of reaction, concentration, and pH determine the efficiency of separation. Because of the difference in basicity, the extent of complex formation is different for each rare earth which is controlled by manipulating pH. However, fractional precipitation by complex formation is a difficult process and requires close control of reaction variables.

Another unique process developed for the separation of REEs was the selective reduction and vacuum distillation of REE halides (Uda et al., 2000). The process utilizes conversion of trivalent chlorides to dihalides in a molten state, and it exploits the difference in redox potential vapor pressure for separation. This method has only been tested on a laboratory scale and no industrial or pilot scale application has been reported to our knowledge.

Currently, solvent extraction (SX) is the most popular and widely used technique in the separation and purification of REEs due to its efficiency and economy. SX utilizes the difference in extractability of metals under equilibrium conditions, like aqueous phase acidity and reactant concentration. The prime reason for the popularity of SX is that it allows easy handling, scalability, fast reaction kinetics, and efficient control of the separation process. Despite being the primary choice, SX has been criticized for requiring a large number of stages to achieve certain purifications and complicated flowsheets for individual separations. Several studies pertaining to REE separation using SX have been performed. The majority of these studies involved testing a new extractant or a combination of extractants to improve the separability among the elements. Table 2.2 summarizes studies performed over the past two decades using different extractants for the separation of REEs. Many of the studies focused on separating a combination of selected rare earths. This is useful in the final stage of separation, when separation between a pair of elements is sought. However, rare earth feeds often contain a large number of elements, hence, for flowsheet design, a comprehensive separation study of feed source is required.

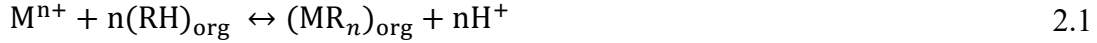
Table 2.2 SX separation studies performed on REEs using various extractants in different media

Elements	Extractant	Media	Author
La and Ce	PC-88A	Nitric	Abdeltawab et al., 2002
Nd and Pr	Saponified PC-88A	Hydrochloric	Banda et al., 2015
Tb, Gd, Eu and Sm	HEHEPA	Hydrochloric	Fontana et al., 2009
Nd, Dy and Y	DEHPA and EHEHPA	Hydrochloric	Mohammadi et al., 2015
Dy and Y	DEHPA, EHEHPA and PC-88A	NA	Thakur, 2000a
La, Nd and Y	TOPO and TRPO	Nitric	El-Nadi, 2012
HREE	α -aminophosphonic acid HEHAPP	Hydrochloric	Kuang et al., 2018
Sm, Gd, Dy and Y	TOPS 99, PC-88A, Cyanex 272, 302, 921 and 923	Hydrochloric	Kim et al., 2012
Y	CA-12–TBP	Hydrochloric	Li et al., 2007

2.3 SOLVENT EXTRACTION (SX)

2.3.1 Fundamentals

Solvent extraction, also known as liquid-liquid extraction, is an extensively used industrial method for the preferential extraction of metals from a pregnant leaching solution (PLS) (Anderson et al., 2009; Rydberg, 2004). The process involves the mixing of two liquid phases, i.e., an aqueous phase containing dissolved metal ions and impurities and an organic phase containing the extractant dissolved in a diluent (). During mixing, the phases are dispersed into one another. The mass transfer of the extractant and the metal ion takes place at the interfacial boundary, wherein the extractant preferentially reacts with the metal ion to form an organo-metallic complex (Figure 2.4). The general form of the chemical reaction that takes place for a typical metal ion when reacting with acidic extractant is given by Free (2013):



where M^{n+} represents metal ion with valance n, $(RH)_{org}$ the organic extractant, $(MR_n)_{org}$ the extractant-metal complex formed during the extraction phase, and H^+ the hydrogen ion released in the process. The subscript ‘org’ in the chemical reaction represents the species in the organic phase.

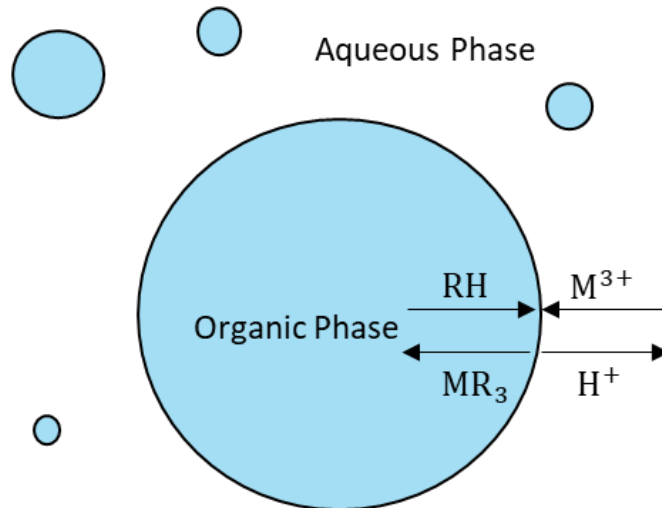


Figure 2.4 Mechanism involved in solvent extraction (adapted from Miller, 1978)

The organo-metallic complex formed during the reaction has more solubility in the organic phase, and hence, it is transferred to the phase resulting in selective extraction of the ion. The mixing time for the process is determined by studying dispersion and reaction kinetics and is selected to allow sufficient contact time between the phases for mass transfer and reaction to take place (Anderson et al., 2009). Mixed liquids are then allowed to stand for a certain time for phase disengagement. The loaded organic phase is separated from the aqueous phase during this process due to its lower density. The extractant-metal complex is thus separated from undesired metal ions during the disengagement due to its high solubility in the non-polar organic solvent. The valuable metal loaded in the organic phase needs to be recovered in the aqueous solution. This is achieved by stripping in the organic phase. A suitable stripping agent, often acid or water, is used for recovering metal ions in the aqueous phase. The stripping agent required is determined experimentally and varies for different metals.

For the REE extraction processes, numerous organic extractants have been identified. These extractants are broadly classified into two categories: ion-exchange and solvating

extractants (Jha et al., 2016). Ion-exchange is further categorized as acidic (cationic) and basic (anionic) extractants. The classification of the extractant is based on the mechanism by which they extract the metal ion and form a complex. Figure 2.5 shows a typical example of the type of complexes formed with trivalent metal ions using different extractant types. For rare earths, acidic extractants, which function using cation-exchange mechanisms, are predominant because of their high-extraction potential. Table 2.3 lists some of the organic extractants used in REE extraction and separation along with their classifications. Of all the listed extractants, PC-88A and DEHPA are popular in industrial rare earth extraction and separation processes (Lyon et al., 2016).

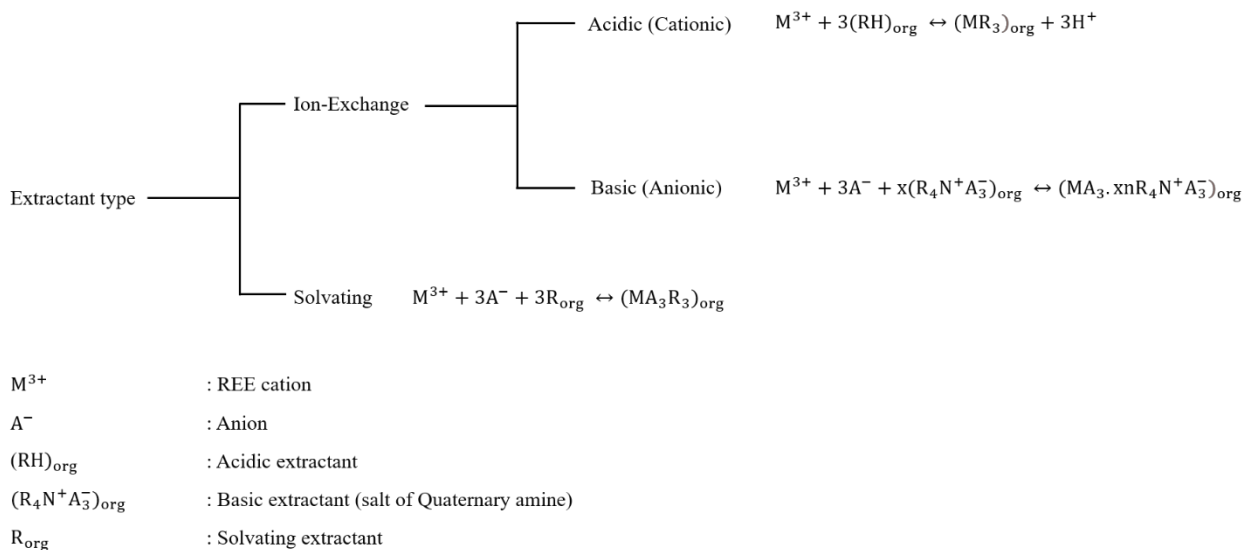


Figure 2.5 Extractant classification on mechanism adapted from Jha et al. (2016) and Xie et al. (2014).

Table 2.3 Extractant based on their classification (ion-exchange and solvating) used in REEs extraction and separation (Jha et al., 2016; Xie et al., 2014)

Extractant	Chemical Name	Type
PC-88A	2-Ethylhexyl phosphonic acid mono-2-ethylhexyl ester	Ion-Exchange (Acidic)
HEHEPA	Bis(2-ethylhexyl) phosphinic acid	
EHEHPA	2-Ethylhexyl phosphonic acid mono-2-ethylhexyl ester	
DEHPA	Di-(2-ethylhexyl) phosphoric acid	
Cyanex 302	Mono thiophosphinic acid	
CA-12	Sec-octylphenoxy acetic acid	Ion-Exchange (Basic)
Alamine 336	Amine based	
Aliquat 336	Trioctyl/decyl methyl ammonium chloride	
TBP	Tributyl phosphate	Solvating
TOPO	Trioctylphosphine oxide	
TRPO	Trialkylphosphine oxide	

Similarly, acids, such as hydrochloric, nitric, and sulfuric, of high concentrations are used for stripping extracted REEs. The extractant and the stripping reagent are selected based

on laboratory tests performed on leaching samples or artificial solutions of metal ion prepared using respective metal salts. The reagents are assessed based on selectivity, extraction efficiency, impurity rejection, operational handling, and cost, etc. The selection of an extractant and stripping reagent is complex and choosing a strong extractant or stripping reagent may not necessarily result in effective separation. Rather, extremes can lead to extraction of undesired components or impurities resulting in low-grade products. Hence, both extractability and selectivity of different reagents need to be determined to select an appropriate reagent scheme to achieve effective separation. For this purpose, different separation performance measures are defined using fundamentals of equilibrium chemistry of the extraction process. For a typical equilibrium reaction given by Eq. 2.1, the reaction equilibrium constant is described by law of mass law of mass action as:

$$K = \frac{a_{(MR_n)_{org}} a_{H^+}^n}{a_{M^{n+}} a_{(RH)_{org}}^n} \quad 2.2$$

where K is the equilibrium constant and “a” followed by subscript is the activity of the respective species. For the reactions occurring in systems assumed to be ideal, “a” is replaced by the concentration and the corresponding equilibrium constant is referred as concentration-based equilibrium constant (K_{conc}). The mathematical formulation of K_{conc} is obtained by substituting the concentration in Eq. 2.2 in place of activities:

$$K_{conc} = \frac{[MR_n]_{org} [H^+]^n}{[M^{n+}] [RH]_{org}^n} \quad 2.3$$

The ratio of metal concentration in the organic phase and aqueous phase in Eq. 2.3 gives the distribution coefficient constant. Distribution coefficient constant (D_c) is a measure of the distribution of the metal species in both phases, and it is also known as the extraction coefficient which is given by:

$$D_c = \frac{[MR_n]_{org}}{[M^{n+}]_{Aq}} \quad 2.4$$

The distribution constant thus provides a measure of the extent of a reaction. However, the distribution constants are not very popular for a complex system involving different ionic states of a metal. Different ionic states lead to multiple equilibrium reactions taking place in the system. Thus, it requires an estimation of multiple equilibrium constants associated with ionic species involved in a reaction, which is not always feasible. Hence for monitoring extraction performance in large industrial processes, variables that can be easily measured and indicate the extent of extraction or separation are used. Discussed below are the important variables used in the hydrometallurgical industry.

2.3.2 Important Variables

2.3.2.1 Distribution Ratio and Percent Extraction

Distribution ratio, unlike the distribution coefficients, are defined for overall metal species (solute) accounting for all the ionic states. Thus, a distribution ratio is described as the ratio of total concentration of metal in the organic phase to total concentration in the aqueous phase given by:

$$D = \frac{[M^p]_{org} + [M^q]_{org}}{[M^p]_{Aq} + [M^q]_{Aq}} \quad 2.5$$

where, p and q reflect different ionic states (oxidation state) of the same metal (M) distributed in both phases. The distribution ratios provide a measure of how metal is distributed between both phases at a given separation condition but not the fraction of metal extracted to organic phase compared to original feed solution. Generally, in an industrial operation, it is more useful to express the metal extraction with respect to aqueous feed

solution. For this purpose, the quantity of metal loaded in the organic phase with respect to the initial quantity present in the aqueous phase (feed) is expressed using a variable called percent extraction. Eq. 2.6 shows the mathematical formulation of the percent extraction, with V_o and V_{aq} representing the volume of organic and aqueous phases, respectively (Rydberg, 2004). An advantage of using percent extraction is that it ranges from 0 to 100, making it easier to comprehend and compare between different metal extractions.

$$E = \frac{V_o[M]_{org}}{V_a[M]_{aq,feed}} * 100 \quad 2.6$$

2.3.2.2 Separation Factor (SF)

On several occasions, during an SX process, a comparison between the extraction and stripping between pair of metals under different conditions is helpful. Distribution ratios evaluated for such cases can be difficult to compare and may have values ranging from zero to infinity. Thus, to have a relative measure of extraction of the two metals in the extraction process separation factors are evaluated. The separation factor between metal pair for a certain condition is defined as the ratio of the distribution ratios, i.e.:

$$S_{A/B} = D_A/D_B \quad 2.7$$

where, $S_{A/B}$ is the separation factor of species A over B and D_A and D_B are the distribution ratios of species A and B, respectively. Separation factors are often used for drawing comparisons between extractants or processing options when separation of multiple elements are sought. Thus, they are used as parameters in identifying conditions that lead to better separation.

2.3.3 Continuous Processes

Industrial SX processes are designed to operate continuously and used in multiple stages to perform loading and stripping of incoming feed material. To maximize the separation, recovery and purity of product, different design configurations, inlet-outlet port arrangements, and flowrates, etc., are tested. Flow types, such as co-current (cascade flow), cross-current (cross flow), and counter-current flows, are used to maximize separation performance (Figure 2.6). If multistage processes are designed to operate, such that the organic and aqueous solvent phases are introduced from the same end and are contacted as they flow down the cascade, the flow type is referred as concurrent flow (Zhang et al., 2016a). Phases, when introduced from opposite ends of the cascade flow type, are referred to as the counter current, crossflow is a distinct case in which fresh solvent is contacted at each stage of the SX process and is used for obtaining pure products when separation factors between elements is very great. Metal solvent extraction usually employs counter current flow arrangement because of greater mass transfer efficiency (Free, 2013).

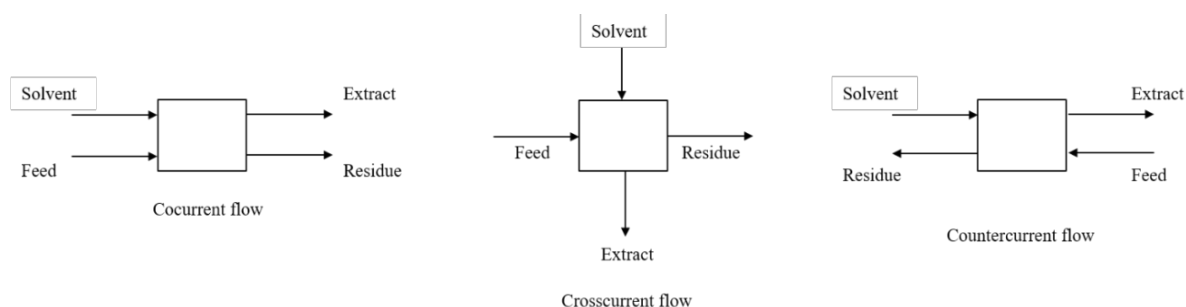


Figure 2.6: Different flow types in solvent extraction (Zhang et al., 2016b)

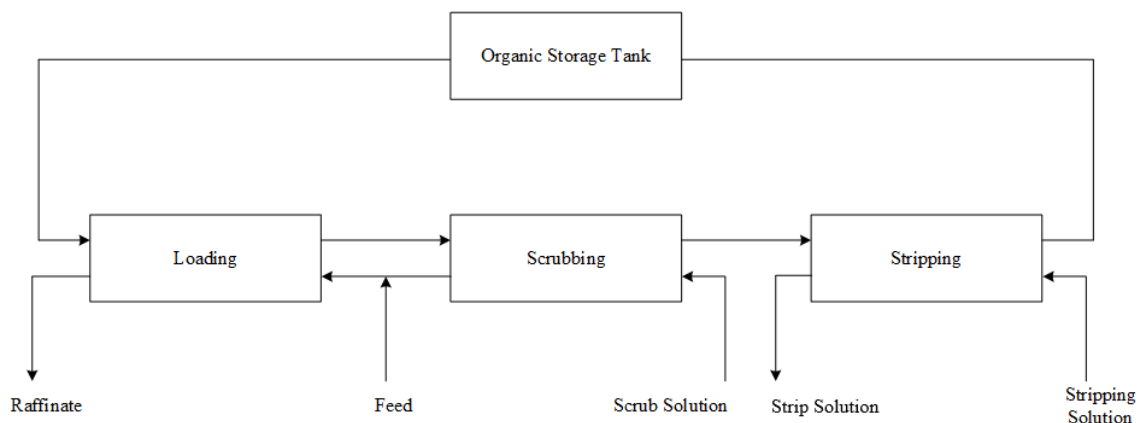


Figure 2.7: Typical solvent extraction train

A typical countercurrent hydrometallurgical separation using SX consists of three main multistage processes, known as loading, scrubbing, and stripping. The loading process is employed to perform the preferential extraction of metal from solution containing dissolved metal to organic phase containing extractant. The loaded organic leaving the loading stage is then scrubbed with a scrubbing agent, usually water, mild acid, or a fraction of strip, circulated to the scrubbing stage. Scrubbing is done to remove undesired components, which are entrained in organic or chemically bounded with the extractant during extraction. The scrubbed organic is then stripped using acid to recover the metal to the aqueous phase. The stripped aqueous solution is, thus, rich in the desired metal as a result of the selectivity achieved through the loading, scrubbing, and stripping steps. Stripped organic solution from stripping process recirculated back to the loading stage whereas the stripped solution containing concentrated metal is processed further. An additional process called saponification is generally applied during continuous operation of a SX process which involves treatment of organic extractant with base, typically sodium hydroxide (NaOH), to prevent pH drift from the release of H^+ during the extraction process. Saponification prevents the reduction in extraction which could have resulted from pH drift.

In some cases, a fraction of the organic or aqueous solution phases in a SX train are recirculated back to alter the extraction performance; this process is known as reflux. Refluxing of a scrubbed solution is very common to minimize losses of metal during a

scrubbing operation. Nevertheless, irrespective of design arrangement and different processes in a SX train, the mechanism is the same, involving mixer and settler configurations arranged in a cascade (Figure 2.8 shows a single mixer/settler stage). A mixer compartment is utilized to disperse the phase, so as to promote the chemical reaction at the interface boundary, and the settler is used for phase disengagement.

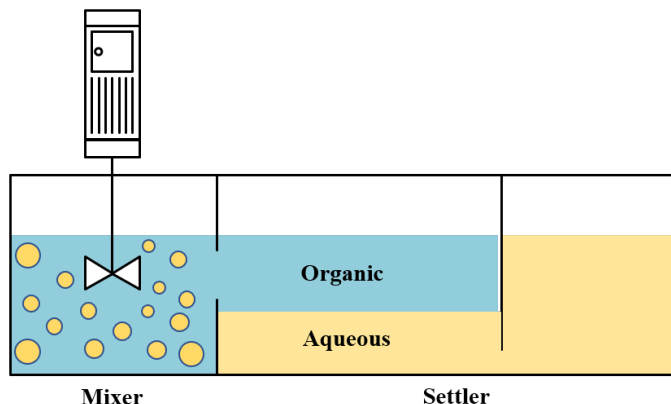


Figure 2.8: Schematic of a single mixer-settler

2.4 EXISTING SX FLOWSHEETS FOR REE SEPARATION

From discussions in previous section, it is evident that substantial development has been made in the chemistry of the REE extraction processes using SX; however, equally important is the knowledge of industrial methods, practices and process flowsheets. Despite SX being the primary process employed for separation of the REEs, the literature for existing pilot and industrial flowsheets for the separation of REEs is very scarce. The majority of resources available are focused on the extraction of REEs into groups. Nevertheless, the available existing REE separation flowsheets discussed in the literature can be categorized based on the number of SX trains applied for separation. These are: 1) Single-train SX process and 2) Multi-train SX processes. The single-train SX process is applied when separation is performed in one step and is primarily used for group separation of REEs or when the number of components are few (2-3). Multi-train configuration

employs multiple steps and trains to stepwise separate REEs with each train aiming to separate one element from the group.

Zhang et al. (2016) detailed different flowsheets which exist for the separation of rare earths. The work catalogs multi-train SX flowsheets based on extractants typically employed in REE separation. The majority of the flowsheets discussed can be classified in this work under two extractants, i.e.:

1. PC-88A
2. DEHPA

Both the extractants are acidic in nature, and they utilize the ion-exchange mechanism. However, the mechanism of extraction is a topic of debate and is shown to vary depending on solution chemistry. This is because of the equilibrium existing between monomeric and dimeric forms of the extractant in the organic phase. In acidic environments, the dimeric state of extractant is more prevalent for extracts using a solvation mechanism. Similarly, in less acidic environments, the monomeric form is more dominant for extracts using the ion-exchange method. It is also reported that the dimeric form transforms to monomeric form to provide extractant availability if the feed has a high metal concentration (Mansur et al., 2002). Irrespective of the mechanism, acidic ion-exchange extractants are popular because of their high extraction potential.

Figure 2.9 shows three different feed compositions (labeled A, B, and C) the flowsheet of which was discussed by Zhang et al. (2016) subjected to separation using PC-88A. For the selected feed distributions, five different flowsheet configurations were presented with slight differences. Figure 2.10 shows two of the flowsheet configurations. Although the specific design and operating variables of the flowsheets were not discussed, it can clearly be observed that the rare earth separation was done by group. The segregation of elements was common to all flowsheets and was based on extractability of the element (HREE, MREE, and LREE). Another observation in the distribution is the presence of a higher proportion of LREEs in the feed shown in Figure 2.9.

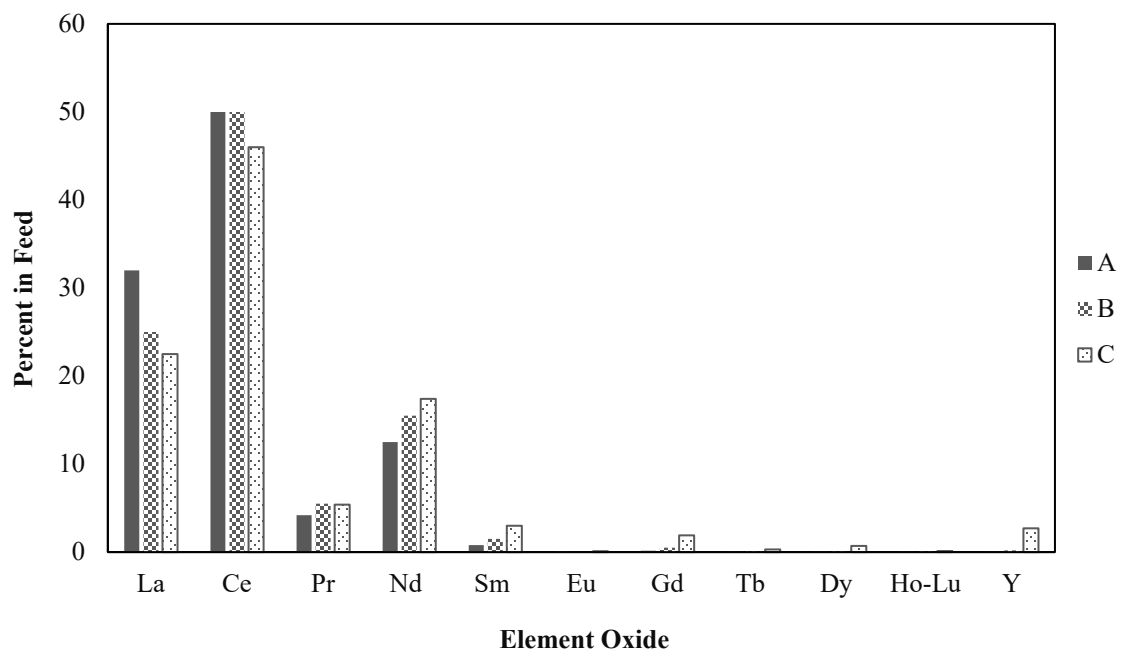


Figure 2.9: Rare earth feed distributions processed using PC-88A (Zhang et al., 2016b)

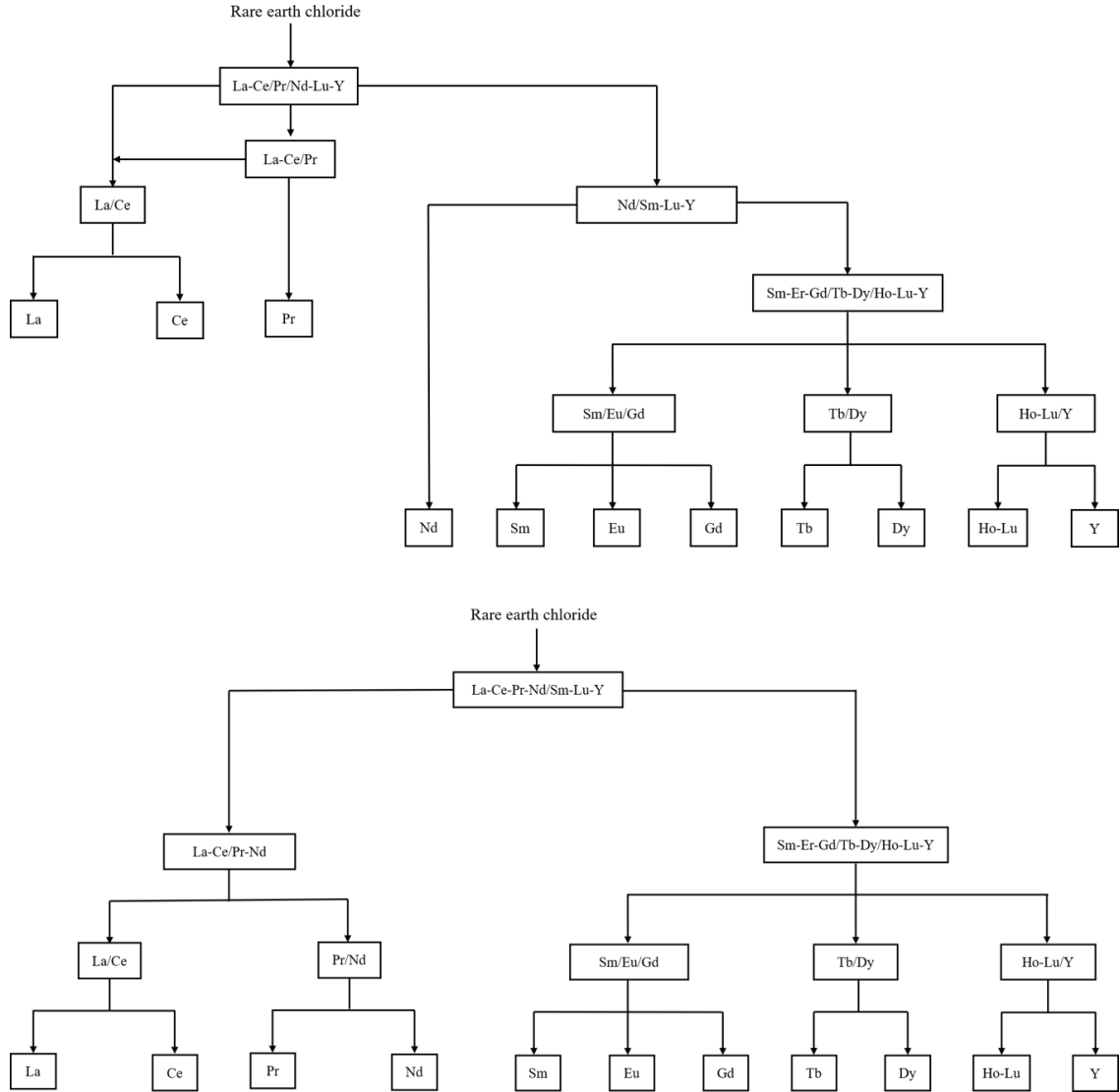


Figure 2.10: Flowsheet configuration for REE separation (Zhang et al., 2016b)

Zhang et al. (2016) also mentioned the use saponification in increasing the extractability of REEs. However, the use of saponification in improving extraction is not as significant as during the extraction H^+ ion in the system, which causes the pH to decrease, thereby decreasing the extractability directly related to pH. In addition, the use of optimization in adopting different routes to separation of LREEs was reported, but no details were provided regarding the method making it difficult to compare the effectiveness and validity of method. Figure 2.11 shows the two-separation route, in which separation process A is the traditional flowsheet, and separation process B is the flowsheet developed using

optimization. It has been reported that the optimized flowsheet has a reduced reagent consumption and organic-storage footprint in the separation of rare earths (Deng et al., 2003).

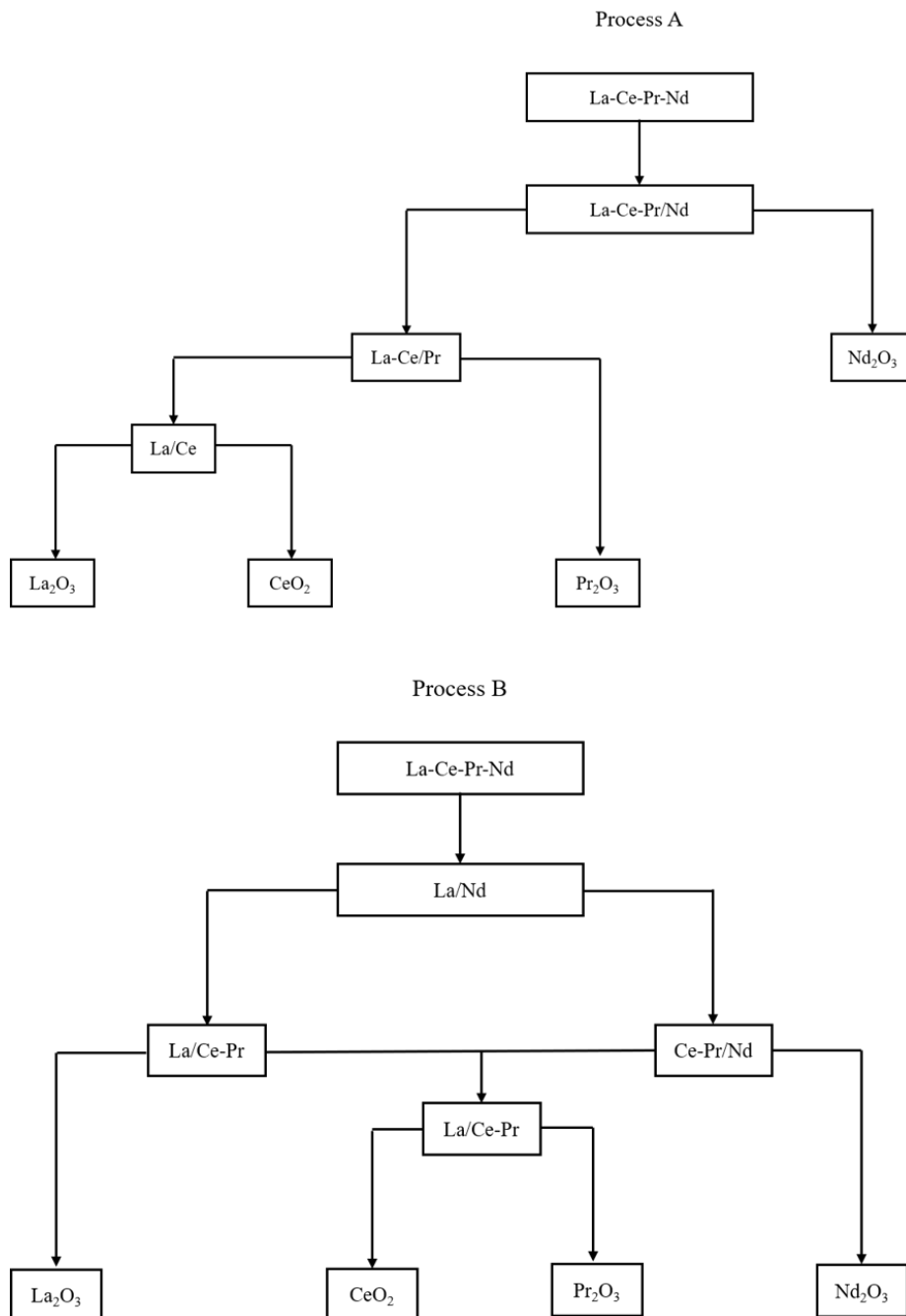


Figure 2.11: Pocess A and B showing separation route developed without and using optimization respectively (Zhang et al., 2016b)

PC-88A has also been used in the separation of HREEs, wherein separation was achieved in stages by the same segregation method, as adopted in the case of LREEs. Figure 2.12 shows feed-distribution of HREE separated using PC-88A. The separation was done in three steps, with the first step extracting erbium (Er) and thulium (Tm). The raffinate from step 1, containing europium (Eu) to holmium (Ho), was treated to separate dysprosium from the group. Finally, the raffinate from step 2, containing europium, gadolinium, and terbium, was processed in step 3 to recover terbium from the feed mixture. The raffinate after each step was concentrated by evaporation to increase the separation efficiency and lower the equipment capacity requirements.

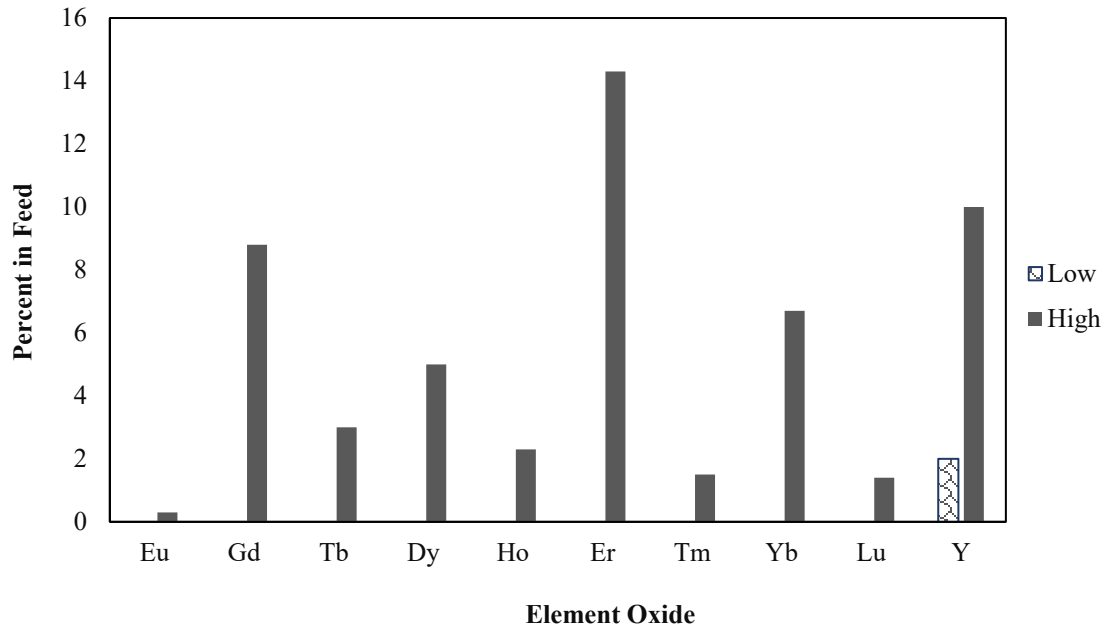


Figure 2.12: Plotted feed composition of HREE source (Zhang et al., 2016b)

In another industrial process used by Molycorp (Gupta et al., 1992), the separation of europium from mixed REE solution, obtained by leaching of bastnaesite ore, was achieved utilizing a two-step SX process. The pregnant leachate solution contained 0.2 gm/L of europium in 100 gm/L of mixed REE, which was separated in multiple steps using two SX trains (Figure 2.13). The first train used five mixer-settler stages to selectively extract

europium into the organic solution using 10% v/v DEHPA. Hydrochloric acid was used as a stripping agent to recover europium to an aqueous phase. The stripped solution contained significant iron, which was removed by precipitation using soda ash. The filtrate containing europium and other rare earths was further processed to improve the purity of europium using a second SX train containing five-mixer settler extraction stages. Europium was loaded in the organic phase selectively, leaving remaining rare earths in the raffinate stream. The loaded organic was stripped using 5 M HCl to obtain a solution rich in europium, which was reduced using zinc amalgam and subjected to precipitation using sulfuric acid to obtain 99.9% pure europium precipitate.

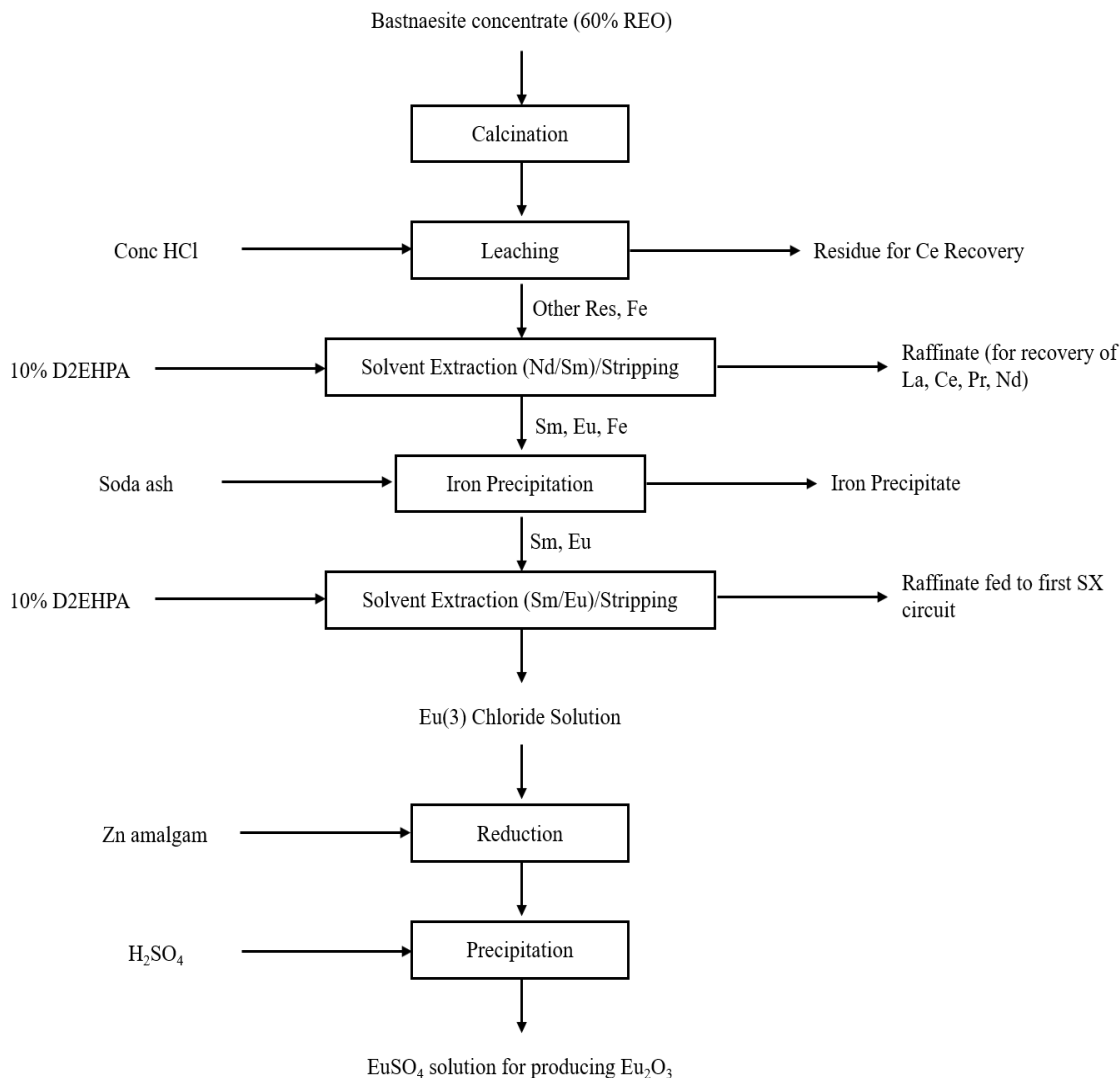


Figure 2.13: Flowsheet used for separation of Europium from bastnaesite (Xie et al., 2014; originally published in Gupta et al., 1992)

Similarly, extraction and separation of REEs using DEHPA on a pilot scale operated continuously has been studied. Like PC-88A, DEHPA extracts through ion exchange and solvation mechanism. Preston et al. 1996 in a series of three papers (Preston et al. 1996a; Preston et al. 1996b; Preston et al. 1996c) first discussed the extraction of mixed REEs. This was then followed by the separation of high purity cerium dioxide using TBP. Finally, the study concluded in the separation of middle and light rare earth fractions using DEHPA in a nitrate matrix. The process involved mini-plant and pilot-plant trials using eight stages

of extraction (E), two-to-four stages of scrubbing (Sc) and six-to-eight stages of stripping (S), followed by secondary stripping (R) as shown in Figure 2.14. The DEHPA concentration was 15% v/v and the equilibrium pH of the extraction was 1. Figure 2.15 shows the concentration profile in the extraction and stripping stages. Considerable extraction of MREEs (Sm-Eu-Gd) can be seen as the concentration decreases in the aqueous phase. Ammonia was added in stage 5 of extraction (E) to increase the pH value to prevent pH drift during processing. This drift was responsible for a slight increase in concentration of LREEs in the aqueous phase. Similarly, the stripping profile indicated elements stripped in reverse order of extraction: Ce > Nd > Sm > Eu > Gd > Tb > Dy. Another unique observation reported was the buildup of Dy in S3 to a value more than the concentration in the strip liquor. The explanation presented was the re-extraction of Dy occurs as acid concentration depletes due to consumption by more easily stripped elements down the stripping stages (Preston et al., 1996).

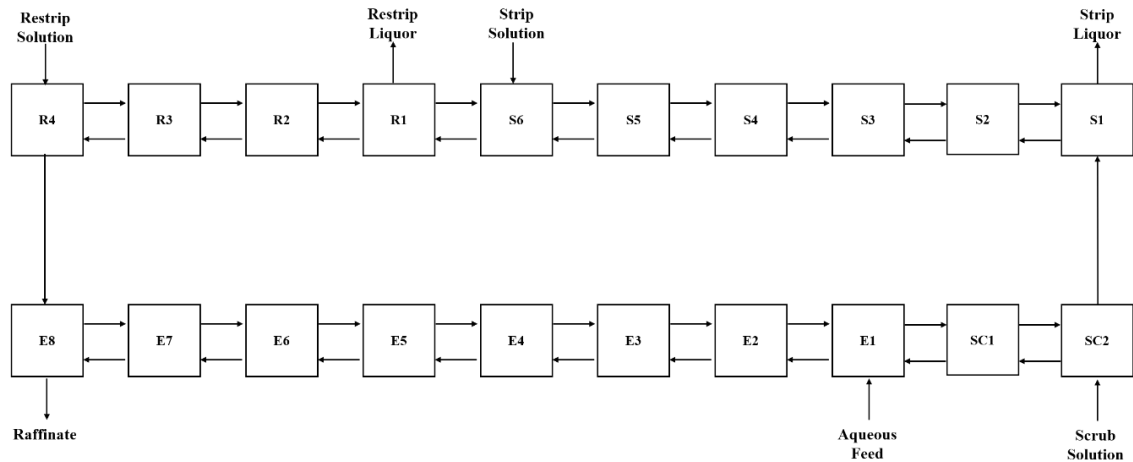


Figure 2.14: Flowsheet for mini plant (Preston et al., 1996)

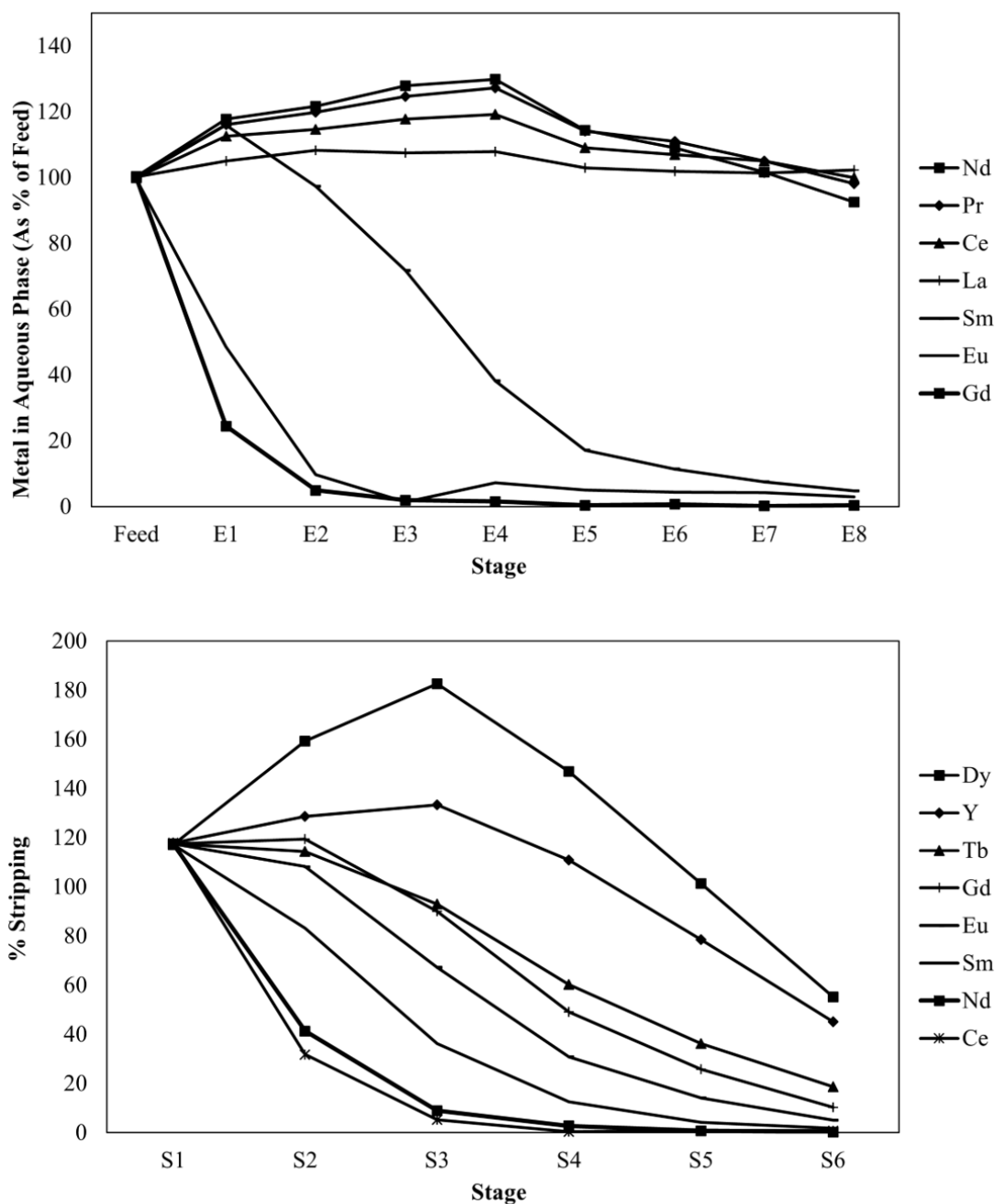


Figure 2.15: Aqueous phase concentration profile for rare earth circuit of mini-plant for loading (top) and stripping (bottom) shown in Figure 2.14 (reconstructed from Preston et al., 1996)

Separation of REEs using different flow configurations and extractants has been applied to individual production of REEs on a batch scale (Brown et al., 1979). Partial and total reflux

of raffinate and strip streams were utilized for concentrating elements in the stages (Figure 2.16). The method was called “force feeding,” a mechanism via which partial reflux was applied. The study was conducted using three different extractants, DEHPA, TBP and Versatic 911, with the common diluent, Shellshol A (trimethyl benzene).

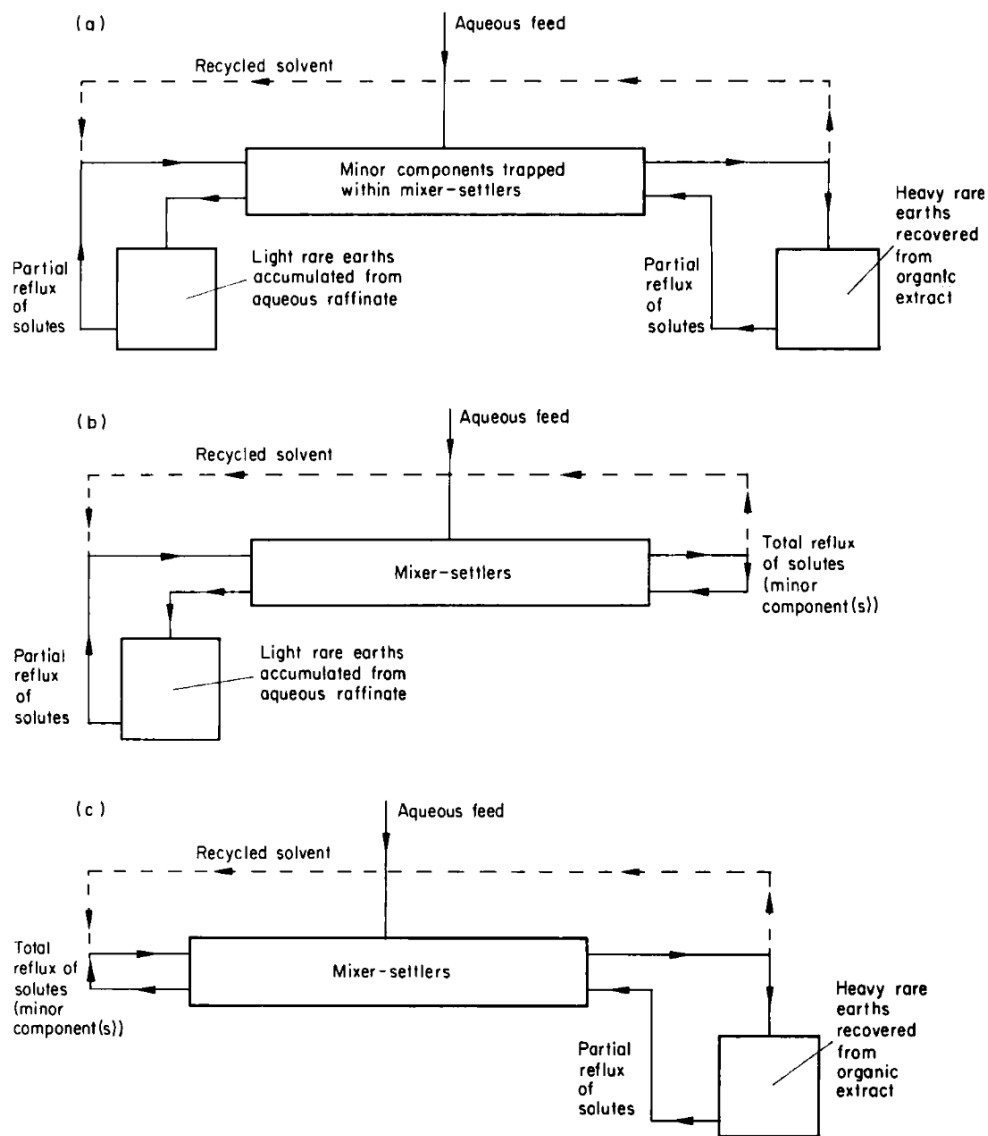


Figure 2.16: Different variants of the force-feeding mechanism (Brown et al., 1979)

The feed source for the separation process was obtained from the leaching of the bastnaesite mineral, having the elemental distribution shown in Table 2.4. MREEs and HREEs present

in minor amounts in the feed were first concentrated in a multistage SX process, as shown in Figure 2.17, using the force-feeding mechanism of Figure 2.16 (b). A seventeen-stage mixer-settler combination was used, of which the last 3 stages were reserved for stripping. The feed solution was introduced at stage 7, and the stripping solution introduced at stage 17. The stripped solution was operated by total refluxing, whereas the raffinate was partially refluxed. MREEs and LREEs present in the feed were trapped within the mixer settler units, and LREEs were allowed to leave the system through the raffinate stream.

Table 2.4: Feed distribution of bastnaesite mineral tested via force feeding mechanism
Brown et al., 1979

Bastnaesite (LnFCO₃)	
Rare earth oxide	70%
La ₂ O ₃	32
CeO ₂	50
Pr ₆ O ₁₁	4
Nd ₂ O ₃	13
Sm ₂ O ₃	0.5
Eu ₂ O ₃	0.08
Gd ₂ O ₃	0.2
Others including	
Y ₂ O ₃	0.22
F	5
BaSO ₄	1
CaO	3

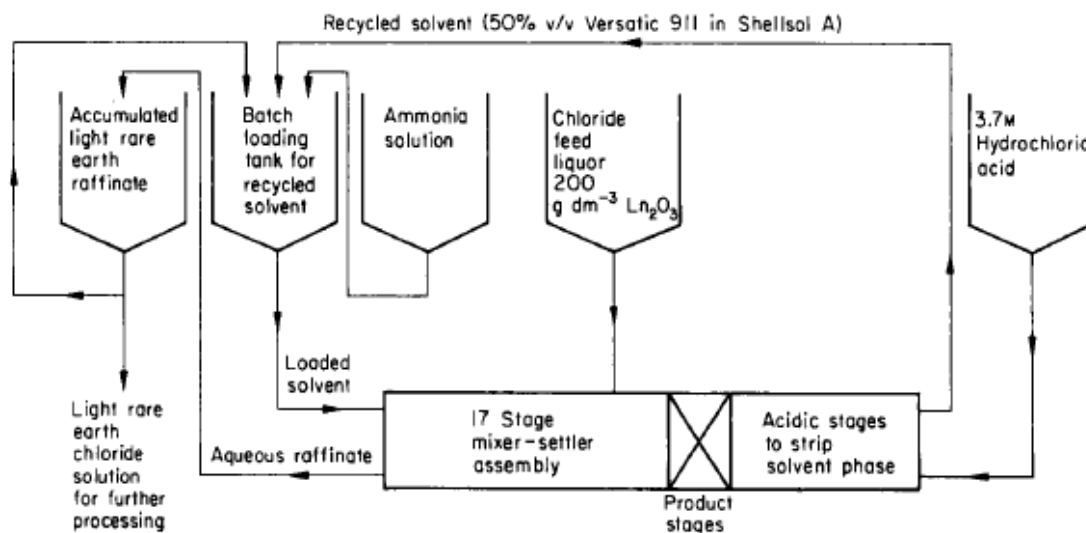


Figure 2.17: Force feeding process for separation of europium (Brown et al., 1979)

The raffinate obtained was further processed, first separating cerium using the precipitation method. Sodium hypochlorite was used as an agent to oxidize cerium (III) to ceric hydroxide (IV), making it insoluble. The remaining solution was processed to remove additional carbonates of sodium by boiling, and it was further converted to nitrate matrix for separation of lanthanum, neodymium, and praseodymium, using SX. Figure 2.18 shows the SX configuration used of separation, which was done in two stages. During the first stage of operation, the force-feeding method was used to concentrate lanthanum in the raffinate stream, whereas neodymium was concentrated in the organic stream, and praseodymium was left together with both elements (see the top of Figure 2.18). In the second stage of operation, mixer settlers were emptied, and the products, after initial treatment, were concentrated by evaporation and then processed using the total reflux method (see the bottom of Figure 2.18). Figure 2.19 shows the concentration profile of the elements from both stages of operation.

The method was successful in obtaining high purity elements (greater than 90 percent) but required significant time for processing in batches: 6-12 hour for SX train shown in Figure 2.17, and a combined 245 hours for SX train shown in Figure 2.18. The process also required many intermediate steps of feed preparation, like evaporation and handling of liquids, when stages were emptied and refilled to adjust configuration.

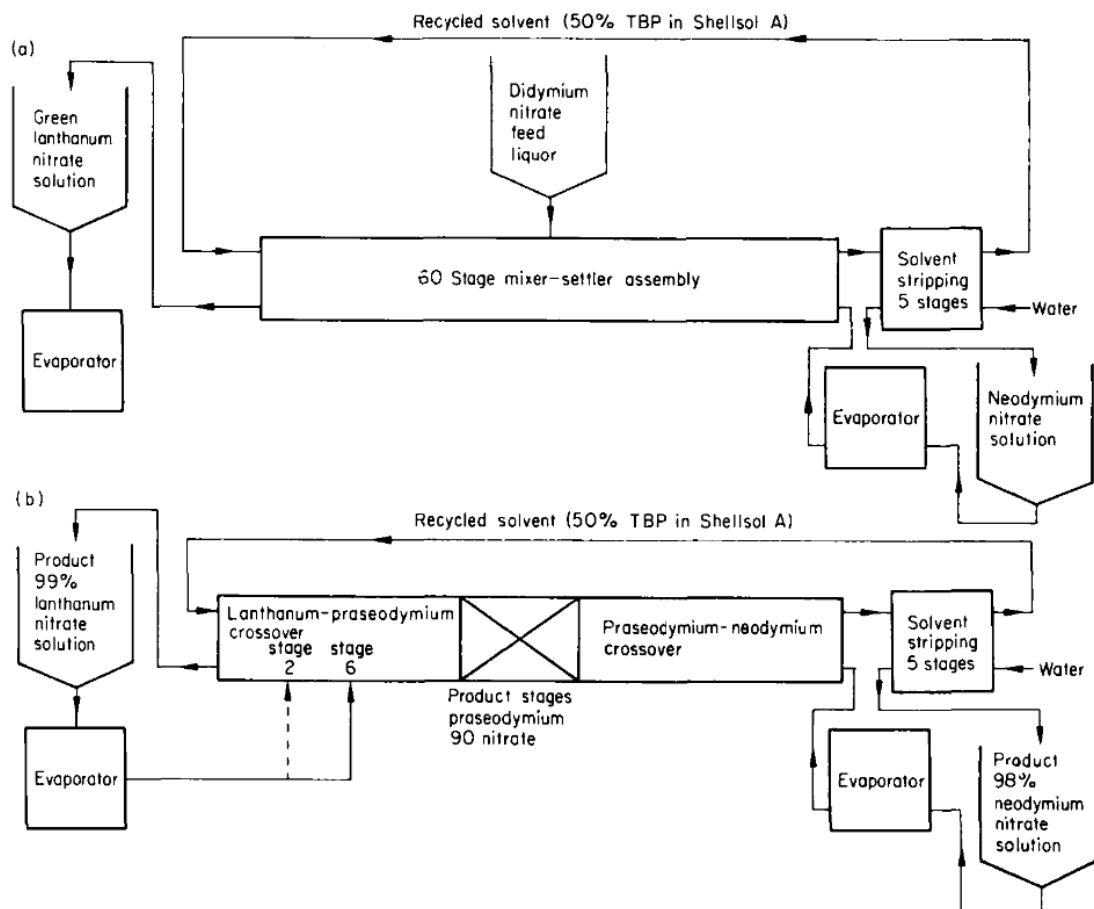


Figure 2.18: Flowsheet used for separation of LREE using partial and total reflux (Brown et al., 1979)

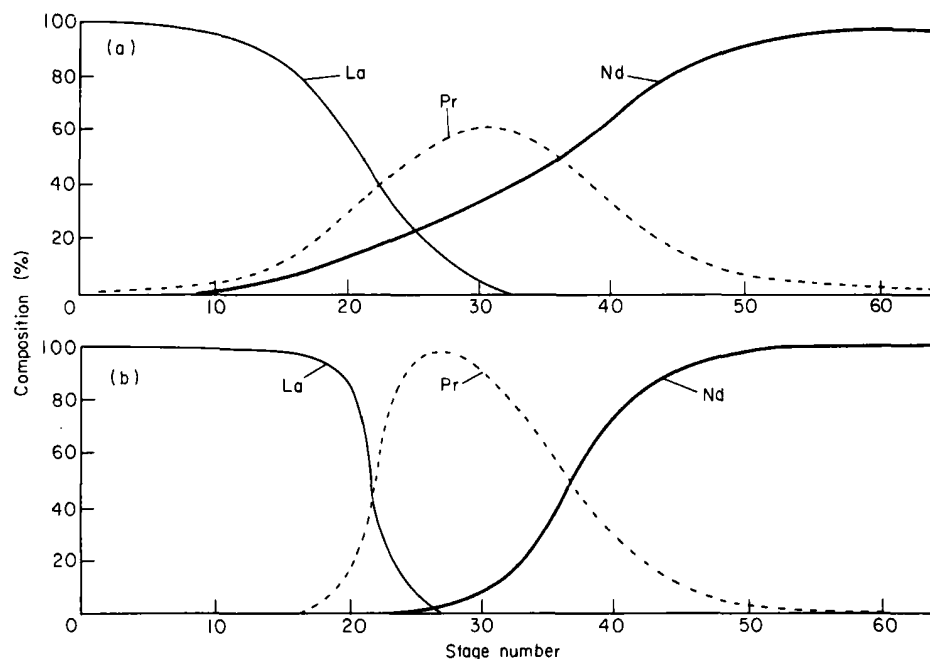


Figure 2.19: Stagewise concentration profile after first treatment (top) and second treatment (bottom) (Brown et al., 1979)

Individual separation of lanthanum, neodymium and yttrium, the major components in Egyptian monazite, was studied by using a combination of extractants, TOPO and TRPO (El-Nadi, 2012). The combined extractant was used to create a synergistic system to improve extraction and separation among elements. The study was performed on an individual element salt solution of 1 gm/L at different extractant concentrations, nitric acid concentrations, and pH conditions. Similarly, stripping studies on the loaded organic solution were also conducted using sulfuric acid (H_2SO_4) and hydrochloric acid (HCl) of different molarities. The results indicated the use of 4 M H_2SO_4 for stripping of Y and 1 M HCl for La and Nd. Based on the findings, a conceptual flowsheet was proposed to separate Y from the La-Nd concentrate. From the flowsheet, it can be deduced that preferential stripping was used in the separation of elements. The McCabe Thiele curve was also developed for individual elements to determine number of stages required for loading. The results suggested the use of seven stages for La and two stages to completely load Nd and Y.

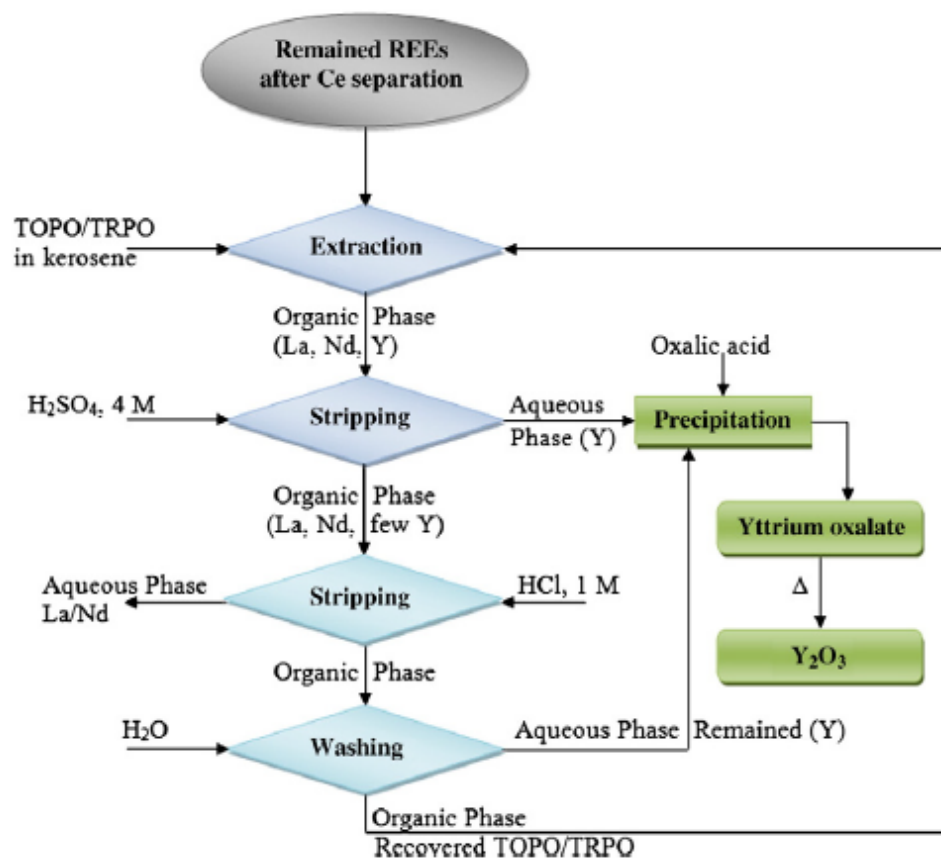


Figure 2.20: Conceptual flowsheet for La-Nd-Y separation using TOPO and TRPO (El-Nadi, 2012)

Application of modern computational techniques such as artificial neural network (ANN) has also been utilized in improving the existing flowsheet (Figure 2.21) for separation of REEs at the Bhabha Atomic Research Centre (Anitha et al., 2008). Neodymium of purity greater than 95% was obtained by development and application of an ANN model to predict the distribution ratio for varying process condition. The improved flowsheet consisted of four extraction and stripping stages each, as well as 20 scrubbing stages operated by refluxing the stripped solution to the scrubbing stages. The lowest separation factor among the elements in feed mixture existed for Nd/Pr, with a value of 1.63, which posed a challenge for the neodymium separation. The 95% purity and 85% recovery of neodymium was made possible by use of a large number of scrubbing stages and refluxing operations.

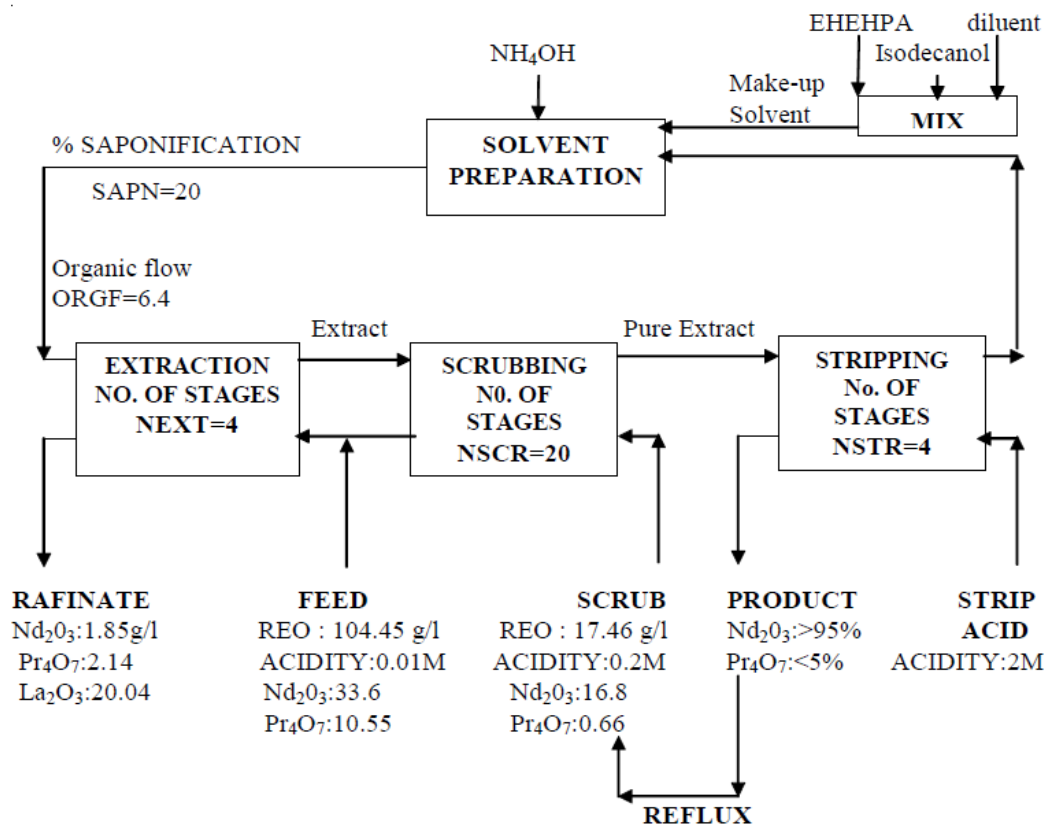


Figure 2.21: Flowsheet post improvement using ANN for separation of Nd from Pr (Anitha et al., 2008)

Thus, from the above discussion, one can articulate that the flowsheets used for REE separation are cumbersome, complex, and influenced by numerous variables. The majority of flowsheets are designed conceptually using laboratory analysis, and many flowsheets do not provide details on the approach for their design. Although information on the design of the SX processes for base metals exist, this is not directly applicable to rare earth separation because of the presence of multiple elements. Also, testing of large-scale, conceptually designed flowsheets on industrial or pilot scales is cost-intensive, hence, an alternate way to design such process is required. One approach is via modeling and simulation. Modeling and simulation can be used in designing process flowsheets, comparing different designs and analyzing the effect of different variables, thereby improving the process. The following section reviews various modeling studies pertaining to REEs and discusses their application and the associated advantages and disadvantages.

2.5 MODELING OF SOLVENT EXTRACTION

Modeling of the SX processes can be broadly classified into two categories: 1) chemical equilibrium modeling (extraction/stripping) and 2) process modeling (Figure 2.22). Chemical equilibrium modeling of the SX process is done to describe the extraction or stripping behavior of the process as a resulting chemical reaction and equilibrium changes. Process modeling, on other hand, is used to study and determine the mass transfer taking place in a multi-stage SX process operated on a pilot or industrial scale.

Research in chemical equilibrium modeling of the SX processes has focused on experimental study of the extraction/stripping process under different chemical conditions. Representation of equilibrium chemical reactions mathematically using the law of mass action (Eq. 2.2) and determining activities of species, i.e., metal ions, complex formed and form of organic extractant by carefully designed experiments, are the most examined areas. The results from the experiments are mostly analyzed using a graphical approach (slope analysis) to determine the stoichiometry associated with the reacting species. For example, Mohammadi et al., (2015) in his work used slope method to determine complexation involved with extraction of neodymium, dysprosium, and yttrium. After identifying associated stoichiometry, the equilibrium is modeled to predict the concentration of species at equilibrium.

Different approaches to modeling, such as thermodynamic and empirical models, have been used to describe the equilibrium process (Figure 2.22). The main goal of all the models was to establish mathematical relationships to predict aqueous and organic phase concentrations of metal(s) under different conditions. However, the approach taken by each method is diametrically opposed. The thermodynamic approach is based on the fundamental analysis of the equilibrium process and focuses on the determination of the equilibrium reaction constant and activities of associated species. On the other hand, the empirical approach uses black box methods to model the process from experimental or industrial data. The choice of the equilibria modeling technique depends upon the complexity of the system and application of the model.

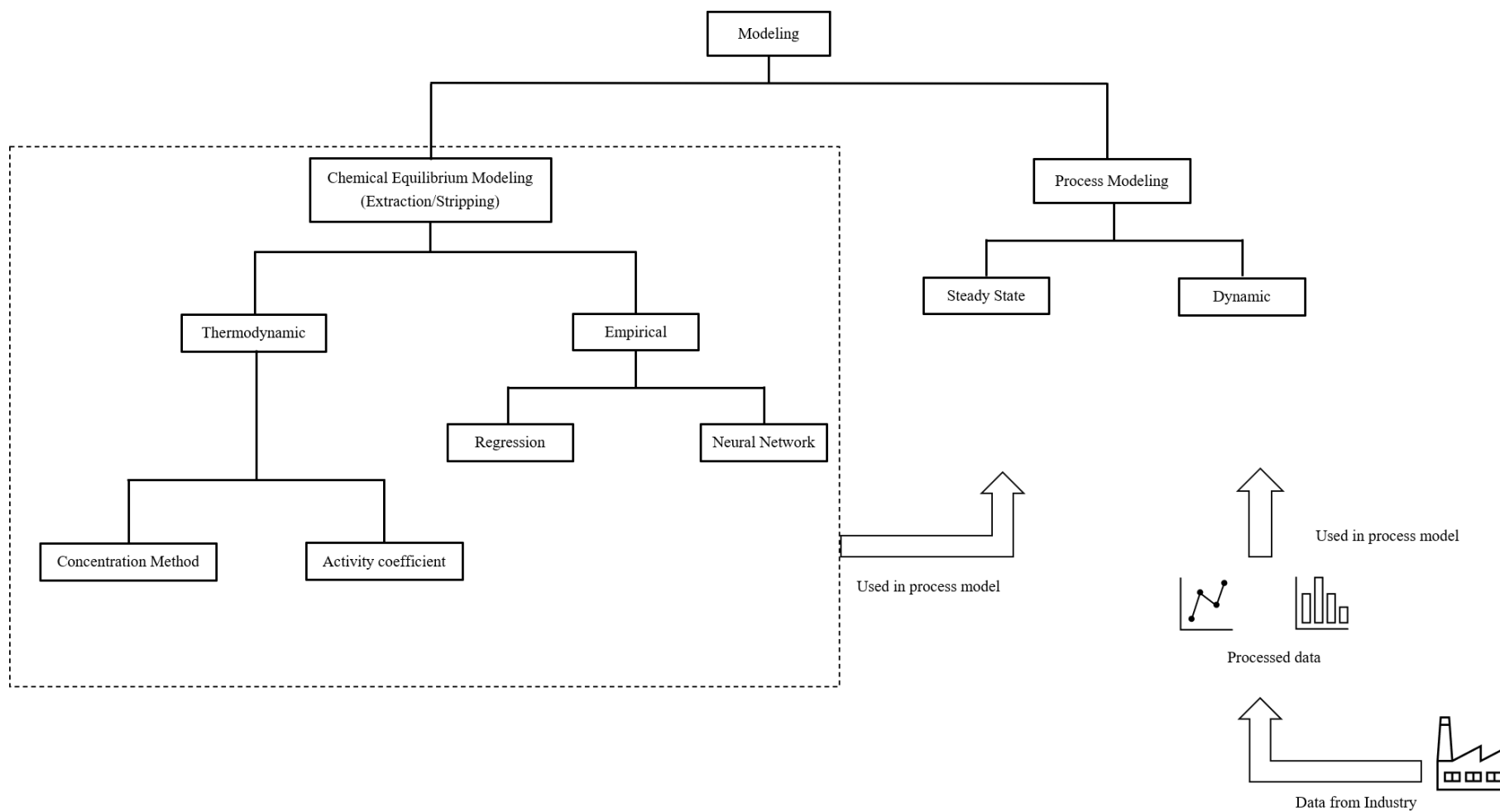


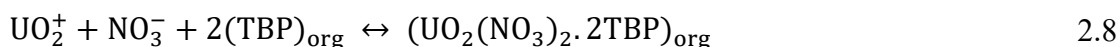
Figure 2.22: Flowchart showing different methods adopted in equilibrium and process modeling and their co-dependence on each other

2.5.1 Thermodynamic Modeling

The thermodynamic modeling of the SX process is based on the fundamentals of equilibrium chemistry. In this method, the equilibrium equations of species taking part in the reaction are defined with the mathematical relationship using the law of mass action. Shake-out test data collected under different conditions are used to estimate equilibrium reaction constants. Several different methods have been established by researchers to model metal distribution constants using this approach. These approaches can be classified into two broad categories: 1) concentration-based methods and 2) activity-coefficient methods. These methods are discussed in the following sections.

2.5.1.1 Concentration Method

In concentration-based methods, the equilibrium data is modeled by measuring the concentration of species at equilibrium after reaction completion. This approach is typical to one described by Eq. 2.3. An initial application of this approach is found in a review by Forrest et al. (1975) where it was used to study the extraction of uranium using TBP: (Eq. 2.8). The equilibrium constant of the reaction was described by the concentration of reacting species at equilibrium given by Eq. 2.9.



$$K = \frac{[\text{UO}_2(\text{NO}_3)_2 \cdot 2\text{TBP}]_{\text{org}}}{[\text{UO}_2^+]_{\text{aq}} [\text{NO}_3^-]_{\text{aq}}^2 [\text{TBP}]_{\text{org}}^2} \quad 2.9$$

$$[\text{TBP}]_{\text{org}} = [\text{TBP}]_{\text{Total}} - 2[\text{UO}_2(\text{NO}_3)_2 \cdot 2\text{TBP}]_{\text{org}} \quad 2.10$$

Where K in above equation is the equilibrium reaction constant (K_{conc} in Eq 2.3). The square brackets [] denote species concentrations in organic and aqueous phases,

subscripted as org and aq. A characteristic of Eq. 2.9, is the complexity, due to four unknown variables. The number of unknowns were reduced to three by substituting the equilibrium TBP concentration, using Eq. 2.10. The substitution was possible because of the known total TBP concentration taken initially and stoichiometry of two associated with TBP during complexation. The Eq. 2.9 was thus solved for various sets of species concentrations to develop a surface at a fixed total TBP concentration. The approach seems convenient and practical; however, it has several major limitations. The first limitation is its applicability to high concentrations, wherein activities of species should be accounted. Secondly, for multiple solute systems, the number of equilibrium reactions increase proportionally to the number of ionic states of each species possible. The complexity of such systems is difficult to negotiate. However, the above method of concentration is valid for a single salt system at tracer-level concentrations where the behavior approximates to an ideal system.

In another concentration-based approach, the distribution of the metal (solute) in the organic phase was modeled as a function of the concentration of metal present in the aqueous phase. The method can be considered analogous to Eq. 2.4, and the functional relationship is called the distribution isotherm, or McCabe Thiele, which is shown in Figure 2.23. The method does not utilize the equilibrium reaction constant K as in the previous method shown in Eq. 2.9 (generic method in Eq. 2.3), and it should not be considered a thermodynamic method. Instead, it uses the concentration relationships between organic and aqueous phases for a specific separation condition such as pH or initial concentration of metal ions.

This method has been widely used in determining the number of stages for the extraction of base metals. However, it is only applicable to systems involving single metal components with experiments performed at specific conditions such as feed composition, extractant concentration and pH. Thus, the downside of this method is that an independent curve needs to be generated for each separation condition. To mitigate this problem, Hughes et al. (1975) developed the distribution surface by combining multiple distribution isotherms at varying conditions, thereby developing a three-dimensional surface plot, as shown in Figure 2.24.

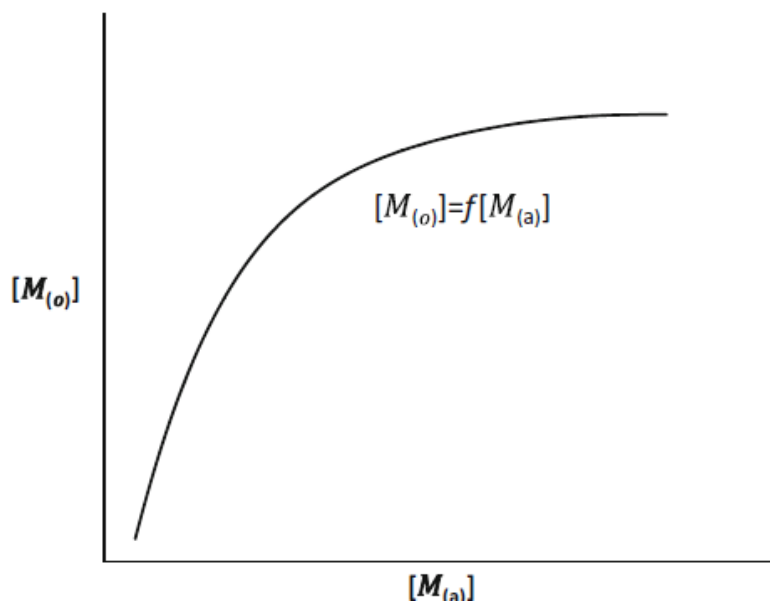


Figure 2.23: Distribution isotherm (Zhang et al., 2016b)

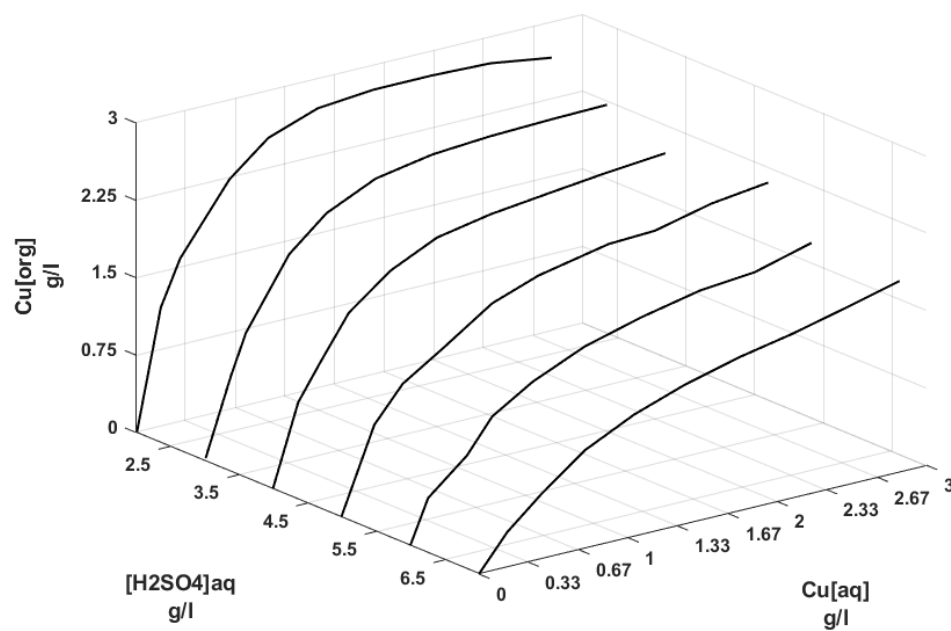


Figure 2.24: Reconstructed distribution isotherm surface developed for copper extraction using LXI64N (Hughes et al., 1975 data originally published in Robinson et al., 1971)

Response surface plots are ideal for single metal systems, but they become complex for multi-component systems that require large number of experiments and surfaces to be developed.

2.5.1.2 Activity-Coefficient Method

The use of concentrations instead of species activities, as described by Eq. 2.3, is only valid for an ideal system. Real solutions deviate from ideal solutions due to numerous interactions taking place between the species (ions), which are responsible for their non-ideal behavior. This deviation from ideality in the system should be accounted for to describe the behavior of the solution, which is done by using activity-based approach (as shown in Eq. 2.2). However, determining the activity of ions is not an easy task because of the presence of a large number of ions and the interacting forces between them. Various thermodynamic methods have been developed to estimate the activities of the species both in aqueous and organic phases. The underlying principle of the thermodynamic methods is based on defining the chemical potential of the species in system. The chemical potential of any species is defined as the partial molar derivate of Gibbs energy, given by Sandler (2017):

$$\mu_i = \left[\frac{\partial G}{\partial n_i} \right]_{T,P,n_j} \quad 2.11$$

where μ_i is the chemical potential of species i ; n_i moles of species; G Gibbs free energy; and T , P , n_i , and n_j are the temperature, pressure and moles of species i and j , respectively. Using the above definition for an ideal system, the chemical potential of species in standard state transforms to (Sandler, 2017):

$$\mu_i^{id} = \mu_i^0 + RT \ln x_i \quad 2.12$$

where μ_i^{id} is the chemical potential under ideal conditions (superscripted), μ_i^0 the molar chemical potential of the pure standard state, R the gas constant, T temperature, and x_i the mole fraction of species in consideration. However, the above equation needs correction to be relevant for real solutions. Hence, an excess term is added to Eq.2.12, to account for non-ideality:

$$\mu_i^{id} = \mu_i^0 + RT \ln x_i + RT \ln \gamma_i \quad 2.13$$

Debye and Huckel first developed the model to estimate the activity coefficient of the ions in an electrolyte solution by describing electrostatic attraction between ions and using a statistical mechanics approach (Debye et al., 1923). The activity coefficient of the ions was evaluated as a function of ionic strength, which is given by:

$$I = \frac{1}{2} \sum_i m_i Z_i^2 \quad 2.14$$

where ‘I’ is the ionic strength, m_i the molality of species i and Z_i the charge on species i. The ionic strength is a measure of total ion concentration in the solution. Table 2.5 contains the model equation given by Debye and Huckel and its variants. The models are useful for solutions having ionic strengths up to 0.005 M. Various modifications of the Debye-Huckel model have been reported that have increased the molality range of the Debye-Huckel model which are summarized in Table 2.5.

Table 2.5 Activity coefficient model based on electrostatic interaction (Newman et al., 1980)

Name	Model Equation	Molality Range
Debye-Huckel	$\log \gamma_i = -AZ^2\sqrt{I}$	$I < 0.005$
Extended Debye-Huckel	$\log \gamma_i = -\frac{AZ^2\sqrt{I}}{1+Ba\sqrt{I}}$	$I < 0.1$
Guntelberg	$\log \gamma_i = -\frac{AZ^2\sqrt{I}}{1+\sqrt{I}}$	$I < 0.1$
Davies	$\log \gamma_i = -\frac{AZ^2\sqrt{I}}{1+\sqrt{I}} + 0.21I$	$I < 0.5$

Despite of wide applicability, the Debye-Huckel models had few shortcomings in accounting various types of molecular interactions. The models only considered ion-ion interactions and omitted ion-dipole, dipole-dipole, and several other interactions depending upon solutes and solvents present in the system. These forces become more significant at higher concentrations due to increased molecular interactions. Another limitation of the Debye-Huckel model is its applicability to low ionic strength solutions. This led to the development of several semi-empirical activity coefficient models by other researchers, i.e., Meissner, Bromley, and Pitzer, which accounted for these interactions and were applicable to strong electrolytes. The model equations for some of such semi-empirical models are given below:

Bromley Model (Bromley, 1973):

$$\log \gamma_{\pm}^{\frac{1}{Z_1 Z_2}} = -\frac{0.511 I^{\frac{1}{2}}}{1+I^{\frac{1}{2}}} + \frac{(0.06+0.6 B)I}{(1+\frac{1.5}{|Z_+ Z_-|}I)^2} + \frac{BI}{|Z_+ Z_-|} \quad 2.15$$

where B is the Bromley coefficient initially published by Bromley (1973) at 25°C for 180 salts; this is valid at ionic strengths up to 6 molal.

Pitzer Model (Sandler, 2017):

$$\frac{G^{ex}}{n_w RT} = f(I) + \sum_i \sum_j \lambda_{ij}(I) M_i M_j + \sum_i \sum_j \sum_k \delta_{ijk} M_i M_j M_k \quad 2.16$$

where $\frac{G^{ex}}{n_w}$ is the excess Gibbs energy, M_i is ion molality or solute in the system, $f(I)$ is the Debye-Huckel term, and λ_{ij} and δ_{ijk} are the second and third virial coefficients, respectively.

Activity-coefficient models have found modest application in metal extraction. Researchers like Chaiko et al. (1988) have used thermodynamic modeling of chemical equilibria to predict the distribution of nitric acid and americium in aqueous and organic phases. In this work, the activity coefficient of the electrolyte solution was calculated using the Bromley method (Chaiko et al., 1988). Similarly, Baes, (2001) developed a series of computer programs to model the SX system thermodynamically. The last in the series programs is called SXFIT, which modeled the SX system by describing the physical chemistry of aqueous and organic phases. Baes' (2001) work included the thermodynamic treatment of:

- Solute and solvent activity coefficient in aqueous phase using Pitzer model;
- Solute and solvent activity coefficient in organic phase by Scatchard-Hildebrand-Scott method;
- Effect of ionization on activity coefficients;
- Non-ideal behavior of solute in non-aqueous phase;
- Heat of mixing of non-aqueous solution.

Activity-coefficient methods have also been used in modeling and simulation of the SX process for metals like cobalt, nickel and lithium. Vasilyev et al. (2019) utilized activity coefficient method to design SX process for separation of cobalt, nickel, and lithium. In their work, SX bench scale tests were conducted on feed mixture sourced from battery leachate using Cyanex 272 as extractant. The results obtained were used in describing

phase equilibrium and determining equilibrium constants. The dissociation of the species in the solution phase was also considered using the equilibrium analysis (Table 2.6). This method used the extended Debye-Huckel model with electrolyte speciation to evaluate the equilibrium concentration of species. Depending upon species concentration in aqueous phase and separation conditions, the metal distribution across interphase was determined. However, the limitation of modeling using an activity-based approach is the complexity and difficulty applying to a real multi-component system.

Table 2.6: Equilibrium and hydrolysis reactions for Co, Ni and Li separation (Vasilyev et al., 2019)

Chemical reaction	Equation for equilibrium constant	logK	
$H^+ + HSO_4^- \rightleftharpoons H_2SO_4$	$K_1 = \frac{a(H_2SO_4)}{a(H^+) \cdot a(HSO_4^-)}$	-3	(1)
$H^+ + SO_4^{2-} \rightleftharpoons HSO_4^-$	$K_2 = \frac{a(HSO_4^-)}{a(H^+) \cdot a(SO_4^{2-})}$	1.98	(2)
$Co^{2+} + SO_4^{2-} \rightleftharpoons CoSO_4$	$K_3 = \frac{a(CoSO_4)}{a(Co^{2+}) \cdot a(SO_4^{2-})}$	2.34	(3)
$Co^{2+} + H_2O \rightleftharpoons H^+ + CoOH^-$	$K_4 = \frac{a(CoOH^-) \cdot a(H^+)}{a(Co^{2+})}$	-9.2	(4)
$Co^{2+} + H_2O \rightleftharpoons 2H^+ + Co(OH)_2$	$K_5 = \frac{a(Co(OH)_2) \cdot a(H^+)^2}{a(Co^{2+})}$	-18.6	(5)
$Co^{2+} + H_2O \rightleftharpoons 2H^+ + Co(OH)_{2,s}$	$K_6 = \frac{a(H^+)^2}{a(Co^{2+})}$	-12.2	(6)
$Co^{2+} + NH_3 \rightleftharpoons CoNH_3^{2+}$	$K_7 = \frac{a(CoNH_3^{2+})}{a(Co^{2+}) \cdot a(NH_3)}$	2.1	(7)
$Ni^{2+} + SO_4^{2-} \rightleftharpoons NiSO_4$	$K_8 = \frac{a(NiSO_4)}{a(Ni^{2+}) \cdot a(SO_4^{2-})}$	2.29	(8)
$Ni^{2+} + H_2O \rightleftharpoons H^+ + NiOH^-$	$K_9 = \frac{a(NiOH^-) \cdot a(H^+)}{a(Ni^{2+})}$	-9.5	(9)
$Ni^{2+} + H_2O \rightleftharpoons 2H^+ + Ni(OH)_2$	$K_{10} = \frac{a(Ni(OH)_2) \cdot a(H^+)^2}{a(Ni^{2+})}$	-20.01	(10)
$Ni^{2+} + H_2O \rightleftharpoons 2H^+ + Ni(OH)_{2,s}$	$K_{11} = \frac{a(H^+)^2}{a(Ni^{2+})}$	-10.5	(11)
$Ni^{2+} + NH_3 \rightleftharpoons NiNH_3^{2+}$	$K_{12} = \frac{a(NiNH_3^{2+})}{a(Ni^{2+}) \cdot a(NH_3)}$	2.73	(12)
$Li^+ + SO_4^{2-} \rightleftharpoons LiSO_4^-$	$K_{13} = \frac{a(LiSO_4^-)}{a(Li^+) \cdot a(SO_4^{2-})}$	2.29	(13)
$Li^+ + H_2O \rightleftharpoons H^+ + LiOH$	$K_{14} = \frac{a(LiOH) \cdot a(H^+)}{a(Li^+)}$	-9.5	(14)
$Li^+ + NH_3 \rightleftharpoons LiNH_3^+$	$K_{15} = \frac{a(LiNH_3^+)}{a(Li^+) \cdot a(NH_3)}$	-0.7	(15)
$H^+ + NH_3 \rightleftharpoons NH_4^+$	$K_{16} = \frac{a(NH_4^+)}{a(H^+) \cdot a(NH_3)}$	9.237	(16)
$H^+ + NH_3 + SO_4^{2-} \rightleftharpoons NH_4SO_4^-$	$K_{17} = \frac{a(NH_4SO_4^-)}{a(H^+) \cdot a(NH_3) \cdot a(SO_4^{2-})}$	9.237	(17)
$H_2O \rightleftharpoons H^+ + OH^-$	$K_{18} = a(H^+) \cdot a(OH^-)$	-14	(18)

2.5.2 Empirical Modeling of the Equilibrium Process

Empirical modeling is often considered one of the convenient ways to model separation processes. Many mathematical non-linear methods have been used in modeling. These methods include regression methods, artificial neural networks, time series analysis etc., (Yun et al., 2016). However, irrespective of the methods utilized, the methods and variables considered for modeling the separation of REEs has not been very systematic or consistent. For example, Thakur (2000b) used empirical models of an exponential form to predict distribution ratios as function of initial acid concentration and initial metal concentration. Whereas Giles et al. (1996) used an artificial neural network method with the crystal radius of the lanthanide elements to generalize separation behavior of rare earth SX processes. In a separate study, a neural network model was developed using extractant concentration, O/A ratio, shaking time, temperature, etc., for the separation of lanthanum (Figure 2.25).

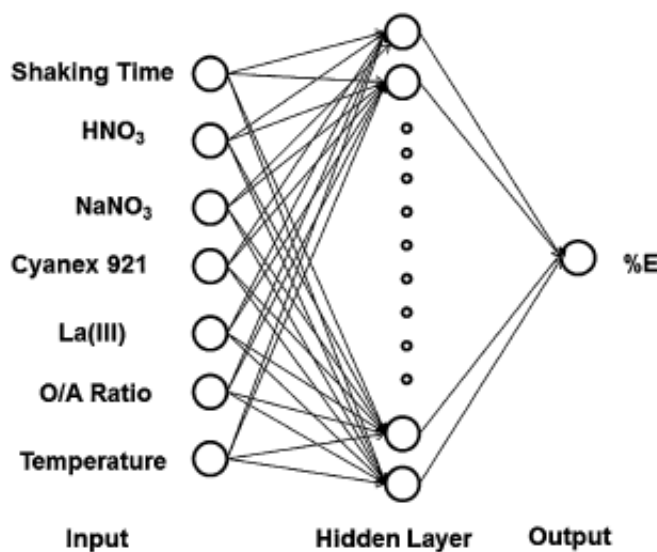


Figure 2.25 Structure of neural network for predicting percent extraction from experimental data (Acharya et al., 2017)

Despite such irregularities in variable selection, empirical methods have been very effective in capturing the interactions and nonlinearities of the separation. Two methods

that have been widely used for rare earth SX modeling are regression and the artificial neural network. In the regression method, the experimental data is fitted using linear and non-linear regression techniques. Table 2.7 shows a typical example of exponential model equations for rare earths extracted using PC-88A, as developed by Thakur (2000b). The model related distribution coefficient of the elements to initial concentration of metal and aqueous phase pH obtained using the regression method. However, no specific reason for the selection of initial pH over equilibrium pH was given, which could lead to inaccuracies in model application because there is significant pH drift after extraction.

Table 2.7: Models developed using power law for La, Ce, Pr, Nd and Sm (Thakur, 2000b)

Element	Model
Lanthanum	$D_{La} = 0.0186. C_i^{-0.94}. \exp (-4.19. C_i^{-0.587}. H_i)$
Cerium	$D_{Ce} = 0.0162. C_i^{-1.204}. \exp (-4.44. C_i^{-0.489}. H_i)$
Praseodymium	$D_{Pr} = 0.0173. C_i^{-1.26}. \exp (-4.277. C_i^{-0.471}. H_i)$
Neodymium	$D_{Nd} = 0.0189. C_i^{-1.31}. \exp (-4.11. C_i^{-0.454}. H_i)$
Samarium	$D_{Sm} = 0.028. C_i^{-1.446}. \exp (-3.22. C_i^{-0.3964}. H_i)$

Neural-network modeling uses a multi-layer network of linear or non-linear weighted transfer functions called neurons. The neurons are connected to each other and arranged in layers, such that the output of one neuron serves as input for the others. The connection between the neurons has associated weight parameters and bias, which is determined while training (or fitting) the network on the data source. Figure 2.26 shows a typical example of

a single neuron to which input data (p) is passed having weight (w) and bias (b) through transfer function f . Different criteria, such as mean-squared error or sum-of-squared error, are used for fitting the models. The data used in model fitting using a neural network is generally divided into three parts. The first part is used for training the network, the second for testing, and the final for validation. The larger the amount of data, the better is the model fit and, hence, the model prediction. Neural networks have found tremendous application in the chemical and processing industry as they can predict the response of complex and interacting processes without understanding the fundamentals of the process (Yang & Chai, 2006). For the same reason, these are referred as black box models.

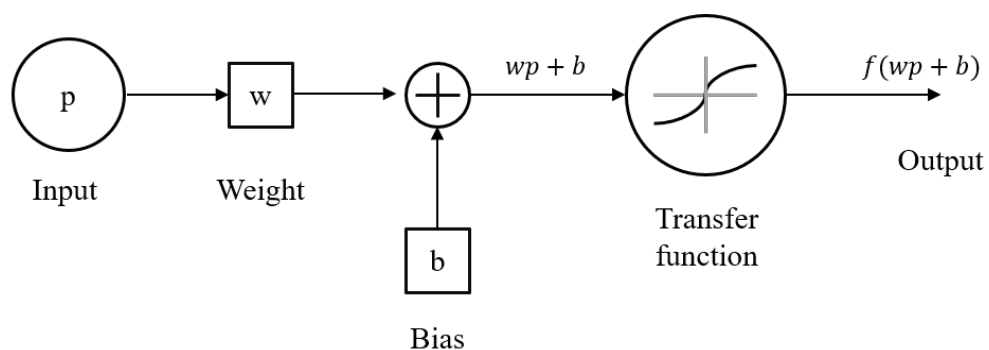


Figure 2.26: Example of working of a single neuron

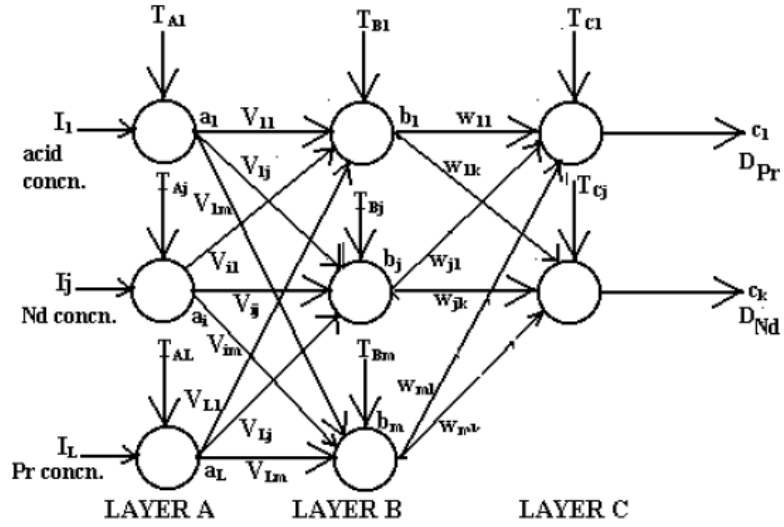


Figure 2.27: Structure of neural network model for distribution ratio of Nd and Pr (Anitha et al., 2008)

Figure 2.27 shows a typical architecture of a three-layer neural network designed to predict distribution ratios of neodymium and praseodymium. The model was developed using the initial metal concentration and acid concentration experimental data, and it was integrated to process model to improve the capacity existing flowsheet shown in Figure 2.21, obtaining the same purity of product. A comparison of the performance of neural networks with an exponential model in the separation Nd and Pr was also made (Anitha et al., 2008). The research reported superior performance on the neural network over exponential model for low acid concentrations. Nonlinear functions, such as sigmoid and hyperbolic tangent were used and compared in the design of the network Eq. 2.17 and 2.18.

$$f(x) = \frac{1}{1+e^{-x}} \text{ (sigmoid)} \quad 2.17$$

$$f(x) = \frac{1 - e^{-2x}}{1 + e^{-2x}} (\tanh) \quad 2.18$$

Similarly, neural networks have also been utilized in modeling synergistic effect of two extractants, LIX984 N and DEHPA, for the separation of zinc from iron (Haghighi et al., 2014). The experimental data of temperature, pH, and ratio of extractants was used to model percent extractants of iron and zinc. Two hidden-layer networks, containing 4, 9, 5, and 1 neuron using the Levenberg-Marquardt algorithm, was used to develop the model. Thus, it is evident that the use of empirical methods, i.e., power law and neural networks using the experimental data, has been successful in modeling SX separation processes of metals. However, the limitation of the methods lies in predicting outside the range of the data set for which they were modeled and selecting of independent variables used.

2.6 PROCESS MODELING

The solvent-extraction modeling discussed in the previous section is useful in understanding the equilibrium chemistry of SX processes, but the significance of the models lies in their application in process design and control. Process design and control requires a method to determine stagewise mass transfer under different design and operational conditions. Estimating mass transfer in a multistage SX process is a challenging task and requires the development of reliable process models. Process models combine the equilibrium extraction principles with mass transfer methods to evaluate the amount of metal transfer taking place in different stages. Mass transfer can be evaluated under two conditions: steady state or transient. Process models developed when the system has attained equilibrium are referred to steady state models and are the primary models used in the process design, whereas models developed to estimate mass transfer in transient conditions are called dynamic models. These models are primarily used in process control. The development and application of process models in REEs extraction and separation has been very limited because of close separation behavior of REEs and a lack of consensus on a general approach to model complex multi-component rare earth systems (Xie et al., 2014). Nevertheless, the existing process-modeling methods and their applications are discussed below.

2.6.1 Steady-state modeling

The roots of the steady state modeling of the SX processes originate from the design of multistage processes, such as distillation and vaporization columns, used in chemical engineering. These processes are operated in co-current or counter-current arrangements, with mass transfer taking place between liquid and vapor phases. Modeling of such processes requires simultaneous solving of the equilibrium-and enthalpy-balance equations between phases. However, in the case of SX processes, enthalpy balance is not useful because of the small energy change associated with phase transformation. Furthermore, the work related to the steady state modeling of rare earth SX processes and the application in design has been primarily focused on counter-current arrangements because of industry practice and acceptance. Hence, the literature available focuses mainly on counter-current arrangements.

The development of the process models for counter-current configurations is proceeded by considering mass balance across a single stage of a “n” stage counter current-process, as shown in Figure 2.28. The mass balance for a metal is expressed by using concentration and flow variables is represented in Eq. 2.19, where, Y and X followed by a subscript represent the concentration in organic and aqueous phase, the subscript indicate the stage number, and V_o and V_a represent volumetric flowrate of organic and aqueous phases.

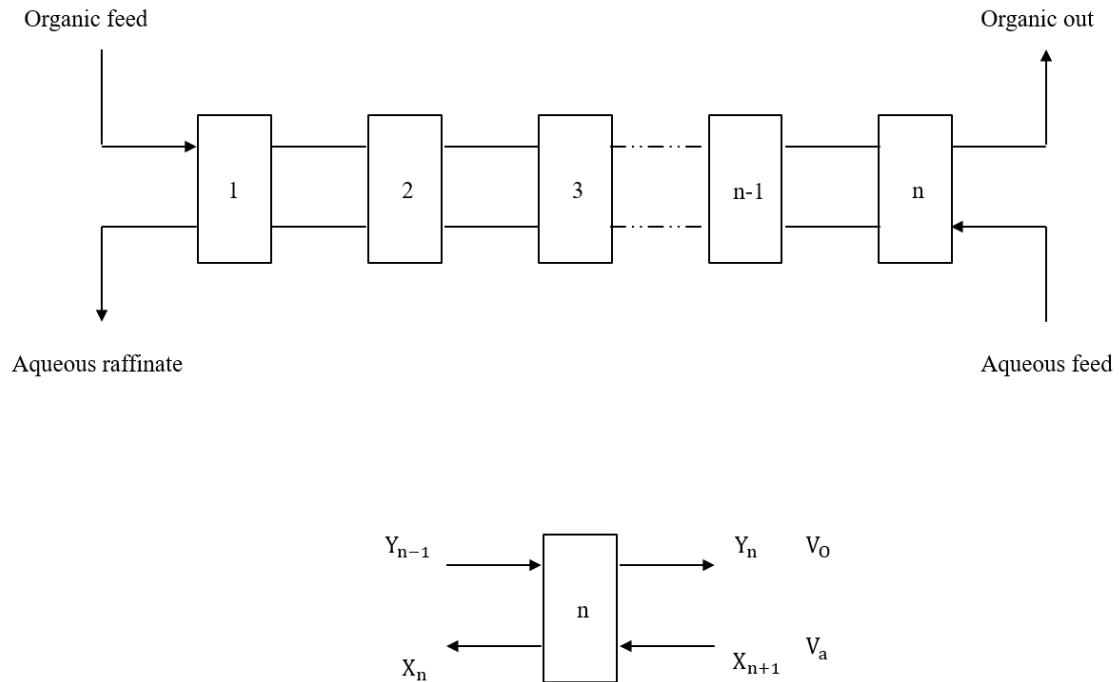


Figure 2.28: Multistage SX process (top, adapted from Xie et al., 2014); mass balance across a single stage showing flow and concentration variables associated with a single stage (bottom)

$$Y_n V_O + X_n V_A = Y_{n-1} V_O + X_{n+1} V_A \quad 2.19$$

Two methods have been primarily used to solve the above equation for SX mass transfer. The first method is an algebraic method and uses distribution coefficients derived experimentally or theoretically to solve for the concentration of metal in streams leaving the system. This method was originally developed by Kremser and is known as the Kremser equation (Klinkenberg, 1951; Kremser, 1930). The second method utilizes a graphical approach to integrate the equilibrium information to evaluate the concentration of metal and stage requirement for extraction, and it is referred as McCabe Thiele method (McCabe et al., 1993).

KREMSER METHOD

In the Kremser method, the solution to Eq. 2.19 is approached by using a simplifying assumption of zero metal concentration of metal in organic feed entering stage 1 of the SX train ($Y_0 = 0$, Figure 2.28). This simplification results in following equation form for stage 1 with one less unknown:

$$X_2 = X_1 + \frac{V_o}{V_a} Y_1 \quad 2.20$$

The transfer or extraction of metal in the stage is then expressed by constant distribution coefficient, as shown in Eq. 2.21, which upon substitution to Eq. 2.20 results in Eq. 2.22.

$$D = \frac{\text{Mass flow rate of metal in organic outlet}}{\text{Mass flow rate of metal in aqueous outlet}} = \frac{Y_n V_o}{X_n V_a} \quad 2.21$$

$$X_2 = X_1(1 + D) \quad 2.22$$

The process, when extended to n stages, leads to the following form:

$$X_{n+1} = X_1(1 + D + D^2 + \dots D^n) \quad 2.23$$

$$X_{n+1} = X_1 \left(\frac{D^{n+1} - 1}{D - 1} \right) \quad 2.24$$

Equation 2.23 is a geometric series with constant ratio of D ; the solution which results in Eq. 2.24. Equation 2.24 can be solved for stage number (n), provided the feed and raffinate composition are known. The Kremser method is useful in designing a simple process involving single ionic states as it utilizes the distribution coefficient of elements; however, it has not been widely used for systems involving multiple ionic states. In addition, assumption of the constant distribution coefficient across multiple stages and zero concentration in organic stream entering stage 1 is not expected in a typical SX train involving loading, scrubbing, and stripping processes.

MCCABE THIELE METHOD

In the McCabe Thiele method, Eq. 2.19 for a multi-stage process is solved by combining equilibrium information graphically which is referred as McCabe Thiele curve. The method involves formulating a system of mass balance expressed by Eq. 2.19 sequentially from one end of the SX train by combining adjacent stages, as shown in Figure 2.29 (McCabe et al., 1967).

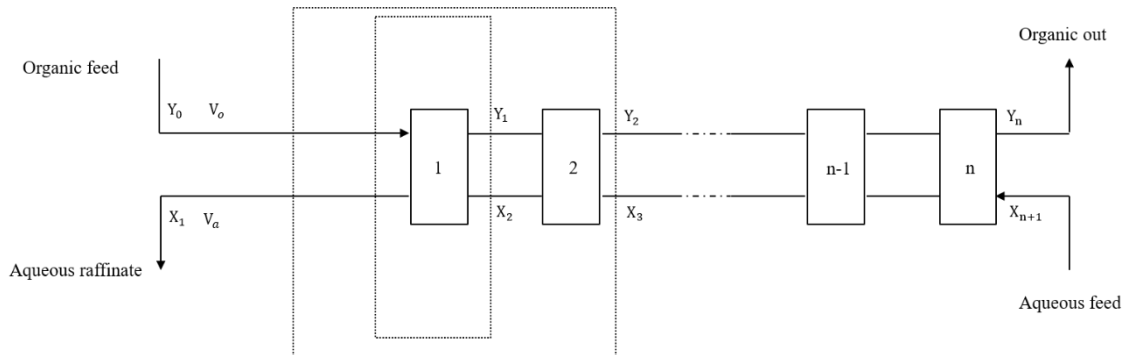


Figure 2.29: Mass balance applied successively to multistage counter-current solvent extraction adapted from Henley et al. (1981)

Thus, mass balance across stage 1 is given by Eq. 2.25, mass balance across stage 1 and 2 combined is given by Eq. 2.26 and similarly across stage 1 and n combined is given by Eq. 2.27.

$$Y_1 = \left(\frac{V_A}{V_O}\right) X_2 + \frac{(Y_0 V_O - X_1 V_A)}{V_A} \quad 2.25$$

$$Y_2 = \left(\frac{V_A}{V_O}\right) X_3 + \frac{(Y_0 V_O - X_1 V_A)}{V_A} \quad 2.26$$

$$Y_n = \left(\frac{V_A}{V_O}\right) X_{n+1} + \frac{\phi}{V_A} ; \phi = (Y_0 V_O - X_1 V_A) \quad 2.27$$

Expressing the stagewise mass balance relationship using this form results in n equations with the first term having a factor of flow ratios (V_A/V_O) and the second term a constant difference of mass flowrate of the raffinate and organic entering/leaving the system (ϕ in Eq. 2.27). The form of equation is linear and is represented graphically as an operating line (AF, as shown in Figure 2.30). The points on the line signify the concentration of metal in organic and aqueous phases entering and leaving a given stage (McCabe et al., 1967).

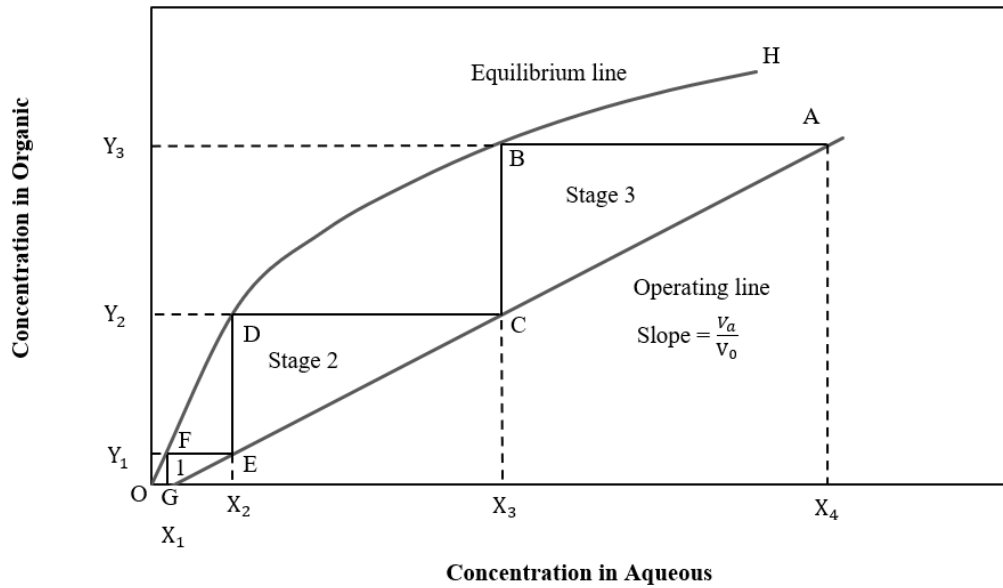


Figure 2.30: McCabe Thiele curve represented as equilibrium line and stagewise mass transfer represented by operating line.

Thus, the operating line is graphed using the phase ratio (V_A/V_o), concentration (X_{n+1}) of an aqueous stream entering any stage, raffinate concentration (X_1) and concentration (Y_0) of metal in organic stream entering stage 1. In most cases the concentration of stream entering any stage is known, however, the raffinate concentration may or may not be known and the organic concentrations is usually assumed to be zero (Eq. 2.27). The equilibrium relationship obtained experimentally or theoretically is then plotted on the same graph and is referred to as the equilibrium line. Figure 2.30 shows a typical example of a three-stage SX process design, with OH representing equilibrium line and GA as operating line.

The number of stages required for extraction is then solved by locating the feed concentration (X_4 in Figure 2.30) on the operating line, which, in this case, is point A and finding the corresponding concentration in the organic phase from equilibrium line, point B (Y_3). The concentration Y_3 represents the metal in the organic phase leaving the last stage of extraction. The concentration corresponding to Y_3 in aqueous phase leaving the system is traced by drawing a line intersecting operating line (BC). The process is repeated till the

concentration in the organic phase reaches zero and X_1 is reached. The number of steps drawn in the process is considered to be the stage number. The difference in concentration in between points X_4 , X_3 , X_2 , and X_1 corresponds to the mass transfer which has taken place as a result of extraction. Similarly, the difference between Y_0 , Y_1 , Y_2 , and Y_3 represents concentration build up in organic phase from subsequent stages.

The method is useful in integrating equilibrium and process relationship to determine the number of stages required. Despite its simplicity, the method suffers from major drawbacks when applied to rare earth separation, which are listed below:

1. The first drawback of the method is the assumption that the concentration in the organic phase as zero, which is required to construct the operating line;
2. The previous McCabe Thiele methods developed for rare earth extraction are created by performing experiments on a single-salt solution, which fails to capture competing ion and saturation effects;
3. Rare earth separation process design, which is a multi-component process, requires solution of multiple equilibrium curves and operating line pairs, which are difficult to solve simultaneously (Figure 2.31). Furthermore, the operating line associated with every component will require the independent assumption of zero concentration in the organic phase, thereby increasing the number of assumptions and, thus, inaccuracy;

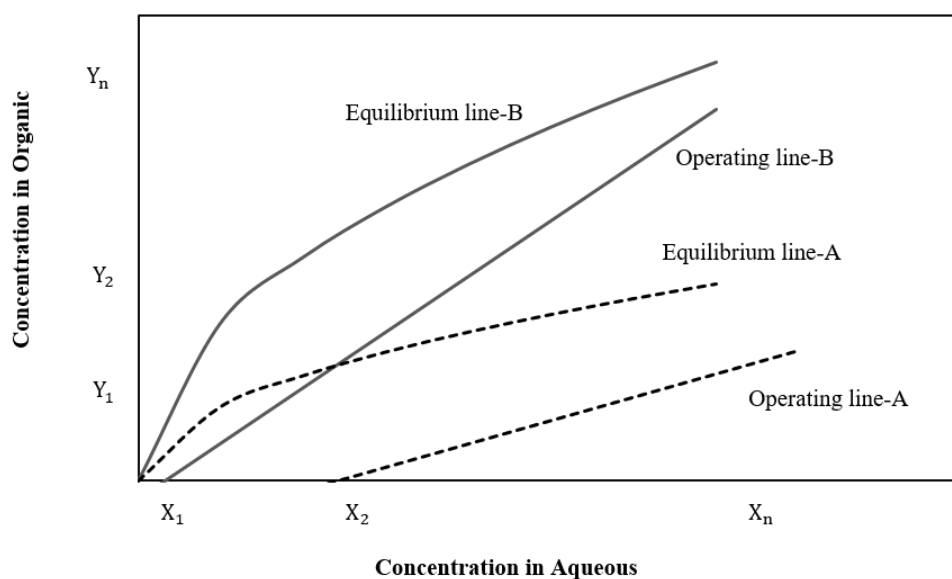


Figure 2.31: Equilibrium curve and operating line pair for two components

4. Complexity further increases as the equilibrium curve can be developed at various pH values. This increases the amount of experimentation, associated costs, and potential design options. With so many unknowns, assumptions, and scenarios to simulate, it becomes very difficult to utilize the above method in flowsheet design and separation.

Various tools and software programs have been developed and tested for process modeling of REEs and different base metals, such as cobalt and nickel. Table 2.8 lists the names of tools and methods used in process modeling of the SX process.

Table 2.8: Programs developed for process modeling of SX

Metal	Method	Tool	Name
Nd	Kremser	-	Voit, 1989
REEs	Kremser	-	Reddy et al., 1992
REEs	Kremser	-	Zhang et al., 2016b
REEs	McCabe Thiele		Sebenik et al., 1966
REEs	-	-	Sharp et al., 1965
REEs	-	by Cytec (no name)	Lyon et al., 2016
REEs	-	ESRECE simulation system	Wenli et al., 2000
Cobalt	-	Aspen custom modeler	Evans et al., 2014
Cobalt/Nickel	-	MINCHEM (Cytec)	Bourget et al., 2011
Cobalt/Nickel/Copper	-	by Cytec (no name)	Soderstrom et al., 2010

2.6.2 Dynamic process modeling

Industrial SX often requires the knowledge of real-time or time dependent behavior of the operational SX circuit for development of process control. Attempts have been made by researchers to develop dynamically model the industrial copper SX process (Komulainen et al., 2006). Similar to steady state models, the dynamic models are based on the fundamental approach of mass balance. However, the difference is the dynamic model describes the time-dependent system behavior by accounting accumulation of material within a mixer settler (Figure 2.32). Equations 2.28 and 2.29 are the typical examples of transient model forms developed by Komulainen et al. (2006) describing stagewise rate of change in concentration in organic and aqueous phase respectively assuming every mixer as a perfect mixing tank. The term on left (d/dt) describes the rate of change (time dependent change) in concentration in organic and aqueous phases in a mixer of stage 1 of an industrial process. The first term on the right in each equation is the mass difference between input and output stream entering and leaving the stage. The second term represents the mass transfer occurring due to extraction, multiplied by a factor K_1 representing the speed of the extraction.

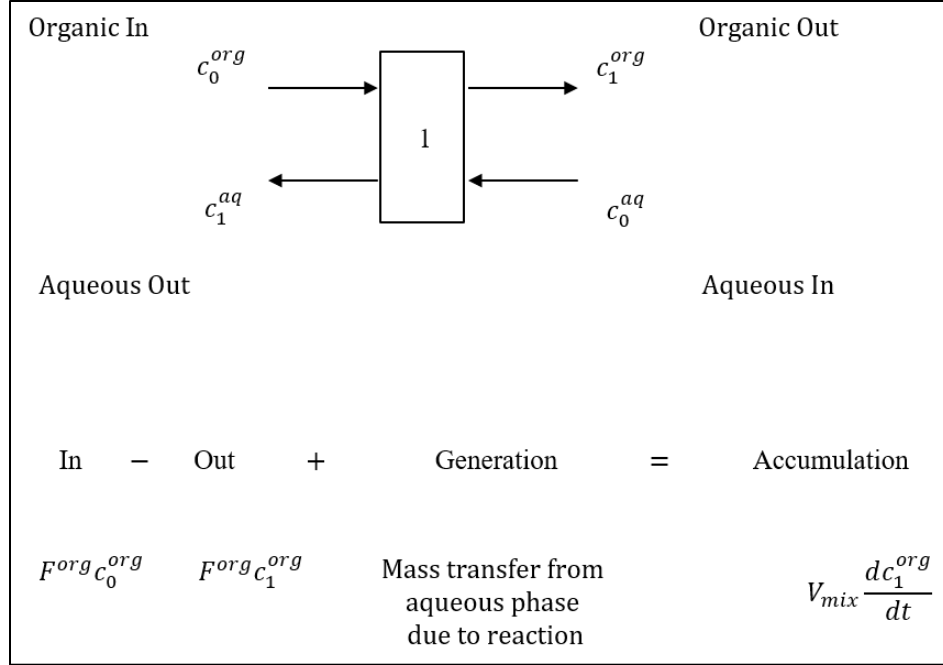


Figure 2.32: Dynamic modeling across a single stage for organic phase

$$\frac{dc_1^{org}(t)}{dt} = \frac{F^{org}}{V_{mix}} (c_0^{org}(t - t_0) - c_1^{org}(t)) + K_1 (c_1^{org}(t) - c_1^{org*}(t)) \quad 2.28$$

$$\frac{dc_1^{aq}(t)}{dt} = \frac{F^{aq}}{V_{mix}} (c_0^{aq}(t) - c_1^{aq}(t)) - K_1 (c_1^{org}(t) - c_1^{org*}(t)) \quad 2.29$$

The c_0 and c_1 followed by superscript indicate the concentration in organic and aqueous phases, entering and leaving stage 1, respectively. F^{org} and F^{aq} represent the flowrate of organic and aqueous phases in mixer, V_{mix} is the volume of mixer, and K_1 is the mass transfer coefficient. c_1^{org*} is the theoretical equilibrium concentration of metal in the organic phase evaluated from plant-specific McCabe Thiele, using on incoming aqueous flow concentration. c_1^{org*} was mathematically described as a function of the following variables α_1 , A , and B , representing efficiency, extraction, and isotherm parameters.

$$c_1^{org*}(t) = f(c_0^{org}(t - t_0), c_0^{aq}(t), F^{org}(t), F^{aq}(t), \alpha_1, A, B) \quad 2.30$$

The method was effective in predicting real-time behavior of the industrial solvent extraction, but it required one month of extensive industrial data collection for parameter estimation and model correction. The data consisted of both offline and online measurements of variables at 4-hour intervals. Flow measurements of aqueous and organic phases were easily available from online measurements, but concentration measurements were obtained from periodic offline sampling and laboratory analysis. In another dynamic model developed by Shahcheraghi et al. (2016), the hydrodynamic behavior of the organic and aqueous phases was modeled separately, following a similar approach but using computational fluid dynamic (CFD) modeling to describe the flow behavior in the mixer/settler. The argument for the use of CFD was the difference in the flow and hydrodynamic behavior of organic and aqueous phases in the settler because of the non-ideal nature of the liquids. The model distinguished the plug flow and perfect mixing assumption for a certain mixer type and used the plug-flow approach for modeling the process. The method was also used in estimating the dispersion and flow patterns through settler and control droplet break-up and coalescence build-up. The simulation was validated with one month of operational data (copper SX). The model predicted well the dynamic extraction and stripping behavior, as well as the process disturbances from input variation.

Dynamic models for the REE SX process for an element pair, Nd and Pr, was also developed using laboratory equilibrium data by Lyon et al. (2017). The model used a similar framework of determining the concentration of metal components across a stage under transient conditions but differed from previous methods in the use of equilibrium data (Lyon et al. 2017). In previous approaches, McCabe Thiele diagrams were used for determining mass transfer in the stages, whereas in the method used by Lyon et al., the experimental data on the distribution coefficient was used. However, the method only considered the pH dependence of the distribution coefficient, and it did not account for

variations due to change in phase ratios. In addition, when using the distribution coefficient, the activities of species were not considered. Nevertheless, the literature (Lyon et al., 2017) reported the model predicted partitioning behavior with reasonable accuracy under steady state conditions but showed some deviation when used for the dynamic condition.

The dynamic models are useful in understanding the dynamics of industrial SX processes, improving and developing process control, but their application in process design is limited. Additionally, the development of dynamic models requires mixer-settler design specifications, flow variables, and extensive computational and data resources, which are typically unavailable in the design phase of the process. For these reasons, steady-state modeling is typically used for process flowsheet design.

2.7 SUMMARY AND GAP ANALYSIS

From the detailed discussion on SX separation of REEs, it can be inferred that significant research has been done on improving separations using various extractants, combinations of extractants, and equilibrium analysis of the SX process. Review of existing industrial and pilot flowsheets showed various configurations of SX trains which followed individual and group separation of elements. However, the details on the method adopted in designing flowsheets, determining performance, and requisite number of stages was limited. Few studies mentioned the use of McCabe Thiele in determining the number of stages for loading and stripping. However, the method was applied by conducting tests on a single salt solution because of experimental complications associated with developing McCabe Thiele for multi-component system. A rare earth system involves multiple components, thereby limiting the use of McCabe Thiele in stage determination because of multiple equilibria and operating line pairs. Process modeling is a solution to design similar complex extracting systems involving multiple components. However, the research relating to the process modeling of REEs are few, summarized in Table 2.8. The previous process models developed for a rare earth system were mostly based on the Kremser method, which is based on assumptions of zero concentration in the organic phase entering system and the constant distribution coefficient across a multistage SX. The method also did not account

for phase ratios' effects, which is critical for stage determination. Thus, process design and stage determination for separation of REEs using SX process is exceedingly challenging due to poor separability and multiplicity of elements. Hence, there is need for design method and determine number of stages required in a SX process for similar extracting multi-component system. This research, therefore, presents an optimal design method of the SX process for the separation of REEs from a mixed rare earth system utilizing bench-scale studies, modeling, and optimization methods.

CHAPTER 3. RESEARCH APPROACH

The broad problem that this research is addressing is the design of a process flowsheet for the separation of REEs. A flowsheet is a combination of different unit processes arranged to achieve a given objective, such as separation or purification. The success of a designed flowsheet lies in its ability to meet the design objective by predicting the behavior of different processes. For this study, the REE separation flowsheet will be a combination of multiple solvent extraction processes (trains), which themselves are combinations of subprocesses (series of specific stages) such as loading, scrubbing, and stripping. Thus, understanding the equilibrium chemical process by studying variables affecting the process and development of extraction/stripping model is essential. The developed extraction/stripping models can then be applied to process models for flowsheet design, as shown in Figure 2.22.

Since solvent extraction is an equilibrium chemical process, the critical variables effecting the process can be identified by reviewing the fundamentals of the equilibrium chemistry, discussed in the subsequent section. Once the variables, have been identified, the experimentation and modeling work can be progressed for design of flowsheet. The general approach taken in this study is summarized in Figure 3.1.

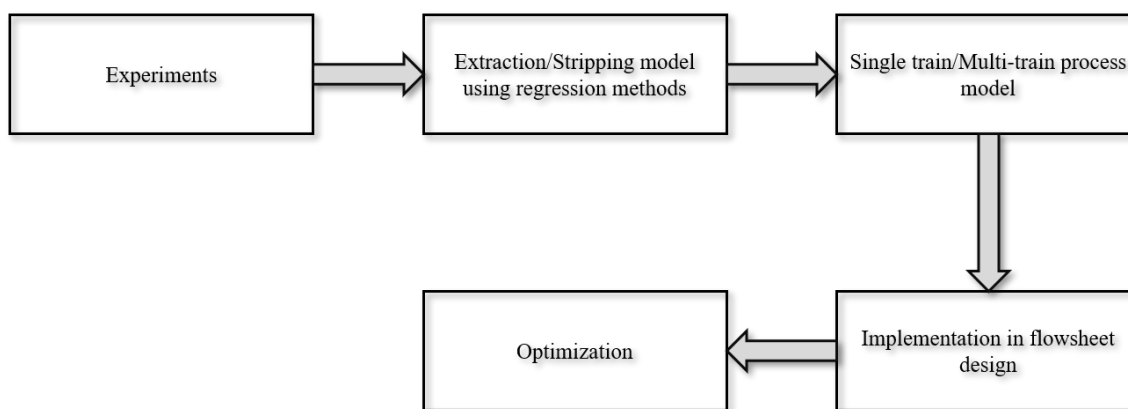
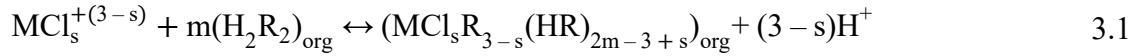


Figure 3.1: Schematic showing step-by-step flow sheet development approach used in this study to model the SX system and use of optimization for flowsheet design

3.1 FUNDAMENTAL BASIS

For an individual REE in the aqueous phase, undergoing equilibrium extraction using an acidic extractant, the general form of possible chemical extraction reactions taking place is expressed as:



where $\text{MCl}_s^{+(3-s)}$ represents the species of the rare earth metal ion in chloride media, H_2R_2 the dimeric form of the organic extractant, $\text{MCl}_s\text{R}_{3-s}(\text{HR})_{2m-3+s}$ the rare earth extractant complex formed during the extraction phase, and H^+ the hydrogen ion released in the process. The subscript “org” in the chemical reaction indicates that the species is in the organic phase. The equilibrium constant (K_i) for the reaction in Eq. 3.1 can be quantified using the following expression:

$$K_i = \frac{a_{\text{MCl}_s\text{R}_{3-s}(\text{HR})_{2m-3+s}} \cdot a_{\text{H}^+}^{3-s}}{a_{\text{MCl}^{3-s}} \cdot a_{(\text{H}_2\text{R}_2)_{\text{org}}}^m} \quad 3.2$$

where ‘a’ followed by a subscript indicates the activities of the respective species at equilibrium and K_i denotes the equilibrium constant. The activities in Eq. 3.2 at low ionic strength, which happens to take place under low concentration (dilute) conditions, can be replaced by the concentration of the respective species, thereby providing a modified equation for the equilibrium constant:

$$K_{i, \text{conc}} = \frac{[\text{MCl}_s\text{R}_{3-s}(\text{HR})_{2m-3+s}]_{\text{org}} [\text{H}^+]^{3-s}}{[\text{MCl}^{(3-s)+}] [\text{H}_2\text{R}_2]_{\text{org}}^m} \quad 3.3$$

where the species in the [] brackets denotes the respective concentration and $K_{i, \text{conc}}$ is the equilibrium concentration constant. During extraction, preferential redistribution of metal

takes place in the organic and aqueous phase, which is an important indicator of the extent of the reaction and measured by the distribution coefficient constant. The distribution constant (D_i^c) for a metal i is defined as:

$$D_i^c = \frac{[MCl_s R_{3-s} (HR)_{2m-3+s}]_{org}}{[MCl^{(3-s)+}]} \quad 3.4$$

Rearranging Eq. 3.3 and 3.4 in terms of distribution coefficient results in following form:

$$D_i^c = \frac{K_{i, conc} [H_2R_2]_{org}^m}{[H^+]^{3-s}} \quad 3.5$$

Further, applying logarithmic transformation to Eq. 3.5 leads to:

$$\log D_i^c = \log K_{i, conc} + m \log [H_2R_2]_{org} - (3-s) \log [H^+] \quad 3.6$$

From Eq. 3.5 and 3.6, it is apparent that the distribution coefficient is a function of extractant and hydrogen ion concentrations at equilibrium. Thus, it can be confirmed that key variables affecting extraction of a single metal ion are:

- Equilibrium hydrogen ion concentration (pH);
- Equilibrium organic concentration.

These factors are a result of the equilibrium chemical reaction. When the process is implemented on continuous scale, variables resulting from the circuit configuration as well as the interconnection of different processes such as loading, scrubbing stripping, recirculation, etc., influence the separation. These variables are referred to as process variables, examples, which include reflux ratio, feed flowrate, and strip flowrate.

Nevertheless, any change in process variables ultimately leads to a change in the equilibrium variables, and thus extraction can be easily described based on the corresponding change. Hence, detailed experimental study of equilibrium pH and organic concentration influences on the equilibrium is necessary.

3.2 MODELING APPROACH USING DISTRIBUTION RATIOS

The discussion in the previous section was useful in identifying the variables affecting the reaction equilibrium. However, the analysis was based on the simplified assumption of replacing activities of ionic species with concentrations and applies to dilute or ideal solutions only. In the real world, this is rarely the case as the extraction of metal is influenced by activities of the ionic species present in the solution.

Modeling the distribution coefficient indicated in Eq. 3.6 for a mixed REE system by a fundamental approach becomes complicated for three reasons. First, it is impractical to identify different ionic species (oxidation states) of a single rare earth existing in the mixed ionic system like M^{3+} , MCl^{2+} , and MCl_2^+ . For instance, if a single rare earth metal such as neodymium is considered, the potential ionic species associated with neodymium will depend upon the ionic interaction and activity as shown in Figure 3.2. The concentration of each ionic state, is determined by dissociation constants k_1 , k_2 , and k_3 , which further determine the extent of reaction of the ionic species with extractant. Hence, for the multi rare earth system used for this research (Figure 4.1), there can be three or more equilibrium constants associated with each rare earth, making the total number of equilibrium constants three times the number of REEs present, which is difficult to model. Second, it has been shown that in the organic phase extractant also exists in equilibrium, with its dimeric and monomeric forms that changes with metal loading (Mansur et al., 2002). When loading increases, a high amount of extractant is required, leading to breakage of dimeric forms to monomeric forms (Figure 3.3).

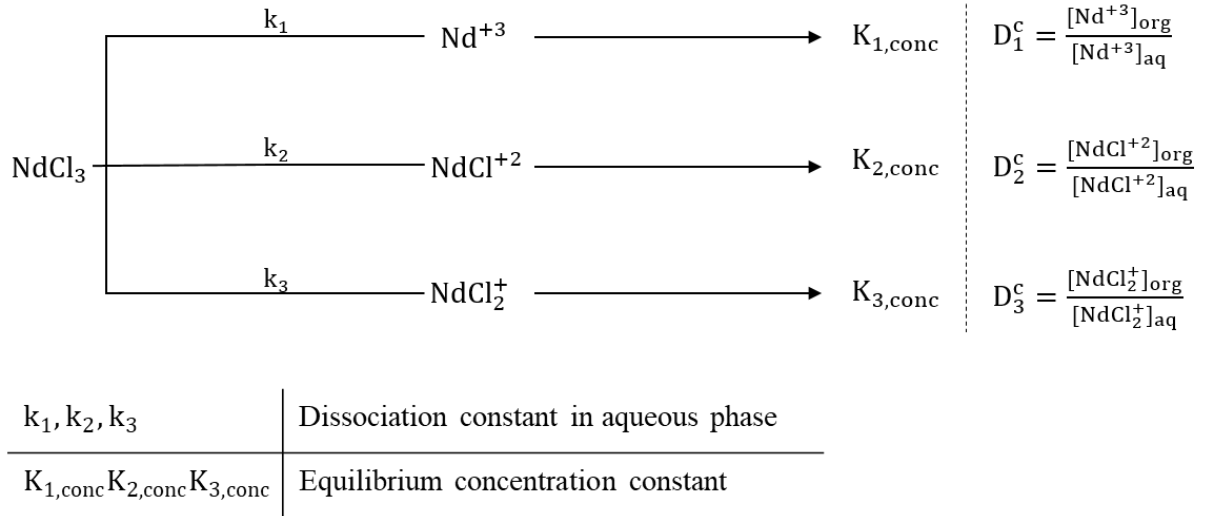


Figure 3.2: Speciation states for an individual rare earth in aqueous phase

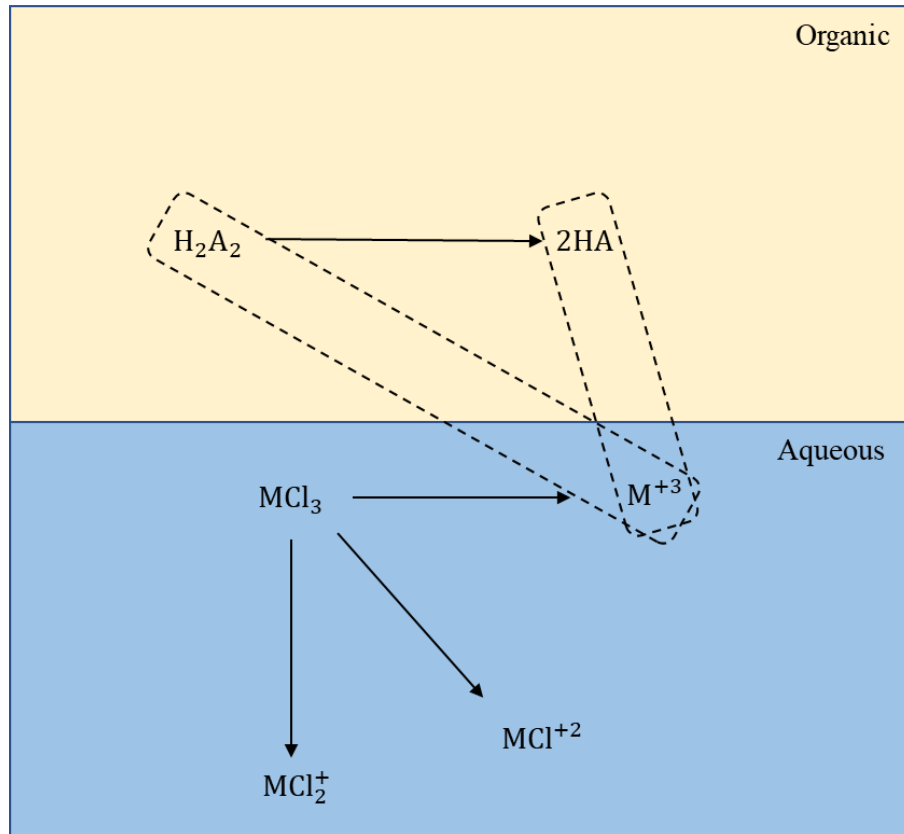


Figure 3.3: Speciation states in organic and aqueous phases

Finally, to model the system for a high ionic strength solution, activity coefficients for each of the species will be required, which is difficult to determine. Hence, a more pragmatic approach to model the separation process is to model the distribution ratio, which is defined as:

$$D_i = \frac{\sum [M_i]_{org}}{\sum [M_i]_{aq}} = \frac{([M^{+3}] + [MCl^{+2}] + [MCl_2^+])_{org}}{([M^{+3}] + [MCl^{+2}] + [MCl_2^+])_{aq}} \quad 3.7$$

where D_i represents the distribution ratio for any species ‘i’ in the system, $[M_i]_{org}$ is the metal concentration in the organic liquid phase, and $[M_i]_{aq}$ is the metal concentration in the aqueous phase. M^{3+} , MCl^{2+} , and MCl_2^+ in [] indicate the concentration of speciation state in respective phases, which is indicated outside the parentheses.

The advantage of using distribution ratios is that it accounts for all the ionic states of metal present in the aqueous phase, which is easy to measure. Since the distribution coefficient is dependent upon equilibrium pH and extractant concentration, it can be proven mathematically that distribution ratios are also dependent on both variables. Thus, one can experimentally investigate the variation in distribution ratios as a function of equilibrium pH and equilibrium extractant concentration, establishing a relationship between them. However, experimentation with respect to equilibrium extractant concentrations is difficult because of the inability to measure metal concentration in the organic phase. Hence, an alternate way of testing is by conducting experiments at different phase ratios. The percent extraction or distribution ratios thus obtained can be used to describe extraction behavior. This approach is also convenient from a process design standpoint as processes are operated at different phase ratios rather than extractant concentrations. The dependence of percent extraction or metal distribution with phase ratio can also be envisioned when considering the fraction of metal extracted with respect to feed, which results in the following expression:

$$E_i = \frac{\left(\frac{O}{A}\right)^{D_i}}{\left(\frac{O}{A}\right)^{D_{i+1}}} * 100 \quad 3.8$$

where E_i is percent extracted, D_i distribution ratio of metal I, and O and A the volumes of organic and aqueous phases. In Eq. 3.8, the dependence of percent extraction on volume is explicit.

Thus, the study of volumes for both phases, referred to as volume ratio, O/A ratio, or phase ratio, is therefore critical for the design of a SX process. Changing phase ratios alters the separation behavior and purity of the product because of the change in available extractant. In a multi-element system, extraction at a low phase ratio (organic-to-aqueous) often leads to competing ion and saturation effects because the large amount of metal ions competing for access to the lower amounts of available extractant. As a result, preferential selection during extraction dominates, thereby changing the expected elemental distribution ratios (Rydberg, 2004). This property is often utilized in industrial SX separation and process design, which, are generally operated at different phase ratios to achieve saturation and desired separation performance. Therefore, to model equilibrium SX process, experiments were designed and performed independently at different equilibrium pH and phase ratios. Generally, statistical factorial design is used in design of experiments, identifying factors (variables), or level of important factors, and develop response surface by single or repeated experiments to locate optimal points. For the current study, the factors affecting the separation are known, i.e., pH and phase ratios. Selecting appropriate value ranges for pH and phase ratio was needed to capture the true relationship with the response variable (Distribution Ratio or Percent Extraction).

Hence, to study variation with pH, experiments were designed to be performed from a starting equilibrium pH 0.5 and ending approximately at 3.0 at a constant phase of 1. The range of pH was determined from an investigative study conducted on a rare earth oxide (REO) sample produced from hydrometallurgical treatment of pregnant leachate solution (PLS) produced from coarse refuse of Western Kentucky No.13 coal. The test involved study and comparison of extraction behavior of REEs at different pH using different extractant types. Two different extractant mixture were tested; 1.) DEHPA Di-(2-ethylhexyl) phosphoric acid) and TBP (Tributyl phosphate) mixture and 2.) Cyanex 572. The tests were performed on 1 gm/L of the REO mixture which had elemental distribution shown in Figure 3.4.

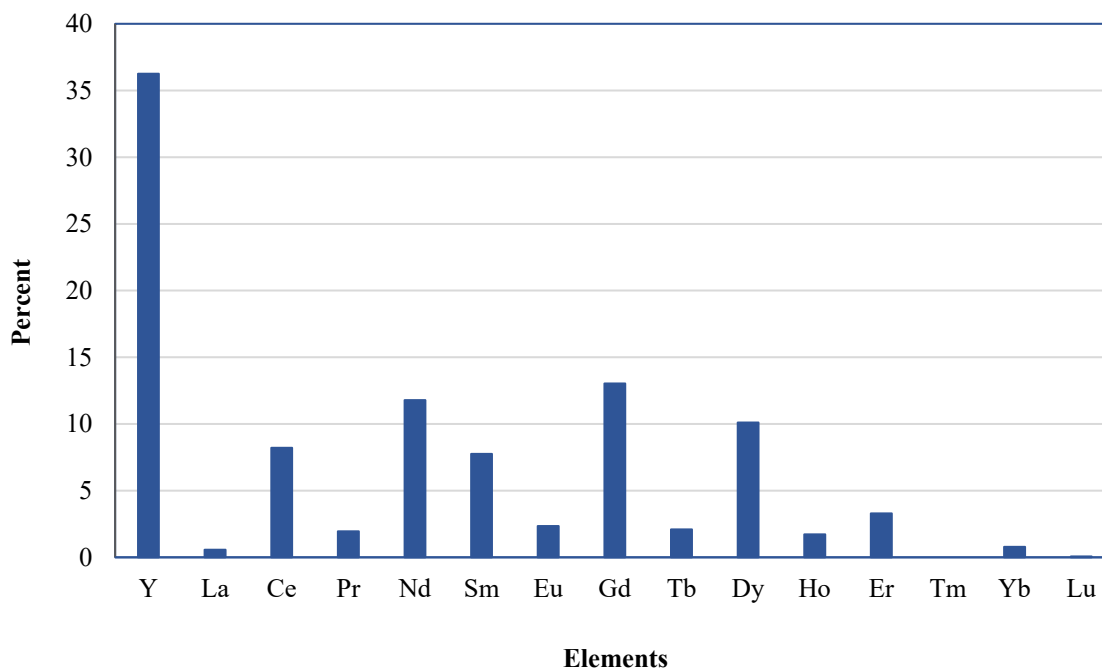


Figure 3.4: Feed distribution of REO obtained from hydrometallurgical treatment of PLS obtained from Western Kentucky No.13 coarse refuse

From the analysis, it was found that the DEHPA and TBP mixture had superior extraction performance in lower pH range compared to DEHPA and Cyanex and, hence, it was selected.

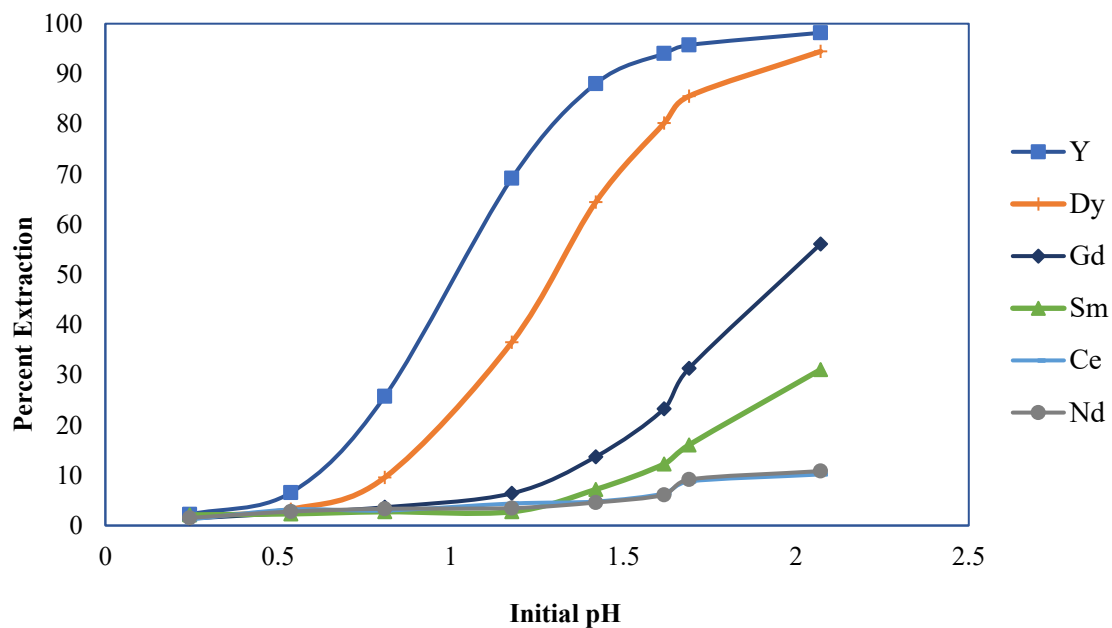


Figure 3.5: Plot showing extraction results of elements present in high concentration from investigative study performed on REO mixture using DEHPA and TBP (2% v/v)

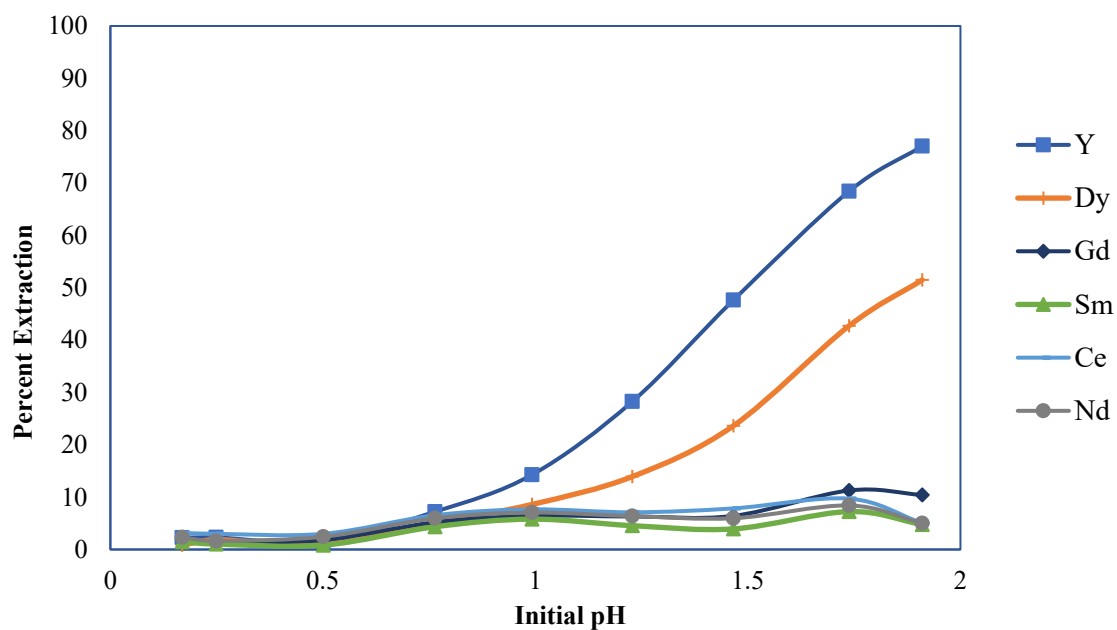


Figure 3.6: Plot showing extraction results of elements present in high concentration from investigative study performed on REO mixture using Cyanex 572 (2% v/v)

Similarly, phase ratios were divided into a five-factor level between 0.1 to 2. However, the difficulty was in selecting the pH to design phase ratio experiments. This is due to dependence of extraction on multiple variables resulting in surface response shown in Figure 3.7. It can be seen from surface plot that numerous pH points can be selected to perform phase ratio (indicated by phase ratio planar surface at pH 1.5 in Figure 3.7). Several such planes can be drawn by conducting test at different pH points. Conventional approach utilize separation factors evaluated from the results of extraction isotherm to select equilibrium pH point and perform experiments to develop phase ratio plane. However, the approach fails to capture the effect of feed composition on separation. Hence, to identify the pH value for the phase ratio experiments, simulation studies were performed utilizing the distribution ratio models developed from pH results.

Figure 3.6 shows the overall approach which was followed for developing models and its implementation in flowsheet design. The first step involved experimentation with pH using selected DEHPA and TBP extractant mixture. The results from the experiments were used in developing distribution ratio model and applied to an SX train using principles of mass balance. The SX train was subjected to sensitivity analysis with pH (simulated at different pH). The purity level obtained from simulation was compared and pH resulting in high purity of elements was selected for phase ratio experiment. The results from phase ratio experiment were then utilized in multi-train modeling for design of multi-train SX flowsheet and stage determination.

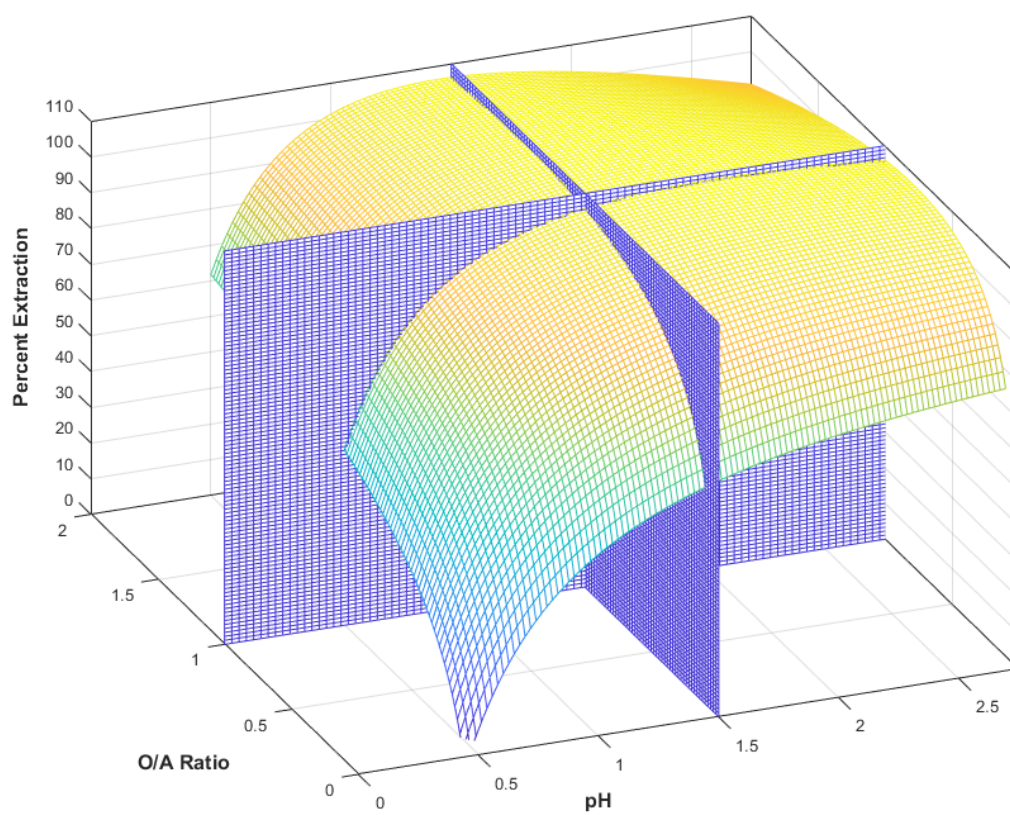


Figure 3.7: Experimental design matrix

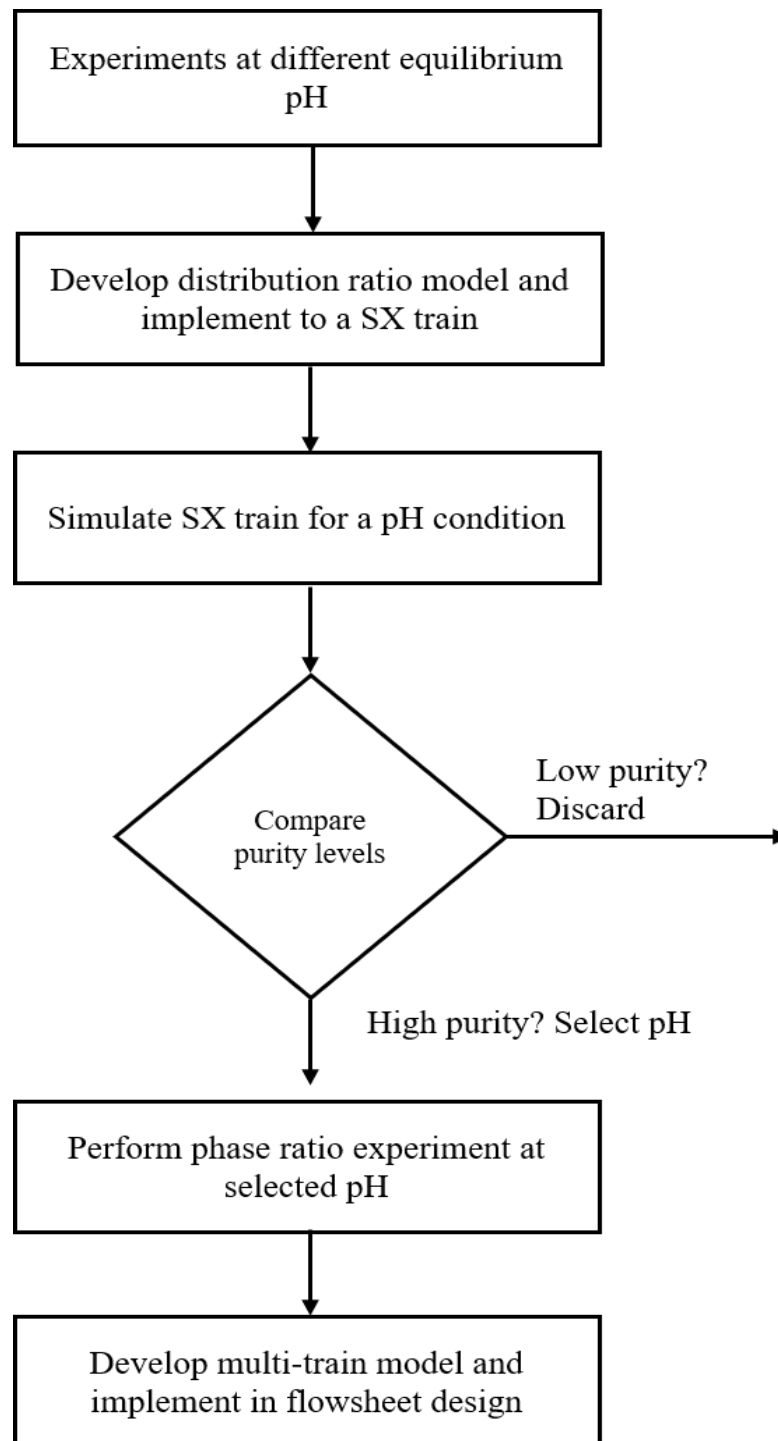


Figure 3.8: Experimental approach and decision making involved in modeling SX process

CHAPTER 4. MATERIALS AND METHOD

4.1 FEED

The feed composition for the current study was derived from the REEs obtained from a coal source. The initial investigative study for REEs in coal source were performed by researchers (Honaker et al., 2014) which determined the potential for extraction REEs. Significant research work has been done since then in extracting REEs from coal and coal sources is conducted at the Western Kentucky Pilot Plant, operated by University of Kentucky (Honaker et al., 2018b). The work involves leaching of roasted coal to recover REEs in a leachate. The leachate is treated following different pathways of precipitation and solvent extraction mechanisms to generate a mixed rare earth oxide product. The elemental distribution of mixed rare earth oxide product generated from the research above was used for determining feed distribution for this research. The coal source used to produce the mixed rare earth oxide was obtained from West Kentucky No. 13 (Baker) seam. Figure 4.1 shows the distribution of elements in the concentrated rare earth oxide (REO). Synthetic solutions were prepared for use in the equilibrium experiments, based on the composition of the REO as shown in Figure 4.1. Elements below 1% were ignored due to their low concentrations. The reconstituted distribution shown in Figure 4.2.

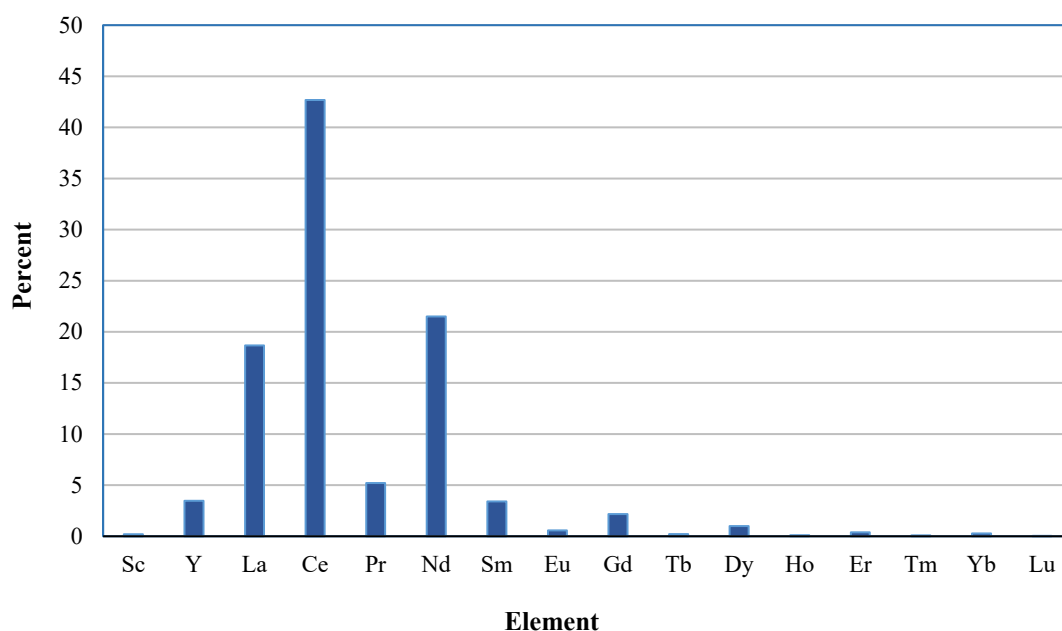


Figure 4.1: REE distribution of the mixed oxide product recovered from West Kentucky No. 13 (Baker) seam coarse refuse

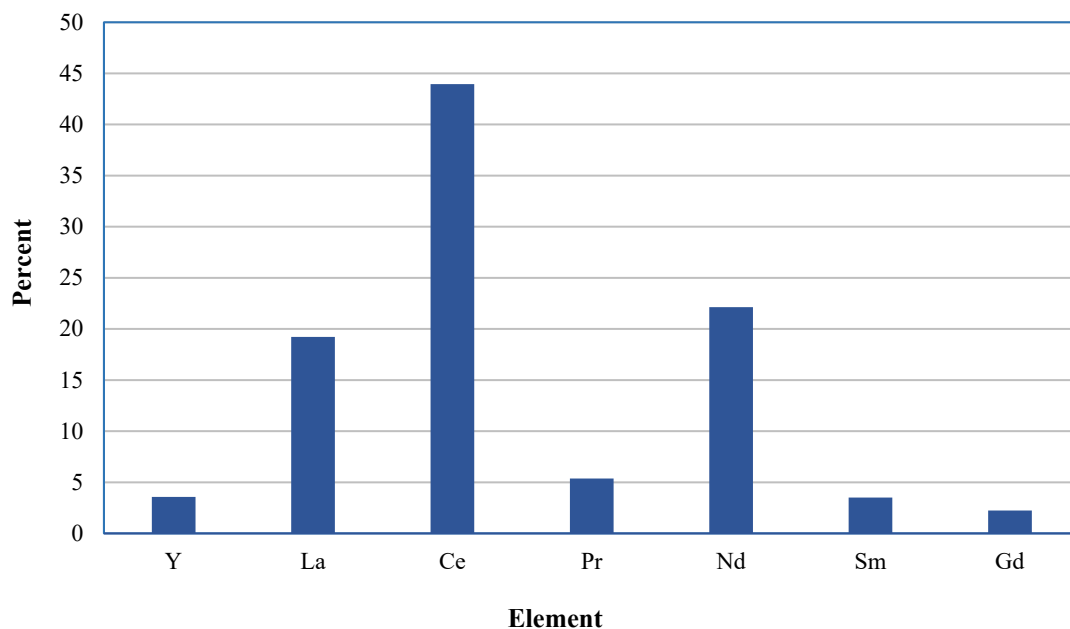


Figure 4.2: Reconstituted REE distribution of the mixed oxide product recovered from West Kentucky No. 13 (Baker) seam coarse refuse after ignoring REEs with less than 1% content

4.2 CHEMICALS

In solvent extraction, the chemical reaction between the extractant and metal ions, and the solubility of product formed drives the separation process. Thus, the primary component required for equilibrium reactions are the extractant dissolved in an organic carrier, called the diluent, and an aqueous phase containing dissolved metal ions and modifiers to control reaction conditions. For this research, Di-(2-ethylhexyl) phosphoric acid (DEHPA) was used as an extractant, and while Orfom (C13-C16 Isoalkanes) served as the diluent. A typical diluent used for a DEHPA system in base metal separation is kerosene. However, Orfom was preferred over kerosene because of the low aromatic content and non-carcinogenic nature, which provided a safer work environment when handling the organic liquid. Tributyl phosphate (TBP) supplied by Beantown Chemicals was used as the phase modifier to prevent a third phase formation during the extraction. In addition, the use TBP was to have a synergistic effect on extraction. TBP is a solvating extractant, which has been shown to improve the separation factor between adjacent rare earths when mixed with DEHPA (Chandra, 2019).

Table 4.1: Specification or organic compound used

Name	Molar Mass (gm)	Density (gm/mL)	Percent used (v/v)	Moles per liter of organic solution
DEHPA	322.43	0.98	5	0.15
TBP	266.32	0.97	10	0.37
Orfom	-	0.84	85	-

The DEHPA and TBP used had purities greater than 95 and 98 percent, respectively. Table 4.1 lists the other chemical specifications of the organic chemical used, and Figure 4.3 shows the chemical structure of the extractants.

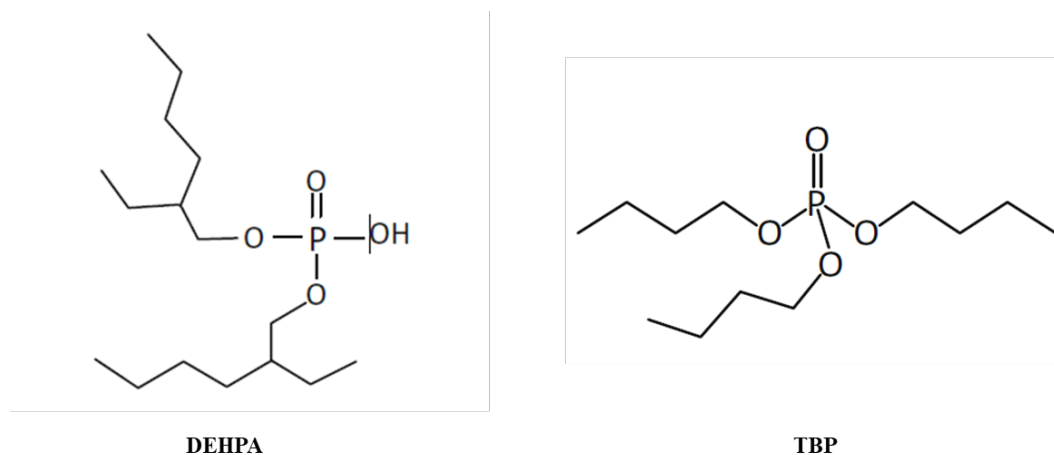


Figure 4.3: Chemical structure of DEHPA and TBP (Zhang et al., 2016b)

The aqueous phase containing the dissolved metal ion was prepared by using rare earth salts. The oxides of yttrium (Y_2O_3), lanthanum (La_2O_3), neodymium (Nd_2O_3), samarium (Sm_2O_3), and gadolinium (Gd_2O_3) were obtained from Fisher Scientific and had purity of 99.9 percent each. However, hydrated chloride of cerium ($\text{CeCl}_3 \cdot 7\text{H}_2\text{O}$) and praseodymium (PrCl_3) were used instead of their respective oxides because of their poor solubility in water; they were also obtained from Fisher Scientific and had purity greater than 99 percent. Trace metal grade hydrochloric acid (37 % w/w) and sodium hydroxide (12.5 M) were used for adjusting the solution pH value. Hydrochloric acid was also used as a stripping agent to recover metal from the organic phase to the aqueous phase.

4.3 EXPERIMENTAL PROCEDURE

To study the complete separation characteristics of the SX process, the experimental plan discussed in Chapter 3 was implemented in two phases. The first phase focused on the effect of the equilibrium aqueous phase acidity (pH) on metal extraction. The second phase involved studying the effect of volume ratios while accounting for the saturation effect in the organic phase. For pH study the tests were conducted between a pH of 0.5 to 3.0 at an approximate interval of 0.5. However, due to saturation and crud formation at pH 3.0, an additional test was performed at pH 2.75 (midpoint of 2.5 and 3), which was considered an upper pH limit. The initial estimate of pH range (or starting pH) was based on results

obtained from the investigative study conducted using DEHPA on 1 gm/L of rare earth oxide, which indicated that most of the REEs are extracted under acidic conditions. Similarly, the second phase of experimentation was performed at different organic-to-aqueous volume ratios at constant pH to construct distribution isotherms (see Figure 3.7). Experiments were performed at phase ratios of 0.1, 0.2, 0.5, 1, and 2, which are typical of any SX study. The solution pH was selected on the basis of purity levels by performing sensitivity analysis with pH for an SX train, which is discussed in CHAPTER 5. Generally, the separation factors are used as an identifier of pH to conduct phase ratio experiments, but they do not capture the effect due to feed distribution and/or changes in feed distribution in an SX train. For this reason, simulations were utilized to identify the pH resulting in good separation between the elements. Three specific pH points, 0.65, 1.5, and 2.2, were identified based on the simulation results to perform the phase 2 experiments.

4.3.1 Extraction

The extraction experiments were carried out by preparing the aqueous and organic liquid feed stocks (Figure 4.4). To make an aqueous feed stock, a solid mixture of 10 grams of REEs was prepared by mixing the oxides and chlorides according to the distribution shown in Table 4.2. The distribution was determined by reconstituting the distribution of feed after removing components less than 1% (Figure 4.1).

Table 4.2: Distribution of rare earth oxides and chlorides in the mixture

Element	Distribution
CeCl ₃ •7H ₂ O	43.34
Nd ₂ O ₃	20.35
La ₂ O ₃	18.91
PrCl ₃	6.20
Gd ₂ O ₃	3.93
Y ₂ O ₃	3.87
Sm ₂ O ₃	3.41
Σ	100.00

The solid mixture was dissolved in 1 liter of 1 M HCl acid. The organic liquid stock containing 5% extractant on a v/v basis was prepared by dissolving 50 mL of DEHPA in the diluent. Similarly, 100 mL of TBP was added to make the 10% v/v phase modifier. The organic solution was then balanced volumetrically with the diluent to make up a total volume of 1 L. After stock preparation, 50 mL of aqueous solution was mixed with the 50 mL of organic solution in a conical flask. Both the phases were mixed for 15 minutes by agitation, and then were transferred to a separatory funnel for phase separation (Figure 4.5). The mixture was allowed to stand for 20 minutes in the separatory funnel to ensure an effective disengagement of both phases. The pH of the equilibrated aqueous phase was measured and a portion of the aqueous phase was analyzed for metal concentration using ICP-OES (Inductively coupled plasma-Optical emission spectrometer; see section 4.4). The metal concentration in the organic phase was back calculated by evaluating the

difference between metal concentration in the aqueous phase before and after the separation using following equation:

$$C_o = \frac{V_{aq}(C_{aq,feed} - C_{aq,eq})}{V_o} \quad 4.1$$

where C_o is the concentration of rare earth metal in the organic phase and $C_{aq,feed}$ and $C_{aq,eq}$ are the concentrations in the aqueous phase, measured before and after extraction, respectively. V_{aq} and V_o are the volumes of the aqueous and organic phases (in mL). The process was repeated to cover the equilibrium aqueous phase pH range, adjusted using NaOH. A blank experiment with the diluent and aqueous phase was also performed to confirm that diluent was not responsible for the transfer of metal ions.

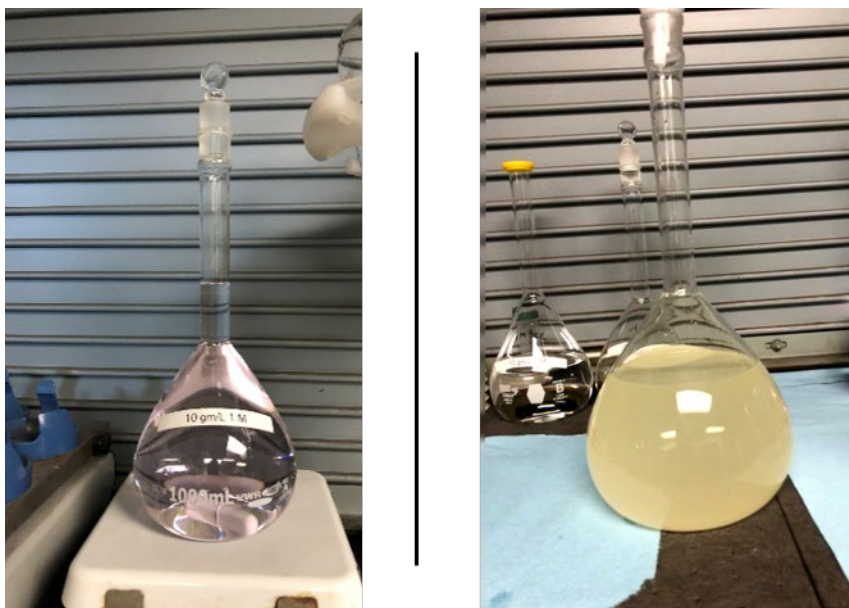


Figure 4.4: Aqueous stock (left) and organic stock (right) prepared for testing

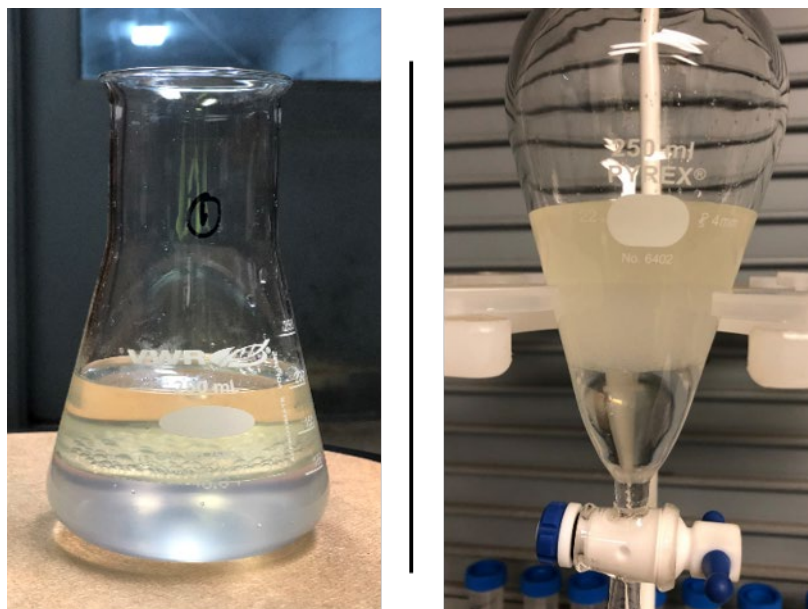


Figure 4.5: Prior mixing (left) and phase separation (right)

4.3.2 Stripping

In order to study the stripping process, 300 mL of the fresh organic stock containing dissolved metal was prepared by loading with aforementioned rare earth to an equilibrium pH of 2.7. The equilibrium pH was the chosen maximum of the equilibrium pH range from extraction experiment. The loaded organic phase mixture so obtained was used for the stripping experiment. The reason for choosing the high equilibrium pH was to maximize the loading of the organic, which happens to be at higher equilibrium pH conditions. Hydrochloric acid of molarities 1, 2, 3, 4, 5, and 6 was used to study the stripping process. The experiment was performed by mixing 50 mL of saturated organic with an equal volume of acid of respective molarity in a conical flask for 15 minutes. After mixing, the phases were separated by allowing them to stand for 20 minutes in the separatory funnel. The resulting aqueous phases after loading and stripping were analyzed for pH and metal concentration. The loading aqueous phase metal concentrations were used to evaluate organic metal concentrations. The organic metal concentrations, together with the stripped aqueous phase concentrations, were used to evaluate the percent of stripping.

4.3.3 Phase 2 experiment

The phase 2 extraction experiments were performed at different organic-aqueous volume ratios by taking 50 mL of aqueous phase and equilibrating it with 5, 10, 25, 50, and 100 mL of organic phase, respectively, to the required equilibrium pH. Mixing was done in a conical flask using a shaker for 15 minutes. Then, the mixtures were allowed to stand for 20 minutes in a separatory funnel for phase disengagement. The pH of the aqueous phase after phase separation was measured. This pH value was compared and adjusted to the required pH level. The process was repeated till required pH value was attained and there was no change in pH after multiple equilibrations. To adjust the pH of the solution after extraction, HCl acid of between 1 and 6 M and sodium hydroxide of molarity 1, 2, 4, and 12.5 were used. The different molarity of HCl and NaOH were selected when adjusting pH to affect a minimum change in volume during multiple equilibrations. The aqueous sample after final extraction was analyzed for rare earth concentration. The concentration in the organic phase was back calculated using Eq. 4.1. The volume ratio in Eq. 4.1 has an impact in the concentration calculation in the organic phase, which was not the case in the phase 1 experiment because the tests were performed at equal volumes (phase ratio of 1).

In the case of stripping, a loaded organic phase was obtained following the same procedure as in the phase 1 experiments. The loaded organic was then divided into five fractions, each a volume of 50 mL, which was stripped with 1 M HCl acid at different volumetric ratios. Five, 10, 25, 50, and 100 mL of HCl were used, and the target equilibrium pH was 0.15. Once the target equilibrium pH was reached, the stripped solutions were analyzed for rare earth content using ICP-OES.

4.4 REE ANALYSIS

Prior to and after the experiments on different aqueous feed samples composition of elements present in the aqueous phase were measured. The elemental analysis of the samples was performed using ICP-OES, a popular technique used for trace metal analysis (Figure 4.6). ICP-OES allows measurement of samples having high total dissolved solids (TDS) and are widely used for ground water and wastewater measurement. It works on the principle of plasma excitation and analyzing the diffraction intensities of the excitation.

The sample to be tested is sprayed into a plasma chamber as an aerosol, where it is irradiated at a temperature range of 6000-8000 K. The radiation produced from the excitation of atoms is diffracted through a prism/lens and is captured on semi-conductor detectors. The intensity of radiation detected from the atoms is measured. The measured intensity is then analyzed using software, which is pre-calibrated with samples prepared before the equipment. The standard samples of concentrations, 0.05, 0.5, 1, 5, and 10 ppm, were prepared for calibrating the ICP. A VHG element calibration standard, containing elements in concentration of 100 µg/L, was mixed in appropriate weight with 5% HNO₃, prepared to the aforementioned standards (Figure 4.7). Upon calibration, the samples to be measured were loaded for measurement under different dilutions, 10x, 100x, and 1000x, of the raw samples. The dilution was done to ensure the elemental concentration of the measured sample is within the calibration range of the equipment.



Figure 4.6: ICP-OES Equipment (adapted form Spectro-Arcos Specofication Sheet)

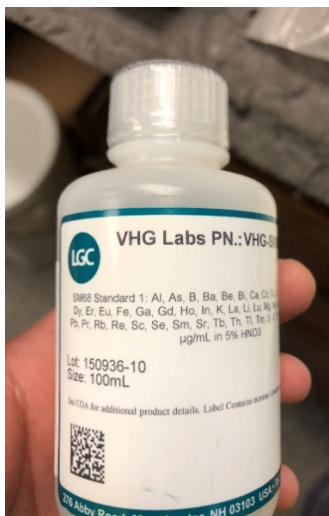


Figure 4.7: Element chemical standard

To ensure the quality of ICP results, the feed solution prepared for different SX test was measured and compared. Figure 4.8 shows whiskers plot from seven measured feed samples used for SX tests. The data inherently contains the experimental error from sample preparation despite that the variability in data is small ensuring less experimental and measurement error. Table 4.3 provides the mean value, standard deviation (std. dev), and std. dev expressed as percent with respect to mean concentration of elements. From Figure 4.8 and Table 4.3 it can be seen the variability in the data is low indicating less experimental and measurement error.

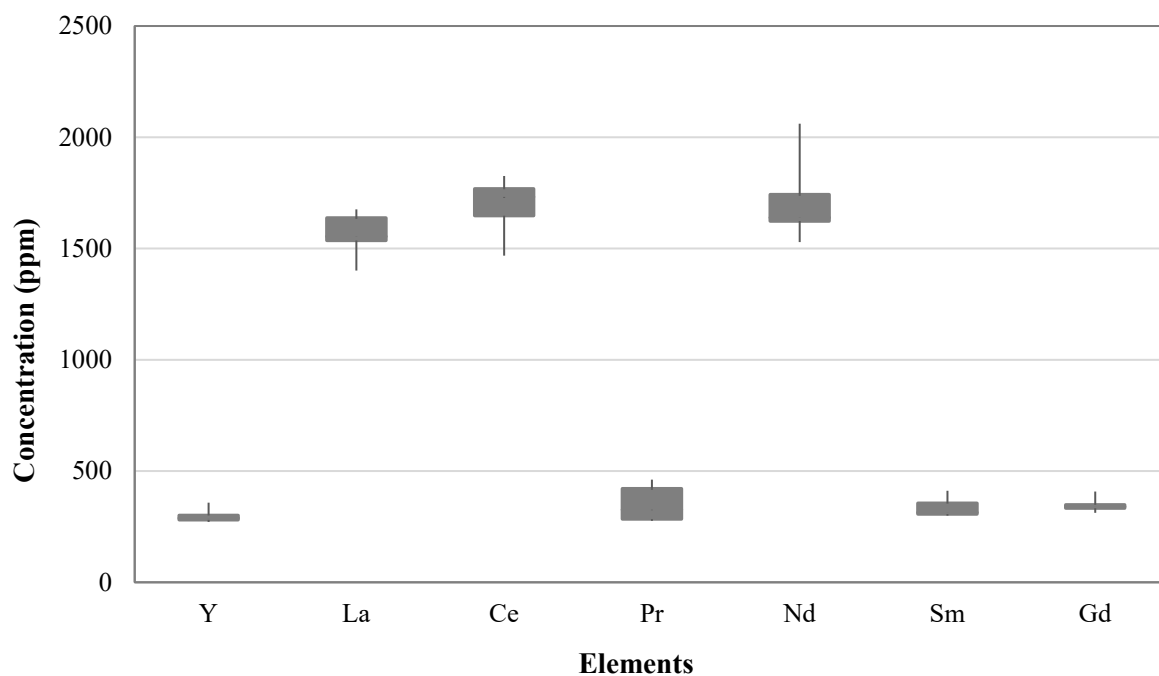


Figure 4.8 Whisker plot of multiple feed stock concentration data used for SX tests

Table 4.3 Mean, standard deviation of measured feed samples

	Y	La	Ce	Pr	Nd	Sm	Gd
Mean	297.37	1568.29	1694.00	353.33	1708.71	335.70	346.07
Std. dev	29.21	94.50	124.01	80.79	175.66	45.91	30.14
Std. dev expressed as percent of mean	9.82	6.03	7.32	22.87	10.28	13.68	8.71

CHAPTER 5. EQUILIBRIUM ISOTHERM

5.1 EXPERIMENTAL RESULTS

The purpose of phase 1 experimentation was to study the distribution of REEs as a function of the equilibrium pH by developing equilibrium extraction and stripping isotherms at fixed phase ratios. Figure 5.1 shows the extraction isotherms created using the experimental results of the loading process. From the plot, it is apparent that the percent extraction for the given system increases with an increase in pH in the following order of extraction: yttrium > gadolinium > samarium > neodymium ~ praseodymium > cerium > lanthanum. The extraction order of elements followed the ionic radii, with the smaller ionic radius being extracted first, as discussed in Section 2.1.1 (Figure 2.2 Ionic radii of rare earths (Eyring et al., 2002)). The extraction order was also in agreement with the classification of REEs as HREEs, MREEs, and LREEs. However, in the case of stripping, no significant change in percent stripped was observed with the equilibrium pH for all elements with exception of yttrium (Figure 5.2). Yttrium showed decreased stripping at higher pH because of its small size, which is believed to be a result of strong association with the extractant, requiring harsh acidic conditions to break the yttrium-extractant complex.

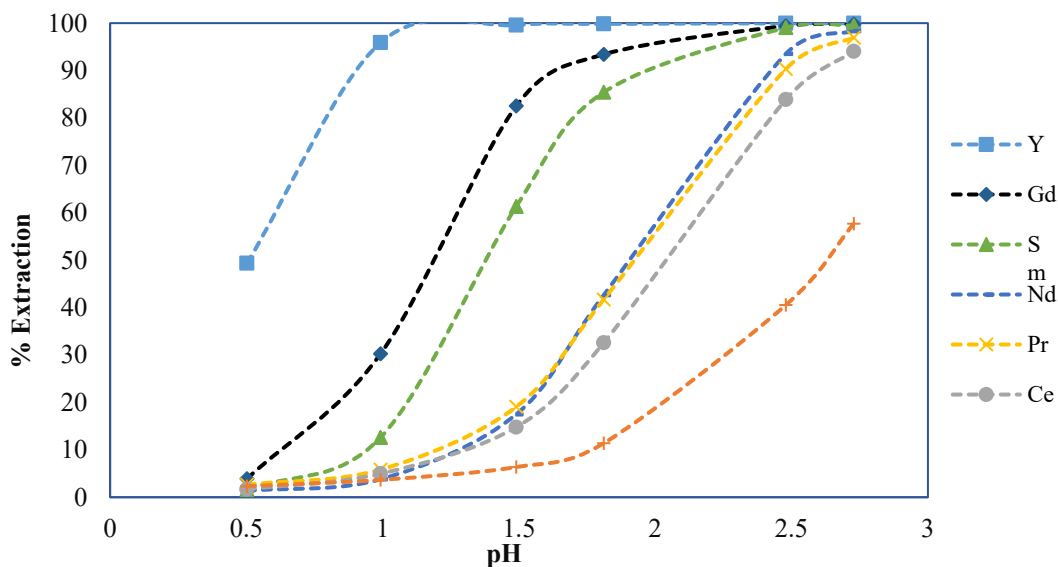


Figure 5.1: Equilibrium isotherm for loading showing percent extraction of REEs at different pH's and phase ratio 1

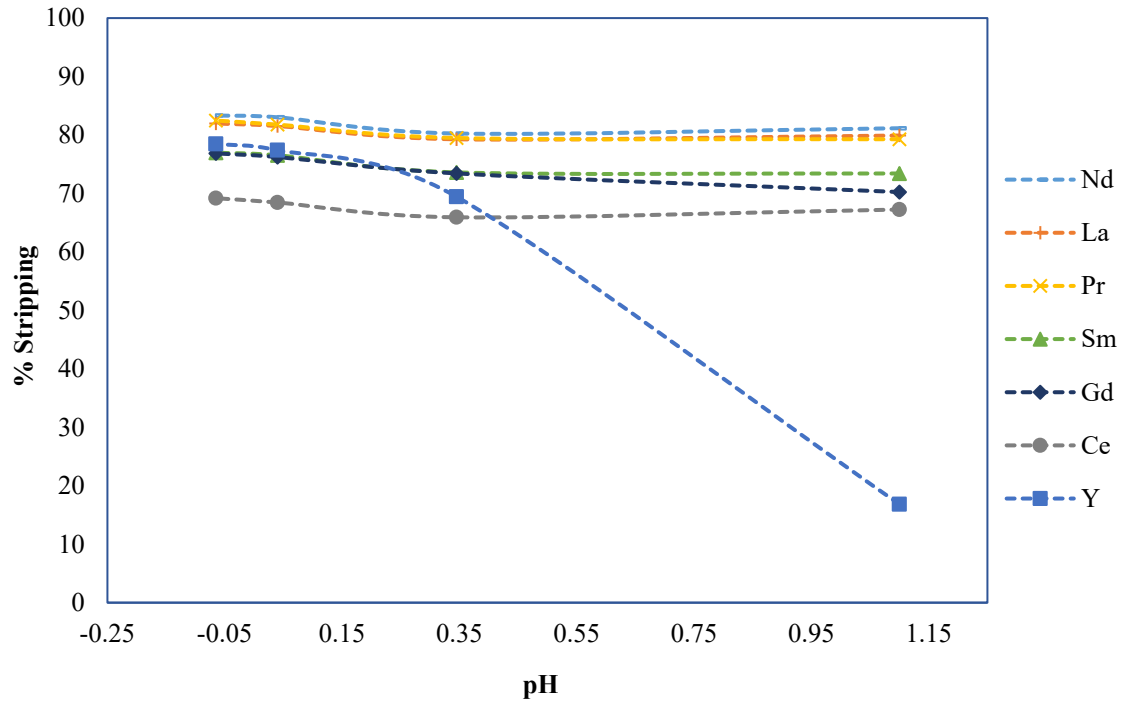


Figure 5.2: Equilibrium isotherm for scrubbing & stripping at a phase ratio of 1

The separation factor, defined as the ratio of percent extraction between element pairs was evaluated using Eq. 5.1 at various equilibrium pH to compare separability. Traditional methods for base metal separation using SX use the separation factor as a criterion for selecting pH. The pH resulting in a high separation factor are preferred to perform the phase ratio experiment.

$$S_{A/B} = \frac{E_A}{E_B} \quad 5.1$$

where E_A and E_B represents the percent extraction of the element A and B at a given phase ratio and $S_{A/B}$ the separation factor.

Table 5.1: Separation factor between element pair at different solution pH values used for extraction

pH	Y/Gd	Gd/Sm	Sm/Nd	Nd/Pr	Pr/Ce	Ce/La
0.50	12.68	2.43	1.19	0.51	1.58	0.72
0.99	3.17	2.40	3.32	0.65	1.17	1.35
1.49	1.21	1.35	3.51	0.92	1.29	2.32
1.81	1.07	1.09	2.00	1.02	1.28	2.86
2.48	1.01	1.00	1.06	1.04	1.08	2.07
2.73	1.00	1.00	1.01	1.01	1.03	1.63
Maximum	12.68	2.43	3.51	1.04	1.58	2.86
Minimum	1.00	1.03	0.51	1.01	1.00	1.00

Table 5.2: Separation factor between element pair at different pH values used for stripping

pH	Ce/Y	Gd/Ce	Sm/Gd	Pr/Sm	La/Pr	Nd/La
1.10	3.99	1.04	1.05	1.08	1.01	1.02
0.35	0.95	1.11	1.00	1.08	1.00	1.01
0.04	0.88	1.11	1.00	1.07	1.00	1.02
-0.07	0.88	1.11	1.00	1.07	0.99	1.02
Maximum	3.99	1.11	1.05	1.08	1.01	1.02
Minimum	0.88	1.04	1.00	1.07	0.99	1.01

Figure 5.3 shows the conceptual separation route developed utilizing the separation factor of the REEs summarized in Table 5.1. The route was developed by identifying pH resulting in high separation factors between adjacent elements in equilibrium isotherm. Thus, Y was separated first at pH 0.5 based on high separation factor of 12.68 between the Y/Gd pair. The process was followed for the next adjacent pair until all the elements were separated from one another. For Nd/Pr which had low separation factor and values close to 1, no separation is possible between the two. Hence following path 1 and 2 in Figure 5.3 Nd and Pr were extracted together. Following this approach, it should be possible to separate Y, Gd, Sm, Ce, and La from the mixture. However, this approach does not reflect true separation as it does not quantify the level of separation achieved and the separation effect in an integrated process.

Another the limitation of using the separation factor to develop flowsheet is that it does not account for separation effects due to feed distribution or concentration in a multi-component system. For example, a feed component, despite showing a high separation factor with other components, may be extracted in considerable amounts if it is present in a major proportion in the feed. In addition, the separation factor can sometimes misrepresent the actual separation between two elements, as in case of Gd/Sm or Pr/Ce pair at pH 0.5, shown in Table 5.1, which indicates high separation factors of 2.43 and 1.58, respectively. However, it can be seen from percent extraction plot in Figure 5.1 that actual extraction of both the elements is small. Hence, a complete evaluation of separation between the elements encompassing pH and feed composition effects is required. Simulation studies are useful in analyzing processes by incorporating all parameters affecting the process. The effect of a particular variable on process can be studied by simulating it in a given range and monitoring the necessary output, this method is called as sensitivity analysis. Hence, to study the effect of pH on separation by incorporating feed composition simulation of a SX train and sensitivity analysis with pH can be applied. Hence, simulation of rare earth SX equilibrium process was approached by modeling extraction behavior by utilizing the results from phase 1 experiments.

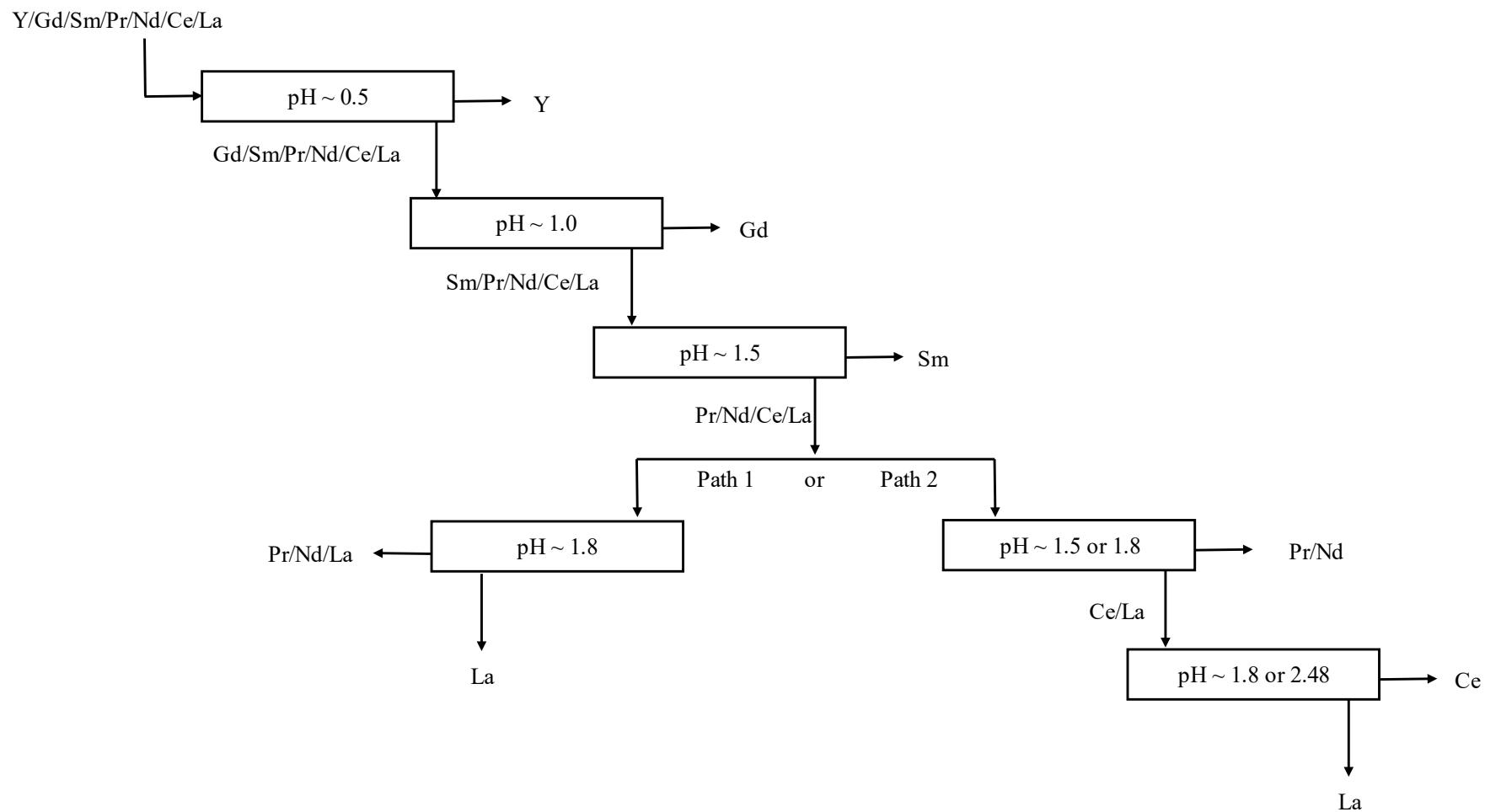


Figure 5.3 Separation route based on separation factor between the elements

The experimental results from the pH study were used to evaluate distribution ratios using Eq. 3.7. The ratios evaluated were log-transformed and plotted with respect to pH. The reason for logarithmic transformation and plotting was to compare whether distribution ratios, like the distribution coefficient as described by Eq. 3.6, follow a linear trend with discrete and integer values of the stoichiometric coefficient associated with H^+ . However, a nonlinear relationship was observed and a polynomial of order two resulted in a better fit for all the elements, as shown in Figure 5.4. The nonlinear behavior suggests the existence of a multiple ionic states of elements occurring in solution. A single ionic state would have resulted in linear relationship, making the distribution ratio and distribution coefficient equal.

The general form of the equation obtained from distribution ratio polynomial fitting can be expressed as:

$$\log D_i = a(\text{pH})^2 + b \text{ pH} + c \quad 5.2$$

where a, b, and c are the model parameters obtained from polynomial fitting. Table 5.3 summarizes the polynomial parameters for each of the REEs found in Figure 5.4.

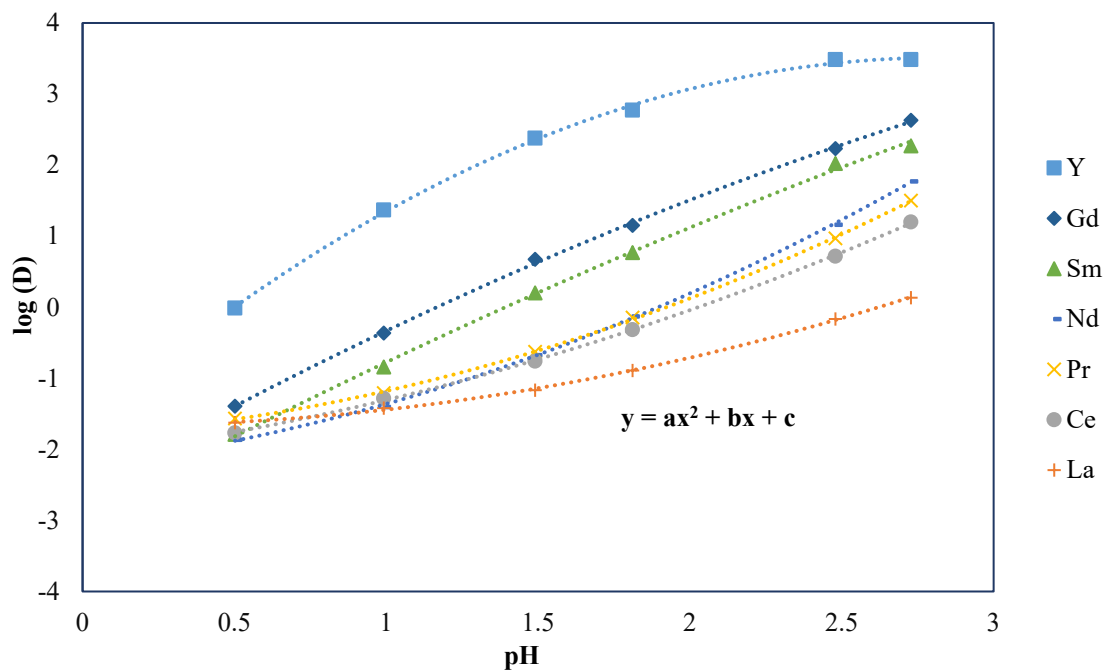


Figure 5.4: Plot of log tranformed distribution ratio with pH for loading of REEs

Table 5.3: Model parameters for distribution ratio and pH - loading

Element	a	b	c	R-squared
Y	-0.65	3.67	-1.67	0.999
La	0.25	-0.03	-1.66	0.999
Ce	0.24	0.54	-2.09	0.997
Pr	0.34	0.30	-1.81	1.000
Nd	0.34	0.52	-2.23	1.000
Sm	-0.13	2.29	-2.93	0.999
Gd	-0.19	2.41	-2.55	0.995

The process was repeated for the stripping distribution data, which is shown in Figure 5.5.

The parameters of the polynomial for stripping have been summarized in Table 5.4.

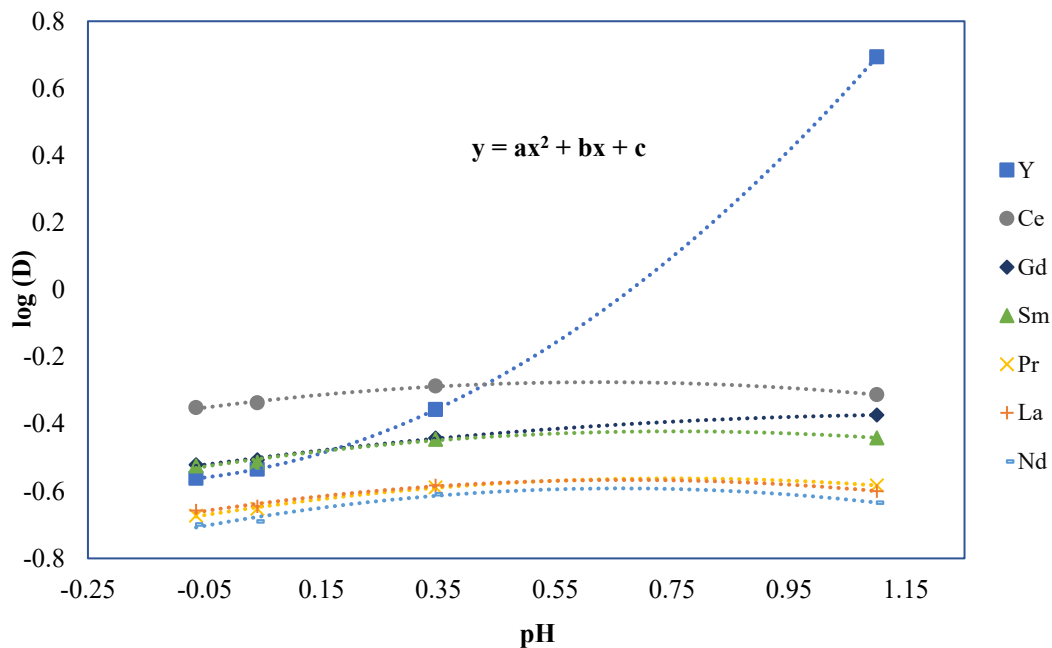


Figure 5.5: Distribution ratio as a function of pH – stripping

Table 5.4: Model parameters for distribution ratio and pH - stripping

Element	a	b	c	R-squared
Y	0.76	0.29	-0.55	1.000
La	-0.18	0.24	-0.65	0.975
Ce	-0.17	0.21	-0.34	0.987
Pr	-0.17	0.26	-0.66	0.996
Nd	-0.22	0.29	-0.69	0.953
Sm	-0.09	0.22	-0.51	0.997
Gd	-0.09	0.22	-0.51	0.997

5.2 MULTI-STAGE PROCESS MODELING

After the extraction and stripping distribution ratio modeling, its application was extended to a multi-stage counter-current SX process (train) involving loading, scrubbing, and stripping processes, as shown in Figure 5.6. The goal was to simulate an SX train at different loading pH and identify equilibrium pH resulting in high concentration and potential separation of elements present in the feed when processed through a continuous SX train. The scrubbing process in the train can be regarded as an extension of stripping process operated at lower flowrates and, hence, stripping models can be utilized for simulating scrubbing process. Although, in the current analysis scrubbing was not incorporated, the goal was to study effect of pH on loading. The fundamental approach of mass balance described using Eq 5.3 was utilized in developing process models to estimate the concentration of elements in organic and aqueous phases from every stage. Figure 5.7 shows a typical single stage of an SX counter-current process with the organic flowing in the opposite direction to the aqueous phase. X's and Y's followed by subscripts are the concentration of element i in the aqueous and organic solutions, respectively, and j indicates the stage number with values ranging from 1 to n. O and A are the organic and aqueous volumetric flow rates. Equation 5.3 shows the mathematical representation of the mass balance across a single stage.

$$OY_{i,j-1} + AX_{i,j+1} = OY_{i,j} + AX_{i,j} \quad 5.3$$

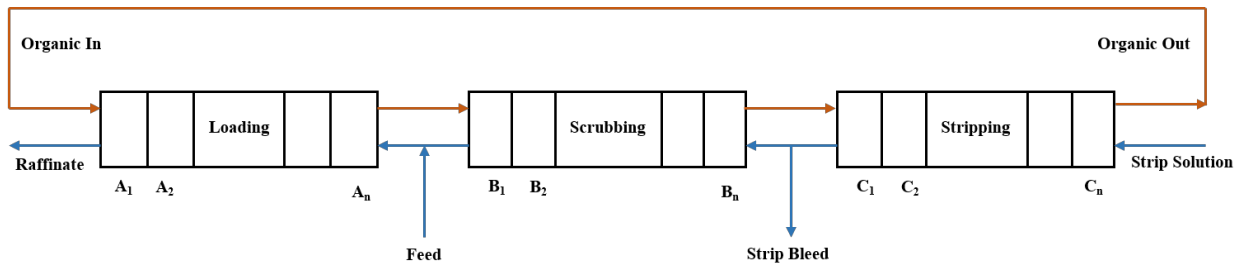


Figure 5.6: Multi-Stage SX-Train



Figure 5.7: Mass balance of a species i for stage j

The relationship assumes steady-state equilibrium, implying no accumulation of material is taking place within the stage. Another attribute of Eq. 5.3 is that it is a six-variable equation with four concentration and two flowrate variables. The flowrate and input concentration are usually known or assumed when designing a process (O , A , X_{j+1} , Y_{j-1}). Substituting known variables (O , A , X_{j+1} , Y_{j-1}) reduces the dimensionality of Eq. 5.3 to two, still unsolvable and requiring separation information. This is where information related to the distribution ratio of elements becomes functional. Substituting the expression of the distribution ratio as the metal concentration in organic to aqueous phases, shown in Eq. 5.4 to Eq.5.3, transforms equations in terms concentration of metal in organic phase, resulting in a form shown in Eq. 5.5.

$$D_{i,j} = \frac{Y_{i,j}}{X_{i,j}} \text{ or } X_{i,j} = \frac{Y_{i,j}}{D_{i,j}} \quad 5.4$$

$$OY_{i,j-1} - \left(O + \frac{A}{D_{i,j}}\right) Y_{i,j} + A \frac{Y_{i,j+1}}{D_{i,j+1}} = 0 \quad 5.5$$

The process, when applied to all the stages, leads to the formation of a system of simultaneous equations. Thus, for the multi-stage SX train, represented in Figure 5.6, which includes loading, scrubbing, and stripping, the general form of equation for a stage j in each process is given by:

$$OY_{i,j-1} - \left(O + \frac{F+RS}{D_{i,j}}\right)Y_{ij} + (F+RS) \frac{Y_{j+1}}{D_{j+1}} = 0 \quad \text{Loading} \quad 5.6$$

$$OY_{i,j-1} - \left(O + \frac{RS}{D_{i,j}}\right)Y_{ij} + RS \frac{Y_{j+1}}{D_{j+1}} = 0 \quad \text{Scrubbing} \quad 5.7$$

$$OY_{i,j-1} - \left(O + \frac{S}{D_{i,j}}\right)Y_{ij} + S \frac{Y_{j+1}}{D_{j+1}} = 0 \quad \text{Stripping} \quad 5.8$$

where, F represents the feed flowrate, S the strip solution flowrate, and R as the reflux ratio; defined as a fraction of the strip solution circulated to scrubbing stage. The number of equations for the processes (SX-train) will depend upon the total number of stages. Thus, for n_1 loading, n_2 scrubbing and n_3 stripping, stages of the system of equations can be formulated and solved to evaluate the concentration of species in the organic phase. A typical example of a system equation matrix for single a rare earth is shown in Figure 5.8. 'O' in Figure 5.8, represents the organic flow rate, whereas ϕ indicates zero, and all the other variables follow the same nomenclature as used in equations 5.5 - 5.8.

$$\begin{bmatrix}
-\left(O + \frac{SR+F}{D_{i,1A}}\right) \frac{(SR+F)}{D_{i,A}} & 0 & 0 & 0 & 0 & 0 & 0 & 0 & 1 \\
0 & \searrow & \searrow & 0 & 0 & 0 & 0 & 0 & 0 \\
0 & 0 & \searrow & \frac{SR}{D_{i,B}} & 0 & 0 & 0 & 0 & 0 \\
0 & 0 & 0 & -\left(O + \frac{RS}{D_{i,B}}\right) \frac{SR}{D_{i,B}} & 0 & 0 & 0 & 0 & 0 \\
0 & 0 & 0 & 0 & \searrow & \searrow & 0 & 0 & 0 \\
0 & 0 & 0 & 0 & 0 & \searrow & \frac{SR}{D_{i,C}} & 0 & 0 \\
0 & 0 & 0 & 0 & 0 & 0 & -\left(O + \frac{S}{D_{i,C}}\right) \frac{S}{D_{i,C}} & 0 & 0 \\
0 & 0 & 0 & 0 & 0 & 0 & 0 & \searrow & \searrow \\
0 & 0 & 0 & 0 & 0 & 0 & 0 & 0 & \searrow
\end{bmatrix}
\cdot
\begin{bmatrix}
Y_{i,1A} \\
Y_{i,2A} \\
Y_{i,3A} \\
Y_{i,1B} \\
Y_{i,2B} \\
Y_{i,3B} \\
Y_{i,1C} \\
Y_{i,2C} \\
Y_{i,3C}
\end{bmatrix}
=
\begin{bmatrix}
0 \\
0 \\
-X_{i,F} \\
0 \\
0 \\
0 \\
0 \\
0 \\
X_{i,SS}
\end{bmatrix}$$

Figure 5.8: System equation matrix for a REE

Solving the above system of equations for different extraction pH, stripping pH, and multiple elements can be cumbersome, hence, a Matlab application was developed to solve the system of linear simultaneous equations. The application computed the concentration of metals in the organic phase and aqueous phase, respectively, for a given set of feed conditions, and it had features to compare the extraction performance by evaluating purity. However, the current model is limited to simulate separation condition involving phase ratio of 1 as it is derived from experimental results conducted at fixed phase ratio.

Figure 5.9 shows the application interface where entries relating to components present in the feed and their associated model parameter for loading and stripping can be entered. The user can enter the element name, feed distribution, and regression coefficients listed in Table 5.3. These entries constitute the distribution ratio model in background and predict distribution ratios ($D_{i,j}$) during simulation. Adjacent to the component description were design variables entries, where stage configuration for an SX train depicted in Figure 5.6 is provided this include number of loading, scrubbing, and stripping stage. Finally, the flow variables for aqueous feed (F), organic flowrate (O), strip solution (S), and reflux (R) are provided in the fillable entries.

The application functions by clicking the calculate tab, which then starts developing the component matrix, iteratively based on the number of stages and elements present in the feed mixtures (Figure 5.8). Thus, a three-dimensional component matrix is created, the rows and columns of which are determined by the total number of stages and number of components determine the layer or size in third dimension. The matrix is then solved for every component (Y_{ij}) to determine the stagewise concentration in the organic phase. Additional features for performing the sensitivity analysis with pH and flowrates were also added to the application as iteration tabs. The iteration tab worked by simulating the SX-train with respect to the variable listed on the tab by constantly updating after each iteration by introducing step change. In the case of pH, a step change of 0.1 was made after each iteration. Sensitivity analysis is useful in understanding the effect of variables on the separation of metal. For SX -train the effect of pH on purity of elements was required at fixed composition. This would provide an insight on how separation is affected from an integrated process involving loading, scrubbing, and stripping accounting distribution of elements in feed.

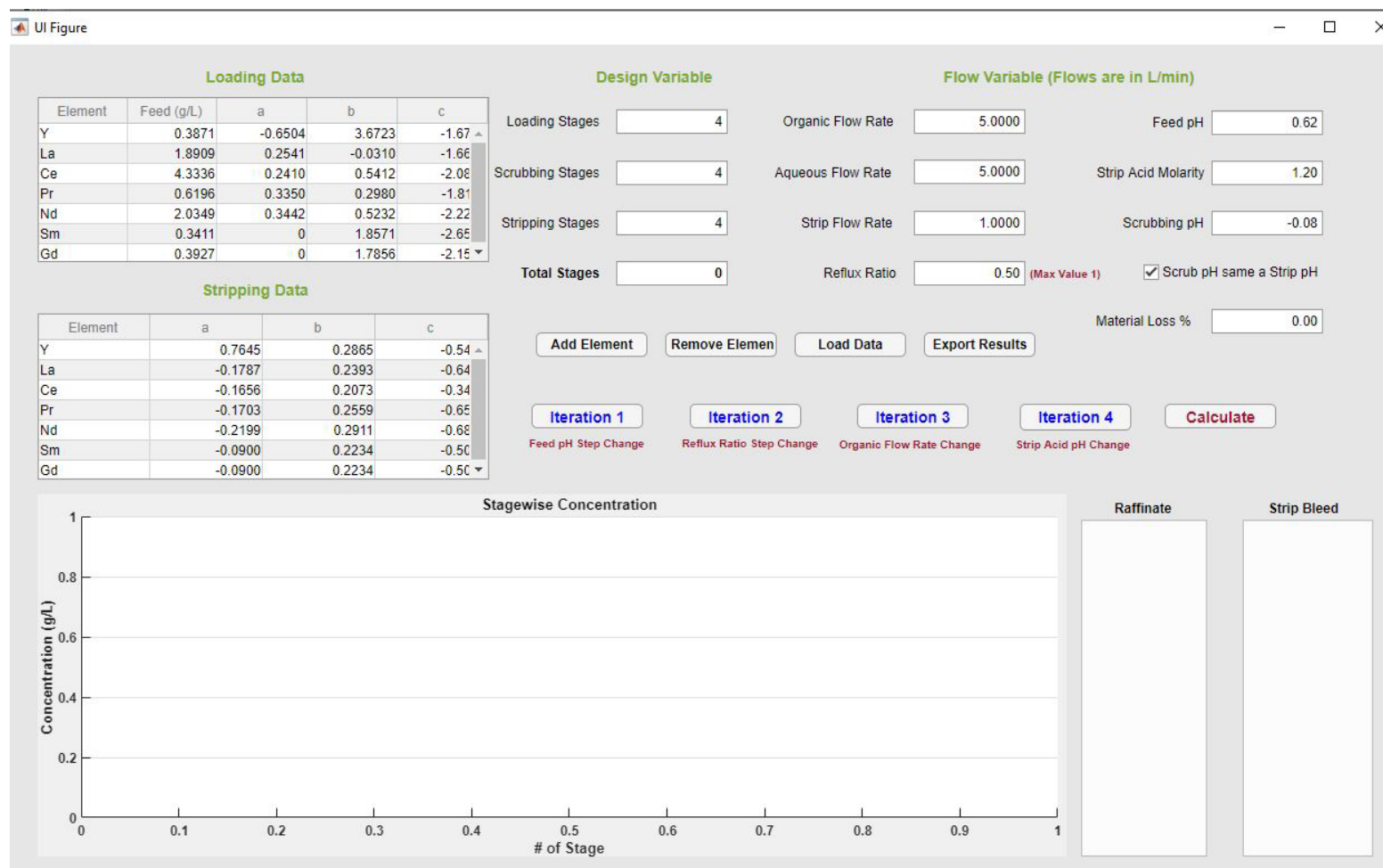


Figure 5.9: Matlab application interface for SX train

5.3 SIMULATION

The developed Matlab application was set up to simulate a SX train by importing the feed composition data and model parameters of the distribution ratios (Table 4.2, Table 5.3, and Table 5.4). To assess the performance of separation, a variable called the “purity factor” was defined as the ratio of concentration of an element of interest to total concentration of all elements in the given stream (strip bleed or raffinate), expressed as a percent. Eq. 5.9 represents the mathematical formulation of the purity factor:

$$P_i = \frac{[M]_i}{\sum_{i=1}^n [M]_i} * 100 \quad 5.9$$

where, P_i is the purification factor of metal i , M_i represents the concentration of metal of interest i in the given stream, and n the number of metal species present in the stream.

The simulation required information on design and operating conditions. The design conditions consisted of a number of stage combinations in loading, scrubbing, and stripping processes, whereas operating conditions was comprised of flowrates of various streams. An initial stage combination of 3-0-1 (loading-scrubbing-stripping) was selected, and other stage combinations were also simulated to see if stage combination had any effect at this point. The goal was not to determine stage combinations, but rather to study the separation of elements when the SX train operates at different loading pH. The reason the models cannot be utilized for stage determination is that they do not account for the changes in distribution ratio due to phase ratio, which is critical in stage determination (Eq. 5.6 - 5.8). The flowrates of organic, feed, and strip streams for the simulation were derived by assigning an initial flowrate of 5 lpm to the organic stream, and the rest were derived from organic flowrate to maintain a phase ratio of 1 in the loading and stripping processes (Table 5.5).

Table 5.5: Parameters used for simulation

Operating Parameters	Value
Loading-Scrubbing-Stripping	3-0-1
Organic Flowrate (lpm)	5
Aqueous Flowrate (lpm)	5
Strip Flowrate (lpm)	5
Initial Strip Acid Concentration	0.707 M (corresponds to equilibrium pH of 0.15)

The simulation run was performed by entering the parameters in the application and varying the equilibrium pH of the system from 0.5 to 2.75. The results indicated a high purity (or concentration) of yttrium in the strip bleed stream when extraction pH was between 0.5 and 1.0. The optimum equilibrium pH for the separation of yttrium was found to be in the range of 0.6-0.7 (avg. 0.65) (Figure 5.10). Small peaks of gadolinium and samarium were also observed at pH 1.3 and 1.5, indicating a concentrating effect of both elements in the strip bleed. Similarly, a moderate concentration of neodymium and cerium were noted for equilibrium extraction when pH is greater than 1.5, with the highest value at an equilibrium pH of 2.2. Despite the difficult separability of neodymium and praseodymium for the given extractant scheme, as shown in Figure 5.1, the simulation showed greater purity of neodymium and cerium compared to other elements. The reason for such behavior is the separation is not only influenced by extraction pH, but the composition of the feed also dictates the resulting product. The feed contained a significantly low concentration of praseodymium; hence, it does not have a significant impact on purity despite being extracted with neodymium.

The simulation was also performed by varying the stage number to ascertain whether the pH effect is unique to the number of stages utilized. Hence a different stage combination with an increased loading stage of 6-0-1 (loading-scrubbing-stripping) was simulated with varying pH. With the change in the loading stage, there was a minor shift (increase) in the

purity curves along the y-axis, but no lateral shift was observed Figure 5.11. Similar observations were made by increasing the stripping stage to 3-0-2 (load-scrub-strip), as shown in Figure 5.12, but there was no or minor shift in purity curves along the x-axis. Changing the stage number only increased the concentration in the strip bleed stream without significantly changing the relative concentration of the elements.

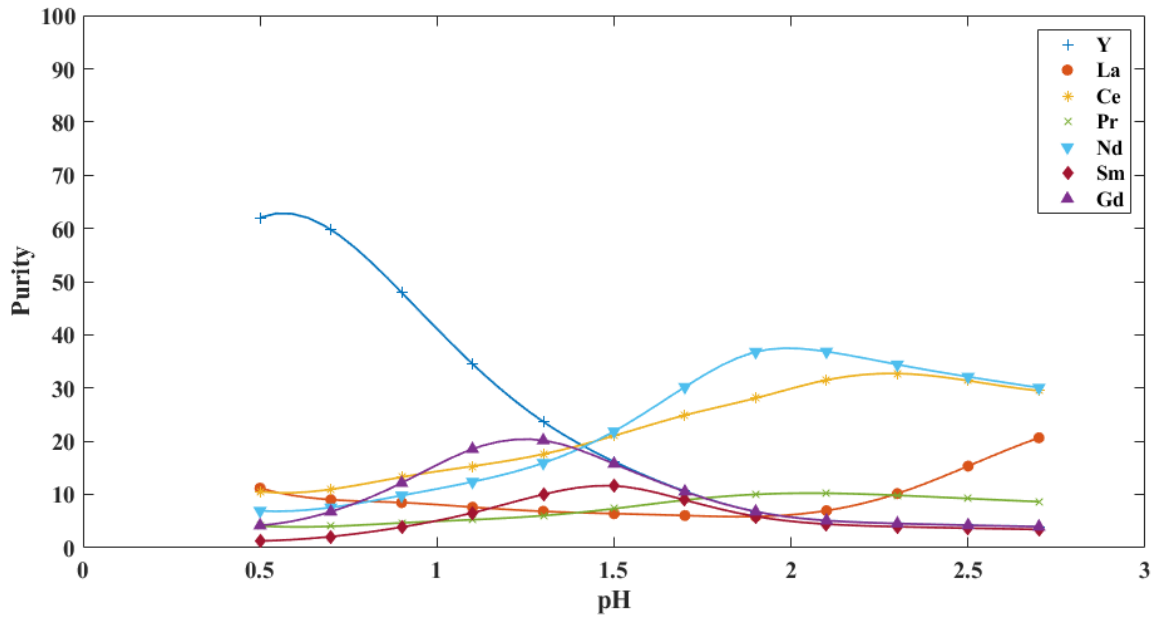


Figure 5.10: Purity in strip bleed stream at different equilibrium pH

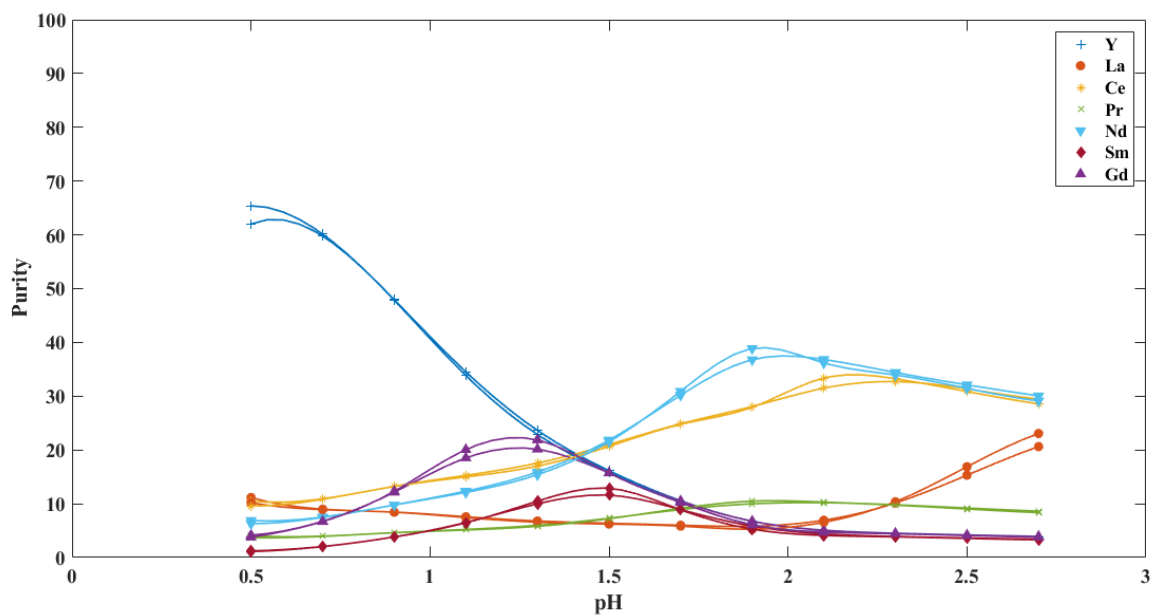


Figure 5.11: : Purity in strip bleed stream at different equilibrium pH for 3-0-1 and 6-0-1 stage combination

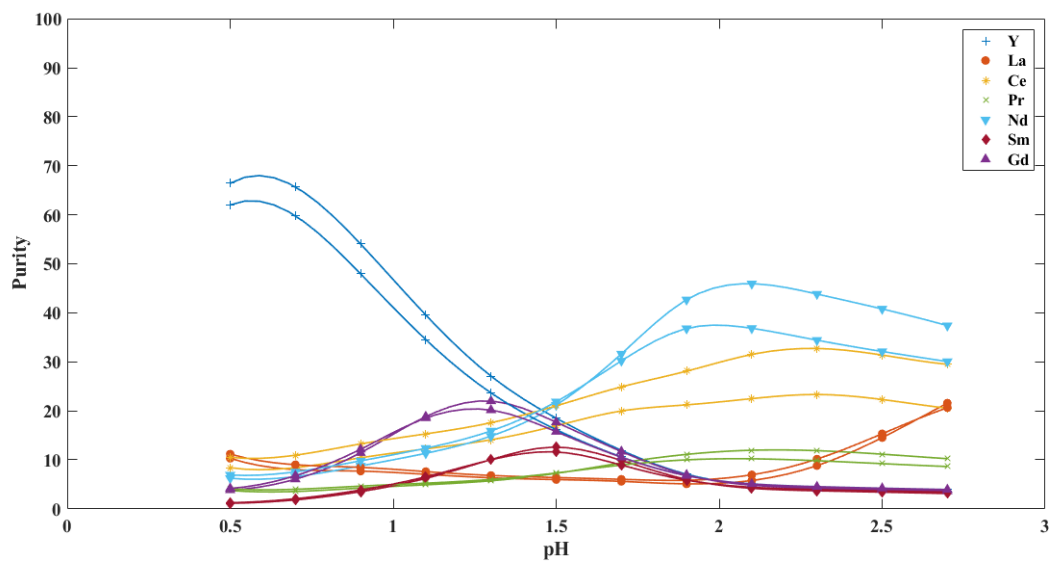


Figure 5.12: Purity in strip bleed stream at different equilibrium pH for 3-0-1 and 3-0-2 stage combination

Thus, based on the following analysis, a conceptual separation scheme was proposed to separate elements individually or in groups. Figure 5.13 shows the proposed separation scheme, in which yttrium from the feed mixture can be separated at pH 0.65 because of its high purity in the strip bleed determined from concentration peaks (Figure 5.10- Figure 5.12). However, the combined separation of gadolinium and samarium is indicated because of low purity peaks, and the small difference in pH between the peaks indicated difficult separability. Similarly, praseodymium, neodymium, and cerium are in moderate purity at pH 2.2 compared to La, which has significantly low purity, hence, it can be separated from the group.

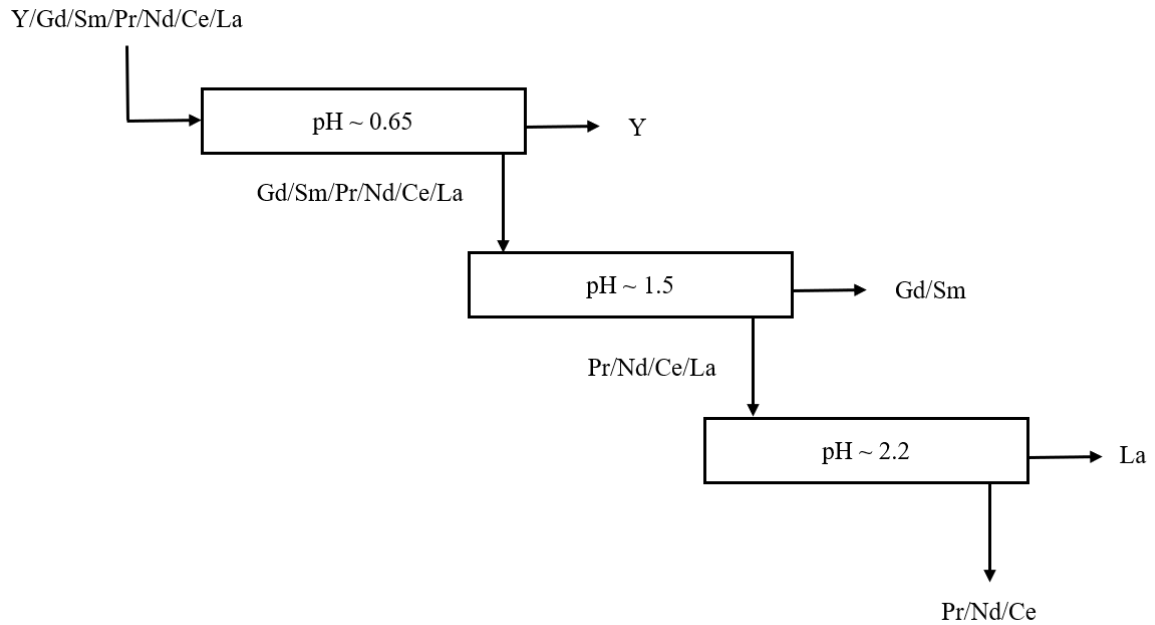


Figure 5.13: Conceptual separation hierarchy

The above analysis was performed by keeping phase ratios constant. However, as discussed in Section 3.2, the extraction behavior of elements is dependent upon the phase ratio. Different phase ratios result in different concentrations of available extractant, thereby altering the extraction characteristics of elements. For the following reason, the study of the phase ratio is included in the design of the SX process. Generally, the phase ratio tests are performed at fixed equilibrium pH, however due numerous pH possibilities it becomes

difficult to select pH to perform phase ratio experiments. The simulation study from this chapter was useful in identifying specific pH points as a way of minimizing the number of pH specific tests compared to large design space shown in Figure 3.7. The pH resulting in peak concentration of elements, as shown in Figure 5.10 and leading to the development of conceptual separation chart shown in Figure 5.13, was therefore selected for phase ratio experimentation.

CHAPTER 6. DISTRIBUTION ISOTHERM

6.1 EXPERIMENTAL RESULTS

The effect of the organic-aqueous phase ratio was studied at three identified equilibrium pH, as determined in the last chapter (Figure 5.13). Table 6.1 lists the target average equilibrium pH values along with measured value of equilibrium pH and associated standard deviations at which the phase ratio experiments were conducted. The pH 0.65 was selected to separate yttrium from the feed mixture. pH 1.5 was chosen for the combined separation of gadolinium and samarium and pH 2.2 for the extraction and separation of cerium, neodymium, and lanthanum (see Figure 5.13).

Table 6.1: pH for distribution isotherm

Targeted equilibrium pH	Average equilibrium pH measured	Standard deviation in measured pH
0.65	0.659	0.003
1.5	1.523	0.014
2.2	2.234	0.028

The results from the phase ratio experiments performed at pH 0.65 indicated yttrium as the only metal extracted in appreciable quantities, whereas extraction of other elements was negligible. Figure 6.1 shows a percent extraction plot of yttrium at different O/A ratios. It can be seen from the plot that 100 percent extraction was not achieved, even at higher O/A ratios, but it was anticipated with the use of multiple stages that a majority of yttrium could be recovered. Also, it would be preferable to utilize low phase ratios as separation conditions to prevent the coextraction of other elements. This is due to the fact that despite having small percent extractions of undesired components their presence in greater proportion be detrimental to the purity of yttrium produced.

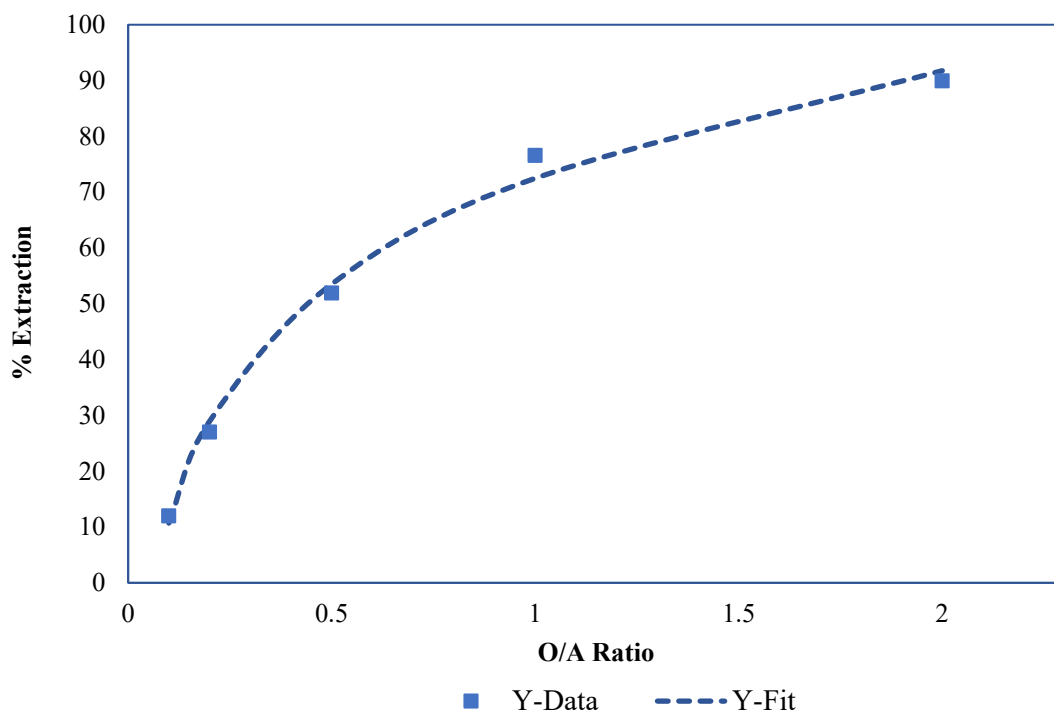


Figure 6.1: Percent Extraction vs O/A Ratio at pH 0.65

At pH 1.52, the extraction of the other components present in the feed increased, confirming the pH dependence of the SX process (Figure 6.2). However, with the increase in phase ratios, a significant increase in extraction for all elements was observed. The extraction at low phase ratios was prominent for yttrium, gadolinium, and samarium, whereas at higher ratios all elements showed improved extraction. The extraction differences of gadolinium and samarium from other elements at low phase ratios can be utilized in separation from other elements, provided the yttrium has been removed. In addition, the separation difference between gadolinium and samarium was also greater at low ratios, favoring separation between them.

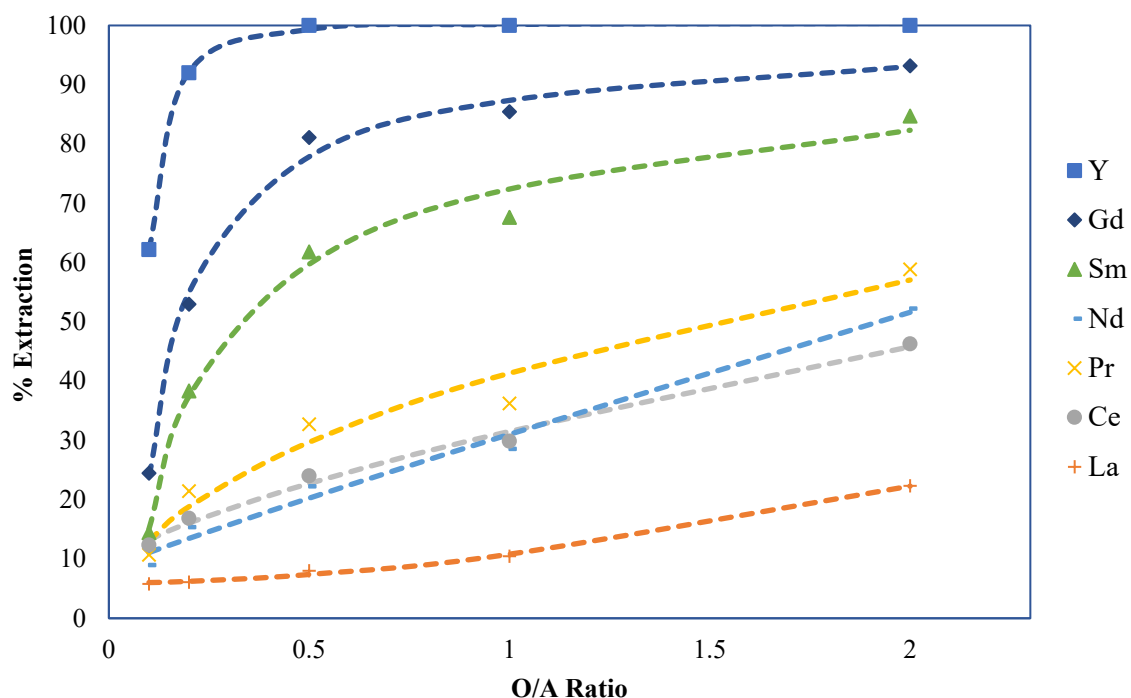


Figure 6.2: Percent Extraction vs O/A Ratio at pH 1.52

Similarly, Figure 6.3 shows percent extraction as a function of O/A ratio at an equilibrium pH of 2.23. As expected, the extraction of all the elements increased considerably, and similar to previous cases, the extraction differential was higher at low phase ratios, which narrowed as the ratio increased. pH 2.23 is important for the separation of neodymium and cerium from the lanthanum, as all three elements are major components in the feed with very close separation curves. Hence, the separation factor was evaluated, in order to identify a suitable phase ratio for flowsheet design (Eq. 5.1). Table 6.2 and Table 6.3 lists the separation factors for both cases.

For combined extraction of gadolinium and samarium from neodymium and other low extracting elements, the separation factor of Sm/Nd should be examined because of their extraction order. Thus, one can see at pH 1.5, an O/A ratio of 0.5 will result in a better separation from neodymium (Table 6.2). Similarly, for the separation of gadolinium and samarium, the O/A ratio of 0.1 at pH 1.5 can be utilized.

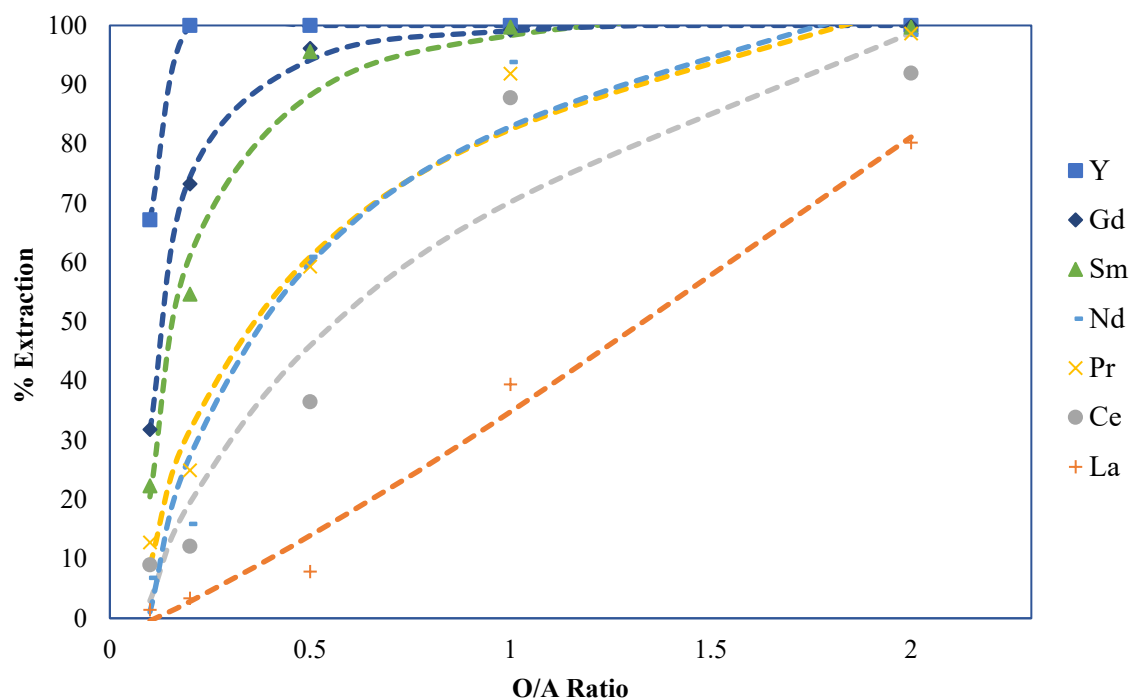


Figure 6.3: Percent Extraction vs O/A Ratio at pH 2.2

Table 6.2: Separation factor for element pairs at pH 1.52

O/A Ratio	Y/Gd	Gd/Sm	Sm/Nd	Nd/Pr	Pr/Ce	Ce/La
0.1	2.54	1.69	1.61	0.84	0.87	2.13
0.2	1.74	1.38	2.49	0.72	1.27	2.76
0.5	1.23	1.31	2.78	0.68	1.36	2.99
1	1.17	1.26	2.37	0.79	1.21	2.85
2	1.07	1.10	1.62	0.89	1.27	2.07
Maximum	2.54	1.69	2.78	0.89	1.36	2.99
Minimum	1.07	1.10	1.62	0.68	1.21	2.07

Table 6.3: Separation factor for element pairs at pH 2.23

O/A Ratio	Y/Gd	Gd/Sm	Sm/Nd	Nd/Pr	Pr/Ce	Nd/Ce	Ce/La
0.1	2.11	1.43	3.27	0.53	1.42	0.76	6.29
0.2	1.36	1.34	3.43	0.64	2.05	1.31	3.59
0.5	1.04	1.01	1.57	1.03	1.62	1.67	4.64
1	1.01	0.99	1.06	1.02	1.05	1.07	2.22
2	1.00	1.00	1.01	1.00	1.07	1.07	1.15
Maximum	2.11	1.43	3.43	1.03	2.05	1.67	6.29
Minimum	1.00	0.99	1.01	0.64	1.05	1.07	1.15

Thus, using the inferences from Table 6.2 and Table 6.3, phase ratio conditions of the loading process for the conceptual flowsheet shown in Figure 5.13 were obtained. Thus, a phase ratio of 1 for SX-train-1 and 0.5 for both SX-train-2 and SX-train-3 were selected. Similarly, stripping phase ratio studies were performed at an equilibrium pH of 0.15. The pH 0.15 was selected because percent stripping, when studied with pH, was mostly constant for majority of elements (see Figure 5.2), hence, a higher pH would minimize acid consumption provided percent stripping is constant. Nevertheless, the stripping phase ratio results indicated that percent stripping of elements was constant with changes in O/A ratio (Figure 6.4). Similar observations were made when percent stripping was studied with respect to pH suggesting stripping characteristics are not effected by for this feed composition when stripping equilibrium pH is lower than 0.15 (Figure 5.2). Nevertheless, the experimental study with phase ratios was useful in identifying phase ratio conditions for the proposed conceptual flowsheet shown in Figure 5.13. The flowsheet can be simulated at the identified conditions of pH and phase ratio using the multi-train model to determine the number of stages required for separation.

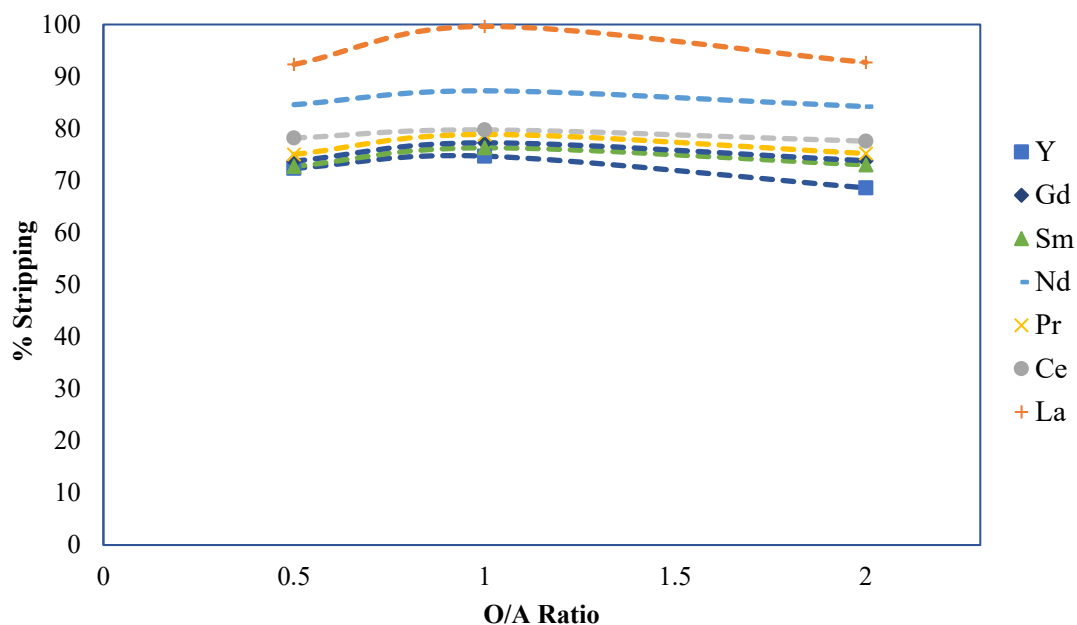


Figure 6.4: Percent Stripping vs O/A Ratio using 1M HCl (0.15 equilibrium pH)

6.1.1 Observance of Saturation Effect

The saturation effect, a common phenomenon observed in continuous industrial SX processes, alters the extraction characteristics of the elements. In industry, the SX processes are operated with aim to utilize maximum extractant by loading organic phase to its maximum capacity; this often results in a contest between similar extracting metal ions in case of the multi-ion system because of less available extractant. During the process due to the selectivity of organic extractant and different affinity of metal ions, certain metal ions replace the less-preferred ions. The effect is more prominent at lower phase-ratio and higher equilibrium pH because of less available extractant and the higher extent of loading in both cases. Saturation effect plays a crucial role in SX towards improving the purity of certain metals present in the system. Hence, it is essential to explore the importance and influence in the extraction process.

For a rare earth system, the extraction preference is given to HREEs, followed by MREEs, and finally LREEs, as mentioned earlier. Thus, elements with higher preference will

replace elements with less extraction potential when the extractant is limited. As the current study was performed on higher concentrations of salt in solution, the saturation effect was observed and accounted for in experimental results. The effects were distinct at an equilibrium pH of 2.2 and higher, and they were viewed from a distribution isotherm plot, showing concentration changes in both phases at different phase ratios. Figure 6.5 and Figure 6.6 show the plot for all elements. It can be seen in Figure 6.5 that, at low phase ratios, the concentration for elements tends to drop. The effect was significant for Nd, Ce, and La because of their large ionic radii, classification as LREEs and presence in high concentration, which led to the shedding of the metal ions back to the aqueous phase, as shown in Figure 6.6. Thus, the saturation effect improves the extraction purity of heavy and middle REEs with smaller ionic radii in the organic phase. When analyzing percent extraction versus phase ratio data, the effect is implicit in the analysis, hence, no separate derivation or method is required to account for the effect.

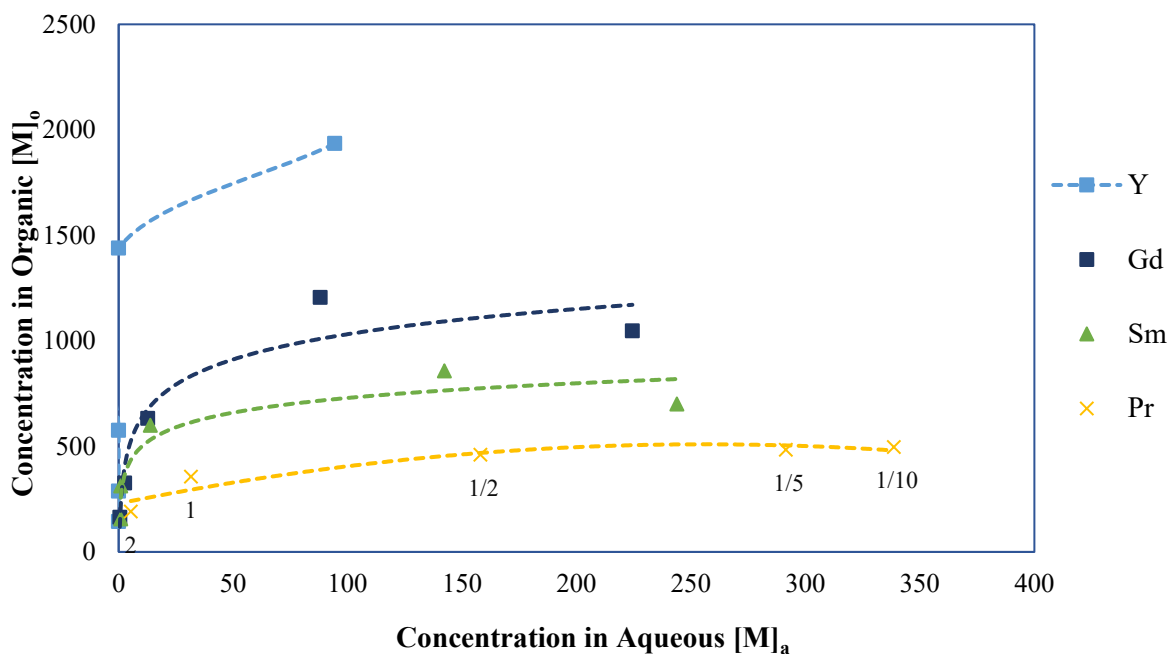


Figure 6.5: Saturation effect at pH 2.2 for Y, Gd, Sm, and Pr

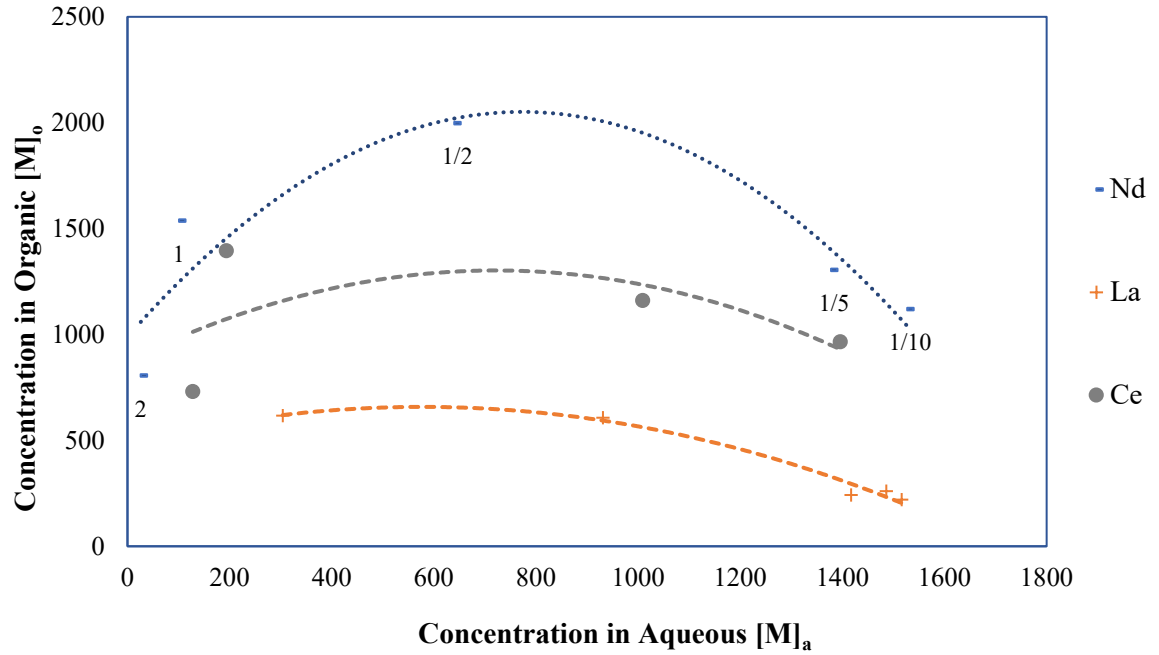


Figure 6.6: Saturation effect at pH 2.2 for Nd, Ce, and La

6.2 MULTI-TRAIN MODEL DEVELOPMENT

Design and simulation of a multi-train SX flowsheet requires the determination of stagewise interphase mass transfer across an SX train for provided separation conditions. The concentration and separation information resulting from the mass transfer of a unit is then utilized by the adjacent units to obtain the overall extraction behavior of a train. Therefore, for an SX process, block representation of a stage describing loading, scrubbing, and stripping process is required. Simulink provides the ability to program models symbolically as a function block. These function blocks can be interconnected with each other to describe any process. For the current study, function blocks for loading, scrubbing, and stripping were developed, which were then interconnected to form an SX train. The individual trains were interconnected to form a multi-train flowsheet design. The following steps were undertaken to develop Simulink function blocks containing SX phase ratio models at defined pH:

- The first step was to develop experimental regression models to describe the percent extraction and stripping with respect to phase ratio and pH. The experimental results were detailed in the previous section;
- The second step was to utilize mass balance stage wise and incorporate the models developed in step 1 to evaluate the transfer of metal in aqueous and organic phases for explicit separation conditions;
- The final step was to develop a library of process unit blocks in Simulink, representing processes such as loading, stripping, SX train, flow mixer, and flow-splitter.

6.2.1 Extraction and Stripping Phase Ratio Model

As a note, the bench-scale extraction data at different phase ratios were shown previously in Figure 6.1, Figure 6.2, and Figure 6.3. The percent extraction was fitted using curve fitting in Matlab to describe extraction with phase ratios. Different non-linear models shown in Table 6.4 were examined, of which power function formed the best extraction relationship determined on the goodness of fit (R^2).

Table 6.4: Functional form explored for curve fitting

Model	Functional form
Polynomial	$y = a.x^2 + b.x + c$
Power	$y = a.x^b + c$
Rational	$y = \frac{a.x+b}{x+d}$
Fourier	$y = a.\cos x.w + b.\sin x.w$
Weibull	$y = a.b.x^{c-1}.exp^{-ax^b}$

The same approach was followed for stripping experimental results shown in Figure 6.4, which were described by linear regression. The method of non-linear least squares was

used as a criterion to determine the goodness of fit and obtain the parameters for the best fit. The mathematical form of the model obtained was:

$$E_{i,j}(x) = a_i(x^{b_i})_{pH1} + c_i \quad 6.1$$

$$S_{i,j}(x) = a_i(x)_{pH1} + b_i \quad 6.2$$

where, $E_{i,j}$ represents the percent extraction to the organic phase of metal; subscripts i and j represent the metal species and stage number; x the organic-aqueous phase ratio at constant equilibrium $pH1$; and a_i , b_i , and c_i represent the model parameters. The same convention follows for Eq. 6.2, with $S_{i,j}$ representing percent stripping of metal from stage j . Table 6.5 lists the model parameters for extraction isotherms.

Table 6.5: Model parameters for extraction

Elements	a	b	c	R ²	Adjusted R ²	Equilibrium pH
Y	1141.29	0.02	-1068.81	0.993	0.987	0.66
Y	-0.23	-2.22	100.40	0.999	0.999	
La	4.87	1.75	5.94	0.997	0.994	
Ce	22.82	0.70	8.70	0.992	0.983	
Pr	44.70	0.44	-3.36	0.961	0.922	1.52
Nd	22.57	0.94	8.46	0.983	0.967	
Sm	-45.70	-0.35	118.10	0.989	0.977	
Gd	-14.30	-0.74	101.67	0.994	0.989	
Y	0.00	-15.07	100.00	1.000	1.000	
La	37.94	1.15	-3.11	0.986	0.972	
Ce	160.41	0.24	-90.20	0.917	0.834	
Pr	-862.16	-0.04	944.61	0.971	0.941	2.23
Nd	-397.83	-0.08	480.77	0.956	0.911	
Sm	-12.29	-0.87	110.61	0.975	0.951	
Gd	-3.21	-1.34	102.30	0.998	0.996	

The developed phase ratio models were utilized in a single-stage function block using steady-state mass balance depicted in Figure 6.7. This method was applied to multiple stages, wherein the stagewise solution from one stage served as the input feed concentration condition to the next (Figure 6.8). X and Y in Figure 6.7 and Figure 6.8 have the same convention of concentration in aqueous and organic phases with the subscript representing the stage number. $E_{i,n}$ in loading represents percent extraction in stage n derived from percent extraction phase ratio model and $S_{i,n}$ indicate percent stripping in stage n derived from percent stripping phase ratio model. For scrubbing, the method developed for stripping was followed, as it is equivalent to the stripping process operating at a low phase ratio.

There was a shift in the utilization of stagewise extraction characteristics in Simulink block model development for the multi-train flowsheet design. Percent extraction and stripping was used in developing a model, unlike distribution ratios that were utilized in the previous chapter: Eq. 5.4. Percent extraction/stripping was used because of mathematical simplicity in terms of scale which percent extraction/stripping offers over distribution ratios. Percent extraction/stripping ranges from 0 to 100, which is easy to analyze and encapsulates flowrates, as it is expressed in terms of mass whereas distribution can range from 0 to any number, making it difficult to analyze because they are expressed in terms of concentration. Nevertheless, both approaches are similar and can be mathematically proven by substituting percent extraction given by Eq. 6.3, instead of the distribution ratio in Eq. 5.3, to solve for concentration in the aqueous stream.

$$E_{i,j} = \frac{O(Y_{i,j} - Y_{i,j-1})}{AX_{i,j+1}} \quad 6.3$$

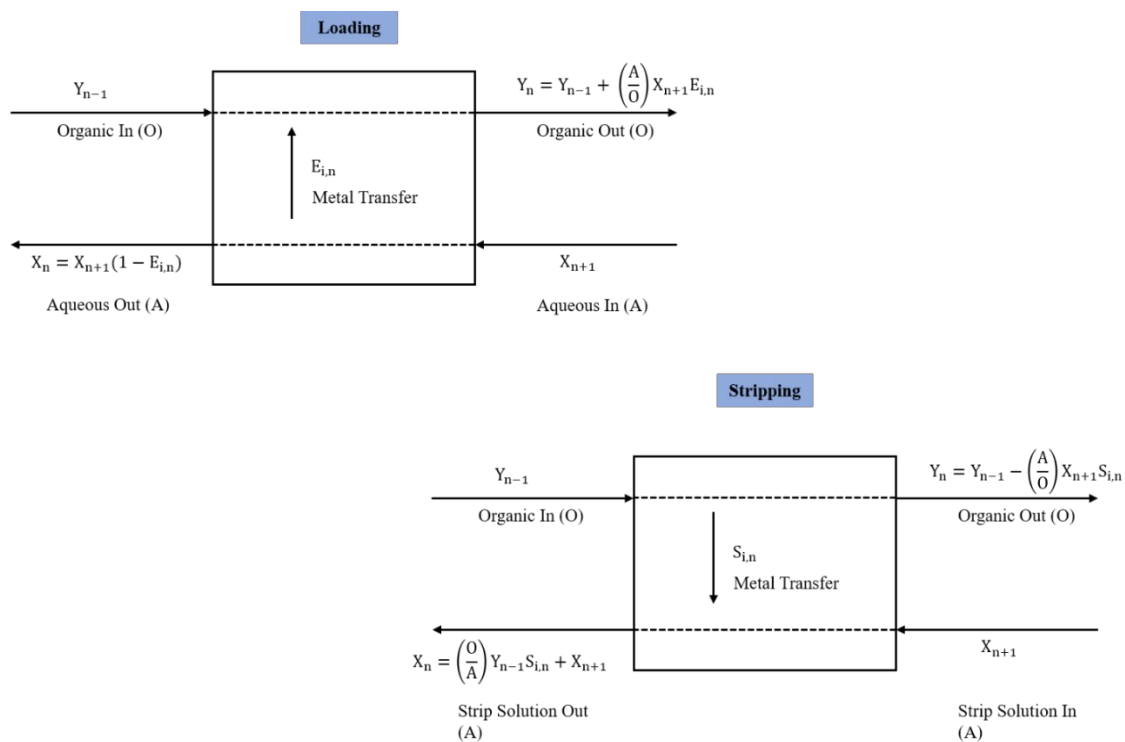


Figure 6.7: Loading and Stripping from a single stage

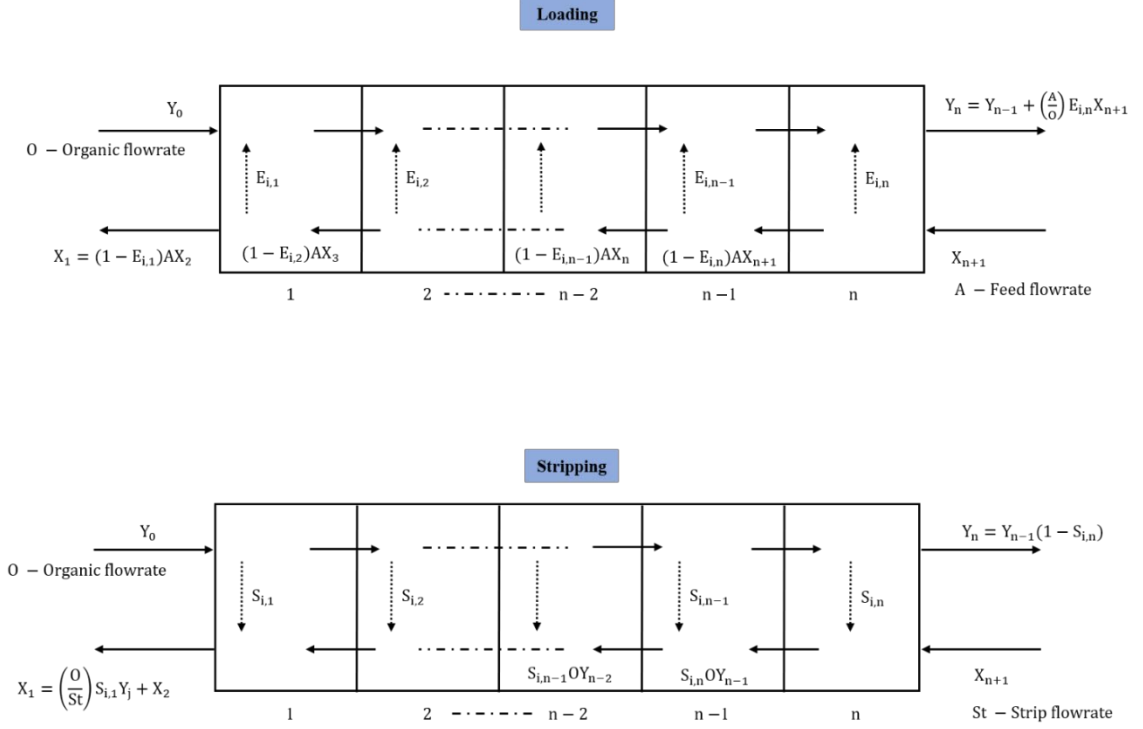


Figure 6.8: Extraction and Stripping from multi-stage loading and stripping process

A general form of the equation to obtain the raffinate and loaded organic concentrations used in a loading process using the method shown in Figure 6.8 is given by:

$$X_1 = X_{n+1}(1 - E_{i,1})(1 - E_{i,2}) \dots (1 - E_{i,n}) \quad 6.4$$

$$Y_n = \left(\frac{A}{O}\right) X_{n+1} [E_{i,n} + E_{i,n-1}(1 - E_{i,n}) + E_{i,n-2}(1 - E_{i,n})(1 - E_{i,n-1}) \dots \dots] + Y_0 \quad 6.5$$

Similarly, for the scrubbing and stripping processes:

$$X_1 = \frac{0}{A} (S_{i,1}Y_0 + S_{i,2}Y_1 + \dots \dots \dots S_{i,n}Y_{n-1}) + X_{n+1} \quad 6.6$$

$$Y_n = Y_1(1 - S_{i,1})(1 - S_{i,2}) \dots (1 - S_{i,n}) \quad 6.7$$

Under the assumption of constant percent extraction in each stage, the Eq 6.4 simplifies to a geometric progression with constant ratio of $E_{i,j}$ which upon solving leads to Kremser's equation discussed in section 2.6.1 (Eq 2.24). Hence, Kremser's equation is a simplified form of Eq 6.4. The limitation of the Kremser method is in applicability in integrated SX process involving loading, scrubbing, and stripping where constant $E_{i,j}$ cannot be assumed between the stages.

6.2.2 Simulink Model Library

Simulink is an application of Matlab widely used for modeling, designing, and simulating steady-state and dynamic processes. It has found wide application in numerous industries such as aerospace, mechanical, and chemical engineering due to its ability to model systems as graphical function blocks (Liu et al., 2004). A function block is essentially a computer program describing a process, and it contains input-output ports to pass inputs and receive processed outputs. Simulink allows features of connecting multiple independent function blocks through signal lines to transfer input-output between other function blocks. The block nature of modeling, and its ability to interconnect multiple blocks, allows for the easy integration of two different processes. Figure 6.9 shows the working of a typical Simulink block, wherein the input information to the block is passed through connected signal lines or provided externally through code.

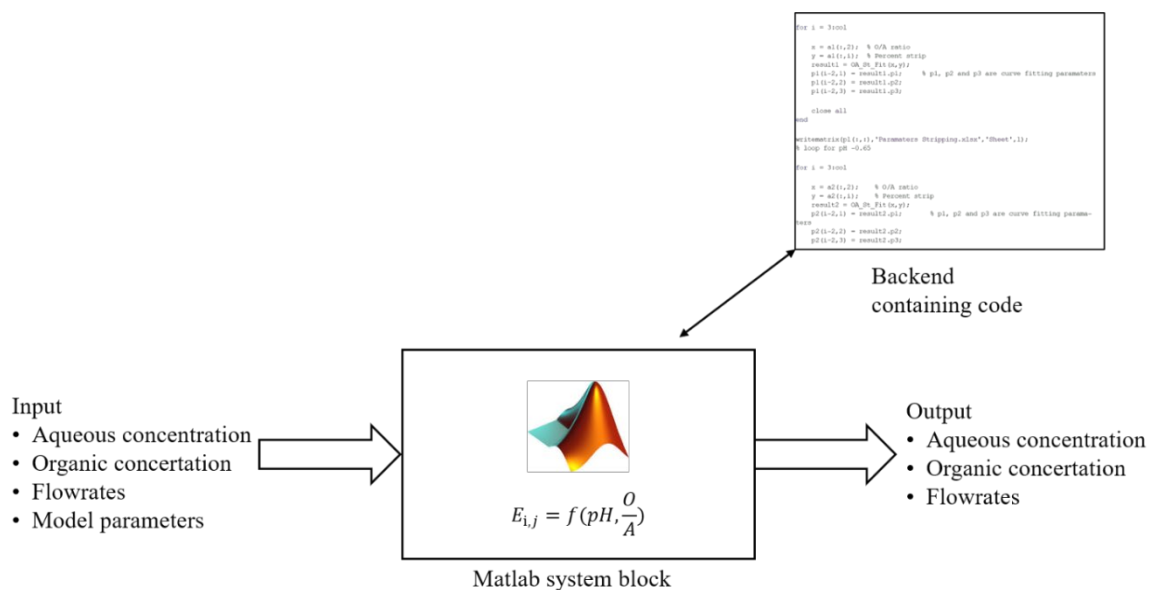


Figure 6.9: Working of a Simulink system block

For the current work of designing a SX flowsheet involving multiple interacting processes, the graphical nature of Simulink is of immense value. SX processes represented as graphical blocks can be easily configured to design and simulate a multiplicity of flowsheets. Signal lines containing organic/aqueous concentration and flowrate information can be used to transfer input-output information between connected blocks. In addition, a function block representation of the SX processes facilitates sub-domain processing, reducing multiple stages to a single programmatic element, allowing the designer to focus on building trains and multi-train elements.

Blocks also improve flowsheet design efficiency because multistage processes are programmed as functions and can be utilized multiple times with updated parameters and conditions. For the following reasons, a graphical block model of different processes was required to simulate an SX flowsheet. The blocks were grouped to form a library and contained process models for loading, scrubbing, stripping, mixer, flow splitters, and useful output variables, such as purity factor and recovery (Figure 6.10). The components of the developed function library for SX processes are discussed in subsequent sections.

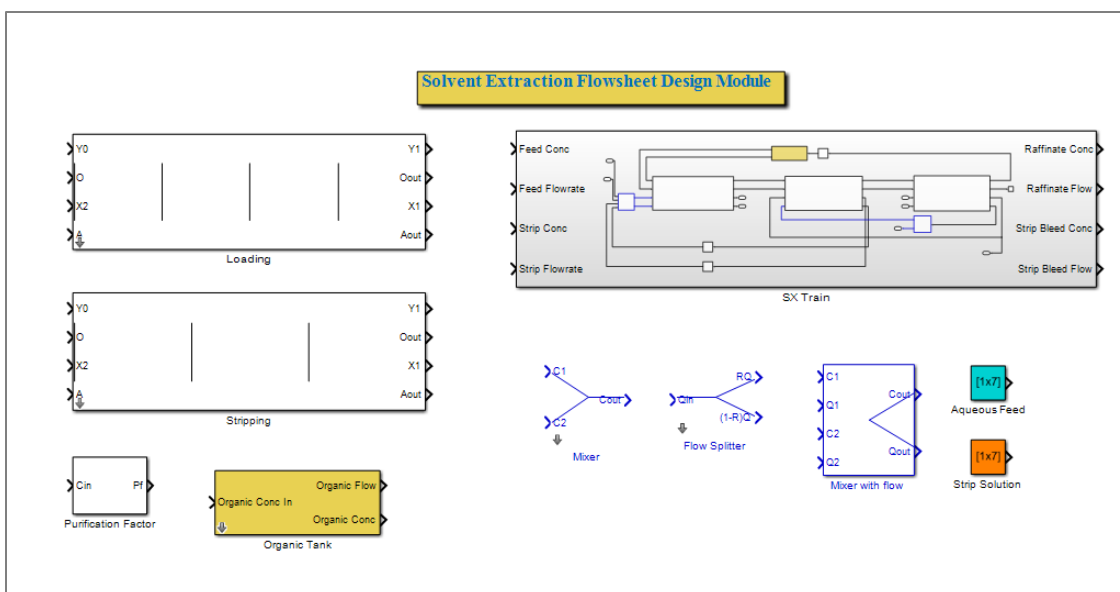


Figure 6.10: Solvent Extraction Model Library in Simulink

6.2.2.1 Loading and Stripping Blocks:

The loading and stripping function blocks evaluated the concentration in organic and aqueous streams exiting the system block using principles described in Figure 6.7 and Figure 6.8. The block had input-output ports through which information related to organic and aqueous streams were passed, as shown in Figure 6.11. The backend contained a Matlab user-defined function block with code for the process involved (see Appendices). The input ports, labeled Y_0 and X_2 , represented an array of concentration of multiple components in organic and aqueous streams entering the block. Similarly, Y_1 and X_1 represented an array concentration of multiple components in organic and aqueous streams, exiting the block obtained using developed models for supplied extraction conditions. Input-output ports, labeled O and A, represented the incoming- outgoing volumetric flowrates of the organic and aqueous streams. A graphical interface shown in Figure 6.12 was also added to the blocks to supply model parameters described in Table 6.5, based on the separation conditions. The feature is called masking of a block in Simulink, and it is useful when the same block is used multiple times but under different separation

conditions. Masking allows for updating model parameters without going into the actual program.

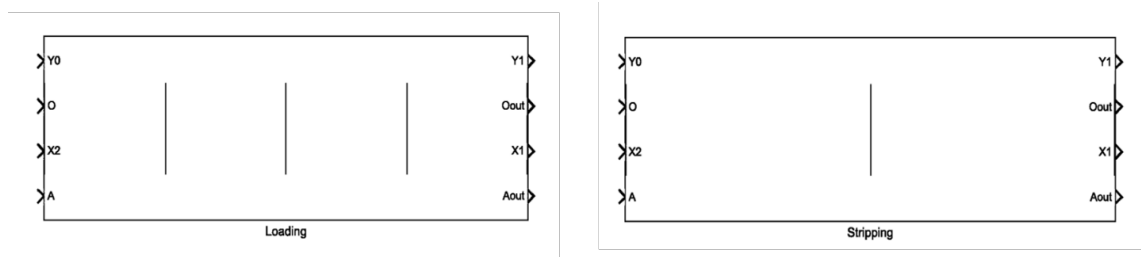


Figure 6.11: Loading and Stripping block in Simulink

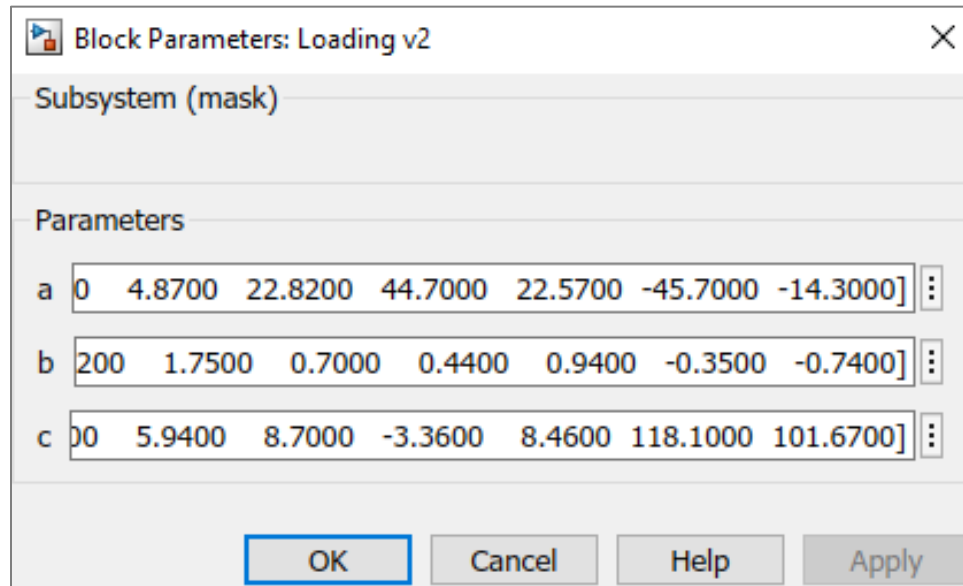


Figure 6.12: Masked loading subsystem

6.2.2.2 Mixer, Splitter, and pH Adjustment:

An SX flowsheet also requires mixers for mixing streams, flow splitters, and pH adjustment during the process. Hence, such features were also added as block modules shown in Figure 6.13. The flow splitter splits the given flow based on a ratio provided by the user.

The mixer block will evaluate the concentration and flow of discharge stream, using the information of incoming stream using Eq. 6.8 under perfect mixing conditions.

$$C_{out} = \frac{(Q_1 C_1 + Q_2 C_2)}{Q_1 + Q_2} \quad 6.8$$

Where, C_{out} is the concentration of output stream, C_1 and C_2 are concentrations of incoming streams, and Q_1 and Q_2 are flow rates of input streams. The flow rate out was evaluated by adding incoming flowrates following the principle of volume conservation. The pH volume adjustment block was developed to account for changes in volume and metal concentration due to the changed volume of any stream from reagent addition to adjust the pH. The block had two input ports for the incoming stream, requiring flowrate and concentration information whose pH was to be adjusted. The input pH, desired output pH, and reagent molarity was provided from the masked interface. The volume due to the reagent addition and resulting change in concentration were included in the discharge stream. The following Eq. was used in estimating the added volume based on the change in moles of the H^+ ion:

$$\Delta Q = \frac{10^{-pH_{int}} - 10^{-pH_f}}{10^{-pH_f} + M} Q_{in} \quad 6.9$$

where ΔQ indicates a change in volume, pH_{int} and pH_f are initial and final pH, M the molarity of reagent, and Q_{in} the flowrate of the input stream. The pH volume adjustment equation is applicable for increasing and decreasing the pH of the incoming stream. However, the method is approximate as it based on the final molarity of H^+/OH^- of the reagent added and assumes complete dissociation and stoichiometry of the added acid or base.

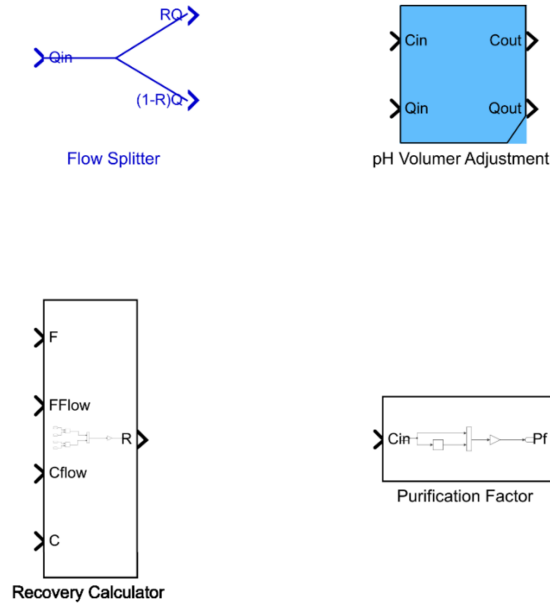


Figure 6.13: Other function blocks

6.2.2.3 Recovery and Purity

The purity factor and recovery block were also developed to evaluate the performance of a unit by measuring the purity of streams leaving the unit and the recovery across the unit. Equation 5.9, described earlier, was used to develop the purity block, and recovery was described using the following relationship:

$$R_i = \frac{[M]_{i,stream} \cdot f_{stream} \cdot 100}{[M]_{i,feed} \cdot f_{feed}} \quad 6.10$$

where, R_i represents the percentage recovery of metal i , $M_{i,stream}$ the concentration of metal of interest i in the given stream, n is the number of metal species present in the stream, and f_{stream} is the flowrate of the subscripted stream.

The developed library consisting of block models can be used to design the SX process or flowsheet of any configuration. An initial application of the block models was in the development of a multistage SX train block model. This was done by placing loading, scrubbing, and stripping blocks in succession to represent the train, as shown in Figure 5.6. The signal lines representing the flow of materials were interconnected with the respective ports of the blocks (Figure 6.14). The reflux flow, from the stripping to the scrubbing unit, was obtained using splitter block, whereas the multiple flow streams were combined using mixer block as in case of scrubbing and feed entering loading process. Similarly, the recovery and purity blocks were added across the strip bleed and feed to evaluate performance during simulation. The SX train was then used to develop the multi-train SX flowsheet, utilizing the train block discussed. The procedural development of the flowsheet, its analysis and optimization, are discussed in the following chapter.

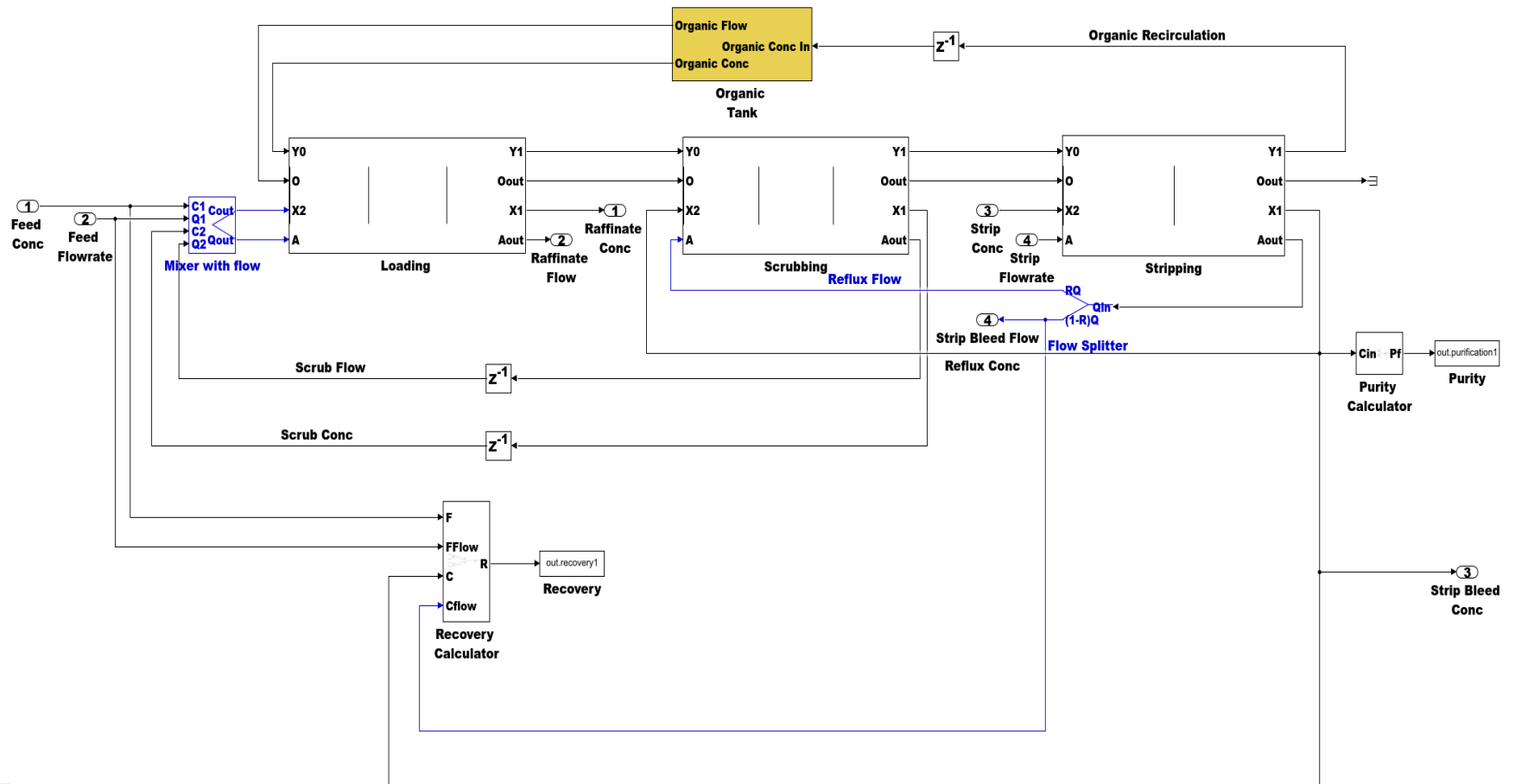


Figure 6.14: Interconnected subsystem of loading, scrubbing, and stripping process to develop SX train block.

6.3 CONCLUSION

Phase ratio is a critical variable in identifying optimum conditions for separation of elements and determining the number of stages required for separation in an SX process. For this reason, industrial solvent extraction circuits, are designed to be operated at different organic-aqueous flowrates to fine-tune phase ratios in order to achieve the desired separation. Therefore, a method or tool which allows design engineers to predict and analyze the separation performance at different phase ratios is essential. The purpose of this chapter is to 1) study the effect of phase ratio on REE separation at pre-determined equilibrium pHs; 2) identify the optimum phase ratio for separation of elements or groups of elements; and 3) provide a block-model framework which can be used to determine the number of stages required in an SX train and design a multi-train SX flowsheet.

The separation factor was used as a criterion in identifying phase ratios for individual and group separation of elements. The key findings from REE separation viewpoints were:

1. At equilibrium pH of 0.65, the extraction of yttrium was dominant at all phase ratios with negligible co-extraction of other components for phase ratios of less than 1. Thus, in flowsheet design, yttrium extraction at low phase ratios is preferred (Figure 6.15);).
2. The combined separation of gadolinium and samarium can be achieved at an equilibrium pH of 1.5 and phase ratio of 0.5;
3. The separation between gadolinium and samarium can be achieved at an equilibrium pH of 1.52 and phase ratio 0.1. These had the highest separation factor of 1.69;
4. Lanthanum, which had lowest extraction potential, can be easily separated from the group containing praseodymium, neodymium, and cerium at pH 2.2 and phase ratios of 0.1 and 0.5.

This chapter also covers the modeling of experimental data using regression methods. Loading process was best described by power function model and stripping by linear models decided on the basis of R^2 when fitting the model. The method of non-linear least squares was used to obtain regression coefficients.

A library of solvent extraction block models was then developed in Simulink. The library contained processes common to industrial SX circuits, which can be simulated by providing the operating conditions and model parameters in order to predict the mass transfer behavior for provided separation conditions. Performance indicators for recovery and purity were defined and included in the model library. The library can be expanded to develop and simulate multi-train flowsheets and understand the intricacy of multi-train separation processes. Thus, essential questions relating to process design, such as number of the stages and number of trains, can be answered using simulation.

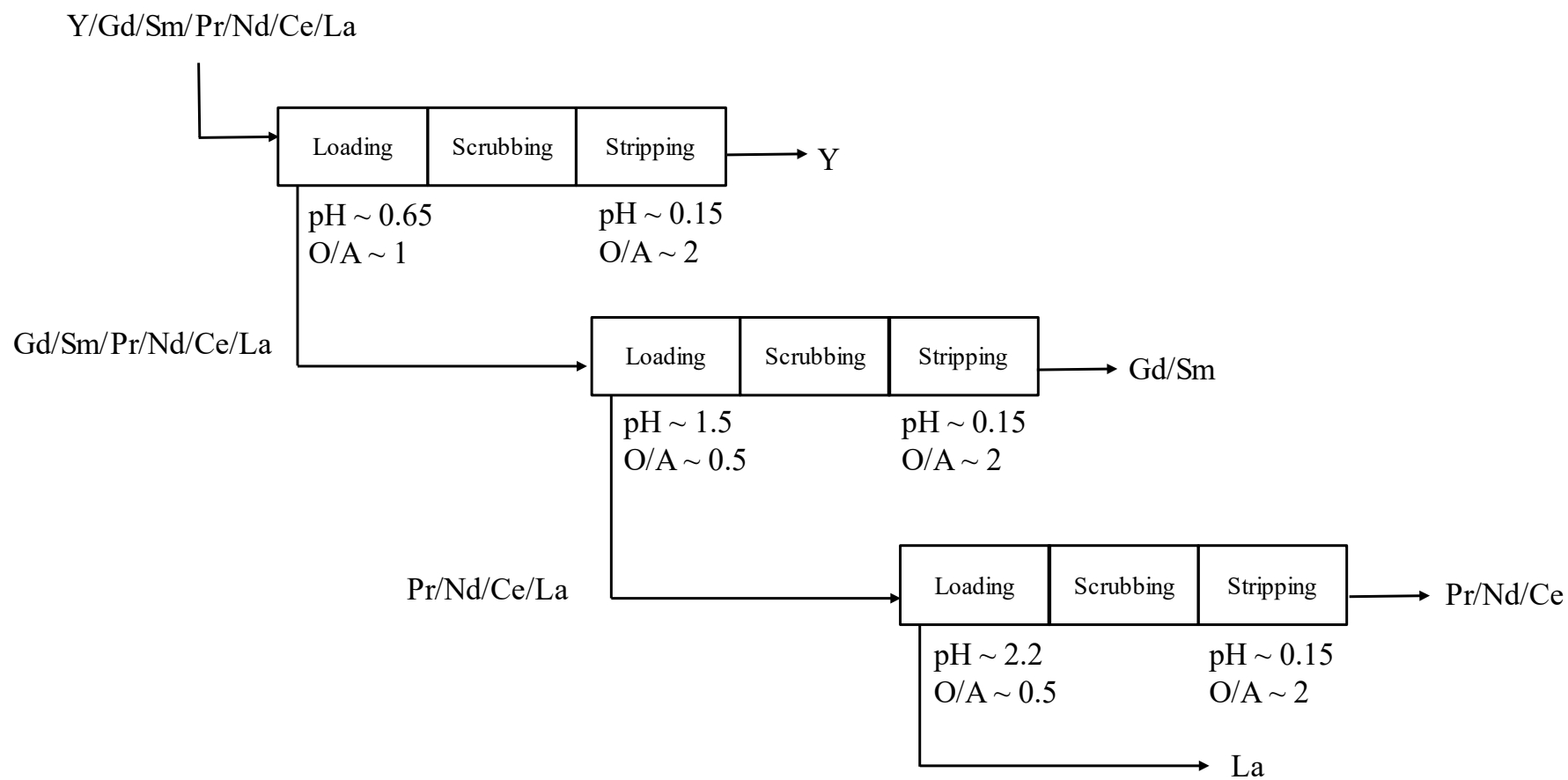


Figure 6.15: Conceptual flowsheet with updated phase ratio conditions

CHAPTER 7. FLOWSHEET DESIGN AND TRAIN OPTIMIZATION

The two previous chapters studied the factors affecting the separation of REEs using an SX process, and then they developed extraction and stripping models by describing the relationship among the factors. The findings from the chapters laid the foundation and initial approach for a multi-train/multi-element flowsheet design for REE separation. However, flowsheet design is a complicated task, as it involves multiple interacting processes and variables, making it difficult to assess performance for various design and operating conditions. The conceptual flowsheet proposed in the previous chapter provides initial multi-train configuration and operating conditions for individual and group separation of elements. Still, the key question facing the proposed flowsheet is in determining the number of stages for best separation performance, assessed in terms of recovery and purity of select elements. Hence the current chapter answers this question by using process modeling and optimization methods.

7.1 FLOWSHEET DESIGN

Any process or flowsheet design task starts with answering the following important questions:

- What are the objectives the designed process or flowsheet is to accomplish?
- What are the indicators for the objective measurement?

For this study, the objective of the flowsheet is to separate REEs from a feed mixture containing multiple rare earths with maximum recovery and purity. Thus, it requires the configuration of multiple SX trains with various stage and separation conditions, in respective trains, in order to achieve required separation. Recovery and purity of the elements can be used as objective measures to assess the extent of separation. The initial SX train configuration with separation conditions was identified from pH and phase ratio studies shown in Figure 6.15. However, the number of stages required for optimum separation and the extent of separation is unknown. Thus, to determine stage number and associated performance, process modeling, as discussed in Section 6.2, was utilized to

design and simulate a multi-train SX flowsheet for different design and operating conditions.

However, simulating a process involving multiple variables that affect the performance can be challenging. The SX train is one such process, the performance of which is influenced by multiple variables, as shown in Figure 7.1. For stage determination, because of known optimum separation conditions for trains, the variables other than design were constant during simulation (highlighted in Figure 7.1), thereby reducing the unknown variables for simulation. Nevertheless, design variables involve multiple unknowns, which are loading, scrubbing, and stripping stages, thereby making stage determination a multivariable unknown problem.

To solve such a multivariable problem, simulation with respect to one variable and analyzing the performance of the variable can be difficult. Hence, for such a complex problem, optimization methods are utilized. Optimization is a mathematical technique of adjusting variables of a process to yield the maximize performance and it is widely used in industrial process design and control. Process optimization ensures smooth operation of any industrial process, thereby confirming good product quality, increased equipment life and reduced cost. Many of the advanced process controls utilize the real-time optimization method to adapt to changes in process conditions due to any external disturbance, such as change in feed composition, pH, etc.

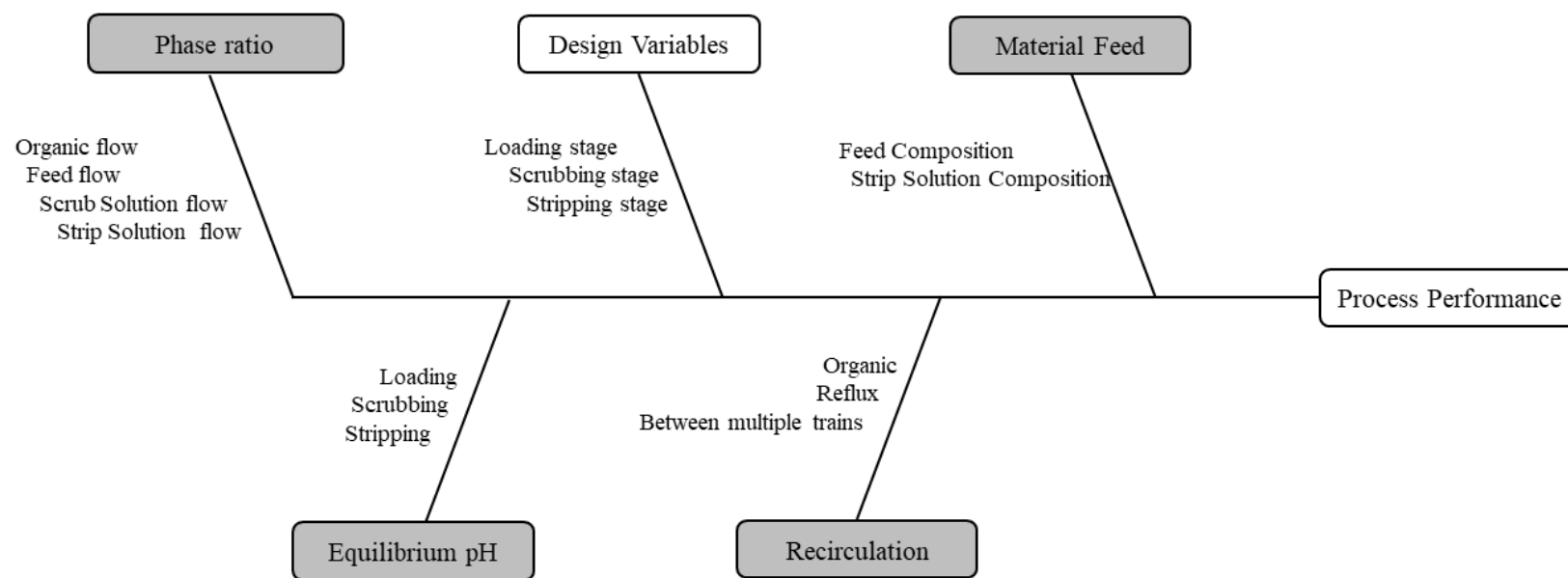
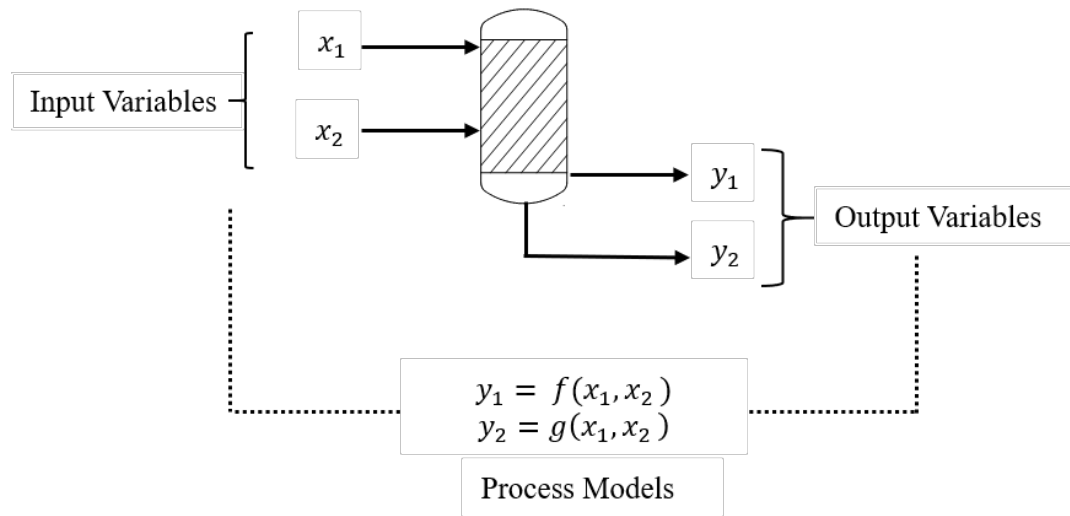


Figure 7.1 Cause and effect diagram showing factor influencing SX performance

Optimization of any process requires the following: 1) a process model to describe the behavior of the system under different conditions within operational constraints; 2) an objective function, representing mathematical formulation of the performance variable as a function of input variables; and 3) an optimization method based on the nature of objective function to achieve optimization.

Figure 7.2 shows an example of the process with x_1 and x_2 as input and y_1 and y_2 , as output variables. The function f and g represent process models describing the relationship between input and output variables. For optimization of the output variable, for example y_2 to attain a certain target value, an objective function is created which describes the difference between a target value and y_2 . The input variables x_1 and x_2 are tuned to minimize the objective function to attains zero value, thereby y_2 reaches the targeted value.



Objective Function : $\Delta = (target\ value - y_2)$

Or : $\Delta = (target\ value - g(x_1, x_2))$

Figure 7.2: Example of a typical system with objective function

For an SX process, the multi-train model developed in Simulink as a function block (section 6.2) can be used in the SX system for a provided separation condition. The unknown variables of the system are the number of stages in loading, scrubbing and

stripping processes and the input to system are concentration and flowrate of incoming streams. Since the objective of trains is to separate elements or groups of elements with maximum purity in the product stream (strip bleed or raffinate), the purity of elements is the primary objective of the function. However, in many situations, recovery of an element is also of importance in order to avoid losing the element in the raffinate/strip bleed stream. Therefore, in such situations, both variables should be accounted, which categorizes design problems as multi-objective optimization problems. Multi-objective optimization problems are solved by converting it to a single objective optimization problem using a weighted average method. It is possible to use a single variable, i.e., either recovery or purity, if both performance variables show similar characteristics in response to a process. However, in the current case, both variables counter optimize one another, i.e., an increase in one results in the decrease of other (Figure 7.3). This is common to mineral and metallurgical processes, increasing in recovery results of undesired components as well, thereby compromising purity.

Hence a transformation method was adopted when the optimization of both recovery and purity were required. An innovative method to transform recovery and purity to a single variable is to consider both variables as vectors, which is possible because both variables are dependent on processes with values ranging from 0 to 100 (Figure 7.3). Resultants of the variables will represent the distance from the origin for a certain design condition, denoted by points A and B on the plane. The maximum distance will indicate the best performance, which is generally the knee of the curve when evaluated using the traditional graphical method. However, in some cases, it is not possible to maximize both recovery and purity; in such cases, either of the variables can be used as objective function criteria depending upon the requirement.

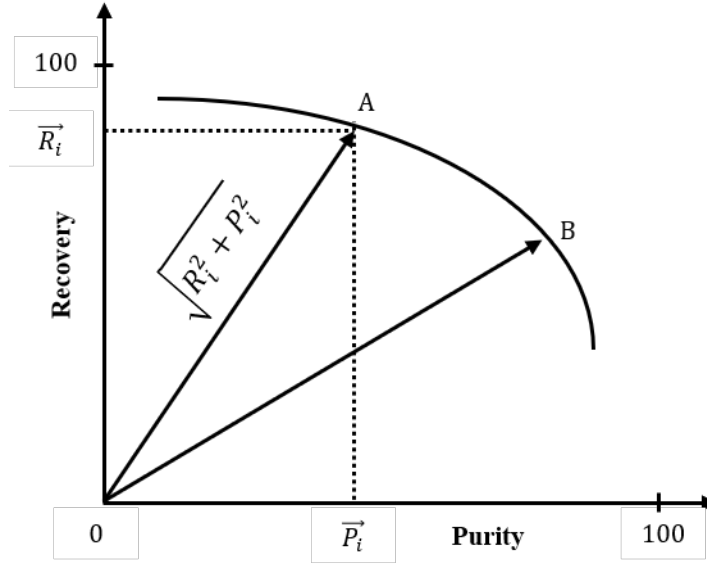


Figure 7.3: Typical recovery-purity curve

The final task was the selection of an optimization method. There are numerous optimization methods available that continue to be developed every year, which makes the determination difficult. To select an optimization method, it is essential to understand the type of optimization problem based on the nature of the input variables. For a continuous variable, such as flowrate, an optimization method that utilizes first-order derivatives to locate maxima and minima can be selected. For discrete variables, integers are utilized. The SX system is a mixed-integer system, i.e., involving discrete and continuous variables with a non-linear objective function, thus falling under the category of mixed-integer, non-linear optimization problems. Hence, gradient-based methods, such as the Newton method or the Newton-Raphson method, do not apply. For this reason, the algorithmic method particle swarm optimization (PSO), which does not require gradient evaluation, was selected. The subsequent section provides details about the method.

7.2 PARTICLE SWARM OPTIMIZATION (PSO)

PSO, a heuristic optimization method used for mixed-integer, non-linear problems, is based on the social model of the flocking of birds or the schooling of fish (Kennedy et al., 1995). The method uses a selected number of particles (birds in the social model) determined at

the start of the optimization. The particles are characterized by position and velocity in multi-dimensional space, with dimensionality determined by a number of unknown variables for optimization. Every particle in a swarm searches for the optimum value in the multi-dimensional search space, with an optimum value representing the best value of the objective function attained by the particle. The particle identifies the position ($p_{best,i}$) associated with the respective optimum of objective function ($f_{pbest,i}$) location. The particles then congregate and then objective function value among the particles is compared and the best objective function value (f_{gbest}) and associated position (p_{gbest}) achieved by the swarm is recorded. The process is repeated iteratively by updating the velocity and position of particles until the global optimum value has been reached. The velocity and position, initially chosen at random within provided boundary conditions, are updated by the following:

$$V_i^{t+1} = wV_i^t + c_1r_1(p_{best,i} - X_i^t) + c_2r_2(g_{best,i} - X_i^t) \quad 7.1$$

$$X_i^{t+1} = X_i^t + V_i^{t+1} \quad 7.2$$

where, V_i^{t+1} indicates the velocity of particle i updated at iteration $t+1$; V_i^t is the velocity of particle i at iteration t , X_i^t is the position of particle at t ; w represents inertia of the particle; c_1 , c_2 weighting constants also called acceleration constants, which prioritize particle or global correction; and $p_{best,i}$ and $g_{best,i}$ are the particle and the group's best positions, respectively. The objective function f_i updates the criteria at every iteration for a minimization problem. These are:

$$f_i < f_{pbest,i} \quad = \quad \begin{cases} p_{best,i} = X_i^t \\ f_{pbest,i} = f_i \end{cases} \quad 7.3$$

$$f_{pbest,i} < f_{gbest} = \begin{cases} p_{gbest} = X_i^t \\ f_{gbest} = f_i \end{cases} \quad 7.4$$

For the flowsheet design, loading, scrubbing, and stripping stage numbers constituted the multi-dimensional search space (position vector X_i) and were represented using variables n_L , n_{Sc} , and n_{St} , respectively. The velocity vector indicated the correction or change that is applied to stage number after each iteration. The correction was based on the stage combination attained by particle and swarm resulting in best value of objective function (purity and recovery). Three different forms of performance variables were used to define the objective function. The variables used were 1) a transformed vector incorporating both recovery and purity (Figure 7.3), 2) recovery, and 3) purity. The objective functions were defined as the difference of maximum value that could be attained by variables as shown in equations below:

$$f_i = 141.42 - \sqrt{R_i^2 + P_i^2} \quad \text{Transformed} \quad 7.5$$

$$f_i = 100 - P_i \quad \text{Purity maximization} \quad 7.6$$

$$f_i = 100 - R_i \quad \text{Recovery maximization} \quad 7.7$$

where f_i represents the objective function utilized in the optimization algorithm shown in Eq. 7.3 and 7.4 and R_i and P_i are the recovery and purity for metal i , evaluated from the process model. The numerical value of 141.42 in Eq. 7.5 is the maximum magnitude of the

sum of two vectors in Figure 7.3, calculated using Eq. 7.8, which can be regarded as the theoretical range of transformed variables.

$$\text{Max Magnitude} = \sqrt{100^2 + 100^2} = 100\sqrt{2} \quad 7.8$$

During flowsheet simulation, one of the objective functions was selected for individual trains. The goal of the PSO was to minimize the objective function for the swarm by identifying optimum loading, scrubbing, and stripping stages. After selection and the development of the optimization routine, the algorithm was implemented in the flowsheet design process. Figure 7.4 is a model flow diagram, showing the implementation in the design process. A flowsheet was first designed using Simulink blocks to which an initial set of operating and design values were provided. The connected Simulink blocks represented the integrated process model with parameters, supplied through a mask system, to each block for a selected separation condition. The flowsheet was then simulated, and mass transfer behavior was predicted for given conditions, which was used to evaluate recovery and purity in the output streams (raffinate and strip bleed). The recovery and purity values were fed into the optimization algorithm, where the performance, i.e., objective function value for all sets of initial values, was evaluated and compared. The condition with the minimum value of objective function was stored and the initial set was updated. The process was repeated until a minimum value of the objective function was reached. The design variables, resulting in maximum value of the objective function, were selected as the optimal design.

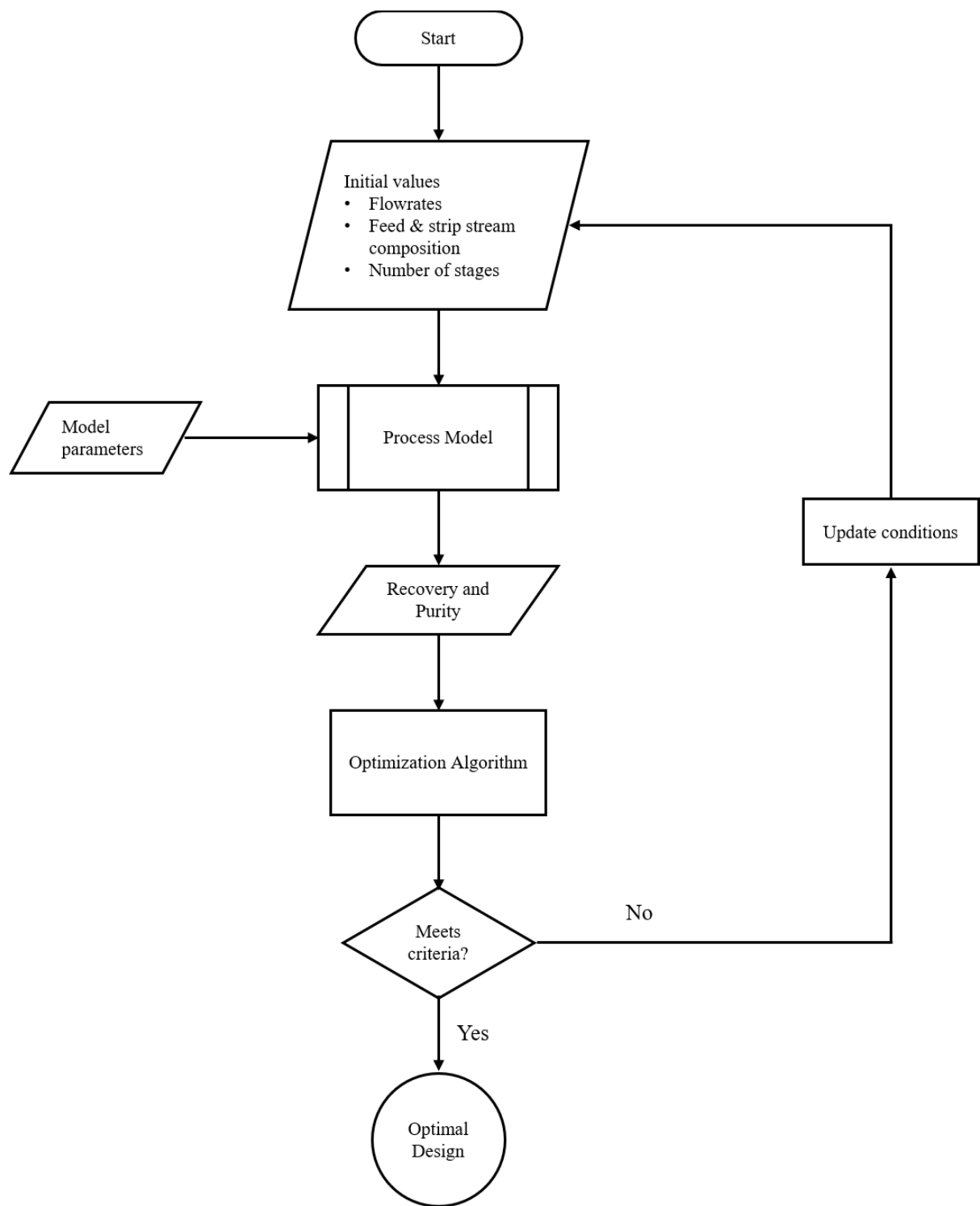


Figure 7.4: Model flow diagram

7.3 YTTRIUM SEPARATION

Based on Figure 6.15, the design and simulation of the conceptual flowsheet was commenced in Simulink using block models, as discussed in Section 6.2.2. The pH and phase ratio conditions described in the conceptual flowsheet were used as settings to derive flowrates of the input streams for the simulation. SX train 1 was configured first to separate the yttrium-based on the order of element extractability. The aqueous feed flowrate to loading stages was set to 0.9 lpm, stripping to 0.5 lpm with a reflux ratio of 0.2 in scrubbing stages, resulting in a total flowrate of 1 in the loading stage (Figure 6.15). This was done to maintain a phase ratio of 1 in loading and 2 in stripping, as proposed by the conceptual flowsheet. At pH 0.65, an organic-aqueous flow ratio below 1 prevents the co-extraction of other components during loading in the feed (see Section 6.1). Stripping is not significantly affected by variations in phase ratio, hence phase ratios of 2 or greater were set in stripping (Figure 6.4). A low-strip acid flowrate reduces the acid consumption cost and results in a concentrated bleed.

The total aqueous-feed flowrate of 1 was selected on the basis of laboratory tests, which were performed using 10 gm of mixed salt in 1 liter of solution in the loading process. Thus, organic flowrate and strip acid flow were derived following the same approach. Table 7.1 lists the input conditions determined and used in the simulation. After confirming the input conditions, the SX train was ready for simulation for determining stage configuration. PSO was implemented across SX train 1, with loading (n_L), scrubbing (n_{sc}) and stripping (n_{st}) stages as unknown variables. The parameters for the PSO listed in Table 7.2 were initialized, and the region for search space, also called boundary conditions, was defined.

Table 7.1: Separation condition for yttrium

Operating Parameters	Value
Feed flowrate (lpm)	0.9
Organic flowrate (lpm)	1
Strip flowrate (lpm)	0.5
Reflux ratio	0.2
Loading equilibrium pH	0.65
Strip equilibrium pH	0.15 (0.70 M)

Table 7.2: Optimization Parameters

Condition	Value
Number of particles	10
Maximum iterations	20
w	0.8
c1	2
c2	2
Boundary conditions for stages	$1 \leq n_L, n_{Sc}, n_{St} \leq 20$

The parameters of PSO were selected based on the understanding of the optimization method and the literature (He et al., 2016). The knowledge used in the selection of parameters are:

1) The number of particles and iteration are decided based on the complexity of the problem. Fewer particles and iterations may lead or not lead to a good solution because fewer particles will be unable to cover the search space within limited steps. Similarly, a larger number may lead to unnecessary computation. A good method for selection is by assessing the dimensionality of the problem, range of search space, and then monitoring the objective function value by multiple trials. The current case involves three dimensions (n_L , n_{Sc} and n_{St}) with a small search space determined by the boundary stage conditions listed in Table 7.2, hence 10 particles were selected with maximum iterations of 20. This allows 10 sets of stage combinations searching for optimum values at every iteration, as shown in Eq. 7.9, thereby resulting in 200 search combinations. The columns in matrix shown in Eq. 7.9 indicate the stage number corresponding to n_L , n_{Sc} and n_{St} and row indicate the number of particles. Thus, 10 rows and 3 columns signify 10 sets of stage combinations simulated iteratively based on iteration number. If the optimum value is unattained, the iteration can be increased.

$$\vec{P} = \begin{bmatrix} 17 & \cdots & 4 \\ \vdots & \ddots & \vdots \\ 3 & \cdots & 12 \end{bmatrix}_{10 \times 3} \quad 7.9$$

2) Inertia weight (w) is a factor in the velocity correction (Eq 7.1), which determines the weightage given the velocity from the previous iteration. It serves as a memory of particles during update at next iteration, generally taken as 0.8. Acceleration coefficients c_1 and c_2 in Eq. 7.1, on other hand, represent the velocity correction weightage towards particle local optimum or swarm global optimum. Both the variables can be tuned based on the problem; however, in general, it is suggested that c_1 and c_2 be set at 2 (Kennedy et al., 1995). In case of SX-train optimization the inertia associated with velocity signify the amount of change applied to stage number (n_L , n_{Sc} , n_{St}) which is retained from previous iteration correction. Similarly, c_1 and c_2 signify the weighting factor to update stage number (n_L , n_{Sc} , n_{St}) based on particle's identified best position (particle's stage combination leading to best purity) and group identified best position (group's stage combination leading to best purity).

3) The boundary condition essentially defines the search space, which is based on the problem being solved. For a stage determination problem, a minimum of one stage is needed in loading, scrubbing and stripping processes, which is established via a lower range of variables. The upper range of 10 was initially selected for trains, which resulted in 10 loading, scrubbing and stripping stages, respectively. If the objective of the SX train was not met, the upper range was updated by 10 more stages. However, there is a possibility that updating the stage number does not result in any change in the objective function value, implying a separation problem.

After defining the PSO parameters, the train was simulated and optimized for stage number, resulting in a minimum value of the objective function described by Eq. 7.5. Recovery of 99.61 and purity of 99.52 was obtained for yttrium extraction in the strip bleed, using a 8-12-3 stage combination of loading, scrubbing, and stripping, respectively. Figure 7.5 shows a convergence plot for SX-train-1, showing error minimization by PSO iteration. Figure 7.6 shows the recovery, purity, and concentration values for the elements in the input and output streams. It was observed that a large number of scrubbing stages are critical for achieving high purity. The strip bleed can be further purified by adding an additional cleaner SX train for the bleed and employing the same method. However, in this case, additional purification was not required. The obtained stage combination was updated in SX train 1, and the flowsheet design progressed to the next SX train, for a combined separation of gadolinium and samarium from the raffinate in SX train 1. The parameter associated with next stage objective function was stage combination of the respective train whereas the optimization parameters were kept same as listed in Table 7.2. This approach of a piecewise optimization of the SX train was adopted because the objective of each SX train proposed in the conceptual flowsheet was different (Figure 6.15). Each train is intended to separate a particular element or element combination with objectives of maximizing recovery and purity described by Eq 7.5. However, when combined objective function was not useful in separation, recovery or purity objective function were used Eq's 7.6 and 7.7. For the proposed conceptual flowsheet shown in Figure 6.15 the purity of Sm was used as objective function for combined separation Gd/Sm. Similarly, for the separation of La from Nd/Pr/Ce, the purity of Ce was selected to maximize combined

extraction of Nd/Pr/Ce in strip bleed stream. The subsequent section discusses the optimization of other trains.

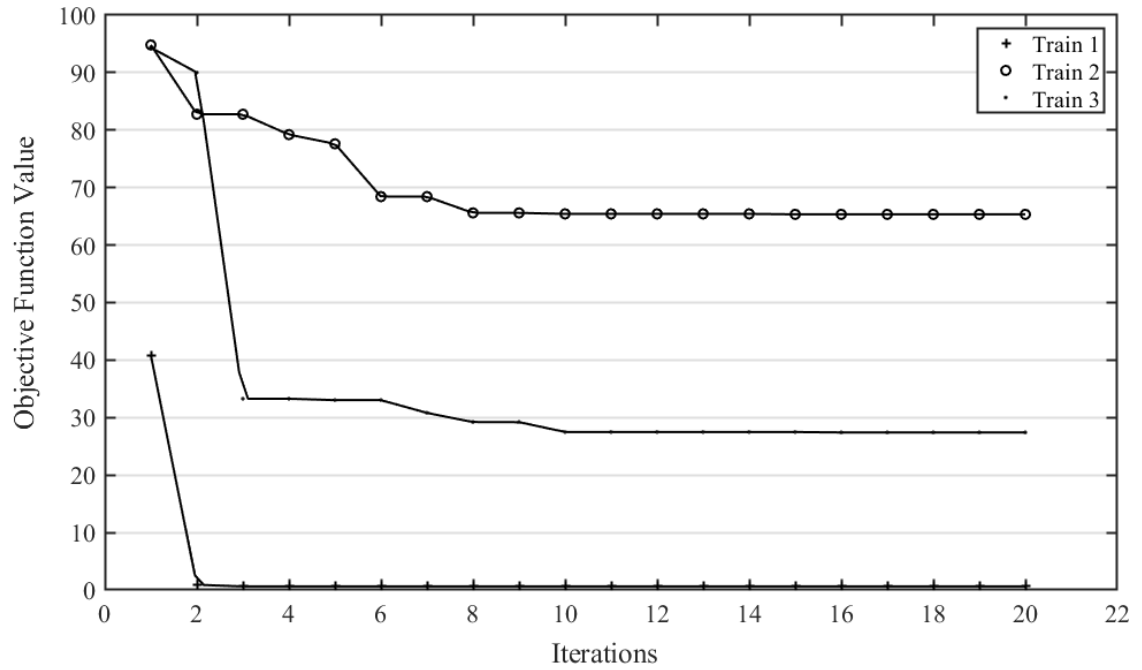


Figure 7.5: Convergence plot for Train 1, Train 2, and Train 3 (optimized independently and plotted together) showing the minimization of objective function with iteration

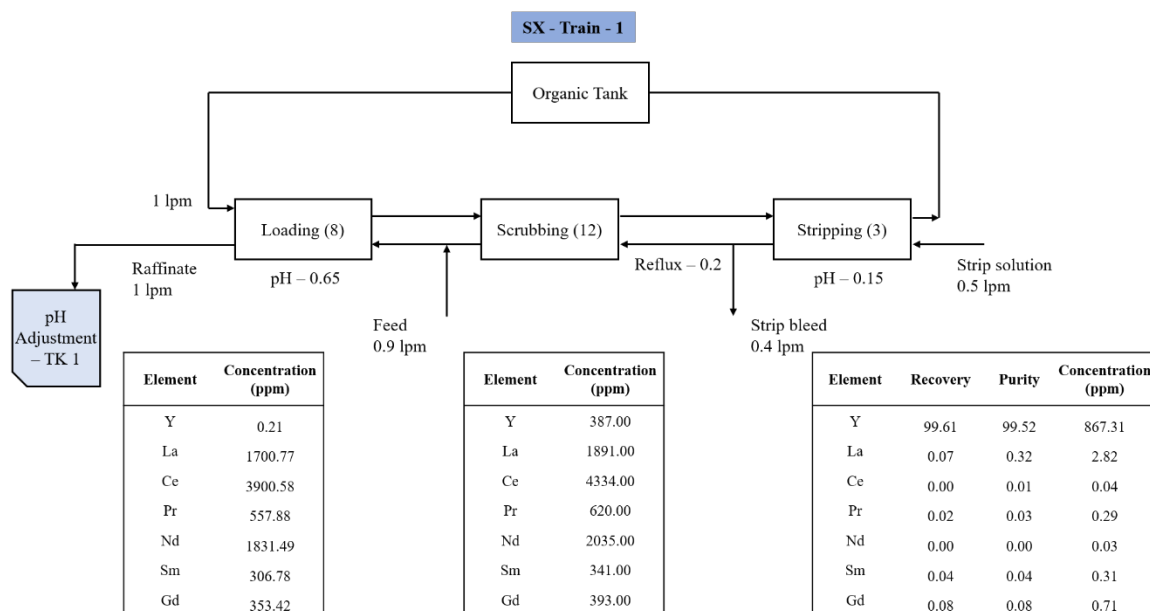


Figure 7.6: Yttrium separation (SX train 1)

7.4 GADOLINIUM AND SAMARIUM SEPARATION

The raffinate from SX train 1, having a minor concentration of Y of 0.21 ppm, was processed in SX train-2 for a combined extraction of Gd and Sm. Following the same approach, train 2 was simulated iteratively to identify stage combinations, using the optimization algorithm to maximize recovery and purity. It was found that the best value attained by the objective function was 41.08 for a 10-3-1 stage combination. The stage combination resulted in high Gd and Sm recovery with values greater than 99 percent; however, the purity was significantly lower, values of 11.20 and 9.71 percent, respectively. The reason for such low purity value is because the concentration of Gd and Sm in the feed is much smaller than Nd and Ce, which despite having a low percent of extraction, are recovered in higher concentrations (Figure 7.7).

Thus, combined separation of both elements from the raffinate mixture by maximizing both recovery and purity is not advantageous. For the following reason, it was sought to maximize combined purity of the Gd and Sm in the strip bleed stream. This was done using the purity of Sm as the objective function given by Eq. 7.6. The reason only the purity of

Sm is considered in the objective function, and not of Gd, is because of the order of extraction of elements shown in Figure 5.1. Setting the objective function as the purity of Sm will automatically maximize Gd because it being extracted before Sm. Nevertheless, the objective function was switched to account for the purity of Sm to achieve lower concentration of the undesired element (Nd, Pr, Ce, and La) in the strip bleed. This resulted in the combined purity of 80.65 percent in the strip bleed for Gd and Sm, and the remaining 19.34 percent of Nd, Pr, Ce and La. Figure 7.5 shows the convergence plot for maximizing the purity of Sm in the strip bleed stream. The recovery of Gd and Sm in the strip bleed was 25.48 and 22.11, respectively, and in the raffinate was 13.62 and 0.23 percent, respectively, indicating a majority of the pair associated with the extractant in the organic stream.

The strip bleed was further processed in SX train 3 to seek potential separation between Gd and Sm, using the purity of Gd in the strip bleed as the objective. The best performance resulted in a purity of 72.59 for Gd and Sm 22.25, indicating the difficult separation of the pair (Figure 7.8). The raffinate from SX train 2, rich in Nd, Pr, Ce, and La, was sent for further processing, while the raffinate from SX train 3 was left untreated, but it can be recycled to train 1 to prevent any loss.

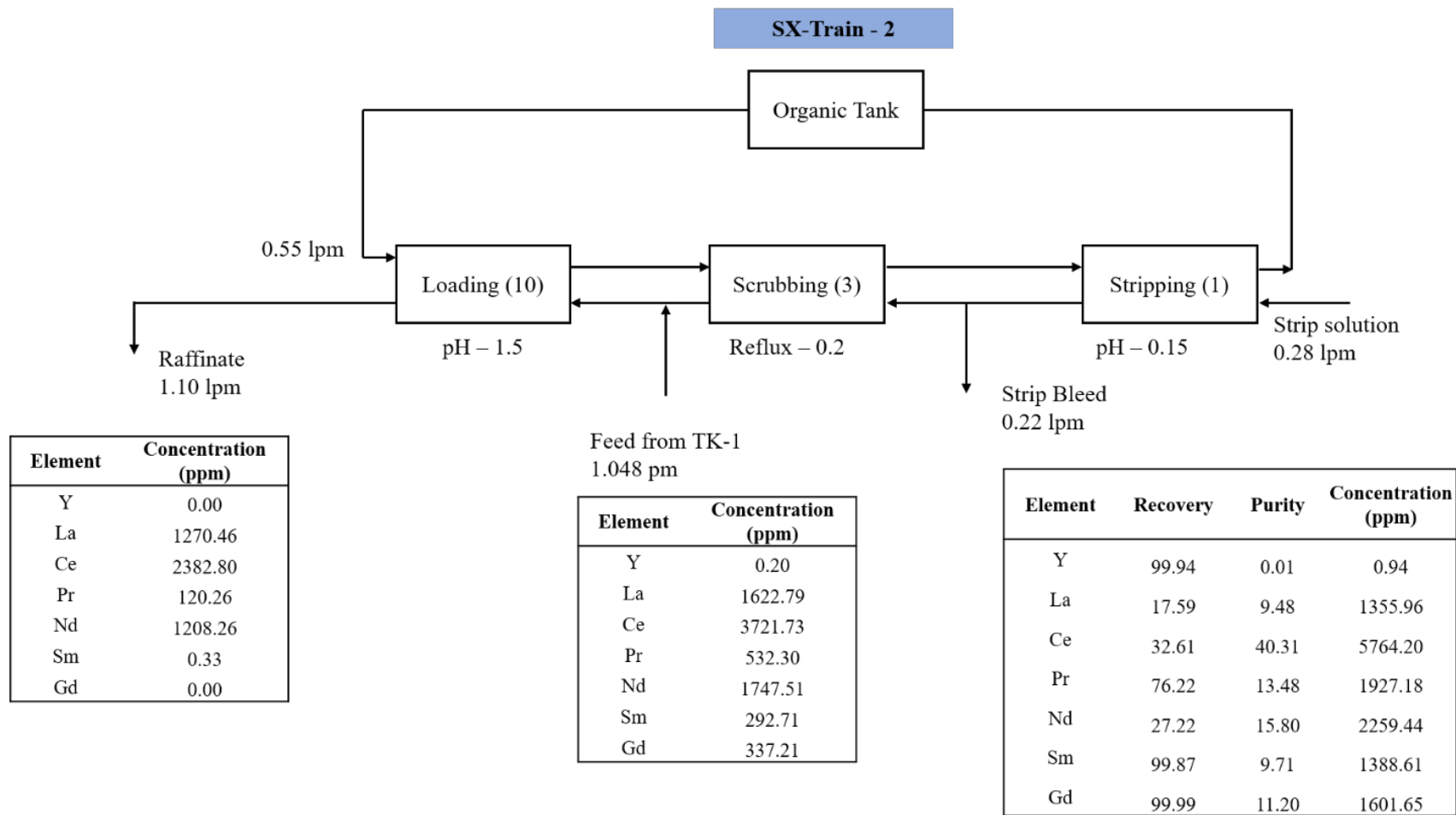


Figure 7.7: Gd-Sm combined extraction train using tramformed objective function

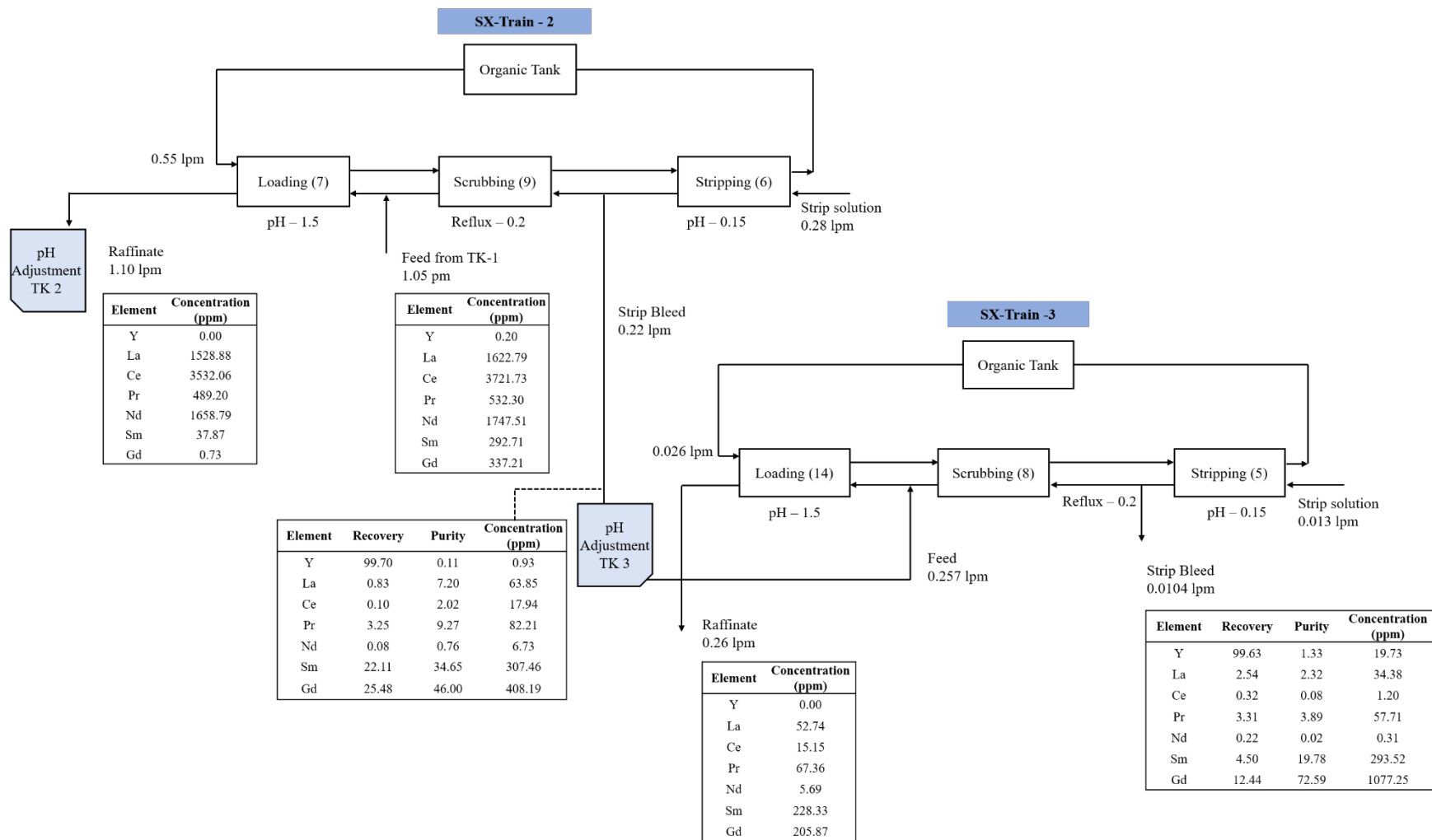


Figure 7.8: Gadolinium and samrium separation (SX Train 2 and Train 3) using purity of gadolinium as objective function

7.5 LANTHANUM SEPARATION

The raffinate stream from SX-train-2 was processed to further separate La from the element mixture consisting of Nd, Pr, Ce, and La. It was done by extracting Nd, Pr, and Ce in the strip bleed and leaving the La in the raffinate stream, using SX train 4 (Figure 7.10). The reason this approach was adopted is due to La having a low percentage of extraction compared to other elements, as shown Figure 6.3, and the ease of extraction of Nd, Pr, and Ce to the organic phase, leaving La in the raffinate. The purity of Ce in the strip bleed was used as the objective function. A 10-3-5 stage combination of loading, scrubbing, and stripping, respectively, yielded a purity 85.41 percent La in the raffinate stream, with the only other major component as Ce with 14.23 percent at a phase ratio of 0.5 in the loading stage (Figure 7.9). Higher purity La can be achieved if the phase ratio of 0.1 is maintained in the loading stage of train 4, as the separation factor is highest, having a value of 6.29 as listed in Table 6.3. The strip bleed resulting from train 4 still contained a considerable amount of La. Hence, it was further processed in train 5, following the same approach applied to train 4 to extract Nd, Pr, and Ce in the organic phase, thereby leaving La in the raffinate. From the simulation, a combined purity of Nd, Pr, and Ce of 93.56 percent was possible using a 8-1-5 (load/scrub/strip) stage combination. Whereas a La raffinate of 77.48 percent purity was predicted and contained 21.37 percent of Ce as a major component. The lanthanum obtained from trains 4 and 5 can be further purified by processing it through additional trains.

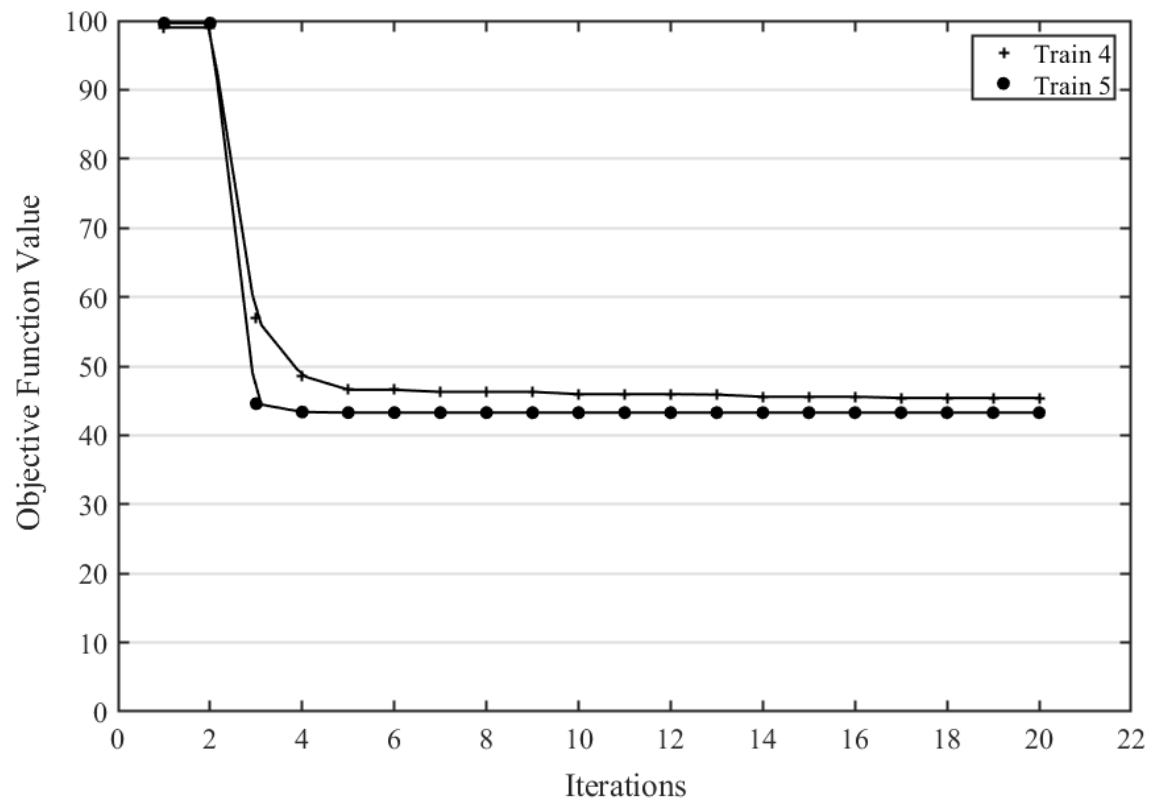


Figure 7.9: Converganice plot for Train 4 and Train 5

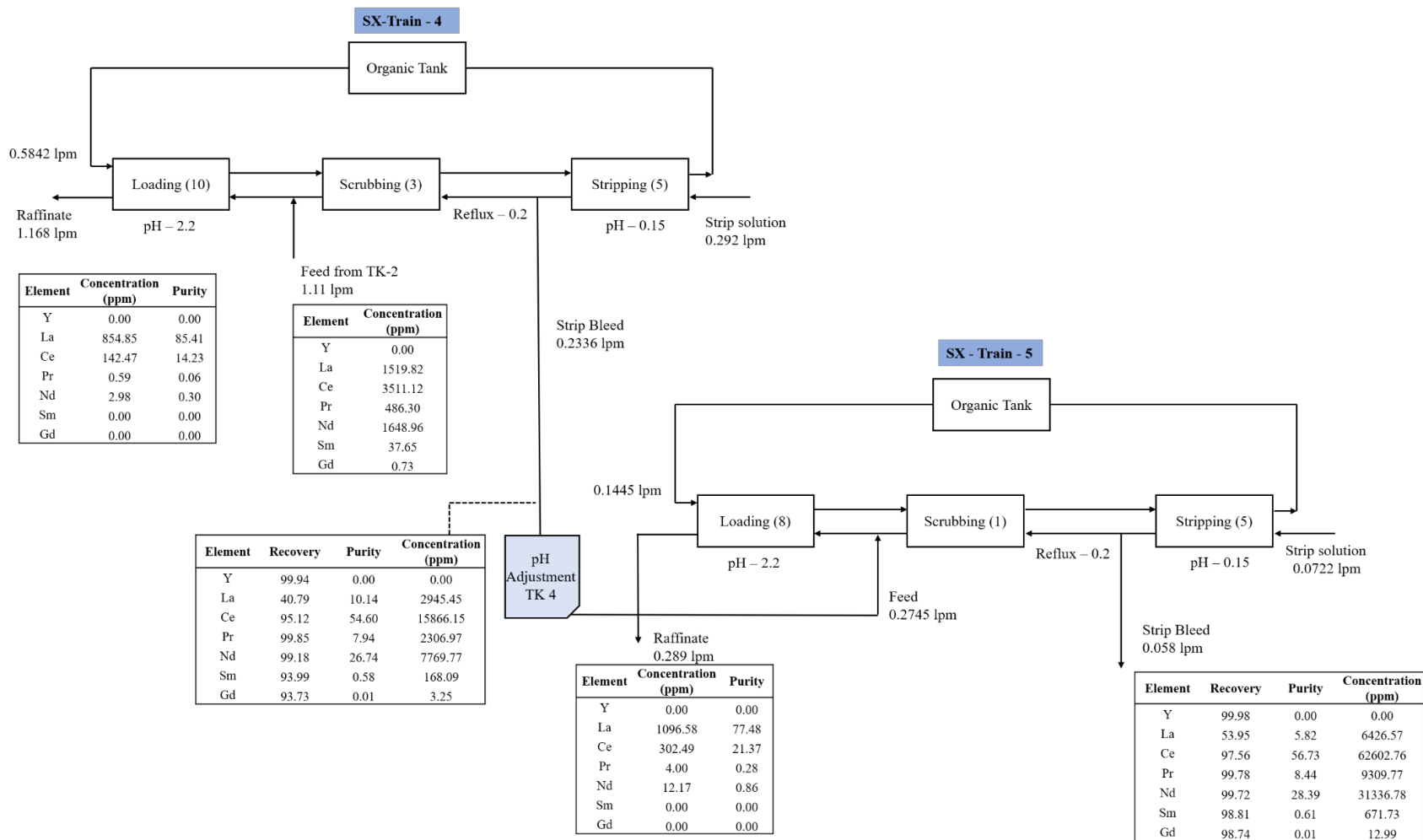


Figure 7.10: Nd-Ce-Pr and La Train 4 and Train 5

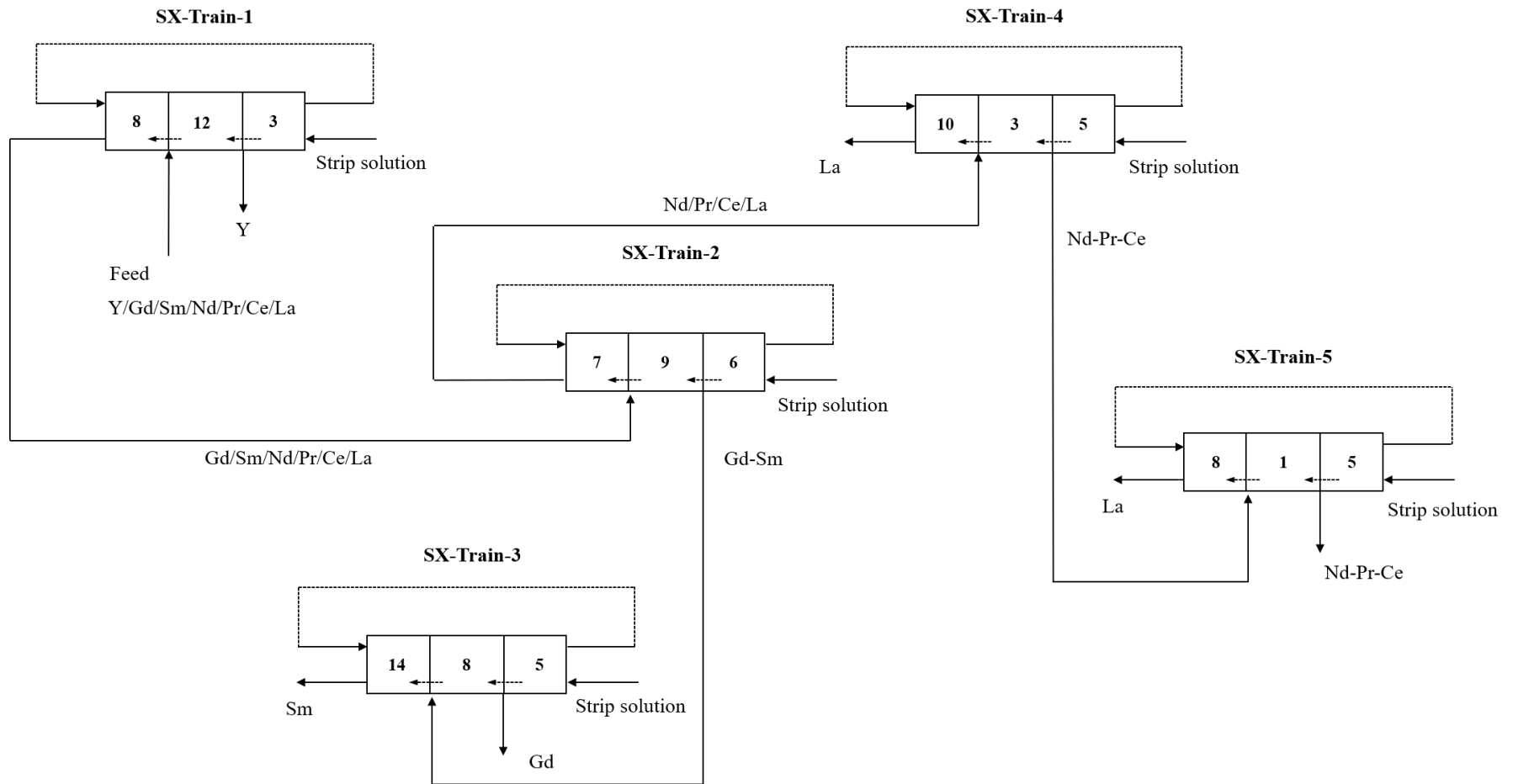


Figure 7.11: Complete flowsheet

Table 7.3: Summary of train optimization objective function and results

Train	Objective Function	Element Separated	Purity	Recovery	Stage Combination (Loading-Scrubbing-Stripping)
Train -1	Recovery and Purity of Y	Y	99.61	99.52	8-12-3
Train -2	Purity of Sm	Gd- Sm combined	46.00/34.65 (80.65)	25.48/22.11	7-9-6
Train -3	Purity of Gd	Gd/Sm	72.59	12.44	14-8-5
Train -4	Purity of Ce	Nd, Pr, Ce combined /La	26.74/7.94/54.60(89.28)	99.18/99.85/95.12	10-3-5
Train -5	Purity of Ce	Nd, Pr, Ce combined /La	28.39/8.44/56.73 (93.56)	99.72/97.78/97.56	8-1-5

After the multi-train flowsheet design and stage determination, the effect of reflux on purity of elements in strip bleed was also studied for each train. The analysis of the reflux essential due to its significance in a continuous operation. Reflux is a variable, other than pH and flowrates, which is manipulated in operation to control the purity of the product. Changing reflux affects the composition of the scrubbed solution leaving the scrubbing process. The changed concentration of the scrubbed solution, after combining with the incoming fresh feed, alters the overall feed composition in the loading stage, thereby altering the loading characteristics. Operating at high reflux has been shown to improve the purity; however, it suffers from the disadvantage of reduced output from the SX-train. Hence, reflux should be selected such that the increase in product quality should not be significantly impacted by decreased output. Figure 7.12 shows the study of the change in reflux ratio on the purity of the elements in the strip bleed that the train was intended to separate. The reflux ratio varied in the range of 0.2 to 0.6, increasing reflux more than 0.6 would essentially mean more recirculation of the stripped solution, which may not be beneficial as it will decrease the output capacity of the train. Nevertheless, from the results, it was observed that an increase in reflux slightly improved the purity in all cases, with a significant change for SX-train-2 (9.8 percent) and SX-train-4 (9.6 percent), wherein the combined separation of elements was sought.

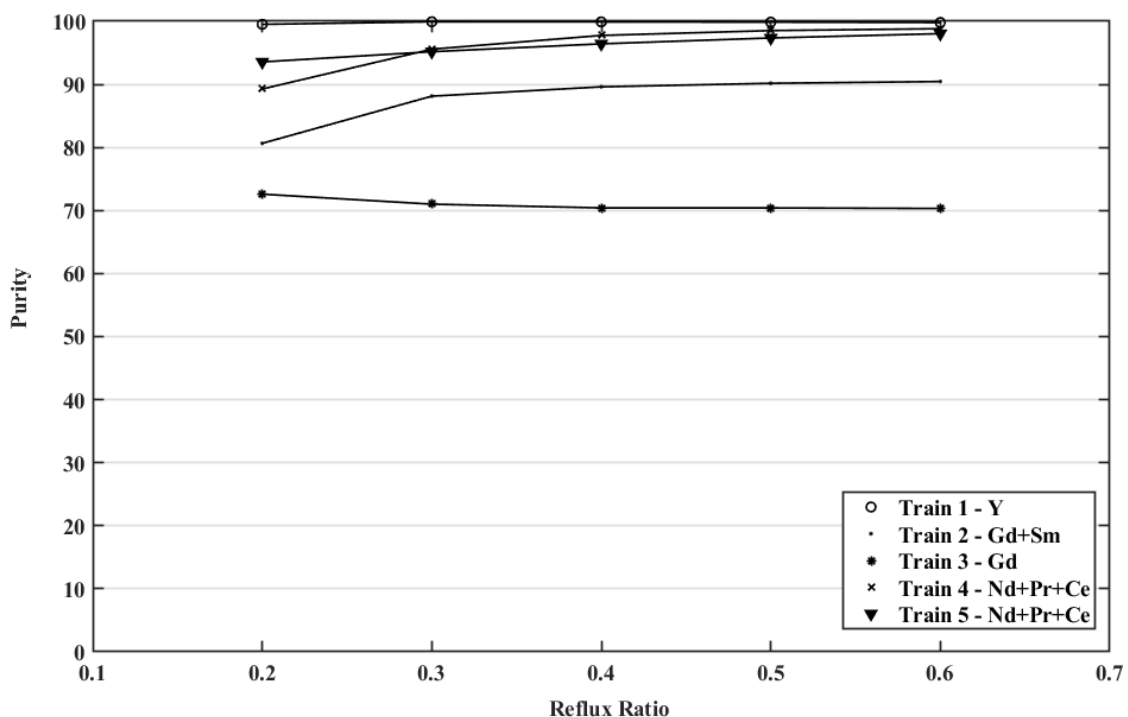


Figure 7.12: Sensitivity to reflux ratio

7.6 CONCLUSION

The chapter discussed the implementation of the separation and process models in developing flowsheets for the separation of elements from a rare earth feed mixture. The design specified the effective separation of yttrium and lanthanum from the feed mixture in high purity, whereas the separation of other elements was also possible to a lesser extent.

The significant challenge associated in the solvent extraction process design, i.e., stage determination, was solved by combining process models with the particle swarm optimization routine. Various stage combinations were tested by the optimization algorithm to yield better separability with recovery and purity of desired elements in the product stream. Nd, Pr, and Ce were difficult to separate and had low separation factors among them. An alternate extractant scheme for the three-element group can be sought for future work and tested using the same methods. Further, the model was used to investigate the sensitivity of the reflux ratio with respect to purity. An increase in reflux showed improved purity for all cases. The developed model and structured approach to design can

be applied to any feed composition, provided the separation variables are recognized and sufficient bench scale data is available.

CHAPTER 8. CONCLUSION AND FUTURE WORK

8.1 CONCLUSION

Solvent extraction is the most popular chemical process used in the extraction and separation of REEs. Significant research relating to the SX process, such as improving extraction and separation characteristics of REEs by using different extractant schemes, has been shown in literature. Still, the key issue facing the industry lays in determining the methodology for developing and designing efficient processes to separate REEs and produce them individually. The current research addressed key issues of flowsheet design and stage number determination for SX to produce individual REEs.

The work was a combination of experimentation and process modeling. Systematic experimental studies were performed on a mixed REE salt solution containing yttrium, gadolinium, samarium, praseodymium, neodymium, cerium, and lanthanum in various proportions. The proportion of the elements in the mixture was derived from the REO concentrate produced by the processing of coal containing REEs. The tests were performed at a high concentration instead of trace concentration to resemble the typical industrial feed and non-ideal nature of the solution.

The experiments involved extraction and stripping tests performed in two blocks with the first varying pH at equal phase ratios, and second varying phase ratios at constant pH. Simulation analysis was preferred in identifying pH conditions for phase ratio experiments, instead of the separation factors to account for feed composition and stripping effects on separation in a multistage process. The results obtained from extraction and stripping tests at different pH were utilized in developing distribution-ratio models. These models were integrated in a mass-balancing framework of an SX train, consisting of loading, scrubbing, and stripping, and they were used in the simulation with respect to change in pH. The pH resulting in high concentration (or purity) of elements in the stripped solution stream were selected for the phase-ratio experiments and developing a conceptual flowsheet. The conceptual flowsheet consisted of multiple trains with selected pH conditions for individual and group separation of elements.

Phase ratio experiments were performed at selected pH to seek further improvement in separation of elements of the proposed flowsheet and develop models for determining the number of stages required. The phase ratios resulting in high separation factors were selected as the operation conditions for the trains. Percent extraction and stripping models were developed using phase-ratio results and were programmed in Simulink as graphical functions. The blocks were used to design and simulate multi-train SX flowsheets. A particle swarm optimization algorithm was applied to the designed flowsheet to identify the number of stages, resulting in high purity, recovery, or both, specific to the train objective. Detailed findings, which were drawn from the study, are listed below.

1. The extraction profile obtained at different equilibrium pH in a range of 0 to 2.75 showed higher extraction of HREEs (Y) and MREEs (Gd, Sm) than LREEs (Pr, Nd, Ce, and La), which take place at a low equilibrium pH for the extractant selected. The profile for elements Y, Gd, and Sm were distinct in a pH range of 0.5 to 1.5 suggesting separability whereas in the case of Nd, Pr, and Ce, showed near-identical extraction characteristics, indicating difficult separability.
2. The stripping characteristics of the elements with change in pH was constant, with the exception of yttrium. Yttrium showed poor stripping at equilibrium pH of 0.35 and higher, indicating a strong association with the extractant. The difference in stripping characteristics between the elements was slight.
3. Non-linear relationships between distribution ratios and equilibrium pH suggested the presence of multiple ionic states of an element (see Section 5.1).
4. Sensitivity analysis with respect to pH, utilizing developed distribution-ratio models applied across a SX train, identified three pH points, 0.65, 1.5, and 2.2, for individual and group separation of elements. The pH points were determined by simulating the SX train at various loading pH and monitoring the purity of elements in the strip-bleed stream. The pH points resulting in high purity were selected for development of a conceptual flowsheet and experimental pH conditions to conduct phase-ratio experiments. The stagewise sensitivity analysis was also performed for multiple design configurations to demonstrate that there was no shift in pH points.
5. Phase-ratio experiment results conducted at specific pH indicated further improvement in separation is possible at low-phase ratios. The combined separation

of gadolinium and samarium from other elements is superior at a phase ratio of around 0.5 at pH 1.5. Similarly, lanthanum can be separated from the group if praseodymium, neodymium, and cerium are extracted together at a phase ratio of 0.5 at pH 2.2.

6. Typical SX experiments are performed at a low concentration of feed, which fails to account for the saturation effect in similar extracting multi-component systems. The current research was performed at a higher concentration of salt solution, which accounted for the saturation effect. The effect was distinct at higher equilibrium pH at low-phase ratios, where a decrease in concentration in experimental results was observed for Gd, Sm, and Pr, whereas a significant decrease was observed for Nd, Ce, and La (see Section 6.1.1).
7. A library of function-block models of different processes was developed in Simulink to design and simulate multi-train SX flowsheets. A conceptual flowsheet was designed consisting of five SX trains. SX-train-1 was tasked to separate Y from the feed mixture and SX-train-2 was aimed to extract Gd and Sm together from the mixture. Additionally, SX-train-3 was added to seek separation between Gd and Sm. Finally, SX-train-4 and SX-train-5 aimed to separate Nd, Pr, and Ce from La (see Figure 7.11).
8. Particle swarm optimization was implemented to determine the number of stages required by each SX train by minimizing the objective function specific to the train. Three different forms of the objective function were defined, which utilized recovery, purity, or a combination of both (Eq. 7.5-7.7). The objective functions were selected so as to maximize separation and purification. The function selection, resulting in the stage combination and performance are summarized in Table 7.3.
9. SX-train-1 used the combined optimization functions of recovery and purity, which resulted in Y recovery and purity of 99.61 and 99.52 percent using a 8-12-3 stage combination for loading-scrubbing-stripping. Similarly, group separation of Gd and Sm used the purity of samarium as the objective function. A 7-9-6 loading-scrubbing-stripping combination resulted in a combined purity of 80.65 percent. The individual separation between Gd and Sm used purity of Gd as the objective function, suggesting the use of 14-8-3 loading-scrubbing-stripping combination

resulting in a purity of 72.59 percent for Gd. Finally, the highest individual separation of La was obtained for SX-train-4, which utilized the purity of cerium as the objective function to concentrate Nd, Pr, and Ce in the strip bleed. This resulted in La in the raffinate of purity 85.41 percent, utilizing a 10-3-5 stage combination.

10. This work shows that scrubbing stages are essential in achieving high purity. Strip bleed used as scrub solution changes the overall composition of the feed entering the loading stage, thereby changing the overall extraction characteristics. For this reason, the SX trains designed for an element or element pair require a large number of scrubbing stages.

8.2 FUTURE WORK

This study covered many of the most important aspects of SX modeling, flowsheet configuration and the number of stages needed to separate REEs from a given feed stream while maximizing the purity of elements. The method and application developed will be applicable to other rare earth feeds with different compositions, provided bench-scale data is available. As with every study, there is often a need for future work and gaps which can be filled by further investigation. Some suggestions for future work are listed below.

1. The SX experiments performed were at a fixed-salt concentration of 10 g/l. Experimental studies at higher salt concentrations can be performed and compared, and they can be used to develop a scaling model. If the separation results do not change by a significant amount, high-concentration solutions can be processed, thereby improving the capacity of SX units.
2. Difficult to separate elements, like Gd-Sm and Pr-Nd -Ce, can be pursued using a different extractant scheme, which could lead to a higher-separation factor for more efficient separation.
3. Similarly, in the case of stripping, the use of a different stripping reagent resulting in greater selectivity can be explored. A selective stripping agent can improve the overall separation tremendously.

4. Dynamic modeling can be pursued by introducing residence time constant in the given model or utilizing transient-state mass balance for a given mixer-settler design. The dynamic model can be used in developing a control system for adjusting pH and flowrate using real-time optimization.
5. An accurate multivariable percent extraction model as function of pH and phase ratio can be developed and utilized in the optimization of both variables.
6. A method to develop a model that accounts for the saturation of the organic and competing ions in the organic phase can be explored.

APPENDICES

APPENDIX 1. SYMBOLS USED

Notation	
a_i	Activity of species i
λ_{ij} and δ_{ijk}	Virial coefficients
μ_i^{id}	Chemical potential under ideal condition
μ_i^0	Standard chemical potential
A	Aqueous Flowrate
c_1 and c_2	Particle acceleration constants
D_i^c	Distribution constant for species i
D	Distribution ratio for metal i
$D_{i,j}$	Distribution ratio for species i in jth stage
E_i or E	Percent extraction for metal i
f_i	Objective function value for element i (PSO)
$f_{pbest,i}$	Best objective function value for particle i (PSO)
f_{gbest}	Best objective function value achieved by the group (PSO)
G^{ex}	Excess Gibbs energy
I	Ionic strength
K_i	Equilibrium constant for species i undergoing reaction in ideal condition
$K_{i, conc}$	Equilibrium concentration constant for species i undergoing reaction
m_i	Molality of species i

O	Organic Flowrate
$p_{best,i}$	Best position of a particle i in any iteration (PSO)
g_{best}	Best position of the group (PSO)
P_i	Purity value for element i
R_i	Recovery value for element i
$S_{A/B}$	Separation factor between metal a and b
R	Gas constant
T	Temperature
V_i^t	Velocity of particle i at time t
w	Particle inertia (PSO)
X_i^t	Position of particle i at time t (PSO)
$X_{i,j}$	Concentration in aqueous phase for species i in j th stage
$Y_{i,j}$	Concentration in organic phase for species i in j th stage
Z_i	Charge on species i

APPENDIX 2. ADDITIONAL PLOTS

The section provides additional plots from a repeat test performed on stripping using acid of different molarity (at fixed phase ratio) and phase ratio test performed at pH 2.75. Additionally, it contains McCabe Thiele plot from phase ratio test conducted at pH 2.75 distinctly showing saturation effects.

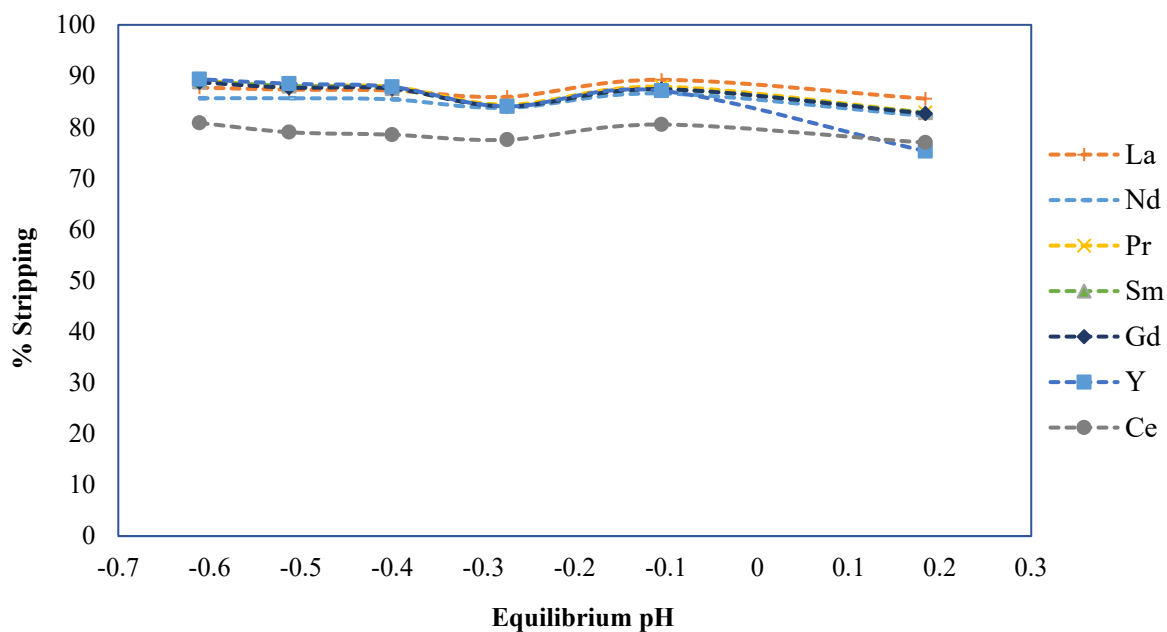


Figure 8.1 Stripping using acid molarity greater than 1 M

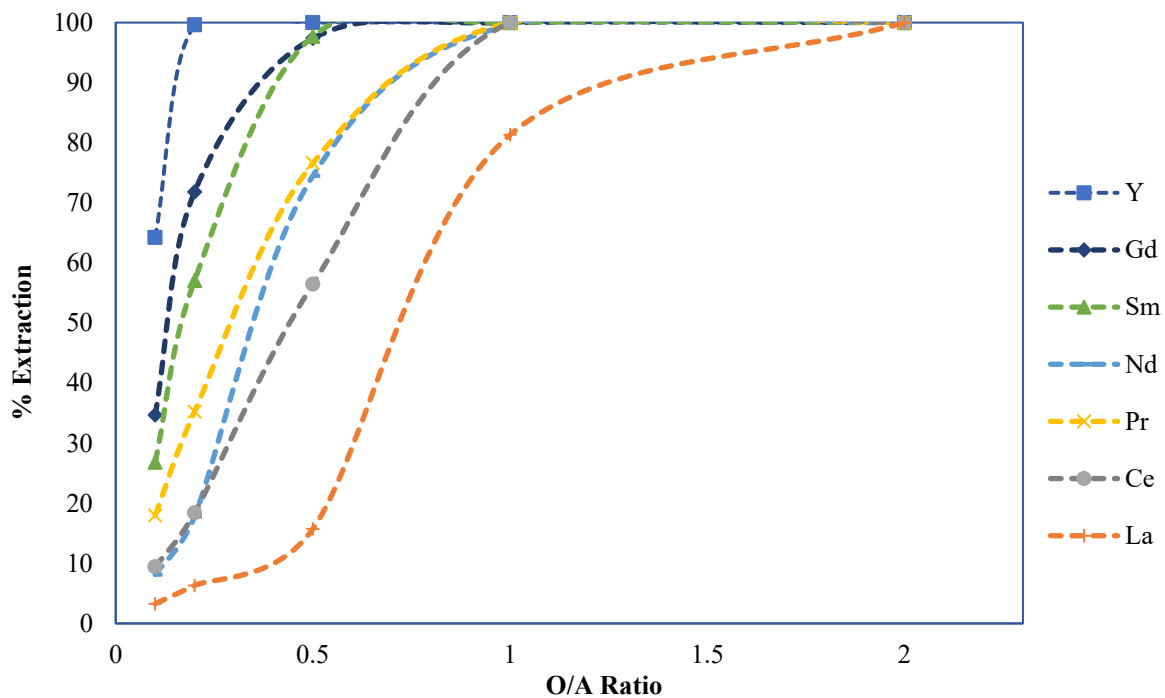


Figure 8.2: Percent Extraction vs O/A Ratio at pH 2.75

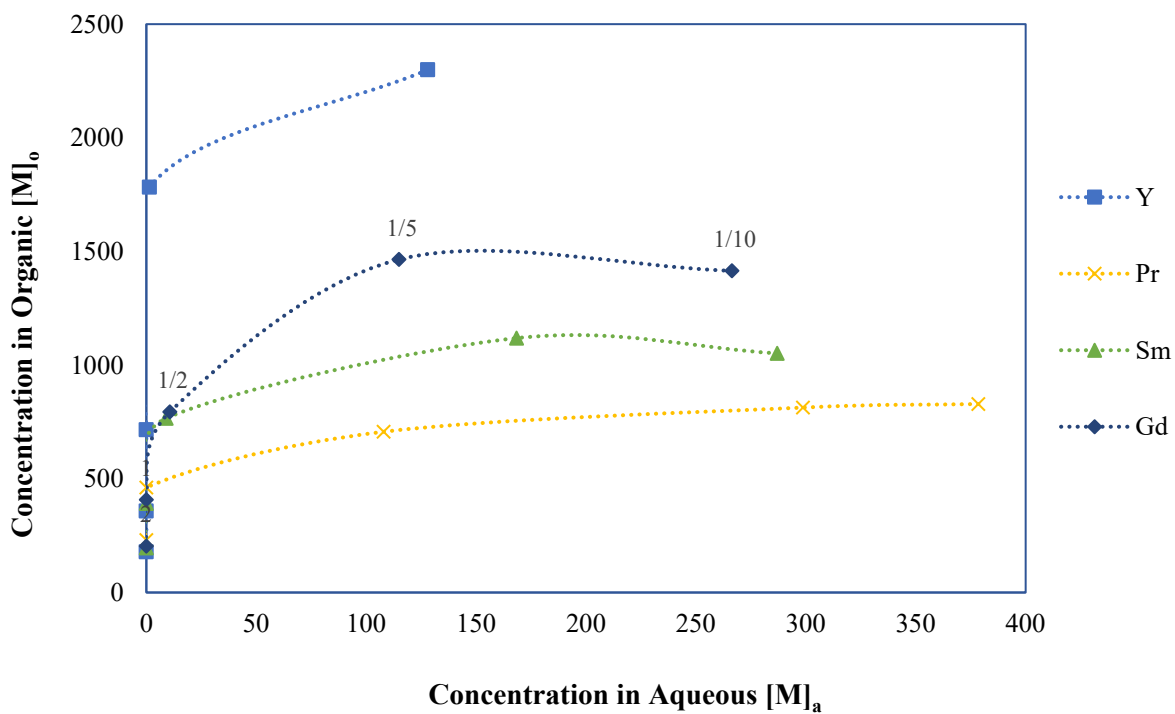


Figure 8.3: Saturation effect at pH 2.75 for Y, Gd, Sm, and Pr

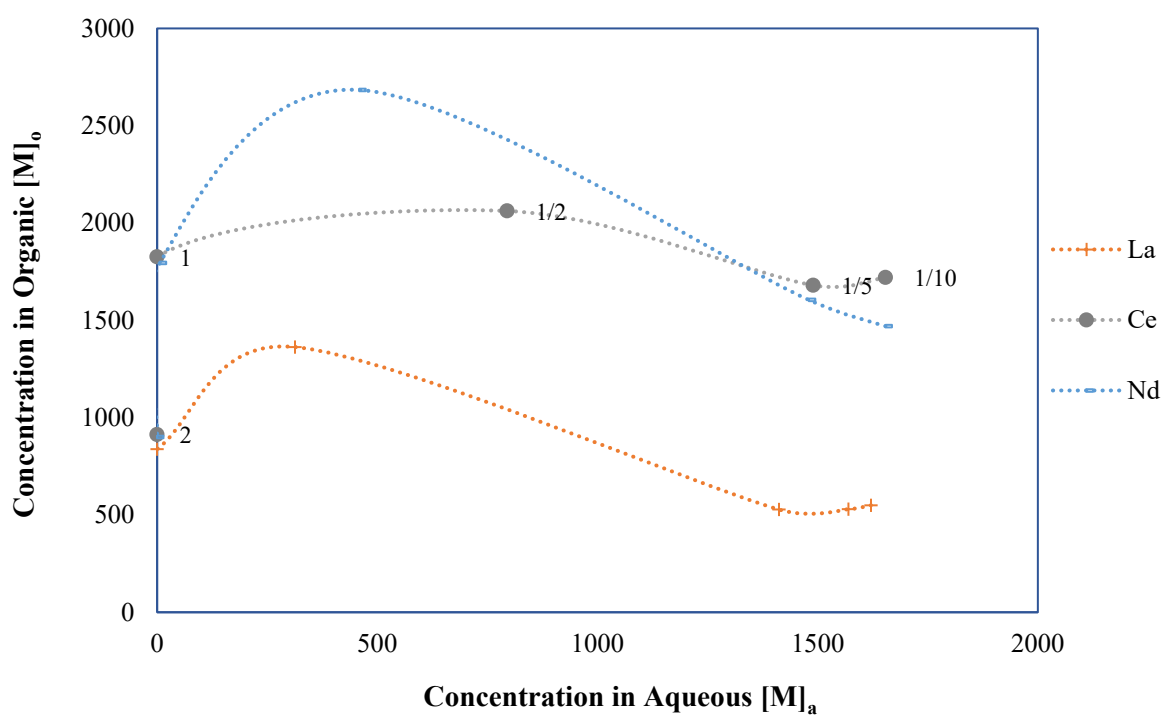


Figure 8.4: Saturation effect at pH 2.75 for La, Ce, and Nd

APPENDIX 3. APPLICATION CODES

LOADING BLOCK

```
function [Y1, X1, A, O] = OA_PE(Y0,X2,A,O,a,b,c,stage)

% Percent Extraction vs O/A Ratio implemented to multi-stage SX

q = O/A;
n = length(X2);
f = cell(n,1);

for i = 1:n
    f{i} = @(x) (a(i)*x^b(i)+c(i));
end

E = zeros(n,1);
Xn = zeros(n,stage);
Yn = zeros(n,stage);
X = X2;

for k = 1:stage

    for j = 1:n

        E(j) = f{j}(q)/100;
        if E(j) > 1
            E(j) = 1;
        end
        Xn(j,k) = X(j)*A*(1-E(j));
        Yn(j,k) = X(j)*A*E(j);

    end

    X = Xn(:,k)./A;

end
O = O;
A = A;
Y1 = (sum(Yn,2)+O.*Y0)./O;
X1 = Xn(:,end)./A;
Xn = Xn./A;
Yn = Yn./O;
```

STRIPPING BLOCK

```
function [Y1,X1,A,O] = Stripping(Y0,X2,A,O,a,b,stage)

% Percent Stripping vs O/A Ratio implemented to multi-stage stripping circuit

q = O/A;
n = length(Y0);
f = cell(n,1);

for i = 1:n
    f{i} = @(x) (a(i)*x + b(i));
end

S = zeros(n,1);
Xn = zeros(n,stage);
Yn = zeros(n,stage);
Y = Y0;

if q >= 1

    for k = 1:stage

        for j = 1:n

            S(j) = f{j}(q)/100;
            if S(j) > 1
                S(j) = 1;
            end
            Yn(j,k) = Y(j)*O*(1-S(j));
            Xn(j,k) = Y(j)*O*S(j);

        end

        Y = Yn(:,k)./O;

    end

else
    for k = 1:stage

        for j = 1:n

            S(j) = f{j}(1)/100;
            if S(j) > 1
                S(j) = 1;
            end
            Yn(j,k) = Y(j)*O*(1-S(j));
            Xn(j,k) = Y(j)*O*S(j);

        end

        Y = Yn(:,k)./O;

    end

end
```

CURVE FITTING CODE FOR LOADING DATA

```
% Script for curve fitting OA vs Percent Extraction at different pH

clc
clear all
load('OA_PercentExtraction_Dtk.mat')

% The experimental data of O/A ratio was stacked as 3-Dimensional matrix
% from 2-D table

a1 = table2array(t1); % pH 0.65, % E vs O/A
a2 = table2array(t2); % pH 1.5, % E vs O/A
a3 = table2array(t3); % pH 2.2, % E vs O/A
a4 = table2array(t4); % pH 2.7, % E vs O/A

all_data = cat(3,a1,a2,a3,a4); % create 3-D matrix

[row col] = size(a1);

% Loop to call function to fit data and store parameters

for j = 1:4

    for i = 3:col

        x = all_data(:,2,j);
        y = all_data(:,i,j);
        result = OA_Ex_Fit(x,y);
        p(i-2,1,j) = result.a;
        p(i-2,2,j) = result.b;
        p(i-2,3,j) = result.c;
        close all

    end

    writematrix(p(:, :, j), 'Paramaters Loading.xlsx', 'Sheet', j); % Export pa-
rameters to excel
end

close all % To close the figure window
```

CURVE FITTING FUNCTION FOR LOADING DATA

```
function [fitresult, gof] = OA_Ex_Fit(x, y)

% Curve fitting function for loading data at different O/A ratio

% x Input data OA Ratio
% y Input data Percent Extraction

[xData, yData] = prepareCurveData( x, y );

% Set up fittype and options.

ft = fittype( 'power2' );
opts = fitoptions( 'Method', 'NonlinearLeastSquares' );
opts.Display = 'Off';
[fitresult, gof] = fit( xData, yData, ft, opts );

% Following lines are for plotting

figure( 'Name', 'Fit' );
h = plot( fitresult, xData, yData);

set(h,'LineWidth',1.8);
set(h,'MarkerSize',12);

ax = gca;
ax.FontSize = 12;
ax.FontName = 'Times New Roman';
ax.YGrid = 'on'
ax.FontWeight = 'bold';
legend( h, '% Extraction vs O/A Ratio','Fitted Curve', 'Location', 'South-
East', 'Interpreter', 'none','FontSize',12,'FontWeight','bold','EdgeColor',
'none');
legend boxoff
xlabel( 'O/A Ratio', 'Interpreter', 'none','FontSize',12,'Font-
Weight','bold','Color','k');
ylabel( 'Percent Extraction', 'Interpreter', 'none','FontSize',12,'Font-
Weight','bold','Color','k' );
xlim([0 2.2]);
ylim([0 100]);
```


CURVE FITTING CODE FOR STRIPPING DATA

```
% Script for curve fitting OA vs Percent Stripping

clc
clear all
load('OA_PercentStripping_Dtk.mat');

a1 = table2array(S1); % pH 0.15; Str vs O/A
a2 = table2array(S2); % pH -0.64; Str vs O/A
all_data = cat(1,a1,a2);

[row col] = size(a1);
% loop for pH 0.15

for i = 3:col

    x = a1(:,2); % O/A ratio
    y = a1(:,i); % Percent strip
    result1 = OA_St_Fit(x,y);
    p1(i-2,1) = result1.p1; % p1, p2 and p3 are curve fitting paramaters
    p1(i-2,2) = result1.p2;
    p1(i-2,3) = result1.p3;

    close all
end

writematrix(p1(:,:),'Paramaters Stripping.xlsx','Sheet',1);
% loop for pH -0.65

for i = 3:col

    x = a2(:,2); % O/A ratio
    y = a2(:,i); % Percent strip
    result2 = OA_St_Fit(x,y);
    p2(i-2,1) = result2.p1; % p1, p2 and p3 are curve fitting parama-
ters
    p2(i-2,2) = result2.p2;
    p2(i-2,3) = result2.p3;

    close all
end

writematrix(p2(:,:),'Paramaters Stripping.xlsx','Sheet',2);
```

CURVE FITTING FUNCTION FOR STRIPPING DATA

```
% Script for curve fitting OA vs Percent Stripping

clc
clear all
load('OA_PercentStripping_Dtk.mat');

a1 = table2array(S1); % pH 0.15; Str vs O/A
a2 = table2array(S2); % pH -0.64; Str vs O/A
all_data = cat(1,a1,a2);

[row col] = size(a1);
% loop for pH 0.15

for i = 3:col

    x = a1(:,2); % O/A ratio
    y = a1(:,i); % Percent strip
    result1 = OA_St_Fit(x,y);
    p1(i-2,1) = result1.p1; % p1, p2 and p3 are curve fitting paramaters
    p1(i-2,2) = result1.p2;
    p1(i-2,3) = result1.p3;

    close all
end

writematrix(p1(:,:),'Paramaters Stripping.xlsx','Sheet',1);
% loop for pH -0.65

for i = 3:col

    x = a2(:,2); % O/A ratio
    y = a2(:,i); % Percent strip
    result2 = OA_St_Fit(x,y);
    p2(i-2,1) = result2.p1; % p1, p2 and p3 are curve fitting parama-
ters
    p2(i-2,2) = result2.p2;
    p2(i-2,3) = result2.p3;

    close all
end

writematrix(p2(:,:),'Paramaters Stripping.xlsx','Sheet',2);
```

PARTICLE SWARM OPTIMIZATION CODE

```
% Particle size optimization applied to SX train for stage calculation

clc
clear all

b = bdroot; % Get file path of current open model
ele = 3; % Specify element based feed distribution array

% Initialize Paramaters -----

Np = 10; % # of particle
itr = 20; % # of iterations
w = 0.8; % inertia
c1 = 2; % Particle coefficient
c2 = 2; % Swarm coefficient

f = zeros(Np,1); % Objective function - Recovery
g = zeros(Np,1); % Objective function - Purification Factor
z = zeros(Np,1); % Combined/Transformed Objective function
lb = [1 1 1]; % Stage # lower bound
ub = [20 20 20]; % Stage # upper bound
l = length(lb);
R = 0.2; % Reflux Ratio

% Initialize position and velocity array -----

P = randi(ub(1),Np,3);
V = randi(ub(1),Np,3);

for i = 1:Np

    nL = P(i,1);
    nSc = P(i,2);
    nSt = P(i,3);
    out = sim(b, 'SaveOutput', 'on');
    f(i) = out.recovery.Data(end,ele); % Recovery
    g(i) = out.purification.Data(end,ele); % Purity
    t(i) = sqrt(f(i).^2 + g(i).^2); % Transformed
    z(i) = 100-g(i);
    % z(i) = 141.42 - t(i); % Objective Func-
tion

end
```

```

particle_best = P; % Particle best
z_pbest = z;
[z_gbest,idx] = max(z_pbest); % Global best
gbest = P(idx,:);
optitr = zeros(itr,1); % Optimum value
optitr(1) = z_gbest;

% Iteration Start -----

for q = 2:itr

    for r = 1:Np

        V(r,:) = round(w*V(r,:) + c1*rand(1,1).*(particle_best(r,:) - P(r,:))
+ c2*rand(1,1).*(gbest - P(r,:)));
        P(r,:) = P(r,:) + V(r,:);
        P(r,:) = max(P(r,:),lb); % boundary condition check
        P(r,:) = min(P(r,:),ub); % boundary condition check

        nL = P(r,1);
        nSc = P(r,2);
        nSt = P(r,3);
        out = sim(b, 'SaveOutput', 'on');
        f(r)= out.recovery.Data(end,ele); % Recovery
        g(r) = out.purification.Data(end,ele); % Purity
        t(r) = sqrt(f(r).^2 + g(r).^2); % Transformed

        z(r) = 100-g(r);
        % z(r) = 141.42-t(r);

        % Condition check -----

        if z(r) < z_pbest(r) %* Objective Minimization for
particle
            z_pbest(r) = z(r);
            particle_best(r,:) = P(r,:);

            if z_pbest(r) < z_gbest %* Objective Minimization for
globe
                z_gbest = z_pbest(r);
                gbest = particle_best(r,:);

            end

        end

    end

    optitr(q) = z_gbest;

end

```

REFLUX SENSITIVITY ANALYSIS

```
% Reflux Sensitivity Analysis

clc
clear all

b = bdroot; % Get file path of current open model
Rf = 0.2:0.1:0.9;
[row, col] = size(Rf);
ele = 3; % sepcify element to analyze

for i = 1:col

    R = Rf(i);
    out = sim(b, 'SaveOutput', 'on');
    f(i) = out.recovery.Data(end,ele);
    g(i) = out.purification.Data(end,ele);
    z(i) = sqrt(f(i).^2 + g(i).^2);
end

x = Rf; % Reflux Ratio
y1 = f; % Recovery
y2 = g; % Purification
y3 = z; % Combined objective function

%-----

xint = linspace(0.1,0.9,100)'; % Reflux Ratio x axis vector
spl2 = spline(x,y2,xint); % Fit y2 data
p2 = plot(x,y2,'o',xint,spl2,'k-'); % Purity Plot

%----- Plot, Axis and label features -----

set(p2,'MarkerSize',8);
set(p2,'LineWidth',1.5);
ax = gca;
ax.FontSize = 12;
ax.FontName = 'Times New Roman';
ax.YGrid = 'on';
ax.FontWeight = 'bold';
xlim([0 1]);
ylim([0 100]);
xlabel('Reflux Ratio');
ylabel('Percent Purity');

%-----
```

REFERENCES

- Abdeltawab, A.Nii, S.Kawaizumi, F., & Takahashi, K. (2002). Separation of La and Ce with PC-88A by counter-current mixer-settler extraction column. *Separation and Purification Technology*, 26(2-3), 265-272.
- Acharya, S.Mishra, S., & Chand, S. (2017). Solvent extraction of La (III) using Cyanex 921 in petrofin and modelling of data by linear and nonlinear techniques. *Journal of Radioanalytical and Nuclear Chemistry*, 314(3), 1813-1824.
- Anderson, C. G.Giralico, M. A.Post, T. A.Robinson, T. G.Tinkler, O. S., & MacMoRan, F. (2009). An Update: Selection Equipment Sizing And Flowsheet Applications In Copper Solvent Extraction And Electrowinning. *Recent Advances in Mineral Processing Plant Design*, 287.
- Anitha, M., & Singh, H. (2008). Artificial neural network simulation of rare earths solvent extraction equilibrium data. *Desalination*, 232(1-3), 59-70.
- Banda, R.Jeon, H. S., & Lee, M. S. (2015). Separation of Nd from mixed chloride solutions with Pr by extraction with saponified PC 88A and scrubbing. *Journal of Industrial and Engineering Chemistry*, 21, 436-442.
- Binnemans, K., & Jones, P. T. (2015). Rare earths and the balance problem. *Journal of Sustainable Metallurgy*, 1(1), 29-38.
- Bourget, C.Soderstrom, M.Jakovljevic, B., & Morrison, J. (2011). Optimization of the Design Parameters of a CYANEX 272 Circuit for Recovery of Nickel and Cobalt. *Solvent Extraction and Ion Exchange*, 29(5-6), 823-836.
- Bromley, L. A. (1973). Thermodynamic properties of strong electrolytes in aqueous solutions. *AIChE Journal*, 19(2), 313-320.
- Brown, C. G., & Sherrington, L. G. (1979). Solvent extraction used in industrial separation of rare earths. *Journal of Chemical Technology and Biotechnology*, 29(4), 193-209.
- Campbell, D. (1973). Rapid rare earth separation by pressurized ion exchange chromatography. *Journal of Inorganic and Nuclear Chemistry*, 35(11), 3911-3919.
- Chaiko, D.Fredrickson, D.Reichley-Yinger, L., & Vandegrift, G. (1988). Thermodynamic modeling of chemical equilibria in metal extraction. *Separation Science and Technology*, 23(12-13), 1435-1451.

- Chandra, A. (2019). *Thermodynamic Modeling and Equilibrium System Design of a Solvent Extraction Process for Dilute Rare Earth Solutions*. (Doctoral Dissertation), University of Kentucky. UKnowledge database. (53)
- Debye, P., & Hückel, E. (1923). De la theorie des electrolytes. I. abaissement du point de congelation et phenomenes associes. *Physikalische Zeitschrift*, 24(9), 185-206.
- Deng, Z.-g.Xu, T.-h., & Yang, F.-l. (2003). Optimization study on the extraction separation process of mixed light rare earth. *Jiangxi Nonferrous Metals*, 17(1), 29-31.
- Dev, S.Sachan, A.Dehghani, F.Ghosh, T.Briggs, B., & Aggarwal, S. (2020). Mechanisms of Biological Recovery of Rare-Earth Elements from Industrial and Electronic Wastes: A Review. *Chemical Engineering Journal*, 124596.
- Du, X., & Graedel, T. E. (2011). Global rare earth in-use stocks in NdFeB permanent magnets. *Journal of Industrial Ecology*, 15(6), 836-843.
- El-Nadi, Y. (2012). Lanthanum and neodymium from Egyptian monazite: synergistic extractive separation using organophosphorus reagents. *Hydrometallurgy*, 119, 23-29.
- Evans, H. A.Bahri, P. A.Vu, L. T., & Barnard, K. R. (2014). Modelling cobalt solvent extraction using Aspen Custom Modeler. In P. S. V. Jiří Jaromír Klemesš, Peng Yen Liew (Ed.), *Computer Aided Chemical Engineering* (Vol. 33, pp. 505-510): Elsevier.
- Eyring, L.Gschneidner, K. A., & Lander, G. H. (2002). *Handbook on the physics and chemistry of rare earths* (Vol. 32): Elsevier.
- Fontana, D., & Pietrelli, L. (2009). Separation of middle rare earths by solvent extraction using 2-ethylhexylphosphonic acid mono-2-ethylhexyl ester as an extractant. *Journal of rare earths*, 27(5), 830-833.
- Free, M. (2013). *Hydrometallurgy: fundamentals and applications*. Hoboken, New Jersey: John Wiley & Sons.
- Gambogi, J., & Cordier, D. J. (2016). Minerals yearbook, rare earths. *US Geological Survey, Virginia, USA*.
- Ganguli, R., & Cook, D. R. (2018). Rare earths: A review of the landscape. *MRS Energy & Sustainability*, 5, E9.

- Goonan, T. G. (2011). *Rare earth elements: End use and recyclability: U.S. Geological Survey Scientific Investigations Report (5094)*. Retrieved from <http://pubs.usgs.gov/sir/2011/5094/>.
- Gupta, C. K., & Krishnamurthy, N. (1992). Extractive metallurgy of rare earths. *International Materials Reviews*, 37(1), 197-248.
- Haghighi, H. K. Moradkhani, D., & Salarirad, M. (2014). Modeling of synergetic effect of LIX 984N and D2EHPA on separation of iron and zinc using artificial neural network. *Transactions of the Indian Institute of Metals*, 67(3), 331-341.
- He, Y. Ma, W. J., & Zhang, J. P. (2016, February 1-3). *The parameters selection of PSO algorithm influencing on performance of fault diagnosis*. Paper presented at the MATEC Web of conferences, Cape Town.
- Honaker, R. Hower, J. Eble, C. Weisenfluh, J. Groppo, J. Rezaee, M., . . . Kiser, M. (2014). Laboratory and bench-scale testing for rare earth elements. *Cell*, 724, 554-3652.
- Honaker, R. Yang, X. Chandra, A. Zhang, W., & Werner, J. (2018a). Hydrometallurgical Extraction of Rare Earth Elements from Coal. In D. B. e. al. (Ed.), *Extraction 2018* (pp. 2309-2322): Springer, Cham.
- Honaker, R. Zhang, W. Yang, X., & Rezaee, M. (2018b). Conception of an integrated flowsheet for rare earth elements recovery from coal coarse refuse. *Minerals Engineering*, 122, 233-240.
- Hughes, M. Andersson, S., & Forrest, C. (1975). Distribution surfaces in solvent extraction systems. *International Journal of Mineral Processing*, 2(3), 267-276.
- Jha, M. K. Kumari, A. Panda, R. Kumar, J. R. Yoo, K., & Lee, J. Y. (2016). Review on hydrometallurgical recovery of rare earth metals. *Hydrometallurgy*, 165, 2-26.
- Kennedy, J., & Eberhart, R. (1995, 27 Nov.-1 Dec.). *Particle swarm optimization*. Paper presented at the Proceedings of ICNN'95-International Conference on Neural Networks, Perth, WA, Australia.
- Kim, J. S. Kumar, B. N. Radhika, S. Kantam, M. L., & Reddy, B. R. (2012). Studies on selection of solvent extractant system for the separation of trivalent Sm, Gd, Dy and Y from chloride solutions. *International Journal of Mineral Processing*, 112, 37-42.

- Klinkenberg, A. (1951). Calculation of the efficiency of counter-current stage-wise mass transfer processes with constant distribution factor, when in the stationary state: I. Distribution of one component only. *Chemical Engineering Science*, 1(2), 86-93.
- Komulainen, T., Pekkala, P., Rantala, A., & Jämsä-Jounela, S.-L. (2006). Dynamic modelling of an industrial copper solvent extraction process. *Hydrometallurgy*, 81(1), 52-61.
- Kremser, A. (1930). Theoretical analysis of absorption process. *National Petroleum News*, 22, 42.
- Krishnamurthy, N., & Gupta, C. K. (2005). *Extractive metallurgy of rare earths*. USA: CRC Press.
- Kronholm, B., Anderson, C. G., & Taylor, P. R. (2013). A primer on hydrometallurgical rare earth separations. *Jom*, 65(10), 1321-1326.
- Kuang, S., Zhang, Z., Li, Y., Wei, H., & Liao, W. (2018). Extraction and separation of heavy rare earths from chloride medium by α -aminophosphonic acid HEHAPP. *Journal of Rare Earths*, 36(3), 304-310.
- Li, W., Wang, X., Meng, S., Li, D., & Xiong, Y. (2007). Extraction and separation of yttrium from the rare earths with sec-octylphenoxy acetic acid in chloride media. *Separation and purification technology*, 54(2), 164-169.
- Liu, Y., & Spencer, S. (2004). Dynamic simulation of grinding circuits. *Minerals Engineering*, 17(11-12), 1189-1198.
- Lusty, P., & Walters, A. (2010). *Rare earth elements*. Retrieved from UK: <http://nora.nerc.ac.uk/id/eprint/12583/>
- Lyon-Utgikar, V. P., & Greenhalgh, M. R. (2017). Dynamic modeling for the separation of rare earth elements using solvent extraction: predicting separation performance using laboratory equilibrium data. *Industrial & Engineering Chemistry Research*, 56(4), 1048-1056.
- Lyon, K., Greenhalgh, M., Herbst, R., Garn, T., Welty, A., Soderstrom, M., & Jakovljevic, B. (2016). *Enhanced separation of rare earth elements* (INL/CON-15-37552). Retrieved from Idaho Falls, ID (United States): <https://www.osti.gov/biblio/1363891>
- Mansur, M., Slater, M., & Biscaia Jr, E. (2002). Equilibrium analysis of the reactive liquid-liquid test system ZnSO₄/D2EHPA/n-heptane. *Hydrometallurgy*, 63(2), 117-126.

- McCabe, W. L. Smith, J. C., & Harriott, P. (1967). *Unit operations of chemical engineering* (Vol. 5): McGraw-Hill New York.
- McCabe, W. L. Smith, J. C., & Harriott, P. (1993). *Unit operations of chemical engineering* (Vol. 5): McGraw-hill New York.
- Miller, J. (1978). Copper Extraction From Ammonia Leach Liquors With Hydroxyoximes.
- Moeller, T., & Kremers, H. E. (1945). The Basicity Characteristics of Scandium, Yttrium, and the Rare Earth Elements. *Chemical Reviews*, 37(1), 97-159.
- Mohammadi, M. Forsberg, K. Kloo, L. De La Cruz, J. M., & Rasmuson, Å. (2015). Separation of Nd (III), Dy (III) and Y (III) by solvent extraction using D2EHPA and EHEHPA. *Hydrometallurgy*, 156, 215-224.
- Nervik, W. E. (1955). An Improved Method for Operating Ion-Exchange Resin Columns in Separating the Rare-Earth Elements. *The Journal of Physical Chemistry*, 59(8), 690-695.
- Newman, S. Barner, H. Klein, M., & Sandler, S. (1980, October 29, 1980). *Thermodynamics of aqueous systems with industrial applications*. Paper presented at the ACS Symposium Series, Washington, DC.
- Preston, J. Du Preez, A. Cole, P., & Fox, M. (1996). The recovery of rare earth oxides from a phosphoric acid by-product. Part 3. The separation of the middle and light rare earth fractions and the preparation of pure europium oxide. *Hydrometallurgy*, 42(2), 131-149.
- Ray, R. Agioutantis, Z., & Kaklis, K. (2019). *Mine Pillar Design Using the Ground Reaction Curve Concept*. Paper presented at the Proceedings of the 38th International Conference on Ground Control in Mining.
- Reddy, M. L. P. Ramamohan, T. Bhat, C. C. S. Shanthi, P., & Damodaran, A. (1992). Mathematical Modelling of the Liquid-Liquid Extraction Separation of Rare Earths. *Mineral Processing and Extractive Metallurgy Review*, 9(1-4), 273-282.
- Robinson, C., & Paynter, J. (1971). *Optimization of the Design of a Countercurrent Liquid-liquid Extraction Plant Using LIX-64N*. Paper presented at the Nat. Inst. Met., Repub. S. Afr.
- Royen, H., & Fortkamp, U. (2016). Rare earth elements-purification, separation and recycling. *Environmental Research Institute: Stockholm, Sweden*.

- Rydberg, J. (2004). *Solvent extraction principles and practice, revised and expanded*. New York: CRC Press.
- Sandler, S. I. (2017). *Chemical, biochemical, and engineering thermodynamics*. Hoboken, NJ: John Wiley & Sons.
- Schmid, M. (2019). Mitigating supply risks through involvement in rare earth projects: Japan's strategies and what the US can learn. *Resources Policy*, 63, 101457.
- Sebenik, R. F. Sharp, B. M., & Smutz, M. (1966). Computer Solution of Solvent-Extraction-Cascade Calculations for the Monazite Rare-Earth Nitrates-Nitric Acid-Tributyl Phosphate-Water System. *Separation Science*, 1(4), 375-386.
- Sharp, B. M., & Smutz, M. (1965). Stagewise Calculation for Solvent Extraction System Monazite Rare Earth Nitrates-Nitric Acid-Tributyl Phosphate-Water. *Industrial & Engineering Chemistry Process Design and Development*, 4(1), 49-54.
- Soderstrom, M. Bourget, C. Jakovljevic, B., & Bednarski, T. (2010). Development of process modeling for CYANEX® 272. *ALTA 2010 Nickel/Cobalt, Copper and Uranium Proceedings*, 1-17.
- Sole, K. C. Feather, A. M., & Cole, P. M. (2005). Solvent extraction in southern Africa: An update of some recent hydrometallurgical developments. *Hydrometallurgy*, 78(1-2), 52-78.
- Srivastava, V., & Werner, J. (2020). *Solvent Extraction Flowsheet Design for the Separation of Rare Earth Elements: Tools, Methods and Application*. Paper presented at the Conference of Metallurgists, COM 2020.
- Thakur, N. (2000a). Separation of dysprosium and yttrium from yttrium concentrate using alkylphosphoric acid (DEHPA) and alkylphosphonic acid (EHEHPA-PC 88A) as extractants. *Solvent Extraction and Ion Exchange*, 18(5), 853-875.
- Thakur, N. (2000b). Separation of rare earths by solvent extraction. *Mineral Processing and Extractive Metallurgy Review*, 21(1-5), 277-306.
- Uda, T. Jacob, T., & Hirasawa, M. (2000). Technique for enhanced rare earth separation. *Science*, 289(5488), 2326-2329.
- Voit, D. O. (1989, 27 Feb - 2 Mar). *Computer simulation of rare earth solvent extraction circuits*. Paper presented at the Rare earth conference: extraction preparation and applications meeting, Las Vegas, NV (USA).

- Weaver, B. (1954). Fractional separation of rare earths by oxalate precipitation from homogeneous solution. *Analytical Chemistry*, 26(3), 479-480.
- Wenli, L., Ascenzo, G., Curini, R., Chunhua, Y., Jianfang, W., Tao, J. J., & Minwen, W. (2000). Simulation of the development automatization control system for rare earth extraction process: combination of ESRECE simulation software and EDXRF analysis technique. *Analytica chimica acta*, 417(1), 111-118.
- Wu, S., Wang, L., Zhao, L., Zhang, P., El-Shall, H., Moudgil, B., . . . Zhang, L. (2018). Recovery of rare earth elements from phosphate rock by hydrometallurgical processes—A critical review. *Chemical Engineering Journal*, 335, 774-800.
- Xie, F., Zhang, T., A. Dreisinger, D., & Doyle, F. (2014). A critical review on solvent extraction of rare earths from aqueous solutions. *Minerals Engineering*, 56, 10-28.
- Yun, C. Y., Lee, C., Lee, G.-G., Jo, S., & Sung, S. W. (2016). Modeling and simulation of multicomponent solvent extraction processes to purify rare earth metals. *Hydrometallurgy*, 159, 40-45.
- Zepf, V. (2016). Neodymium Use and Recycling Potential *Rare Earths Industry* (pp. 305-318): Elsevier.
- Zhang, J., Zhao, B., & Schreiner, B. (2016a). *Separation hydrometallurgy of rare earth elements*: Springer.
- Zhang, J., & Zhao, B. S., Bryan. (2016b). *Separation hydrometallurgy of rare earth elements*: Springer.

VITA

EDUCATION

- M.S., Mineral Preparation Engineering, University of Alaska Fairbanks
Thesis Title: “Dynamic Simulator for a Grinding Circuit”
August 2017
- Bachelors, Mineral Preparation Engineering, Indian Institute of Technology (Indian School of Mines), Dhanbad
Thesis Title: “Beneficiation of fine coal using Water Only Cyclone”
June 2013

AREA OF EXPERTISE

Process Improvement, Process Design and Control, Modeling and Simulation, Hydrometallurgy, Mineral Processing, Neural Networks, Bayesian Methods

RESEARCH EXPERIENCE

- 05/2018-05/2020 - Graduate Research Assistant, Department of Mining Engineering, University of Kentucky, Lexington, KY, USA
- 08/2017-05/2018 - Research Fellow, Department of Mining Engineering, University of Kentucky, Lexington, KY, USA
- 01/2015-06/2017 - Graduate Research Assistant, Department of Mining and Geological Engineering, University of Alaska Fairbanks, Fairbanks, AK, USA

INDUSTRIAL EXPERIENCE

- 05/2019-08/2019 - Summer Intern - Mineral Processing and Metallurgy Freeport McMoRan, AZ
- 07/2013-01/2015 - Process Shift Engineer – Ore Dressing – Hindustan Zinc, Vedanta Resources, Rampura Agucha Mines, Bhilwara, Rajasthan, India

PUBLICATIONS

- Srivastava, V., & Werner, J. (2020). Solvent Extraction Flowsheet Design for the Separation of Rare Earth Elements: Tools, Methods and Application. Paper presented at the Conference of Metallurgists, COM 2020.
- Srivastava, V., Akdogan, G., Ghosh, T., & Ganguli, R. (2018). Dynamic modeling and simulation of a SAG mill for mill charge characterization. *Minerals & Metallurgical Processing Journal*, 35(2), 61-68.
- Khamkhash, A., Srivastava, V., Ghosh, T., Akdogan, G., Ganguli, R., & Aggarwal, S. (2017). Mining-Related Selenium Contamination in Alaska, and the State of Current Knowledge. *Minerals*, 7(3), 46.
- Gupta, T., Ghosh, T., Akdogan, G., & Srivastava, V. (2017). Characterizing rare earth elements in Alaskan coal and ash. *Minerals & Metallurgical Processing*, 34(3).
- Conference Presentation on Dynamic Simulator Module of a Grinding Circuit, Phoenix, Arizona: *Society of Mining and Metallurgical Engineering*, 2016.

ACTIVITIES AND HONORS

- Engineer in Training, Commonwealth of Kentucky, 2018
- WAAIME Scholarship, Society of Mining & Metallurgical Engineering, 2018
- Mineral & Metallurgical Processing Division Scholarship 2016 and 2017, Society of Mining & Metallurgical Engineering.